TECHNICAL REPORT

Illinois Institute of Technology, Chicago, Illinois 60616

MEASUREMENTS NEAR BLUFF BODIES IN TURBULENT BOUNDARY LAYERS INTENDED TO SIMULATE ATMOSPHERIC SURFACE LAYERS

by

Jimmy Tan-atichat and Hassan M. Nagib

IIT Fluids & Heat Transfer Report R74-2
May, 1974

Supported under AFOSR-Themis Contract F44620-29-C-0022
and NSF Grant GK-41466X

MEASUREMENTS NEAR BLUFF BODIES IN TURBULENT BOUNDARY LAYERS INTENDED TO SIMULATE ATMOSPHERIC SURFACE LAYERS

by
Jimmy Tan-atichat and Hassan M. Nagib

IIT Fluids & Heat Transfer Report R74-2

Mechanics and Mechanical and Aerospace Engineering Department
Illinois Institute of Technology
Chicago, Illinois 60616

May, 1974

ACKNOWLEDGMENT

Many thanks are due Professors Mark V. Morkovin and Andrew A. Fejer for the very valuable consultations throughout the study; to John L. Way, who provided many stimulating discussions and helped with the instrumentation; and to Professor L. N. Tao for providing important comments on the first draft. Special thanks go to Perry Deutsch, for the design and construction of the three-dimensional traversing mechanism and his help in the modification of the Environmental Wind Tunnel. We are most grateful for the help provided by Rick Roberts, Gene Ginani, and other staff members of the Mechanics and Mechanical and Aerospace Engineering Department Machine Shop. The skill and patience of Tom Corke in the reduction of data for the velocity profiles are deeply acknowledged. Tom Hajek and Rich Wlezien provided valuable assistance in the preparation of the figures. Special appreciation is due Marsha Faulkner and Debra Mertens for typing several drafts of the manuscript. This research has been supported by USAF OSR Themis Contract F44620-69-C-0022 and by NSF Grant GK-41466X, Division of Engineering, Fluid Mechanics Program.

J. T. & H. M. N.

TABLE OF CONTENTS

LIST OF FIGURES

NOTATION

A	Total plan area of roughness fetch
A_r	Combined plan area of all roughness elements
d_i	Inner diameter of counter-jet manifold
d_j	Diameter of the jet exits in the counter-jet manifold
d_o	Outer diameter of the counter-jet manifold
f	Length of the roughness fetch
k	Height of the roughness elements
n	Reciprocal of the power law exponent = $1/\alpha$
$\dot{q}$	Volumetric flow rate of compressed air through the counter-jet manifold
s	Distance between centers of the jet exit holes of the counter-jet manifold
$U(z), \bar{U}$	Mean longitudinal velocity
U_j	Jet velocity from the counter-jet generator (manifold) measured one hole diameter downstream of the exit plane
U_∞	Wind tunnel free-stream mean velocity
u'	Root-mean-square value of the fluctuating component of the longitudinal velocity
x	Longitudinal (axial) distance measured downstream from the counter-jet manifold
x^+	Longitudinal distance from counter-jet manifold to the perforated plate at station VI
x_m	Longitudinal distance downstream measured from the center of the model
y	Transverse distance measured from inside edge of the wind tunnel test section
z	Elevation above the wind tunnel floor

z_o	A characteristic roughness length found by extrapolating the power law velocity profiles to zero log ($\bar{U}$)
α	Exponent of the power law profiles defined by $U(z)/U_\infty = (z/\delta)^\alpha$
δ	Boundary layer thickness (see text for definition)
θ	Angle between counter-jets and the horizontal plane through the center of the counter-jet manifold (θ is positive when the jets are aimed towards the floor)

ABSTRACT

The relatively new counter-jet technique is shown to be suitable for producing thick turbulent boundary layers which may be used to simulate neutral atmospheric surface layers in wind tunnels of moderate length. The increased thickness is achieved in the "I.I.T. Environmental Wind Tunnel" by providing large momentum defects at the wall through upstream-oriented, spanwise-discrete wall jets, with changeable jet velocities and controllable jet angles. This technique permits rapid alteration of reproducible boundary layers from outside the tunnel while the experiments are in progress. It is demonstrated how various mean velocity profiles (which can be represented by a wide range of power law exponents) and turbulence intensity distributions of the boundary layer are obtained at the same streamwise position using different settings of the counter-jet parameters and different types of artificial surface roughness. The transverse uniformity of these layers is also documented. Selected measurements of the flowfield near a bluff body for two wind directions in three different layers are compared in order to examine the sensitivity of measured effects to changes in the characteristics of the turbulent layers. While small changes are observed when results obtained in the two thick boundary layers are compared, large differences are noted between these and those obtained from tests in the thinner "natural" boundary layer of the tunnel. It is in this boundary layer (thickness of

boundary layer equal to approximately half of the model height) that the effect of the wind direction with respect to the bluff body is most evident. The data consistently demonstrate that the higher turbulence level within the two thicker layers increases the spreading and decay rates of the wake of the model. Influence of the wind direction on the flowfield on top of the bluff body is much stronger than that due to changes in the boundary layers. Similar sensitivity to the orientation of the bluff body is observed downstream of the model at low elevations.

CHAPTER I

INTRODUCTION

The concern for the effects of skyscrapers on the local wind condition or the flowfield in large, and highly built-up cities has revealed a number of important questions. In the downtown area of large cities, the high buildings can create adverse effects on the pedestrians, vegetation planted in the plazas, and other buildings in their vicinity under certain "atmospheric wind" conditions. It is much simpler and very often more economical to be able to make measurements on models rather than to do full-scale measurements on site. However, for the measurements on the models to be useful, the results should correlate with the full-scale conditions. This brings up the problem of trying to "scale-down" as to simulate the atmospheric boundary layer in a wind tunnel.

Thick turbulent boundary layers intended to simulate neutral atmospheric surface layers have been generated in many wind tunnels using different techniques. These generally aim at modeling selected statistically long-time average gust characteristics and velocity profiles. Actually, the target atmospheric layers consist of a succession of quasi-equilibrium boundary layers diffusing within older boundary layers as the wind, the ground roughness and the topography change. The information from tests in simulated surface layers such as steady and unsteady loads on

structures, smoke and contaminant dispersion, pedestrian safety and comfort, etc., depends to an unknown extent on the details of the above changing profiles.

Some of the most up-to-date information regarding the atmospheric surface layer (i.e., the lower part of the planetary boundary layer where the wind is not strongly influenced by the rotation of the earth and hence its direction does not change with height) is contained in various reviews and summarys[1-4*]. The uncertainties in the information as well as the lack of some types of them stands in the way of any attempts at evaluating the different wind-tunnel simulation techniques. For example, Davenport[5] has proposed 1500 to 2000 feet for the thickness of the neutral atmospheric boundary layer over built-up terrain, while Hanna[6] has suggested 2400 feet for the same conditions. In the case of the characteristics of the turbulence, the limited information available, even as far as the turbulence intensity profiles[1-4], does not permit us to predict the conditions within an urban area.

The changes of wind direction and consequently the ground conditions just upstream of the area of interest and the gustiness and slow variations of the wind and the velocity profiles complicates the problem even further. In light of these uncertainties, it is felt that model testing

---

*Numbers in superscript refer to the order of listing of references in the Bibliography section.

should include the examination of the sensitivity of measured effects to changes in the thickness, velocity profiles and turbulence scales of the simulated boundary layer.

Background and Philosophy

When we analyze similarities and differences between simulation of atmospheric surface layers in "long tunnels"[7,8] (or "boundary layer tunnels") and in "short tunnels"[9-15], it becomes clear that all these techniques must ultimately rely on wall roughness to produce a quasi-equilibrium layer. The target atmospheric surface layers under near-neutral conditions are controlled by the roughness as the shear stress diffuses freely from the ground. The adverb "freely" is emphasized by the advocates of "long tunnels" where generally no solid boundaries protrude above the roughness height. (Recently it seems that here and there a drag-producing body has sneaked into the "long tunnels.") On the other hand, the very length of the "long tunnels" makes the sidewall effects more critical and limits the quality of the boundary layers, in particular their transverse uniformity and structure.

In most of the "short tunnel" techniques a drag-producing device is introduced upstream of the roughness fetch from which the shear stress $\overline{uw}$ diffuses. Those devices, which protrude beyond the normal roughness, bring about vortical wakes which are then convected directly downstream into the body of the test layer. As the pro-

ponents of long tunnels point out, such relatively slowly decaying wakes[16] could impose artificial scales not present in the atmospheric layer. The same worry about extraneous scales beyond those of the thickness of the boundary layer itself, δ, and of the height of the wall roughness, k, applies to schemes in which upstream or downstream jets are combined with drag-wake producing grids to "shape the mean velocity profiles." The dominant turbulence structure then appears to be that of the wakes and jets, rather than that of the freely diffusing wall-controlled boundary layer[17,18].

One should be asking: What does a test in a single simulation of an ideal atmospheric layer really tell us? Over urban areas the idealized standard layer loses most of its theoretical underpinnings (there is inhomogeneity and large roughness) and becomes a rather arbitrary, somewhat fuzzy average. It follows that for the type of interactions between the urban wind and the building which we hope to understand and control, matching exactly the "prescribed" power of the velocity profile α in the wind tunnel should not be the overriding consideration. Rather, we should test for sensitivity to velocity profiles near the "official profile" and to alterations of the turbulence structure. Even for the determination of specific load factors, this procedure, combined with judicious bracketing of the results, seems justified in light of the uncertainties. Added to these uncertainties is the difficulty in modeling the scales of the turbulence in the wind-tunnel simulated

layers[19, 20]. The purposeful variation of the wind profiles by Colin and Olivari[21] and by Torrance[22] representsexamples of the systematic testing for sensitivity to poorly known parameters.

At IIT the problem of generating thick turbulent layers capable of simulating the variable ground-conditioned neutral atmospheric layer - without artificial scales and wakes - then appeared two-fold. (a) Production of large momentum defects with a freely mixing, spanwise homogeneous, wall-attached, large-scale turbulent structure. (b) Within this thick layer, a build-up of a faster-diffusing, quasi-equilibrium, roughness-controlled boundary layer. Thus, thickness and quasi-equilibrium might be achieved in layers with wall-conditioned scales δ and k alone if (a) were successful. Preliminary results by Nagib, et al.[24] and Gunnarsson[23] have shown that the counter-jet technique, namely the direct utilization of simple, controllable wall jets, oriented upstream, proved to be highly effective and versatile.

The counter-jet technique, schematically represented in Figure 1, provides large momentum defects at the wall through active, upstream-oriented, spanwise-discrete wall jets, with rapidly changeable jet velocities U_j and controllable angle θ of the jets with respect to the ground. From still limited experience with the counter-jet technique, we believe that the mean profiles and turbulence

characteristics are at least comparable in quality to those of other tunnels. In addition, this technique permits the modification of the profiles and the turbulence characteristics in a matter of minutes. Thus it provides at least a partial answer to Cermak's criticism[7] of "short tunnel" techniques: "However, these methods give no control of the turbulent structure." The turbulent layers can be altered rapidly and reproducibly from outside of the tunnel while the experiments are in progress; they can even be pulsated rapidly around a mean state. It is this flexibility which makes the technique very attractive for the important but neglected study of sensitivity of measured effects to changes in surface layer characteristics. In the work[24] performed in the smaller test-section of the same wind tunnel, the separate and combined effects of U_j, θ and wall roughness were illustrated.

Objectives

It was the objective of this investigation to develop further the counter-jet technique and to document the effects of the parameter values on the turbulent boundary layers generated. In particular, the first goal was to alleviate some of the difficulties encountered when Gunnarsson worked[25] on the implementation of the counter-jet technique (previously developed[24] in the small test-section of the I.I.T. Environmental Wind Tunnel) to the larger test-section of the tunnel. This included substantial modifica-

tions of the wind tunnel in order to improve the free-stream conditions of the low-speed test section.

It is, however, the main objective of this study to investigate the salient features of flow around a simple "building" in different boundary layers. In 1971, frustrated by a report on wind-loads based on 200,000 pressure readings on a model similar to ours, Morkovin[26], in his "Approach to flow engineering via functional flow modules," more concisely formulated ideas inherent in the efforts of many pioneers. The focus is on salient features which are grouped into coherent modules, i.e., "identifiable, morphologically invariant, mildly interacting flow structures," which were illustrated for flows around three-dimensional obstacles in laminar boundary layers of Norman[27] and for flows associated with screens, honeycombs, perforated plates and other flow and turbulence manipulators of Loehrke and Nagib[30]. We adapt here the modular flow concept to our studies in turbulent layers.

In short, our objectives are to demonstrate the counter-jet technique and to illustrate the sensitivity approach and the modular-flow approach in a simple instructive case.

CHAPTER II

EXPERIMENTAL FACILITIES AND TECHNIQUES

Experimental Facilities

The main experimental facility used in this investigation was the I.I.T. Environmental Wind Tunnel. The tunnel was used previously by Yung[28], Gunnarsson[25] and Way, Nagib and Tan-atichat[29] and is described in the following. A discussion of the evaluation and modification of the free-stream in the test section used for the present study is presented in Appendix A.

Environmental Wind Tunnel. The newly constructed I.I.T. Environmental Wind Tunnel is represented schematically in Figures 2 and 3. The tunnel operates in a recirculating mode and it has two separate test sections. A photograph of the low-speed test section is shown in Figure 4. Air is blown by the fan (Axivan Series 2000, Model 45-26 1/2-BD-CP made by Joy Manufacturing Company) through the low-speed test section, which is located in the "return" leg of the tunnel, and is drawn through the high-speed test section. The pitch angle of all the fan blades is adjustable by a continuous control which is located outside the tunnel. A variable speed 150 h.p. d.c. motor (G.E. Type C0505) is used to drive the fan through a set of V-belts. The motor speed is governed by a feedback-type speed control unit (G.E.Silicon-VI Industrial Drive System) at any desired value from 0-1750 r.p.m. The motor speed is monitored by

a tachometer-generator and is displayed on the remote control console. The maximum variation and drift in the free-stream speed are approximately 0.1% and 1% of the set velocity respectively. The flexibility offered by the motor speed control and the adjustable pitch angle of the fan provides steady operation of the tunnel under broadly different flow conditions and pressure drops in the two test sections. It also facilitates excellent speed control at low and high free-stream velocities. Uniform and steady velocities as low as 3 ft/sec have been maintained in the high-speed test section; i.e., as low as 0.8 ft/sec in the low-speed test section. The maximum speed in the small test section (2 ft. deep x 3 ft. high x 10 ft. long) is 100 ft/sec while in the large test section (4 ft. deep x 6 ft. high x 22 ft. long) is 25 ft/sec.

In addition to the turning vanes, flow manipulators (e.g., honeycombs, screens, and perforated plates) were used to damp out the turbulence level as well as secondary flows in the wind tunnel and to help prevent the diffuser stall at the entrance to the large test section.

The details of the side of the tunnel in which the high-speed test section is located are shown in Figure 2. A honeycomb section made of closely-packed plastic drinking straws is used just downstream of the turning vanes. The honeycomb is similar to ones used by Loehrke and Nagib[30] (mesh = 0.175 inch, solidity = 0.2) and is 8.25 inches long.

Located downstream of the honeycomb are: a series of eight screens (28 mesh, 0.007 in. wire diameter and 0.35 solidity; made of stainless steel) followed by a 4 ft. long settling chamber and a slow 4:1 contraction leading to the test section. Attention to the turning vanes, honeycomb and screens, together with provision for adequate decay time has brought the turbulence level u'/U_∞ at the entrance to the test section to as low as 0.03% at U_∞ = 70 ft/sec. The test section is followed by a pressure relief gap and a 16 ft. long small-angle diffuser.

Two plexiglas windows are located on the front face of the test section and are hinged by precision hinges on the extreme ends of the section permitting easy access to the inside of the tunnel. Two similar plexiglas windows which can be easily removed and replaced in position (possibly by other plates with traversing mechanisms attached to them) are found on the back face of the test section. A traversing mechanism which is driven by two variable speed d.c. motors (Bodine Type NSH-12R with Type BSH 200 d.c. motor control and Bodine type NSH-34RH with ASH 400 d.c. motor control) capable of traversing two probes in the streamwise and vertical directions is mounted on top of this test section along a 5/16 in. slot. The side walls of the test section between the windows are made of two removable aluminum plates (12 in. wide, 40 in. high) which are utilized for additional probe mounting and continuous vertical

and spanwise traversing or for supporting models. The floor of the test section is made of finished wood and can also be removed and replaced easily.

The present investigation was performed in the low-speed test section which will be described in detail next. Air flows from the variable-pitch fan into a transition section (circular to square) and enters the diffuser which is followed by the test section. At the entrance to the diffuser, a bank of plastic straws packed in a honeycomb-like matrix is used to suppress any swirling motion or secondary flows in the air. In addition, a perforated plate is utilized upstream of the honeycomb to reduce the large-scale eddies. A screen downstream of the straws is used to keep them from being blown away since they are only held in place by friction. The screen also reduces the level of turbulence downstream of the straws (see Loehrke and Nagib[30]). At the midsection and the exit of the diffuser, perforated plates provide the necessary back pressure to prevent stall due to the large angle (17.5°) of the diffuser[31]. Originally, splitter plates were used to prevent the stall but it was found that they lead to undesirable wakes that were detected far downstream in the test section[25]. Another perforated plate is installed 1.5 ft. from the diffuser exit to aid in uniformizing the flow in the test section.

All three perforated plates downstream of the honey-

comb matrix were stretched prior to being fastened and aircraft control cables, 0.021 in. diameter, were used to keep them tightly stretched across the section. The orientations of the cables were carefully selected so that their influence on the flow was minimal. An additional measure was used to ensure the tightness of the perforated plates. The plates were carefully heated to relieve the residual stresses in order to provide additional tightness after installation into the wind tunnel. The justification for using extensive measures in tightening the plates is that a vibrating perforated plate can cause flow anomalies due to the fluctuations in pressure across it and to the periodically shed vorticity from its holes.

The perforated plates used are made of 1/16 in. thick punched steel plates with 0.25 in. holes, 0.313 in. apart arranged in a hexagonal array resulting in a solidity of 0.42. The straws are 8.25 in. long plastic drinking straws with 1/8 in. diameter. The screen is made of 0.0065 in. stainless steel wire which forms a square mesh of 30 per inch having a solidity of 0.352.

Measurements at various stations of the 22 ft. test section were made and some of them are reported in Appendix A. After the final modifications, performed during the early stages of this study, the maximum spatial variation in mean free-stream velocity was found to be less than ±5% of the average velocity. The turbulence intensity along

the test section for the range of flows used here was approximately 1%. A calibration curve for the low-speed test section showing the relation between the motor r.p.m. and the free-stream velocity, at a fan setting of 2, is displayed in Figure 5.

Traversing Mechanism. The measurements reported in the present investigation were made using a hot-wire probe mounted on a specially designed minimum blockage traversing mechanism capable of traversing in three directions. The mechanism utilizes linear "Thompson" bearings and guide shafts and is mounted at an adjustable height inside the test-section. Vertical (z) motion was achieved through a guide tube mounted on a DISA 55H01 traversing mechanism powered by a DISA 52C01-2 high torque stepper motor and controlled by a DISA 52B01 sweep-drive unit. The maximum continuous traverse is 24.2 in. (615mm). At the present setting of the traversing mechanism, the hot-wire can probe down to within 1/8 in. above the tunnel floor and up to a height of 27.75 in. The vertical traversing speed used was two inches per minute.

In the lateral or transverse (y) direction, the probe can move to within 5.75 in. from either side of the test section width which is 48 in. In the axial or streamwise (x) direction the traversing length is seven feet. Both the transverse and streamwise traversing were accomplished through the use of Bodine Model 557 high torque (52 in.-lb.)

d.c. gear motors and Model 902 speed controllers driving .021 in. diameter aircraft cables via pulleys. Lateral traversing was done at a speed of three inches per minute. The entire traversing mechanism can be mounted at different heights and/or axial positions to give a wider range of coordinates that can be surveyed. A photograph of the traversing mechanism (looking downstream) with the probe mounted in position is shown in Figure 6. The bluff-body model can also be seen in the photograph.

Surface Roughness. As in most of the classical studies of turbulent boundary layers over rough walls[16,32], two-dimensional roughness was used in this work instead of randomly or orderly spaced three-dimensional roughness elements. Although the latter was tried initially, two-dimensional roughness was decided upon with one of the important motives being the ease by which one can reproduce it in any wind tunnel at any time. Artificial roughening of the test-section floor was, therefore, achieved by placing "Unistrut" members (1-5/8 to 3-1/4 in. high) across the entire width of the tunnel. The two types of roughnesses used are shown schematically in Figure 7. The design of the two types was based on the optimum roughness parameters found by Liu et al.[33] Roughness II with all the elements of uniform height (k = 1-5/8 inch) was the primary type used in the second phase of this investigation (Chapter V). The roughness surface density, A_r/A, for types I and II are 0.17 and 0.20 respectively. The roughness fetch

length for the two types is approximately 13.7 and 11.5 ft.

Bluff Body Model. The "building" model selected was a 4-inch square wooden block, 7.75 in. high. The model was placed in two orientations. In orientation I the model has the diagonal of its cross-section aligned with the mean flow and in orientation II one of its sides is facing the flow. The tunnel blockage due to the model for orientations I and II is 1.27% and 0.90% respectively.

Instrumentation

A tungsten hot-wire (0.00015 in. diameter, 0.1 in. long) mounted normal to the mean flow direction provided a signal primarily sensitive to the streamwise velocity. The hot-wire signal is processed in the manner shown schematically in Figure 8. The frequency response of the wire measured by the square wave method, was found to be up to 30 kHz when using the DISA 55D01 constant temperature anemometer. The output of the anemometer was linearized by a DISA 55D10 linearizer using an exponent of 2.0. Both the non-linear and the linearized hot-wire signals were monitored on a dual beam Type 5031 Tektronix storage oscilloscope.

The output of the linearizer was also fed into a DISA 55D25 auxiliary unit and a DISA 55D35 true r.m.s. meter. The optimum integration time for the r.m.s. meter was found to be 3-10 seconds. The output of the r.m.s. meter was then recorded by one channel of a Hewlett-Packard Model 7100BM dual channel strip-chart recorder. The

DISA 55D25 Auxiliary unit was used primarily to isolate the low pass network. A 1000 microfarad capacitor in conjunction with the output impedence of the auxiliary unit and the input impedences of the other instruments connected to it comprised the network. The output of the low pass filter was fed to the second channel of the strip-chart recorder and to a DISA 55D30 DC digital voltmeter that indicated the mean velocity. The network served to smooth the mean velocity signal recorded on the strip chart. Care was taken in evaluating the circuit and making sure the records were proportional to the true mean and r.m.s. velocity signals.

Data Acquisition and Experimental Procedures

If roughness elements were to be used, the first step was to place them into position along with the counter-jet generator (which will be described in Chapter III) in the test section. Next, the instrumentation and the wind tunnel were turned on at the operating conditions and allowed to warm up for a period of 2-3 hours. During this time the air temperature inside the tunnel reached a value of approximately 100°F. After the warm-up period, the hot-wire anemometer was calibrated with the aid of a pitot-static probe located in the free-stream of the test section. Slowing down the tunnel speed, the roughness elements were then checked for proper placement and the counter-jet was set at the required angle of attack. The traversing mechanism was then positioned for the starting point of the

first acquisition traverse. Next, the wind tunnel drive was brought up to the desired speed and compressed air was supplied to the counter-jet generator via a rotameter which monitored the flow rate.

After the transients of the start-up subsided, the traversing mechanism was started and synchronized with the strip-chart recorder to obtain various types (transverse or vertical) of velocity profiles (both mean and r.m.s.). After the end of the traverse, the hot-wire probe position was reset, the required parameter changes made, and the next traverse was carried out. The values of the parameters U_∞, U_j, θ, roughness type, etc., the instruments' settings and various observations were recorded for each traverse.

Using the above procedure, a record of both the mean velocity and the r.m.s. of the fluctuating velocity was obtained for each traverse. These records were then reduced to page-size with the aid of a Model 7000 Xerox copying machine. Whenever needed, corrections for air temperature variation were incorporated. The reduced strip-chart records were finally traced on the figures presented here. When data points are shown on the figures, this means that they were obtained by reading points off one of the continuous records.

CHAPTER III

DESIGN AND EVALUATION OF THE COUNTER-JET GENERATOR

The primary objective of the counter-jets is to produce near the surface a large momentum in the opposite direction to the free-stream. After the flow reattaches downstream of the jets, the resulting large momentum defect near the surface produces a thick boundary layer in a relatively short downstream distance.

The counter-jet generator was constructed from a 1/8 in. thick stainless steel tube with a 2-3/8 in. outside diameter. The generator is 47.8 inches long and it spans the width of the low-speed test section of the Environmental Wind Tunnel. Thirty-eight holes, 0.25 in. diameter, were drilled on a milling machine to ensure their alignment. The holes are located along a straight line at equal distances of 1.25 in. between centers. Diametrically opposite the jet exit holes, three inlet holes of 3/8 in. diameter supplied the counter-jet manifold with compressed air. The flow rate of the air through the generator was monitored by a Fischer and Porter Model 356184 flow rotameter. Approximately 132 CFM of air passes through the manifold at U_j = 175 ft/sec. This flow rate corresponds to less than 3% of the air flowing through the generated boundary layer when U_∞ = 12.5 ft/sec. A photograph of the counter-jet generator (mounted onto a 0.25 in. thick plywood sheet with 3 steel bands) in place in the wind

tunnel is found in Figure 9. Some of the roughness elements can also be seen in the background of the above figure. The steel bands that fasten the manifold to the plywood base could be easily loosened to permit changing the angle of the counter-jets with respect to the floor. Guide marks on the bands and on the blower body (calibrated for the range ± 20° with respect to horizontal) facilitated changing the angle of attack of the jets.

Counter-Jet Generator Modifications

In order to minimize the transverse non-uniformities downstream of the counter-jet, the momentum supplied by the generator across the tunnel should be as uniform as possible. This means that the counter-jets should have equal velocities (i.e., flow rates) exiting from them along the entire length of the manifold.

It was discovered early during the investigation that the uniformity of the distribution of air between the jets is sensitive to the design of the inlet tubes providing air to the manifold. Using the original inlet tubes[25] which extended about halfway into the manifold body with 4 holes drilled in their sides and a hole at their downstream end, it was discovered that the jet-velocity distribution at the exit of the holes is highly non-uniform. From Figure 10 one can easily conclude that the ratio of the highest to the lowest velocity among the jets is on the order of 4 to 5. Various methods were then tried with the

goal of achieving a uniform velocity distribution out of the generator.

It was conjectured that in order to uniformize the jet velocities, the pressure gradient along the manifold length should be kept very small compared to the pressure drop across each jet orifice. Various flow manipulators[30] were experimented with, both singly or in combinations by placing them inside the manifold. Different results were obtained with the most successful flow manipulator being a perforated plate (P.P. #3) and a "Scott" foam slab combination.

During the course of designing and evaluating the various types of inlets to the counter-jet manifold, an alternate location of the air inlet to the generator was tried. In this case the compressed air was supplied at one end of the manifold body rather than through the side, as indicated in Figure 11. The side inlets were sealed temporarily during the following experiments. Figure 12 demonstrates that the velocities from the counter-jets were very uniform except in the entrance region near the inlet pipe. The flow manipulator used inside the blower was a perforated plate and foam combination similar to the one shown in Figure 11 except the small patches of foam were not present. A hemispherical plug made of foam was also placed over the air inlet at the end of the manifold. The velocity distribution for the configuration was very uniform except for the first 9 to 10 jets which experienced

suction due to the entrainment created by the high velocity inlet jet. To achieve this type of uniform jet velocity distribution in the test section of the wind tunnel the manifold body would have to be longer than the width of the test section. This would necessitate cutting through the wind tunnel wall. Such a modification would prohibit the flexibility of moving the counter-jet generator upstream or downstream inside the test section to achieve optimum boundary layers. However, once the best position is found, this type of air inlet can be used.

In view of the above limitation the following modification of the counter-jet was used for the present investigation. The air inlet tubes were redesigned so that they were approximately flush with the inside of the manifold. A 2-1/8 in. wide strip of a steel perforated plate (P.P. #3 of Reference 30) 47 in. long, which was lined with one-inch thick "Scott" foam on one side, was inserted into the manifold so the foam faces the exit jets, as shown in Figure 11. Three pieces of 1/4 in. thick foam (2.5 in. x 1.75 in.) were also attached to the perforated plate opposite the inlet jets. The plate-foam assembly was held in place by friction and the ends of the manifold were sealed.

This modification produced the jet velocity distribution displayed in Figure 13. Because of the method used for the modifications of the counter-jet manifold, its first exit hole was plugged. It can be seen that the

variations in jet velocities occurred opposite the air inlets to the generator. However, they were small (the lowest jet velocity being only 8.6% below the average) compared to the original counter-jet results (compare with Figure 10). To completely eliminate the inlet effects on the counter-jet velocity distribution the compressed air should be supplied at the end of the manifold in the manner described earlier, making sure that an adequate entrance length is provided outside the test section. This will be implemented at I.I.T. in the near future.

Effects of Counter-Jet Position

At the beginning of the low-speed test section, at station VI (see Figure 3), a perforated plate (P.P. #3) provided the final flow conditioning needed for the test-section. It was, therefore, desirable to study the effect of the generator placement relative to this perforated plate in order to avoid any adverse interaction between the perforated plate and the counter-jets. Vertical profiles of mean velocity and turbulence intensity were obtained in the test section for various distances between the counter-jet blower and the perforated plate (denoted by x^+). Profiles for various angles of attack of the counter-jets θ (positive toward the floor) were recorded. All the measurements in this part of the study were taken along the test section center (y = 24 in.) and at a constant distance of 16 feet between the measuring station and the counter-jet generator.

Figures 14 and 15 show the mean and the turbulence intensity profiles for $\theta = +20°$. The counter-jet velocity was set at 175 ft/sec for all cases. Corresponding to $x^+ =$ 1 ft. the turbulence intensity was lower than that for $x^+ =$ 2.5 ft. or $x^+ = 3.0$ ft. The difference, however, was minimal between $x^+ = 2.5$ ft. and $x^+ = 3.0$ ft. as can be seen in Figure 15. Reducing the angle of attack of the counter-jets to +10° in Figures 16 and 17 one can again see the same trend of increasing turbulence intensity (at a given height z) as the distance x^+ is increased. The portions of the mean velocity profiles shown in the figures were not affected to any great extent, except for $x^+ = 1$ ft. The profiles for $\theta = 0°$ and $\theta = -10°$ are shown in Figures 18 and 19, and Figures 20 and 21 respectively. In general, the farther the counter-jet generator was from the perforated plate the higher the turbulence intensity at a given height until some critical distance was reached; e.g., for x^+ distances of 3 or 4 ft. the turbulence intensity distribution was approximately the same. In the case of $\theta = -10°$, Figure 20 shows that the mean velocity profiles had inflection points and the effect of x^+ on the turbulence intensity (Figure 21) was similar to the previous cases.

A lower free-stream velocity of 8 ft/sec was then used to obtain the next profiles. Figures 22, 23, 24 and 25 indicate that at the lower free-stream velocity, the mean velocity and turbulence intensity profiles for $x^+ = 3.0$,

3.5 and 4.0 are practically identical for $\theta = 0°$ and $\theta = -10°$. It should be noted that at the higher free-stream velocity the case of $\theta = -10°$ was more sensitive to x^+ variation than the rest. Since the effect of x^+ diminished when x^+ was between 3.0 and 3.5 ft. regardless of the orientation of the jets, the value of x^+ for all the remaining studies was fixed at 4 ft. This position of the generator assures no interaction between the jets and the perforated plate. A smaller x^+ could have been used; however, it was considered wiser to be on the safe side although sacrificing some short fetch of the test section.

Having fixed x^+ at 4 ft., the effects of changing the angle of attack, θ, on the mean velocity and turbulence intensity profiles were obtained in Figures 26 and 27. As θ decreases, the turbulence intensity increases at the lower values of z. Since these results are very similar to the ones obtained by Nagib et al.[24], it was considered unnecessary to proceed with a complete study of the effects of the jets angle θ on the generated boundary layers. Instead their results[24] were relied upon and the value of θ found by them to yield boundary layers most representative of the accepted neutral atmospheric conditions (i.e., $\theta = +10°$) was utilized for the remaining tests.

CHAPTER IV

MEASUREMENTS OF GENERATED BOUNDARY LAYERS

In an attempt to contrast some techniques of simulating atmospheric surface layers and to examine the sensitivity of the flowfield near the "building" model to changes in boundary layer velocity profiles, measurements of different turbulent boundary layers are performed in this chapter. Based on these measurements, selected layers are used in the next chapter to model atmospheric surface layers. Although the simulation is by no means complete, it was considered adequate in view of all the uncertainties in defining the atmospheric conditions inside urban areas. (See discussion of Chapter I.)

Tunnel Boundary Layer

The first of the boundary layers was generated by a tunnel floor fetch of 20 ft. with no artificial surface roughness. Its transverse uniformity is shown in Figures 28, 29, 30 and 31. The mean velocity at the five different transverse positions is found to be uniform to within ±4.52% of the free-stream velocity. The free-stream turbulence intensity at this position as obtained from Figure 113 is approximately 1.1% for this velocity. If the boundary layer thickness δ is defined as the height z at which the mean velocity and turbulence intensity approach the values of the free-stream, δ for the natural boundary layer of the wind tunnel is found to be approximately 4-6 in.

depending on the lateral position.

Definition of the boundary layer thickness using the mean velocity or turbulence intensity alone was difficult and insufficient. Although this is partly due to residual uncertainty of approximately 2% in the measurements resulting from the compensation for air temperature drift[34], the fact that the turbulence intensity at the maximum height of some of the traverses did not yet reach the free-stream level made the discrimination between the boundary layer and the flow outside of it difficult. In addition, in some profiles at heights corresponding to the "free-stream" $\partial\bar{U}/\partial z$ was not always zero. Certain transverse non-uniformities in some velocity profiles also discouraged the use of a restrictive and precise definition of the boundary layer thickness.

The log-linear and log-log plots (see Reference 32) of Figure 28, shown in Figures 32 and 33, confirm our estimate of the tunnel boundary layer thickness. The average power law exponent $\bar{\alpha}$ for this boundary layer is 0.15.

Roughness-Generated Boundary Layers

The next type of boundary layers was obtained by adding surface roughness elements of type I or II (for details see Figure 7) to the same length of the test section. Figures 34 and 35 display the boundary layer mean velocity and turbulence intensity profiles respectively. The log-linear plot in Figure 36 indicates that both

velocity profiles follow a logarithmic variation for $4 < z < 14$. From Figure 37 the characteristic roughness length z_o was found to be equal to 0.055 and 0.018 in. for roughnesses type I and type II respectively; the corresponding α values are 0.45 and 0.38. The boundary layer thicknesses as noted from Figures 34 and 35 are approximately 17 in. for type I roughness and 15 in. for type II. The peak turbulence intensity is about 14% occurring at a height of 5 in. for type I roughness and about 12.5% at $z \simeq 3$ in. for type II. Both diminish quite rapidly to the free-stream level at the boundary layer edge.

Counter-Jet Generated Boundary Layers

Without Surface Roughness. Vertical centerline velocity profiles of the boundary layers generated using various counter-jet velocities at different streamwise locations x are shown next. In obtaining the profiles of Figures 38, 39, 40 and 41, no artificial roughness was introduced in the tunnel except the blower body and its air supply tubes which were kept as close to the floor as possible. The effect of the presence of the generator (with no air supplied to it) can be detected when the turbulence intensity profiles of Figures 29 and 31 (no blower inside test section) are compared with those of Figure 41. The passive manifold in position created a boundary layer with a moderate turbulence intensity of about 5-6% (at x = 16 ft.) up to a height of roughly 12 in. where it rapidly drops off to the free-stream level. Examining only the mean velocity profiles of Figures

28 and 40 one can hardly distinguish between the two conditions.

Blowing moderately with the counter-jets (U_j = 122.5 ft/sec), not much increase in turbulence intensity or change in boundary layer mean profile shape are noted as we compare Figures 38 and 39 with 42 and 43 for x = 9 ft. or as we compare two of the curves (U_j = 0 and U_j = 122.5) of Figures 40 and 41 for x = 16 ft. Increasing U_j to 148.8 ft/sec produced a more dramatic change in the turbulence intensity profile at both x locations (see Figures 39 and 41). Blowing even stronger at U_j = 175 ft/sec removes the small non-uniformity in the mean velocity profiles and increases the turbulence level still further. As in the case of the measurements of Nagib et al.[24], one concludes that the counter-jet technique is reasonably effective only when U_j is larger than some threshold value. Below this value the effect of U_j diminishes. It is conjectured that this threshold value is associated with the full establishment of the separation line between the jets and the oncoming free-stream.

The variation of u'/U_∞ with height in Figure 41 for U_j = 175 ft/sec and x = 16 ft. is small for $2 < z < 17$ in. At the maximum height of the traverse the turbulence intensity has not yet reached its free-stream level although the mean velocity is changing very little with height as depicted by Figure 40. In this case, using a criterion on

$\overline{U}$ (such as $\overline{U}(\delta) \simeq U_\infty$) alone to determine the boundary layer thickness would indicate a δ different from the one obtained from a definition based on u'/U_∞ alone. Hopefully, by looking at both one gets a better idea of what might be happening and one may avoid contradictory conclusions on δ values.

Much of the same data plotted in a different manner showing the variation of the profiles with distance x for constant U_j values are shown in Figures 42 through 49. With increasing x distances we see a decrease in the turbulence intensity but a much more uniform distribution among the heights z. For the large x values the sensitivity of the profiles to downstream distance diminishes.

The transverse uniformity for the vertical profiles at x = 16 ft. with U_j = 175 ft/sec and no surface roughness is shown in Figures 50 and 51. Up to about z = 16 in. the turbulence intensity for the different transverse positions remained uniform. Above this level the centerline turbulence intensity decays at a faster rate, compared to the other two y positions, to a value of less than 4% at $z \simeq$ 27.5 in. This value is still higher than the free-stream intensity indicating the extent of the boundary layer to higher elevations. The lateral uniformity at different heights is again shown in the y-traverses of Figures 52 and 53, obtained at a lower U_∞. Based on the above results, the counter-jet velocity was fixed at the value of 175 ft/

sec for all the remaining measurements.

With Surface Roughness. In addition to setting the counter-jet velocity at 175 ft/sec, roughness elements of type I and II (see Figure 7) were placed on the surface of the test section. The resulting velocity profiles, displayed in Figures 54 and 55, depict a slightly higher velocity defect in the lower portion of the boundary layer $z \leq 16$ in. for type I roughness compared to type II. A peak turbulence intensity of about 14.5% is obtained for type I roughness while the corresponding value for type II is approximately 13.5%. Comparing these values to those generated by roughness alone (14% for type I and 12.5% for type II) indicated that the peak values are approximately the same; however, the profiles are different. The turbulence intensity generated by the roughness alone without U_j dropped to the free-stream level of the tunnel at $z = 15$ to 17 in., while in the case of roughness combined with high U_j, u'/U_∞ was still about 4% at a height of 24 in. The turbulence intensity along the centerline of the counter-jet generated layer with no artificial roughness and $U_j = 175$ is about 8% over the lower portion $2 < z < 12$ in. reaching a value of 4% at $z \simeq 27.5$ in. (for details see Figure 51).

Figures 56 and 57 show the log-linear and log-log plots of Figure 54. The range where the data follows a logarithmic profile is $4 < z < 18$ in. and the power law

exponents are .35 and .26 for type I and type II roughnesses respectively; the corresponding z_o's are 0.013 and 0.0015 in. The power law relationship seems to be valid for $2 < z < 19$.

The transverse uniformity of these layers is indicated in Figures 58 through 61 with the aid of vertical profiles. Additional evidence is given in the form of y-traverses across the test section in Figures 62 and 63. The mean velocity was fairly uniform in the 2 ft. central section up to about z = 24 in. The turbulence intensity and mean velocity plots indicated that near the top edge of the floor boundary layer the side-wall boundary layers have begun to merge with it, producing lower mean velocities and higher turbulence intensity levels at the sides. An assessment of the three-dimensionality of the turbulence in the boundary layer can be made from the undulations in the u' surveys. This evidence is in support of the arguments for the two-dimensional type of roughness used here and in most of the classical work on turbulent boundary layers.

Figures 64 through 67 represent surveys of mean and fluctuating velocity from x = 9.14 ft. moving progressively downstream to x = 13.77 ft. These profiles were taken with the hot-wire probe at a streamwise position midway between the roughness elements. The similarity between the profiles is an indication that the generated boundary layer is at near "equilibrium." In Figures 66 and 67 at x = 14.44 and 14.71 ft., the probe was placed one-half and one full

spacing of the roughness element beyond the last downstream roughness element. These profiles depict the relaxation of the boundary layer downstream of the roughness fetch.

CHAPTER V

MEASUREMENTS OF THE FLOWFIELD NEAR BLUFF BODIES IN SIMULATED SURFACE LAYERS

Simulated Surface Layers

The first of the three boundary layers selected for testing the model was the natural boundary layer produced over a fetch of 20 feet in the test section of the wind tunnel. The second was obtained by adding a roughness of type II (see Figure 7) to the same length of the test section. The third boundary layer was generated by the counter-jet technique in conjuction with surface roughness of type II. The mean velocity and turbulence intensity profiles for these three boundary layers along the tunnel vertical centerline, at the same streamwise position, are shown in Figures 68 and 69. Additional information is presented in Chapter IV. For the purposes of this discussion these three layers will be referred to as: the tunnel boundary layer, the roughness-generated boundary layer and the counter-jet generated boundary layer. (Note that the counter-jet generated boundary layer also uses artificial surface roughness.) A detailed discussion concerning these and other thick turbulent boundary layers is included in Chapter IV.

The selection of these boundary layers was based on several factors. First, the tunnel boundary layer was included as an extreme or reference case in order to contrast

the results from the other boundary layers with those which are obtained if essentially no effort is made to simulate the atmospheric surface layer.

In view of all the uncertainties regarding the true conditions within the atmospheric boundary layer (see discussion in Chapter I), complete modeling is almost impossible to date. A total simulation of the planetary boundary layer requires matching the mean velocity and turbulence intensity profiles, the spectral energy content of the velocity fluctuations, the Reynolds numbers overall model surfaces, the temperature gradients and the changes in wind direction with height. If one is only interested in high winds in neutral atmospheric conditions and if the simulation is limited to the lower part of the boundary layer (i.e., the surface layer) the problem is reduced to modeling the mean velocity and turbulence intensity profiles and the scales of the turbulence (i.e., the spectra of the velocity fluctuations). Since the main objective here is to study the flowfield near a "building model", such limited simulation is adequate.

It is believed at I.I.T. that the testing of the flowfield of interest in different boundary layers and the evaluation of the sensitivity of the main characteristics of this flowfield (i.e., the flow modules[26]) to the changes between these boundary layers is a more effective approach than to attempt to model some handbook description of the

planetary surface layer (especially when such handbook information is by no means complete and, at times, even inaccurate).

The two thicker boundary layers used here are not far from simulating the mean velocity and turbulence intensity profiles of the surface layer in the streamwise direction. Unfortunately, no complete measurements of the spectra of u or the profiles of other components of velocity were obtained during this study.

The model shown in Figure 70 was tested in each of the three boundary layers displayed in Figures 68 and 69. Two wind directions were studied by changing the model orientation as represented in Figure 70. A number of hot-wire probe surveys were made in each case; a summary of these, their range and coordinate positions are listed in the table of Figure 70. The measurements presented here deal with characterizing the wake of the model and the shear-layer module[26] on top of the bluff body as well as the interaction between them.

Measurements Downstream of Model

Vertical Profiles. The two downstream distances at which the mean velocity and turbulence intensity profiles were recorded for both orientations of the model, were roughly one and two model heights downstream of the model. Figures 71 and 72 show the profiles at x_m = 8.75 in. (the closer distance) for orientation I in which one of the

corners of the model is facing the flow. From Figure 71 one can see that the wake profile produced when the model flowfield was measured using the tunnel boundary layer has a sharp mean velocity gradient near the top (the model was 7.75 in. high), whereas those produced when either the roughness-generated layer or the counter-jet generated layer was used did not have as high a shear. The ones obtained from the two thicker boundary layers are similar in shape while the one produced by the tunnel boundary layer had quite a different shape. The peak turbulence intensities for all three profiles occur at a height approximately equal to the height of the model and are of about the same magnitude. However, shape distinction between them is still observed. Above $z = 12$ in., the influence of the model diminishes and the turbulence characteristics revert to those representative of the respective boundary layers. Profiles obtained using the second orientation (II) of the model, again at $x_m = 8.75$ in. are given in Figures 73 and 74. In the case of mean velocity profiles, the contrast between the different boundary layers used was not as sharp as it was with orientation I. The turbulence intensity profiles indicate, however, that while the elevation at which the peak of the turbulence intensity occurs is approximately the same as that of the corresponding ones in orientation I the peaks are much wider for orientation II. This can be explained in terms of the thicker shear layer on top of the model present in orientation II. Measure-

ments made on top of the model confirmed this observation (see Figure 97 through 102).

Velocity profiles taken at about 2 model heights downstream, for orientations I and II, are given in Figures 75-78. The mean velocity profiles of Figures 75 and 77 show that for orientations I and II, the profile shapes are quite similar. Comparing the turbulence intensity profiles of Figure 76 with those of Figure 78 reveals an interesting point. Using the tunnel boundary layer, the region of high turbulence for orientation I is confined to a lower z than that for orientation II. For the roughness-generated and counter-jet generated boundary layers, the turbulence intensity profiles for orientation I and II look similar except for some differences in the peak levels.

Transverse Profiles. At different elevations above the tunnel floor the hot-wire probe was traversed across the test section to obtain different transverse profiles of the model wake. Again the model was placed in the center of the test section (y = 24 in.) and both orientations I and II were tested. Velocity profiles at about a quarter of the model height (z = 2 in.) and x_m = 8.75 in. are shown for orientation I in Figures 79 and 80 and for orientation II in Figures 81 and 82. The wakes produced by the tunnel boundary layer for both orientations I and II had much higher velocity gradients at the edge of the wake compared to those produced by the two other boundary layers. This

indicates a large effect on the wake spreading and decay by the turbulence within the boundary layer.

The same may be said for the profiles taken at $z = 4$ in. for both orientations as shown in Figures 82 through 86. While these profiles are not very sensitive to the orientations tested, the ones at the lower elevation, $z = 2$ in., displayed a much more evident sensitivity. However, at $z = 7$ in., which is roughly at the same height as the model, the mean velocity profiles in Figures 87 and 89 look drastically different.

Comparing among the different mean velocity profiles in Figure 87, the wake produced by the tunnel boundary layer has a peak at the center. This peak diminishes in size due to the increased turbulence for the roughness-generated layer and it could not be detected for the even more turbulent counter-jet generated boundary layer. The same peak was not found at $z = 4$ in. as demonstrated by Figures 83 and 84. At a height of 10 inches for both orientation I and II the mean velocity profile could hardly sense the presence of the upstream obstacle (see Figure 91). However, the turbulence intensity profile obtained in the tunnel boundary layer and to a small extent that from the roughness-generated layer could sense the presence of the bluff body through an increase in turbulence level. At about two model heights downstream and an elevation of 4 in. for orientation I, the small mean velocity peak at the

center, which was felt somewhat upstream at z = 7 in., is noted indicating a down draft of some sort (see Figures 83, 87 and 93). It is conjectured that the shear layer generated by the top of the model in that case approaches the ground downstream of the bluff body.

Measurements on Top of Model

Vertical Profiles. Figures 97 through 102 display the effect of the model orientation with respect to the wind direction on the flowfield above the roof of the "building" for the three different boundary layers. All the profiles obtained along the model centerline on top of the roof indicate a large difference with elevation in the velocity gradient and turbulence intensity for the case of a building facing the wind direction with one of its sides (in particular when compared with orientation I). This type of behavior of orientation II is typical of a shear layer which separates along the top front edge of the bluff body. The sensitivity of these profiles to the boundary layers is almost negligible.

Transverse Profiles. From the traverses across the top of the model shown in Figures 103 through 108 for the three boundary layers, it is evident that for orientation II, with one of the sides facing the oncoming velocity stream, large gradients in the mean velocity and turbulence intensity are found using the tunnel boundary layer. With the roughness-generated or the counter-jet generated

boundary layers, the mean velocity gradient and defect are much less. Note the evidence pointing to the presence of two rolled-up vortices for orientation I in all these figures in particular Figures 103 and 104 and the extent by which the vertical gradient and the higher turbulence level of the roughness and counter-jet generated boundary layers inhibit the formation and smear these vortices in Figures 105 through 108. Differences in the profiles resulting from the use of the roughness or counter-jet generated boundary layers were found to be insignificant for both orientations I and II. (Compare Figure 105 to Figure 107 and Figure 106 to Figure 108.)

CHAPTER VI

CONCLUSIONS AND RECOMMENDATIONS

Conclusions

1. As a result of substantial modifications of the wind tunnel with the aid of various turbulence manipulators, the free-stream conditions in the low-speed test section, including the uniformity of the mean velocity distribution and the level of free-stream turbulence, were considerably improved.

2. A study of the counter-jet technique lead to three major modifications of the system as implemented by Gunnarsson[25]. The modifications were: a) an improvement of the design of the counter-jet manifold resulting in a more uniform distribution of the flow among the various jets; b) increased counter-jet velocities; and c) increased effectiveness of the jets by the elimination of the interaction between them and the perforated plate located at the entrance to the test section. As a result of these changes, considerable improvements in the generated boundary layers were achieved.

3. The relatively new counter-jet technique was shown to be suitable for producing thick turbulent boundary layers which may be used to simulate neutral atmospheric surface layers in wind tunnels of moderate length. The technique permits rapid alteration of reproducible boundary layers from outside the tunnel while the experiments are in

progress. It was demonstrated how various mean velocity profiles (which can be represented by a wide range of power law exponents) can be obtained at the same streamwise position using different settings of the counter-jet parameters and different types of artificial surface roughness.

4. The transverse uniformity of the generated turbulent layers was documented. In addition, the similarity between various streamwise locations (sufficiently downstream of the counter-jets) of both mean velocity and turbulence intensity profiles provided some evidence that the boundary layer may be at equilibrium.

5. Selected measurements of the flowfield near a bluff body for two wind directions in three different boundary layers were compared to study the sensitivity of the measured effects to changes in the characteristics of the turbulent layers. While small changes are observed when results obtained in the two thick boundary layers were compared, large differences were noted between these results and those obtained from tests in the thinner "natural" boundary layer of the tunnel. It is in this boundary layer (δ equal to approximately half of the model height) that the effect of the wind direction with respect to the model was most evident. The data consistently demonstrated that the higher turbulence levels within the two thicker boundary layers increased the spreading and

decay rates of the wake of the bluff body.

6. Downstream of the "building model" near ground level higher turbulence intensities were measured for the model orientation with one corner facing the flow compared to the other orientation in which one of the sides was facing the wind direction. For the former orientation, evidence was provided by the data which pointed to the presence of two rolled-up vortices initiating at the leading edges on top of the model. In the thicker boundary layers the higher turbulence level inhibited and smeared these vortices. However, the measurements provided sufficient evidence of their existence and indicated that they tend to approach the ground downstream of the bluff body. In the case of the latter orientation, a behavior typical of a shear layer which separates along the top front edge of the bluff body was documented. Compared to the other one, this orientation was found to be consistently less sensitive to changes of the boundary layers.

7. The influence of the wind direction on the flowfield on top of the bluff body was much stronger than that due to the changes in the boundary layers. Similar sensitivity to model orientation was evident downstream of the model at low elevations.

Recommendations

1. The spectra and scales of the simulated boundary layers and possibly of the flowfields near bluff-body models

should be obtained so that detailed characterization of the turbulence would be available. Results obtained may then be compared with atmospheric data whenever possible.

2. A thorough investigation of the different characteristics of roughnesses (artificial or natural; two- or three-dimensional; random or orderly placed) and their effects on different flows must be carried out. This investigation should be preceded by a comprehensive survey of the literature.

3. A temperature compensation system (similar to the one described in Reference 34) capable of automatic correction of the anemometer output drift due to changes in air temperature inside the wind tunnel should be used for future measurements since temperature compensation of the data records, after collecting them, is very time-consuming and limited in accuracy.

4. Since the optimum distance for the location of the counter-jet generator has been determined, a new one utilizing air inlet at the end(s) can be installed to provide exceptionally uniform velocity distribution from the exit holes. Provisions for changing the counter-jet angle θ rapidly and accurately should be included. If incorporated, an air compressor capable of supplying a large amount of air (> 132 CFM) steadily to the counter-jet manifold could extend the U_j range.

5. The transverse (v) and vertical (w) velocity components in the simulated boundary layers should be measured along with the u component. An estimate of the Reynolds stresses could then be obtained.

6. Windows located near the floor of the test section would provide easier access to the test section and would facilitate flow visualization studies.

7. To expedite and simplify the study of flowfields around bluff-body models, the installation of a turntable, built into the floor of the tunnel, on which the models are placed is highly recommended.

APPENDIX A

MODIFICATION AND EVALUATION OF THE WIND TUNNEL FREE-STREAM

Prior to performing the measurements of generated boundary layers reported in Chapter IV, the low-speed section of the I.I.T. Environmental Wind Tunnel was extensively modified to provide better free-stream conditions. One of the conclusions of the investigation conducted by Gunnarsson[25] is that transverse uniformity of the generated boundary layers was difficult to achieve. Different barriers[25] were therefore used under various flow conditions to reduce the transverse non-uniformities. Based on the work reported in Reference 30 and other experiences in suppression of turbulence and secondary flows at I.I.T., several modifications involving the use of additional flow manipulators were implemented in the wind tunnel during the summer of 1973.

The tunnel sections between stations II and VII (for relative positions see Figure 3) were removed to gain easy access and then replaced in position after the following changes were incorporated. Honeycombs consisting of 8.25 in. long, 0.125 in. diameter plastic drinking straws (approximately 70,000) were hand-packed into the tunnel section between stations II and III. The perforated plate, P.P. #3, previously installed in station II was retained. Detailed information including the pressure drop, solidity, hole size and arrangement of the perforated plate, and the

performance of it under different flow conditions can be found in References 29 and 30. The plate served to cut down large eddies, and the honeycomb suppressed any swirls or secondary flows initiating from the tunnel fan and the right-angle turn just downstream of it. A 30 mesh per inch stainless steel screen (0.0065 in. wire diameter and 0.352 solidity) was placed immediately downstream of the honeycomb (plastic drinking straws) to reduce the turbulence level and also to support the straws, since they were only held together by friction.

Two type P.P. #3 perforated plates were installed at stations IV and V in the diffuser providing the necessary back pressure to prevent stall[31] due to the large diffusion angle (17.5°). To aid in uniformizing the flow entering the large test section another P.P. #3 was installed at station VI. The plates at station V and VI were originally installed by Gunnarsson[25]. As discussed in Chapter II, extreme care was taken this time to ensure that the perforated plates were tightly held in place.

The conditions in the test section prior to the present modifications were carefully determined by Gunnarsson[25]. Two of his surveys are reproduced here in Figures 109 and 110 for the purpose of comparison. The free-stream conditions were actually worse than indicated in these two figures. In particular, Gunnarsson's boundary layer profiles appeared to be influenced by swirling or secondary flows.

After completion of the modifications, mean velocity measurements were made at various locations of the test section. Contours of mean velocity obtained between stations IX and X just upstream of the plexiglas windows are shown in Figures 111 and 112 for two different air speeds. The free-stream turbulence level (for the section between stations IX and XII) of 4% prior to the present modifications was reduced to less than 1.5% over the range of free-stream velocities shown in Figure 113. Figures 28 to 31 indicate that the free-stream mean velocities are within ±5% of the average value.

Additional pressure drops from the added flow manipulators reduced the maximum velocity of the wind tunnel by a factor of two (from 200 ft/sec to 100 ft/sec in the high-speed test section and from 50 ft/sec to 25 ft/sec in the low-speed test section). The increased flow resistance led to a faster rate of increase in the air temperature inside the tunnel when operated at high speeds. Air temperature inside the wind tunnel can and usually does exceed 100°F (70°F ambient) in a couple of hours. Before performing hot-wire calibrations the tunnel was operated at the desired speed for 2-3 hours until the equilibrium temperature was approached. Temperature corrections[34] were sometimes performed after the data were collected.

APPENDIX B

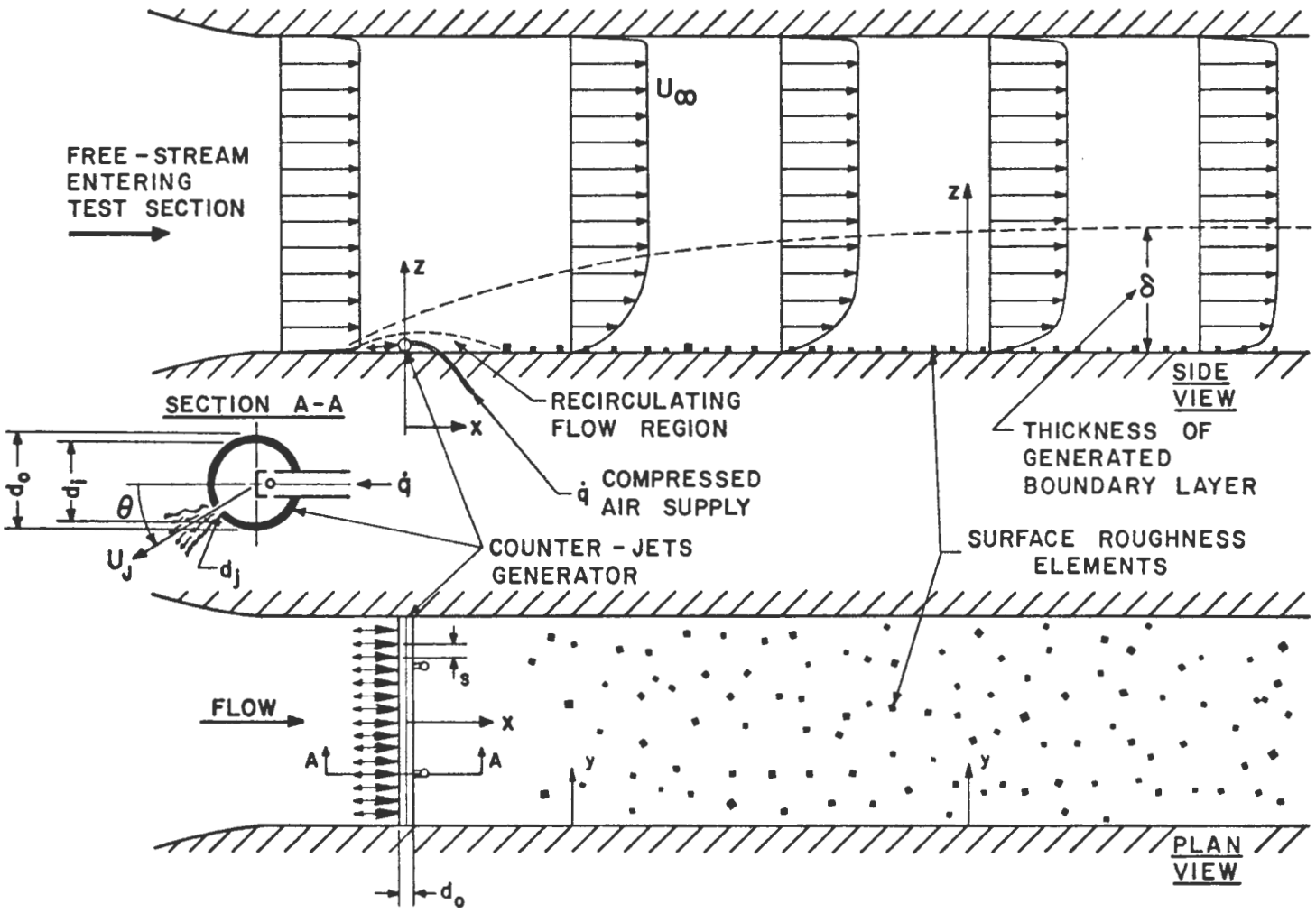

Figure 1. Schematic Representation of Counter-Jet Technique Used for Modeling of Atmospheric Surface Layers

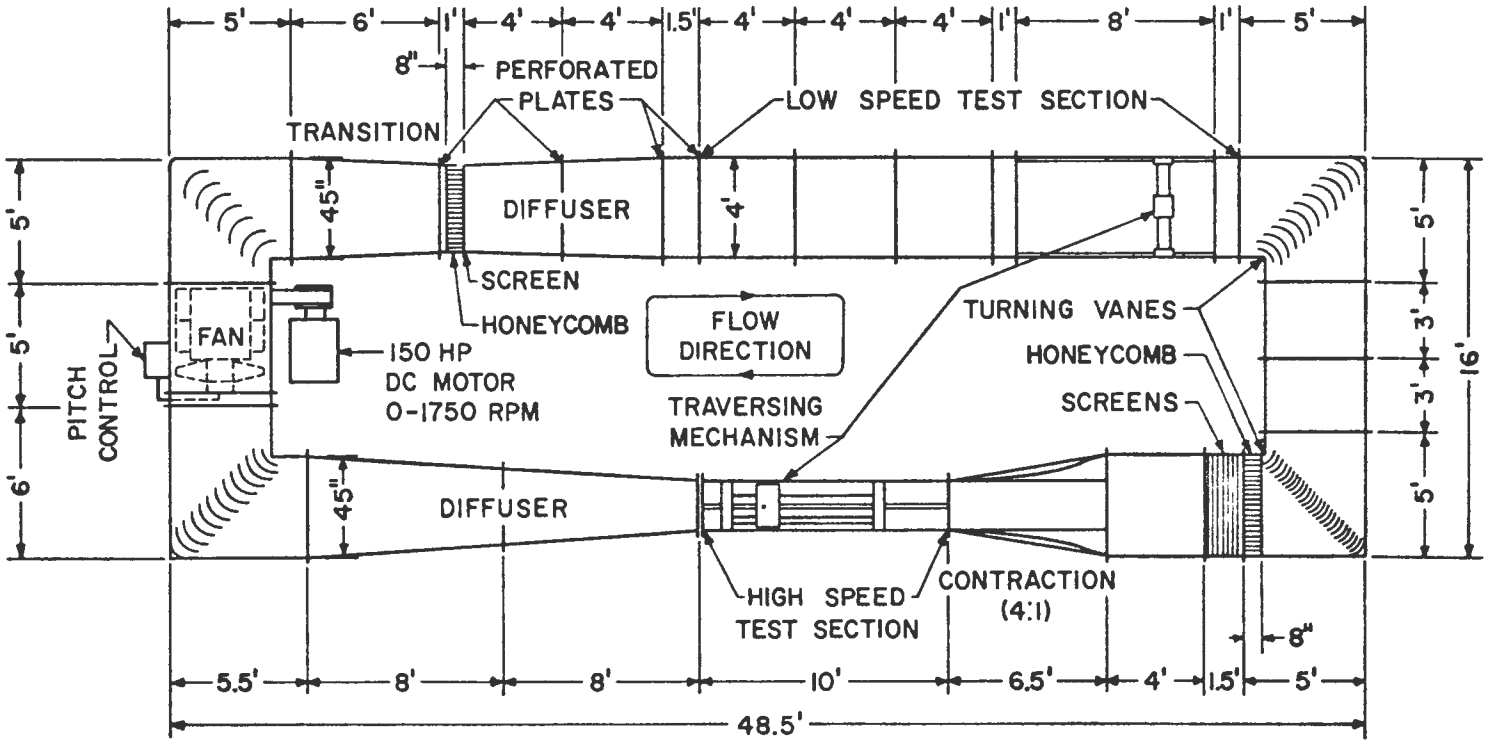

ILLINOIS INSTITUTE OF TECHNOLOGY
ENVIRONMENTAL WIND TUNNEL
PLAN VIEW – 1/6"=1'

HIGH SPEED TEST SECTION – 2'x 3'x 10' ; MAXIMUM VELOCITY = 100 FT/SEC
LOW SPEED TEST SECTION – 4'x 6'x 22' ; MAXIMUM VELOCITY = 25 FT/SEC
FLOW – CLOCKWISE ; CONTRACTION – 4:1 ; MAXIMUM POWER = 150 HP

Figure 2. Schematic of the I.I.T. Environmental Wind Tunnel

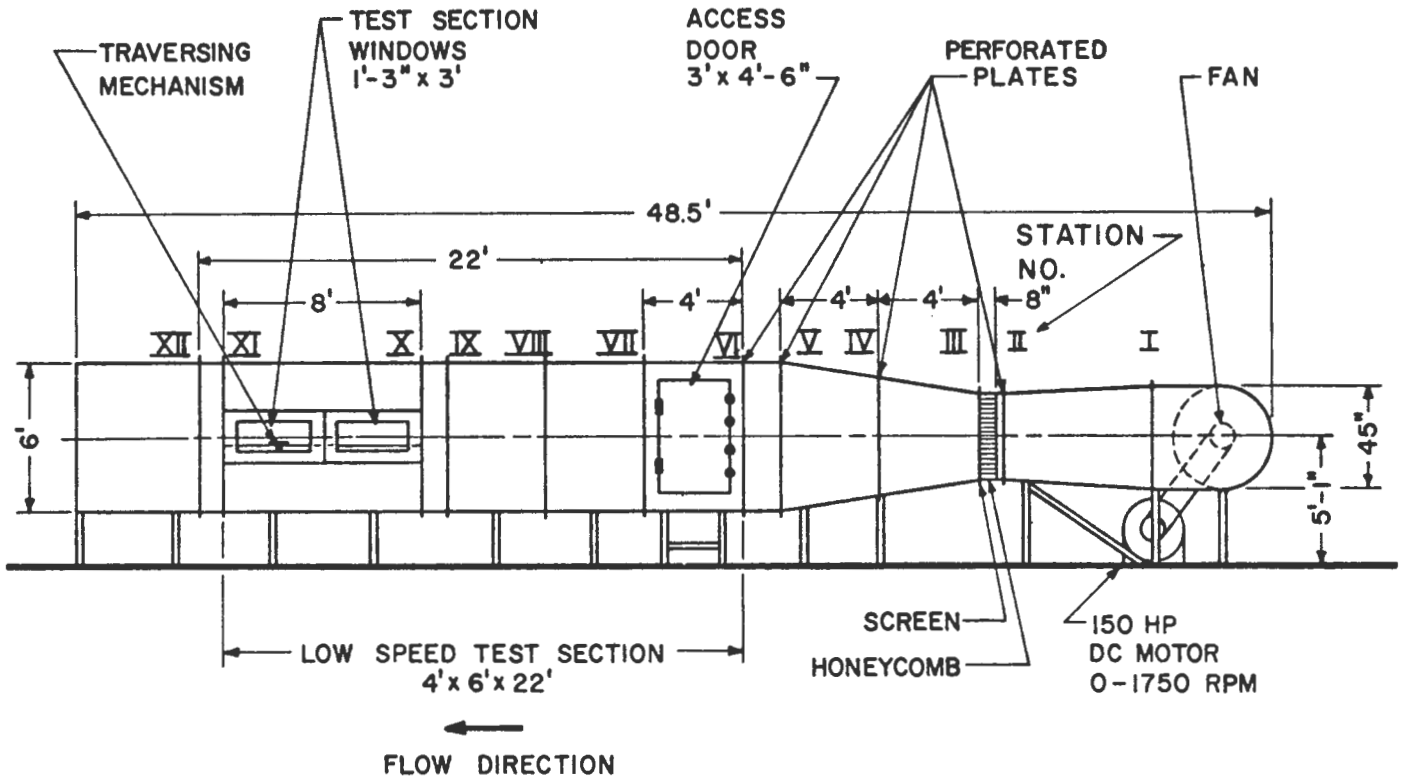

ILLINOIS INSTITUTE OF TECHNOLOGY
ENVIRONMENTAL WIND TUNNEL
SIDE VIEW — LOW SPEED TEST SECTION
1/6" = 1'

Figure 3. Side View of Low-Speed Test Section of the I.I.T. Environmental Wind Tunnel With Labeled Station Numbers

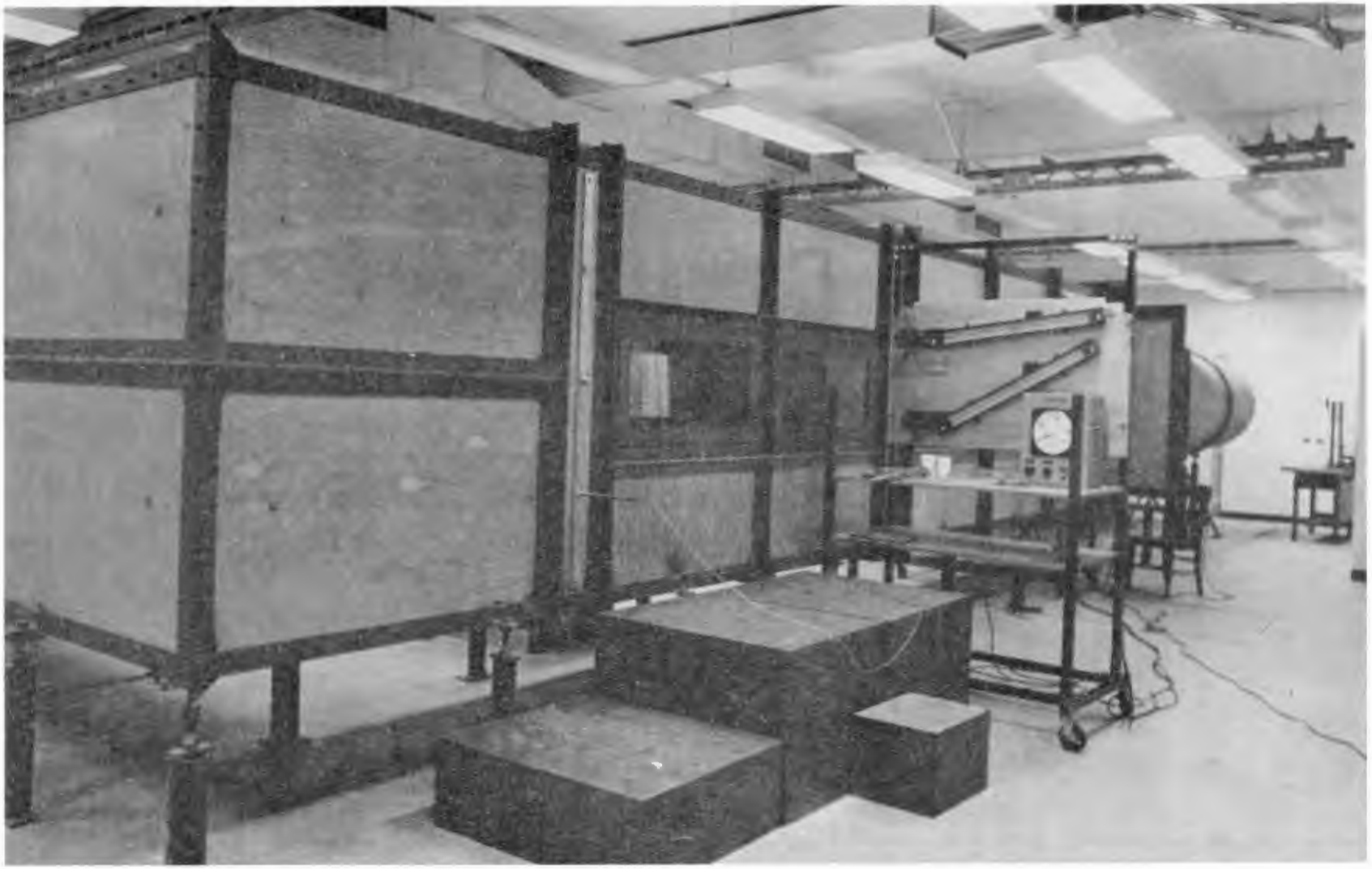

Figure 4. Low-Speed Test Section of the I.I.T. Environmental Wind Tunnel

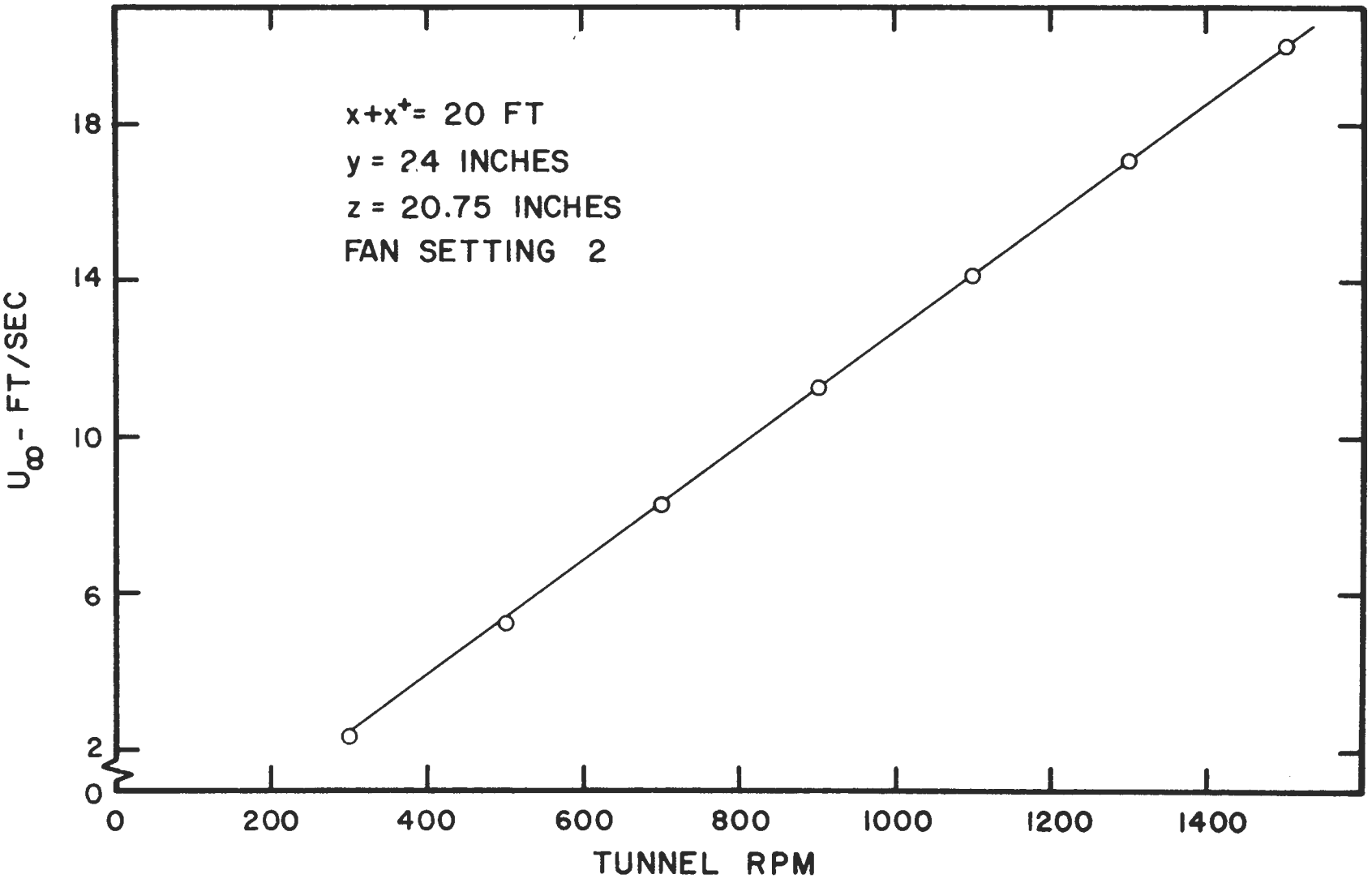

Figure 5. Calibration Curve of Free-Stream Velocity in Low-Speed Test Section of the I.I.T. Environmental Wind Tunnel

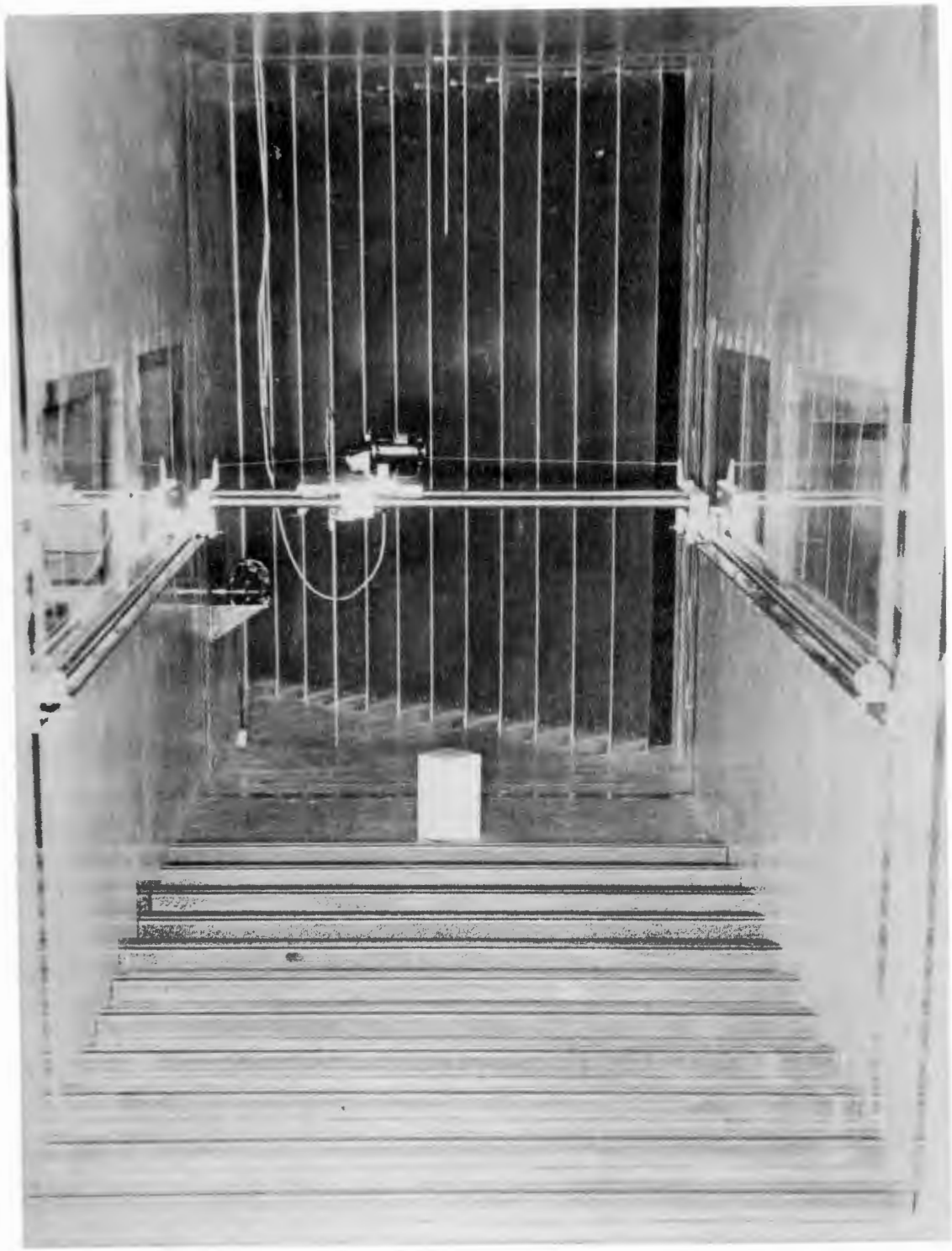

Figure 6. View of Low-Speed Test Section Looking Downstream with Traversing Mechanism, Model and Surface Roughness in Position

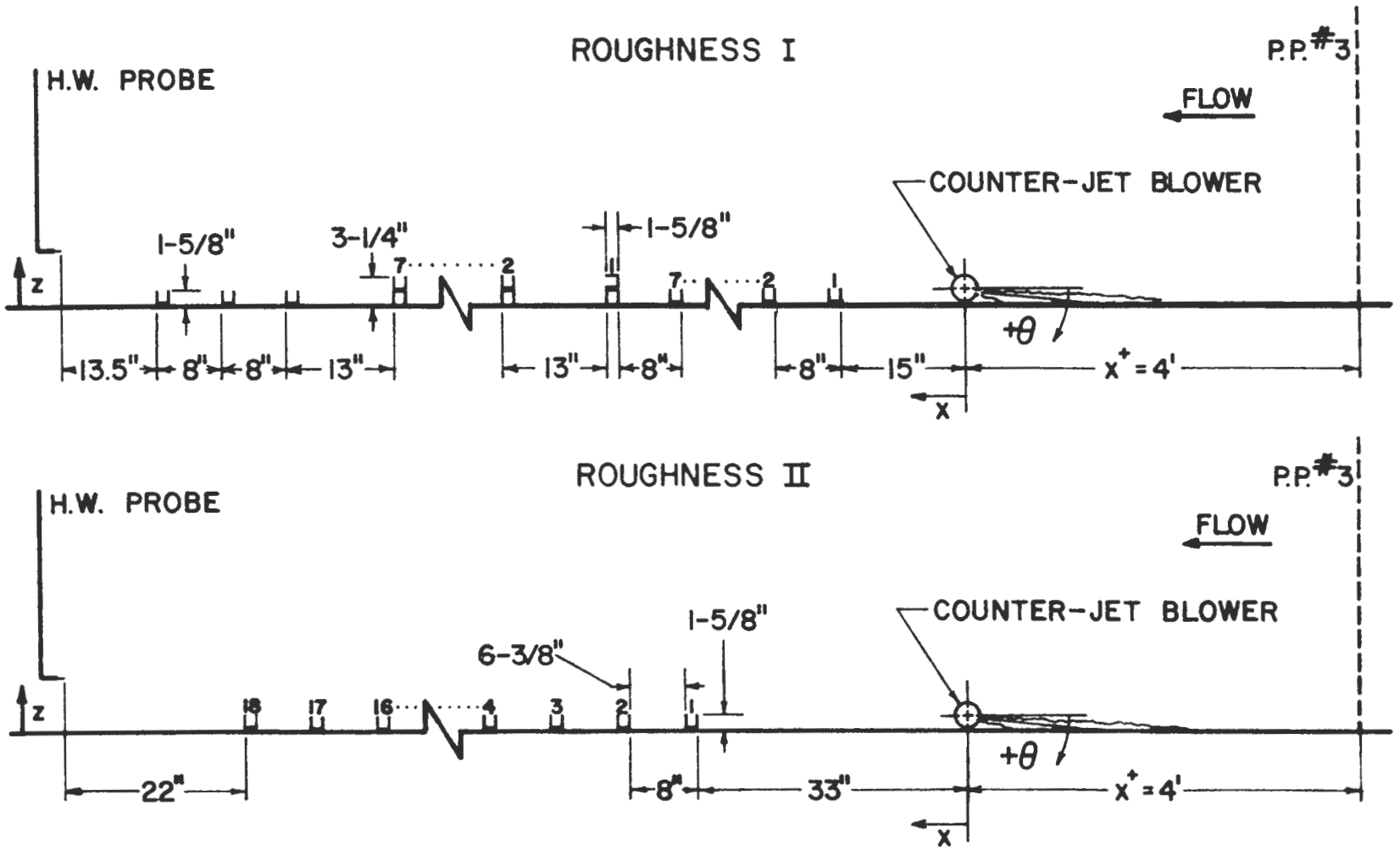

Figure 7. Schematic Representation of Surface Roughnesses Used

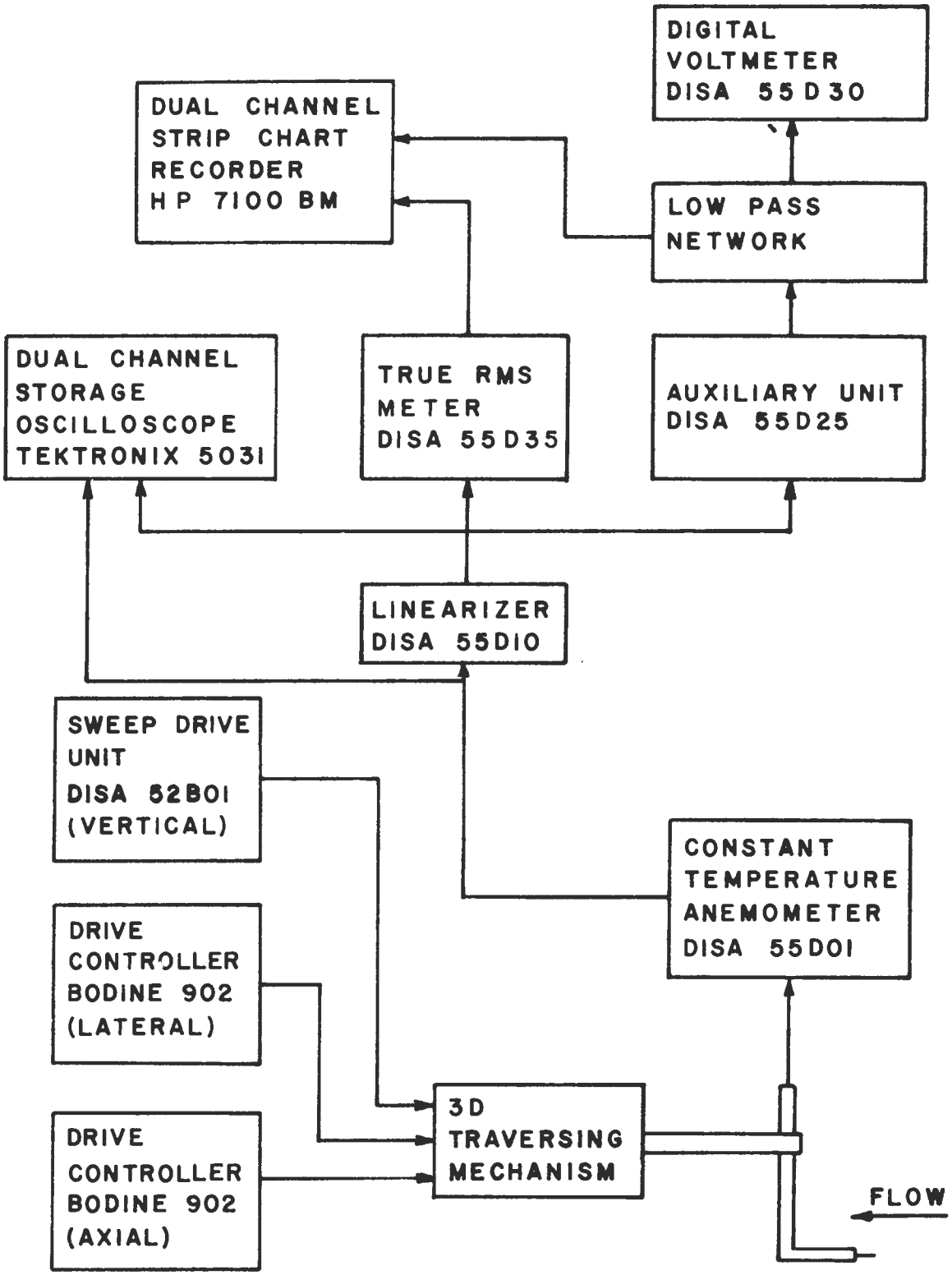

Figure 8. Instrumentation Schematic

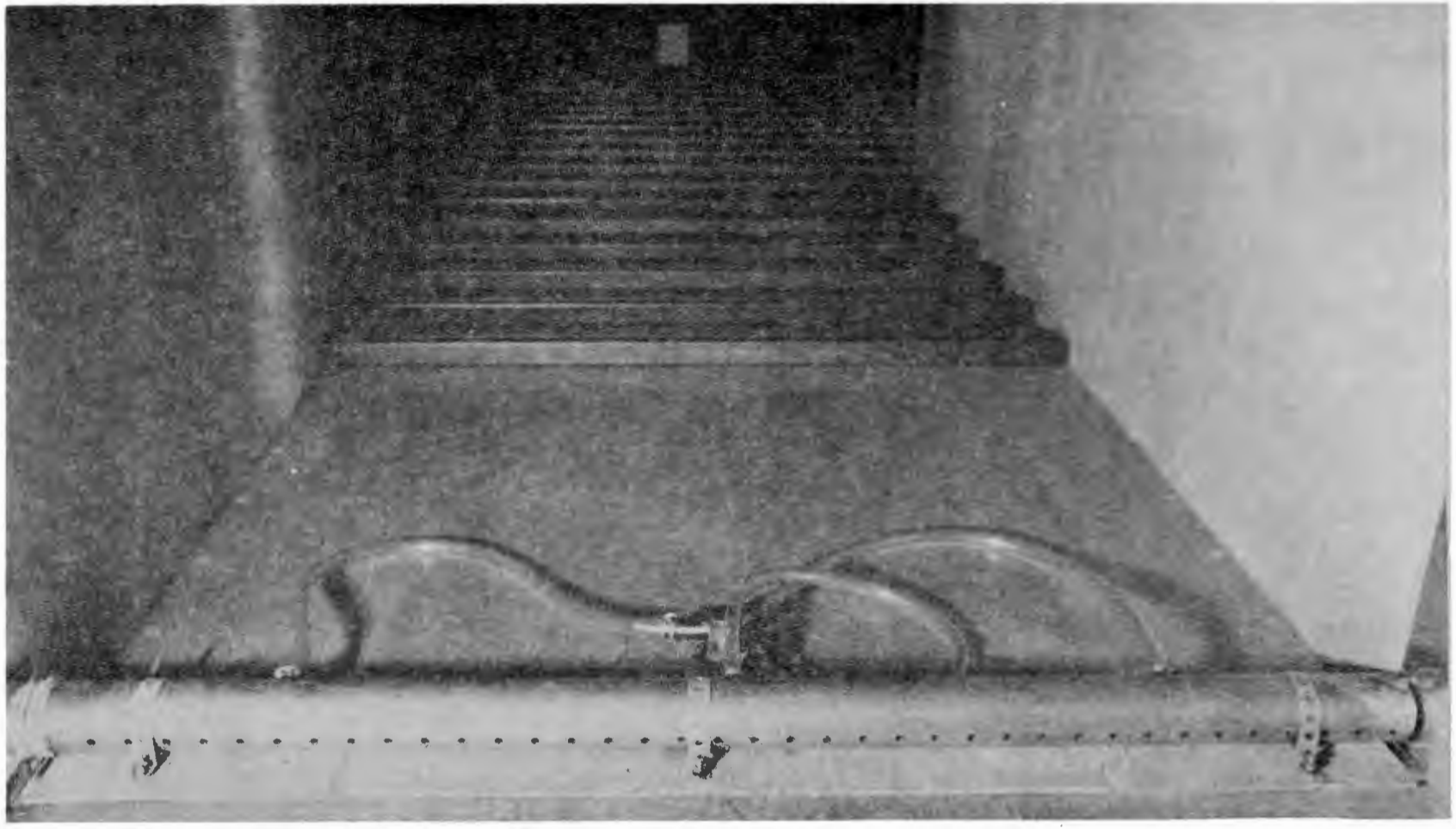

Figure 9. Counter-Jet Generator in Position on Floor of Low-Speed Test Section

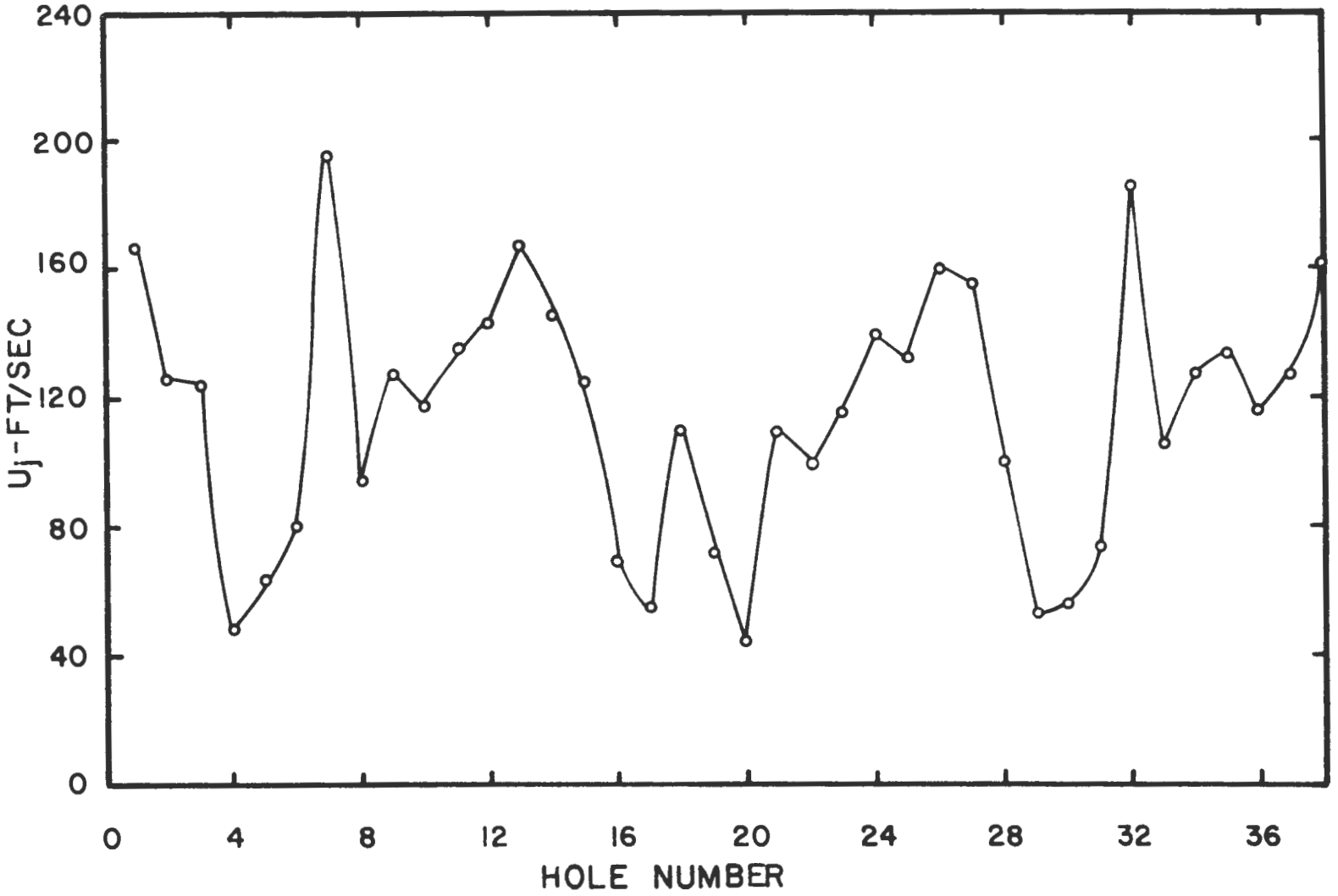

Figure 10. Initial Velocity Distribution Out of Counter-Jet Generator

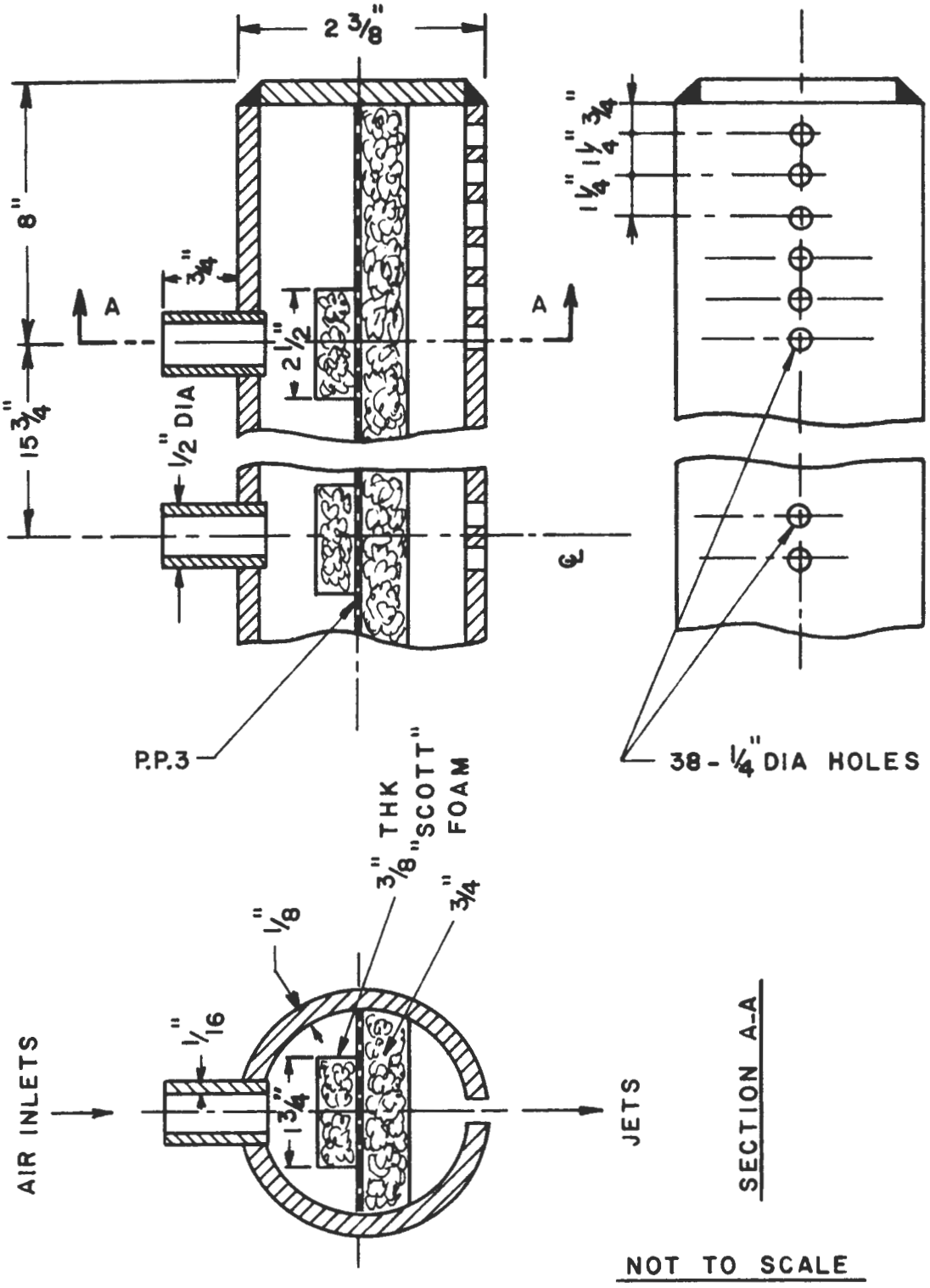

Figure 11. Schematic of Modified Counter-Jet Generator

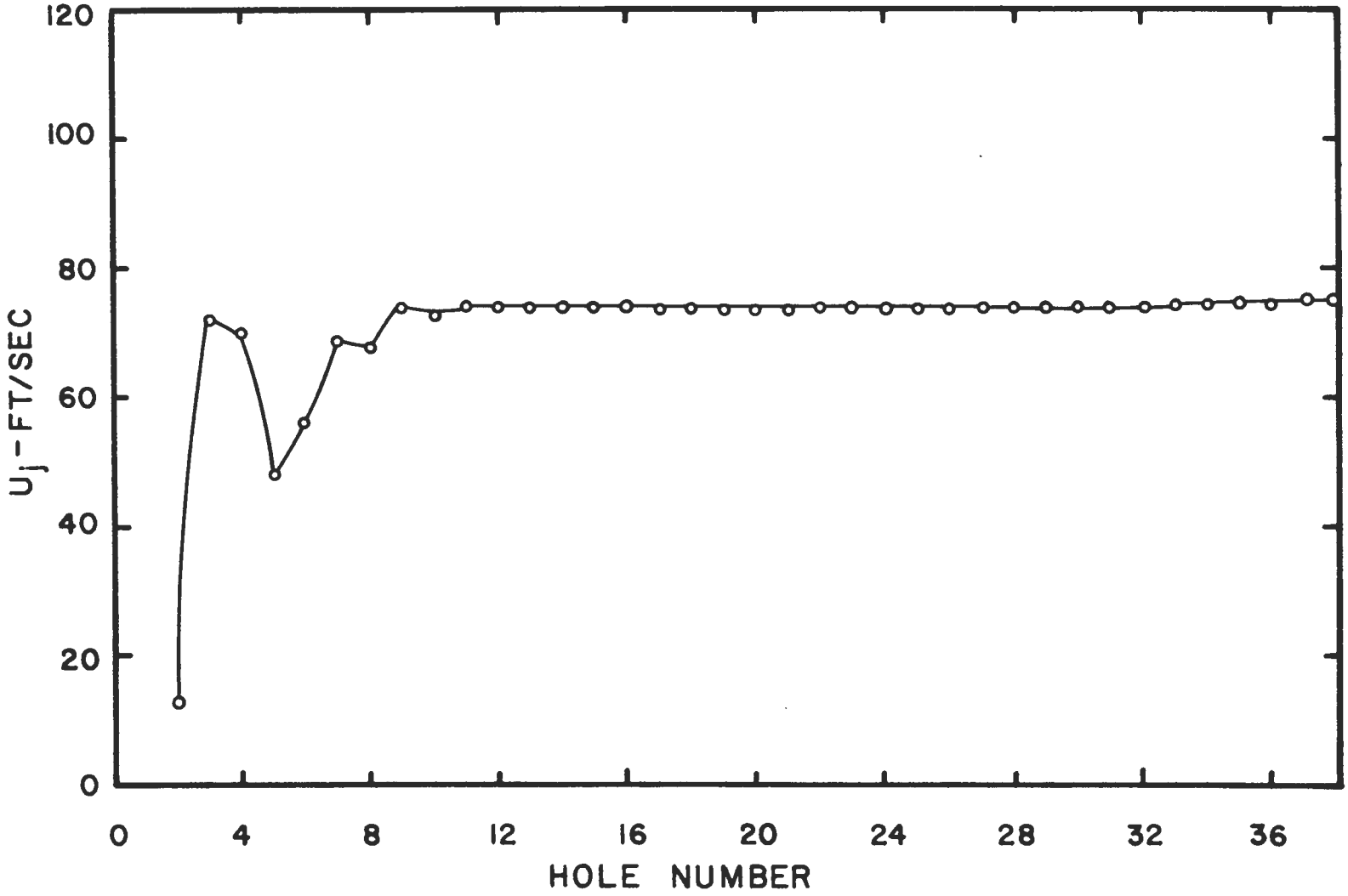

Figure 12. Velocity Distribution Out of Counter-Jet Generator Utilizing End Air Inlet

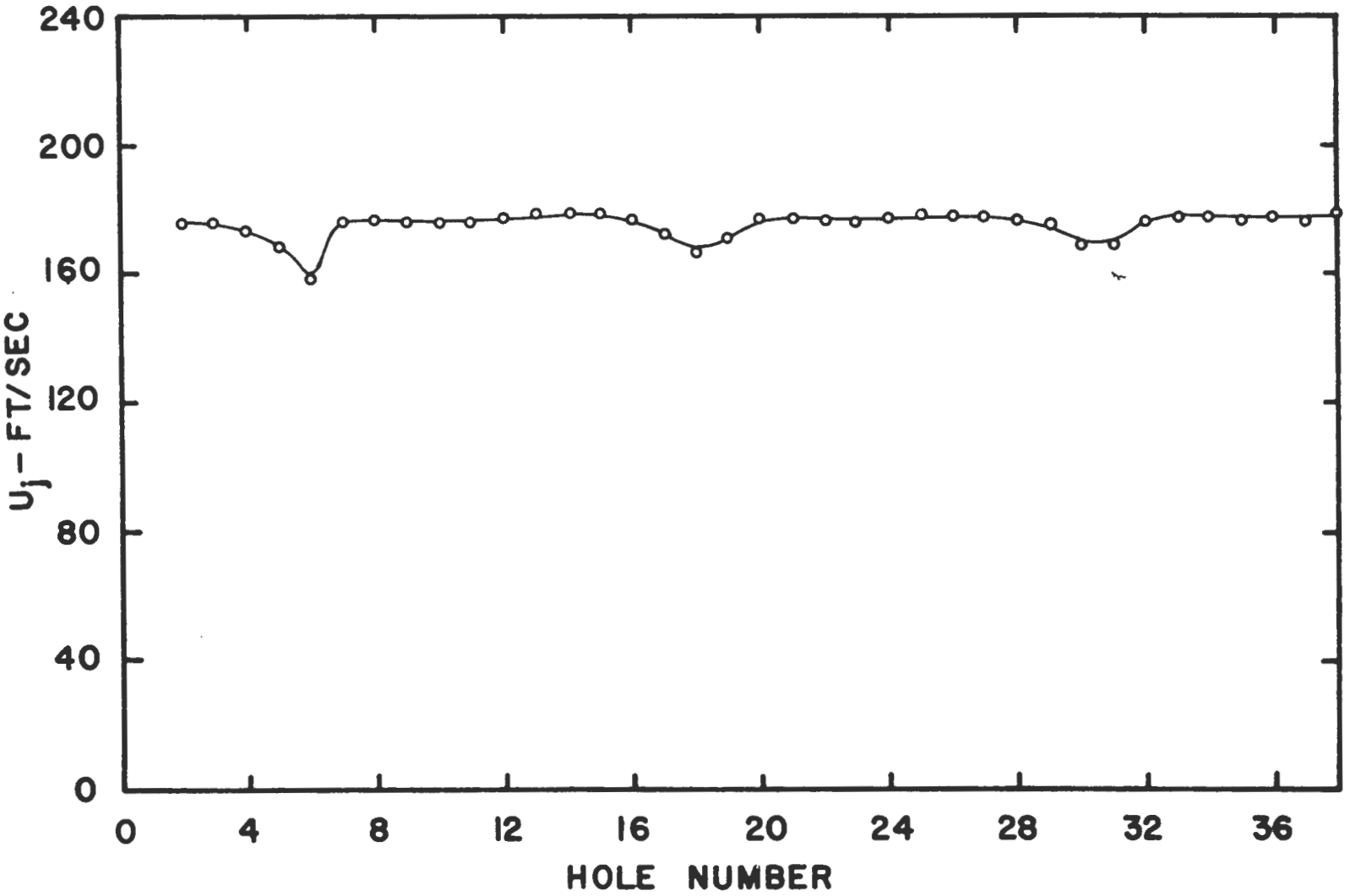

Figure 13. Velocity Distribution Out of Modified Counter-Jet Generator

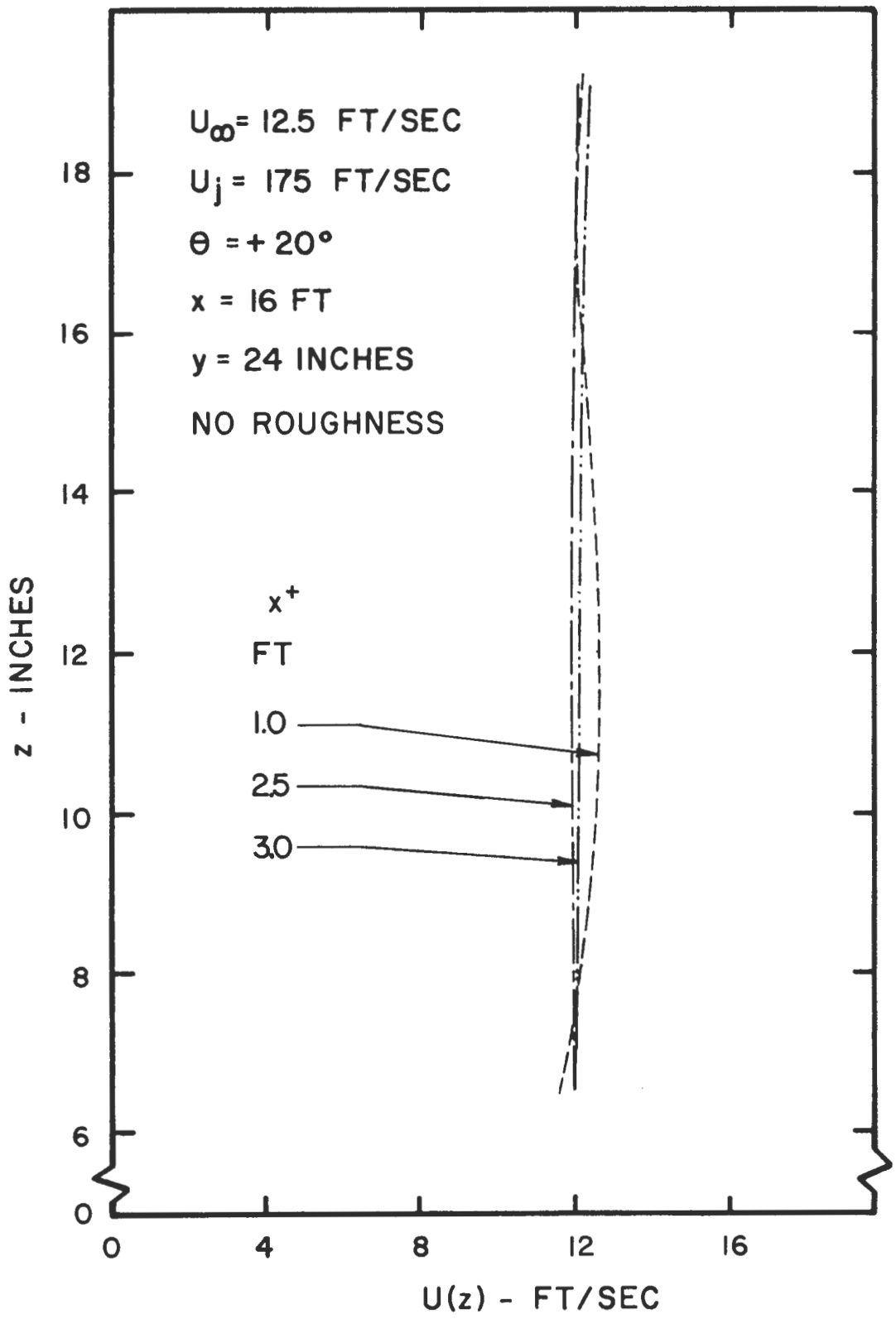

Figure 14. Effect of Position of Counter-Jet Generator With Respect to P.P. #3 on Boundary Layer Mean Velocity Distribution for $\theta = +20°$

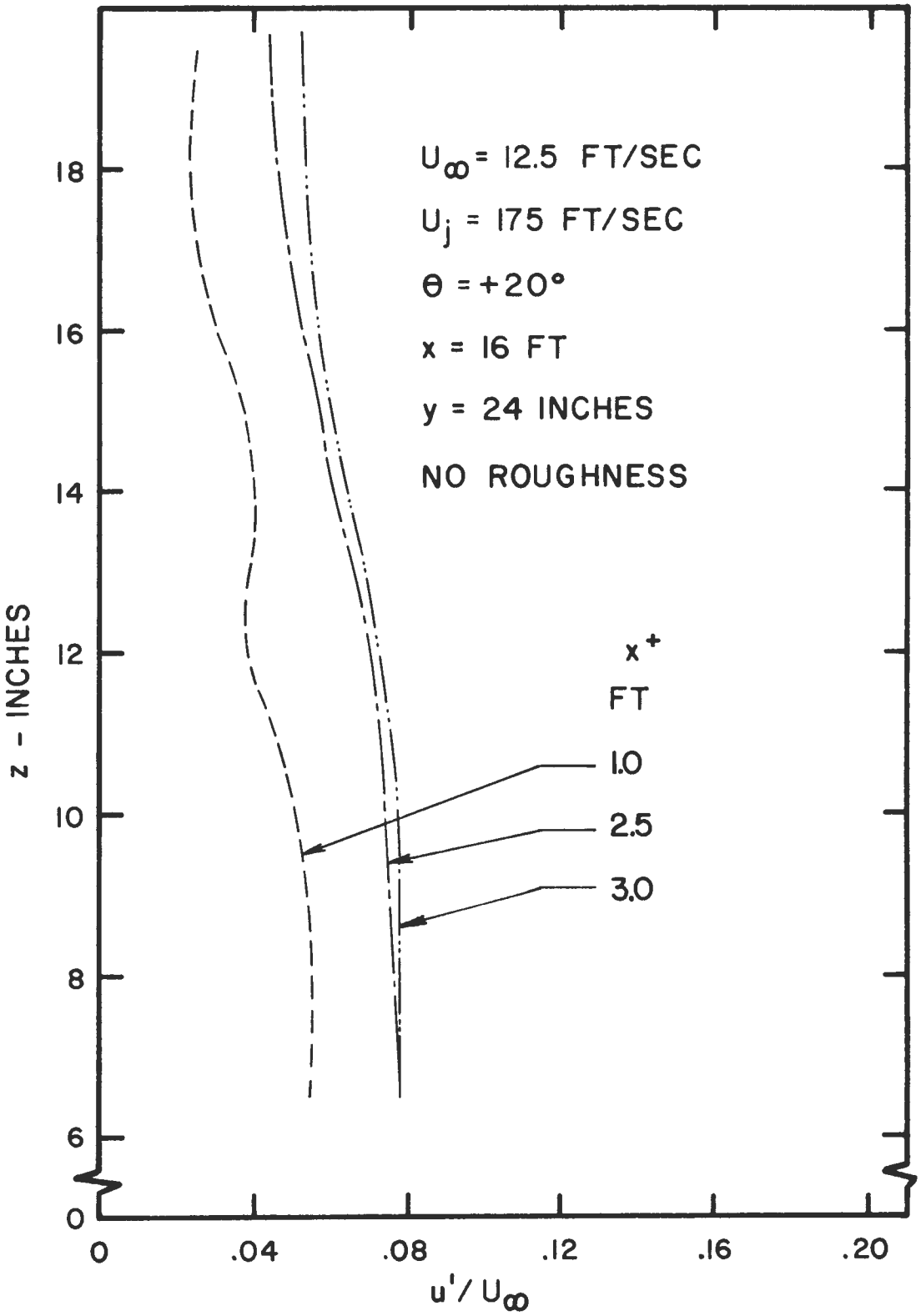

Figure 15. Effect of Position of Counter-Jet Generator With Respect to P.P. #3 on Boundary Layer Turbulence Intensity Distribution for $\theta = +20°$

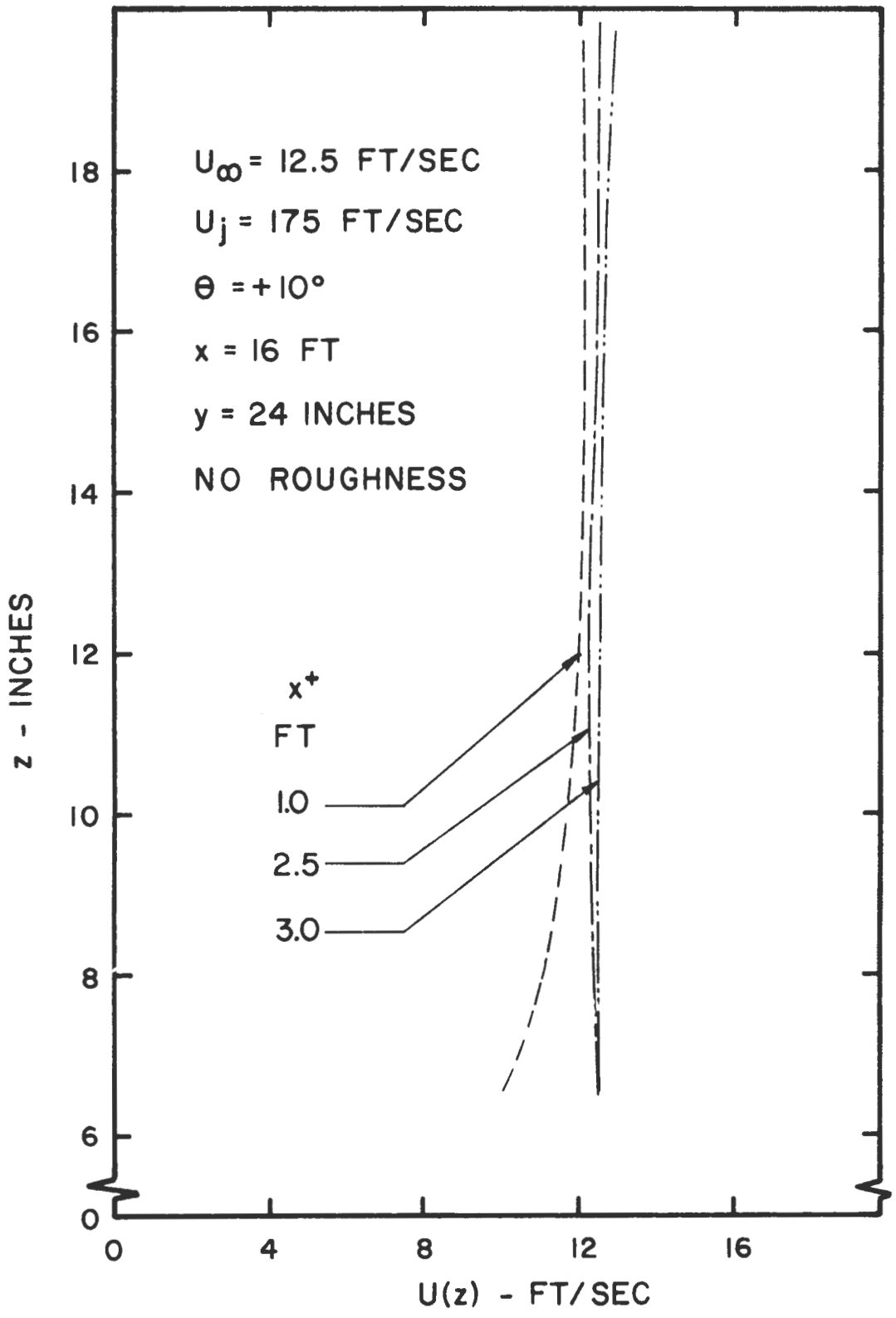

Figure 16. Effect of Position of Counter-Jet Generator With Respect to P.P. #3 on Boundary Layer Mean Velocity Distribution for $\theta = +10°$

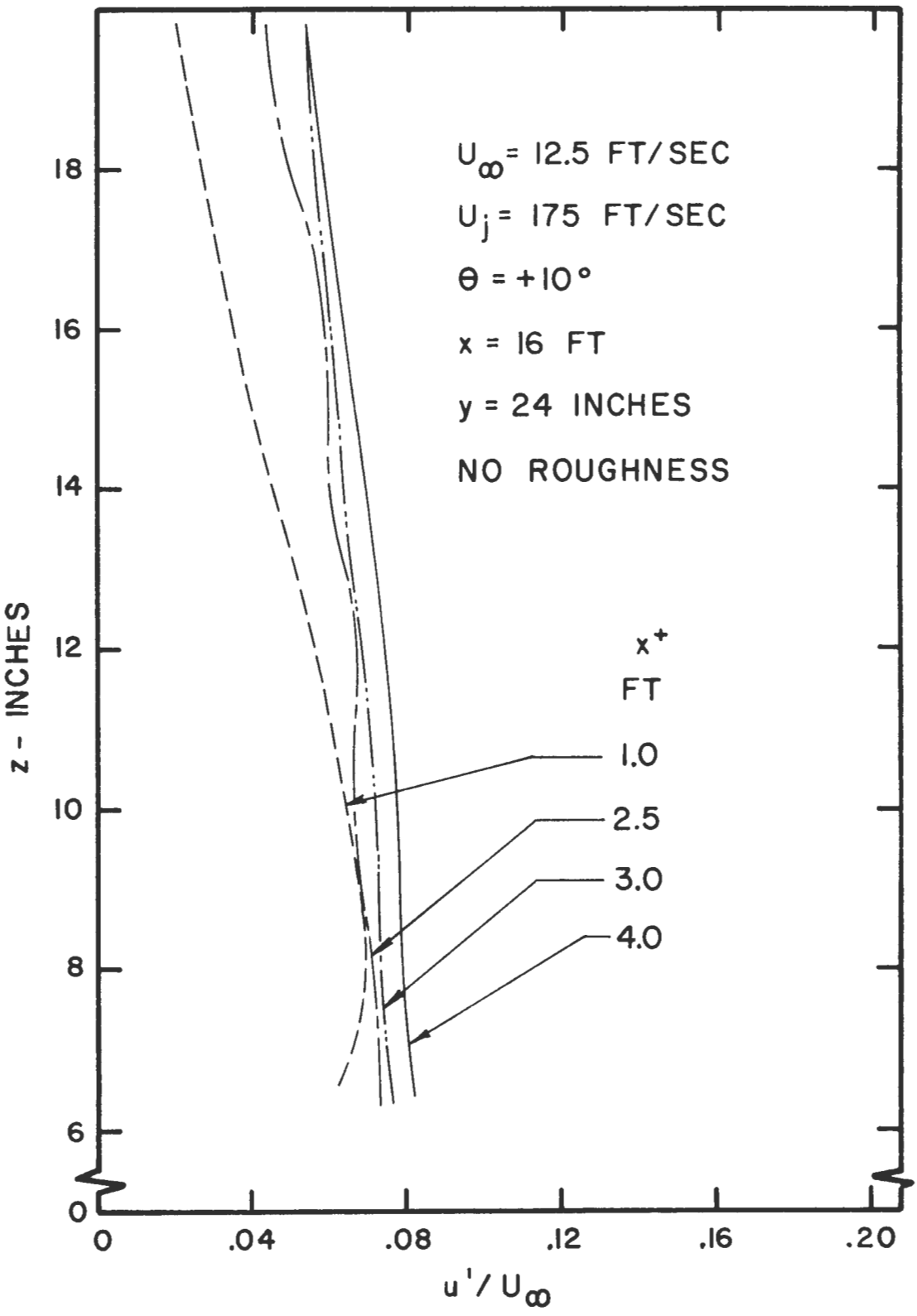

Figure 17. Effect of Position of Counter-Jet Generator With Respect to P.P. #3 on Boundary Layer Turbulence Intensity Distribution for $\theta = +10°$

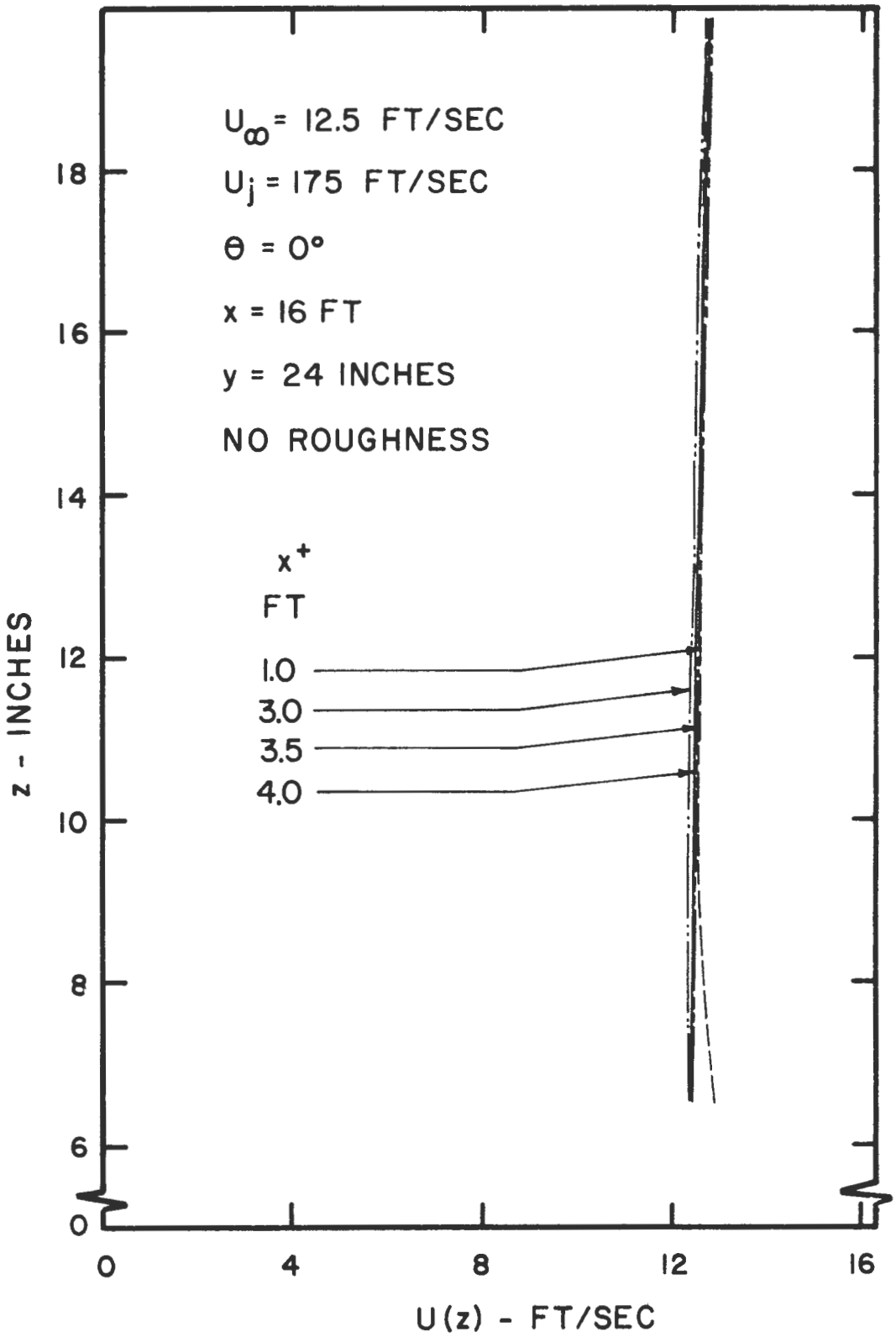

Figure 18. Effect of Position of Counter-Jet Generator With Respect to P.P. #3 on Boundary Layer Mean Velocity Distribution for $\theta = 0°$

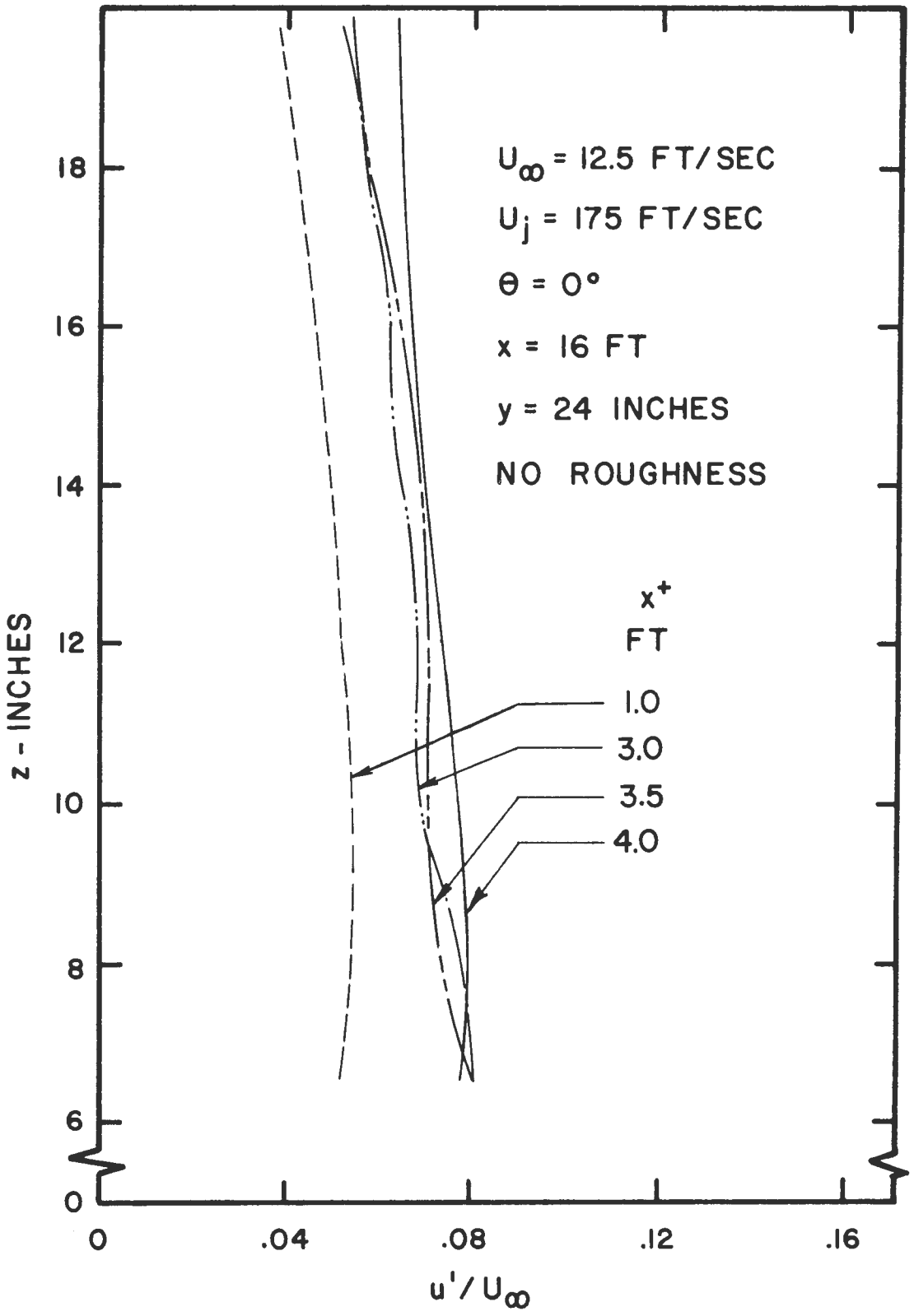

Figure 19. Effect of Position of Counter-Jet Generator With Respect to P.P. #3 on Boundary Layer Turbulence Intensity Distribution for $\theta = 0°$

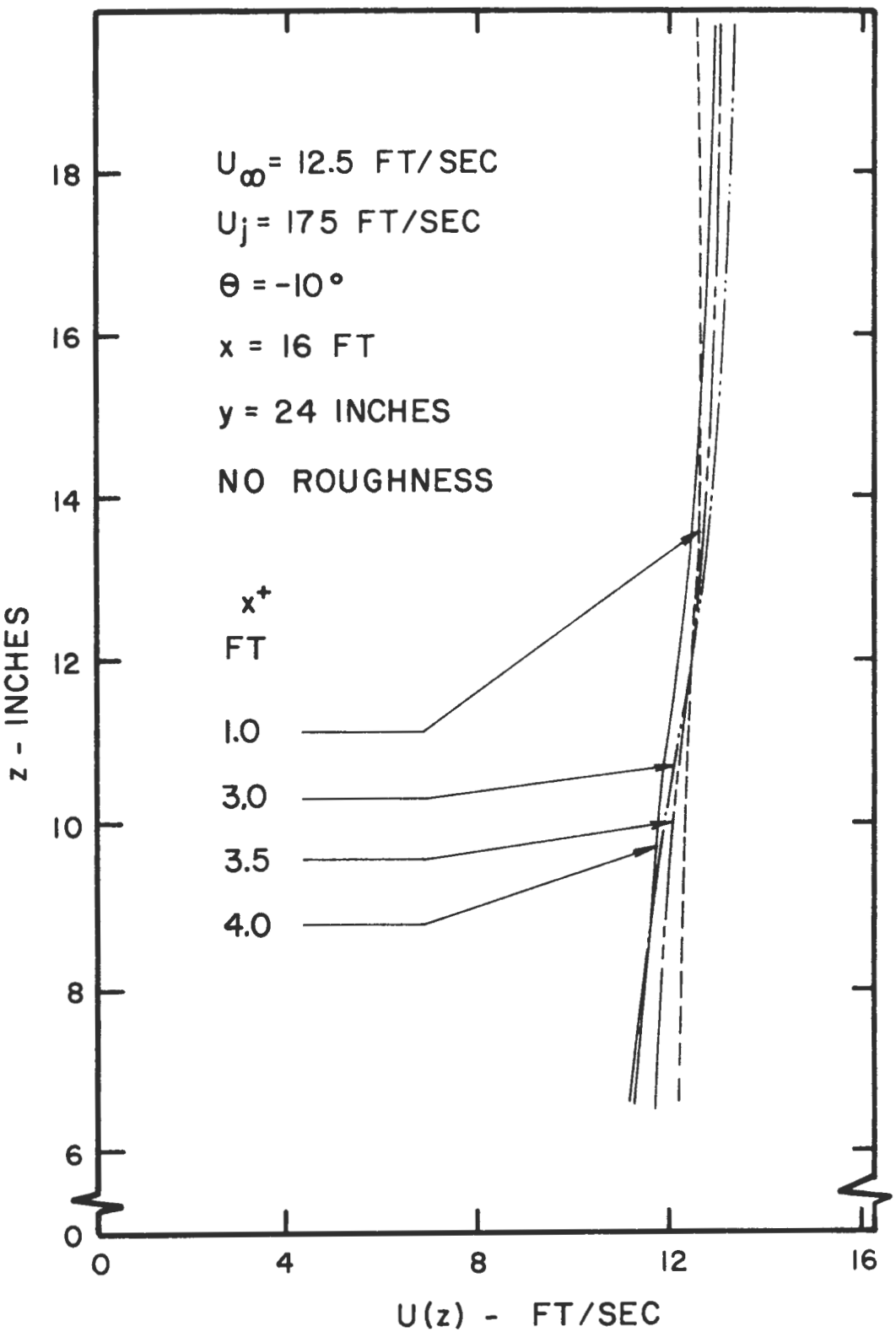

Figure 20. Effect of Position of Counter-Jet Generator With Respect to P.P. #3 on Boundary Layer Mean Velocity Distribution for $\theta = -10°$

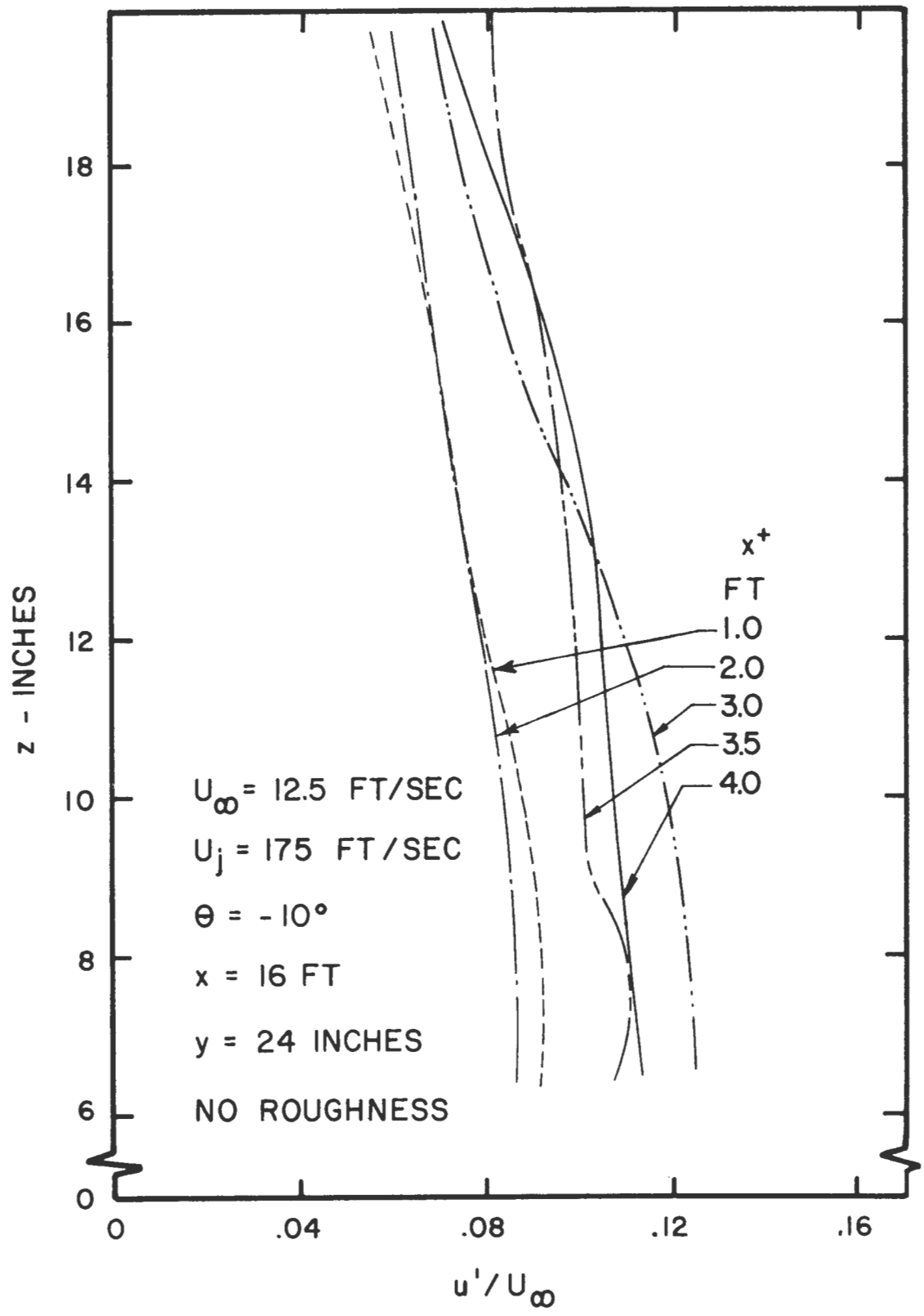

Figure 21. Effect of Position of Counter-Jet Generator With Respect to P.P. #3 on Boundary Layer Turbulence Intensity Distribution for $\theta = -10°$

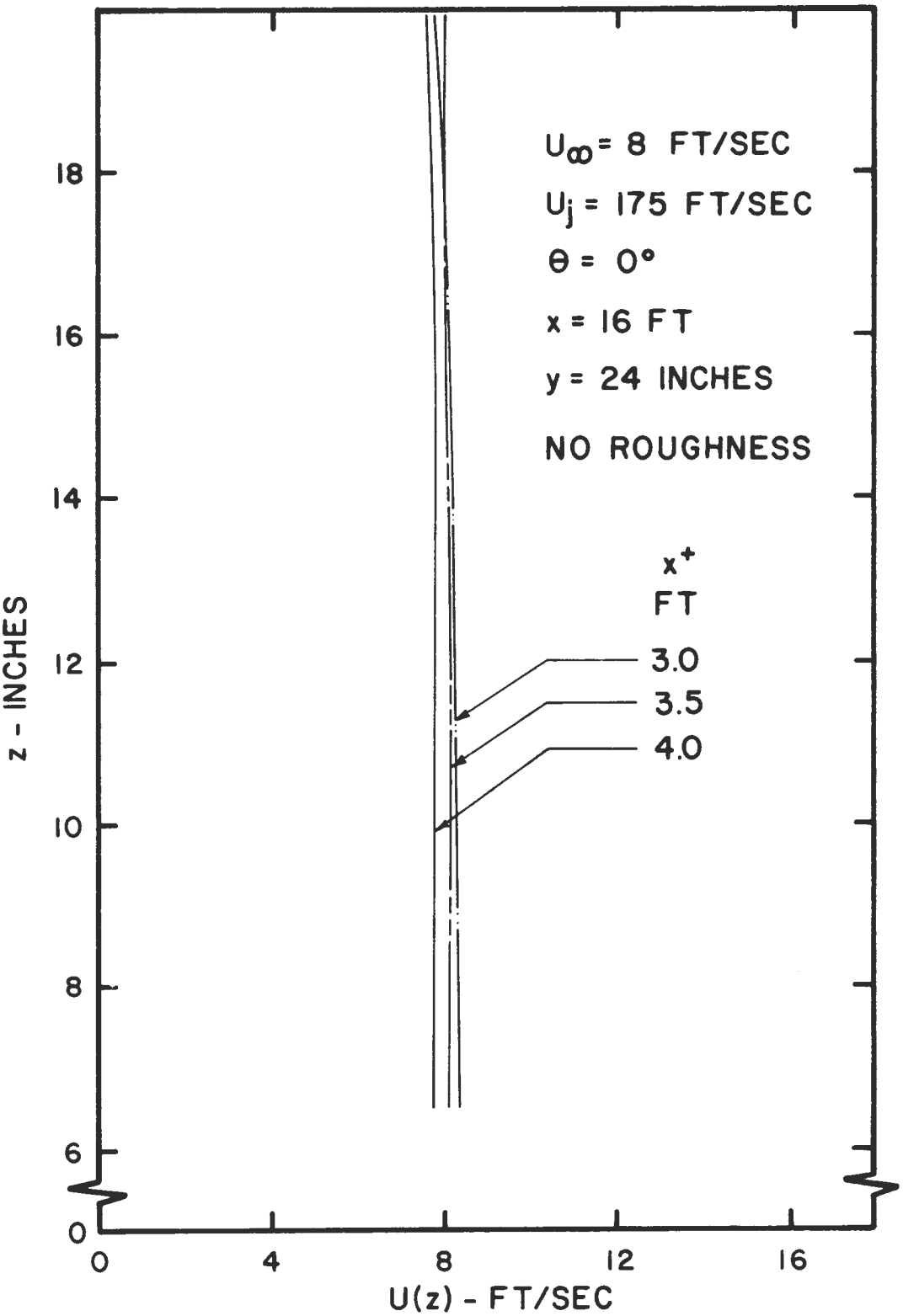

Figure 22. Effect of Position of Counter-Jet Generator With Respect to P.P. #3 on Boundary Layer Mean Velocity Distribution for $\theta = 0°$ at Low Free-Stream Velocity

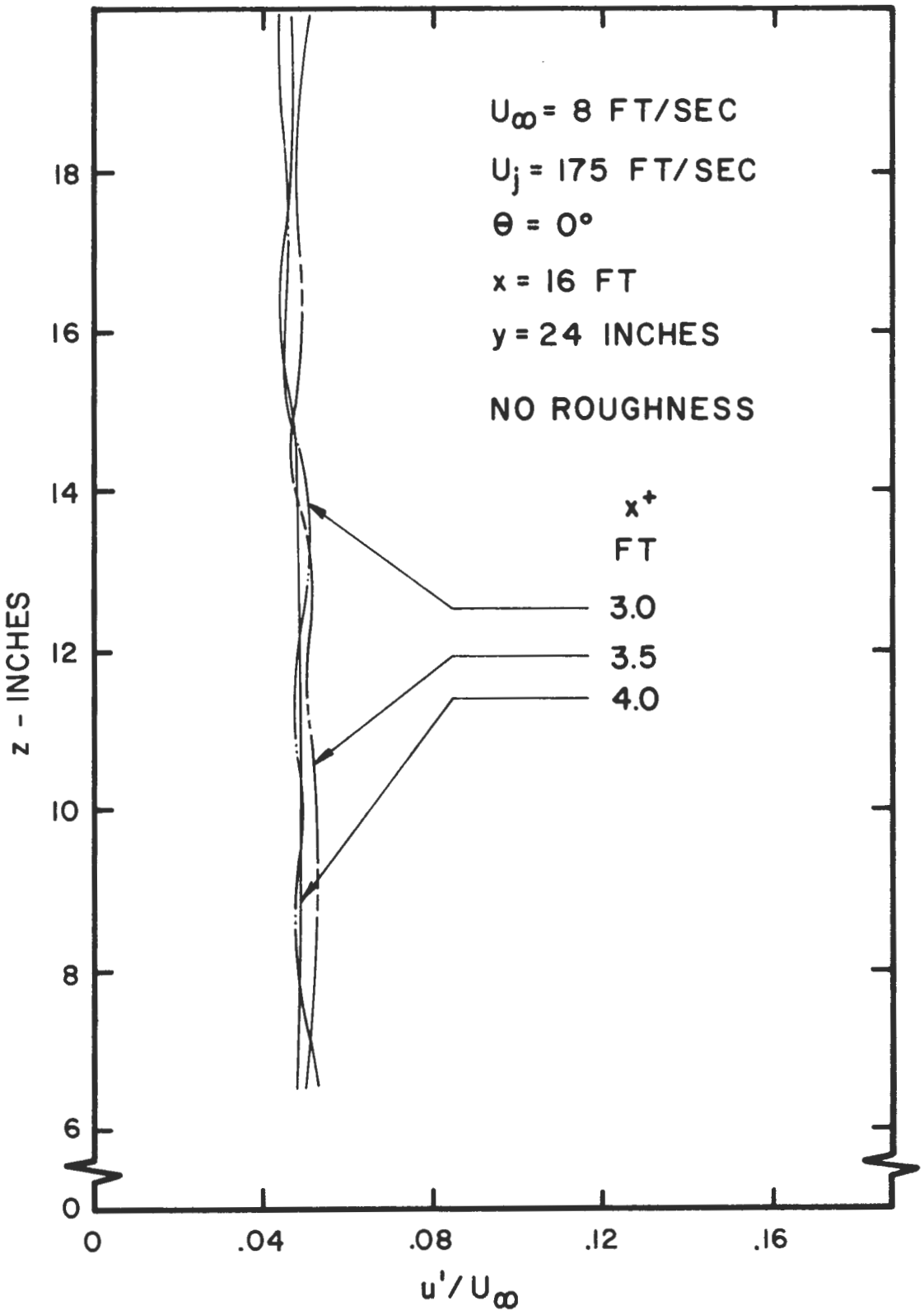

Figure 23. Effect of Position of Counter-Jet Generator With Respect to P.P. #3 on Boundary Layer Turbulence Intensity Distribution for $\theta = 0°$ at Low Free-Stream Velocity

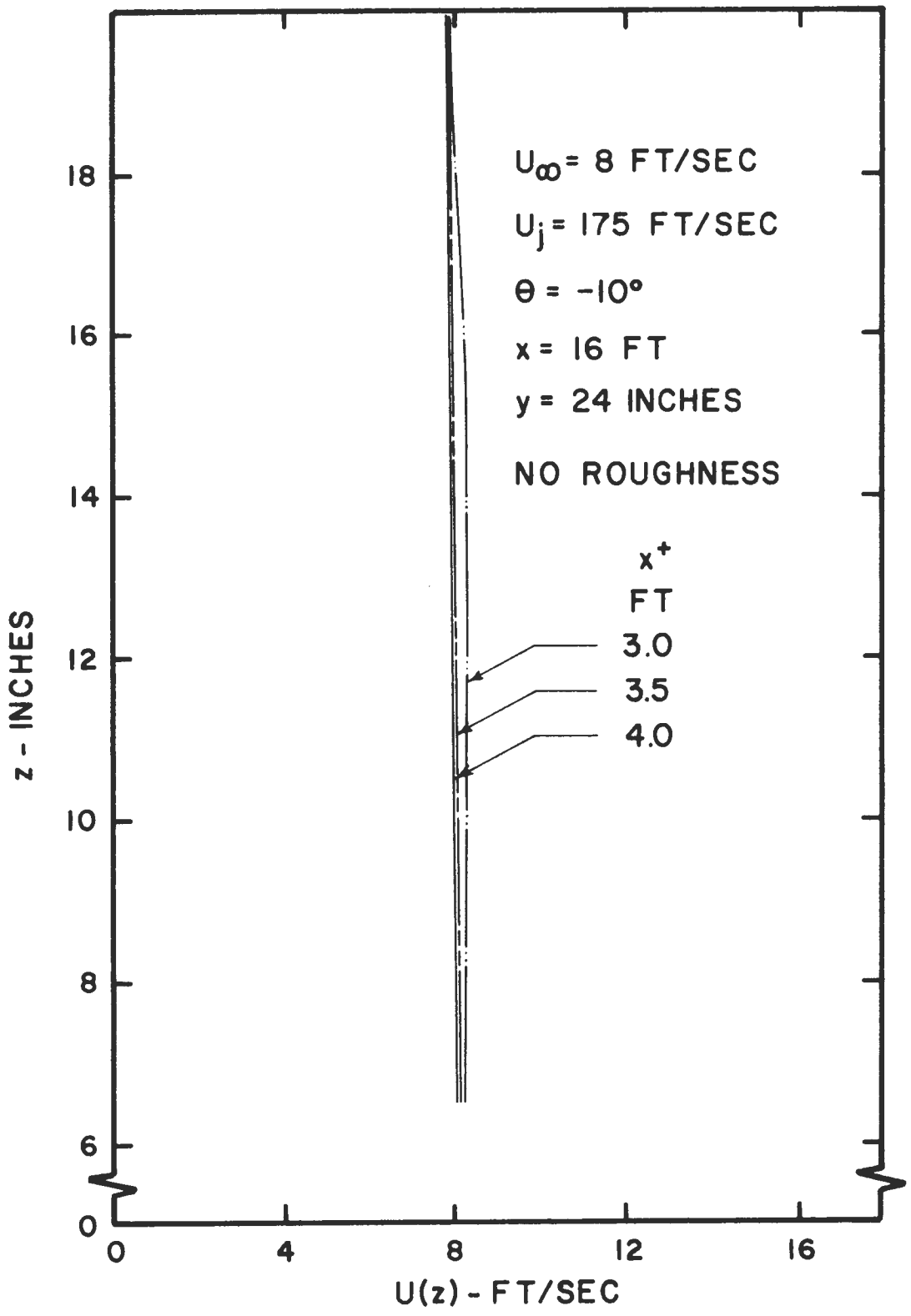

Figure 24. Effect of Position of Counter-Jet Generator With Respect to P.P. #3 on Boundary Layer Mean Velocity Distribution for $\theta = -10°$ at Low Free-Stream Velocity

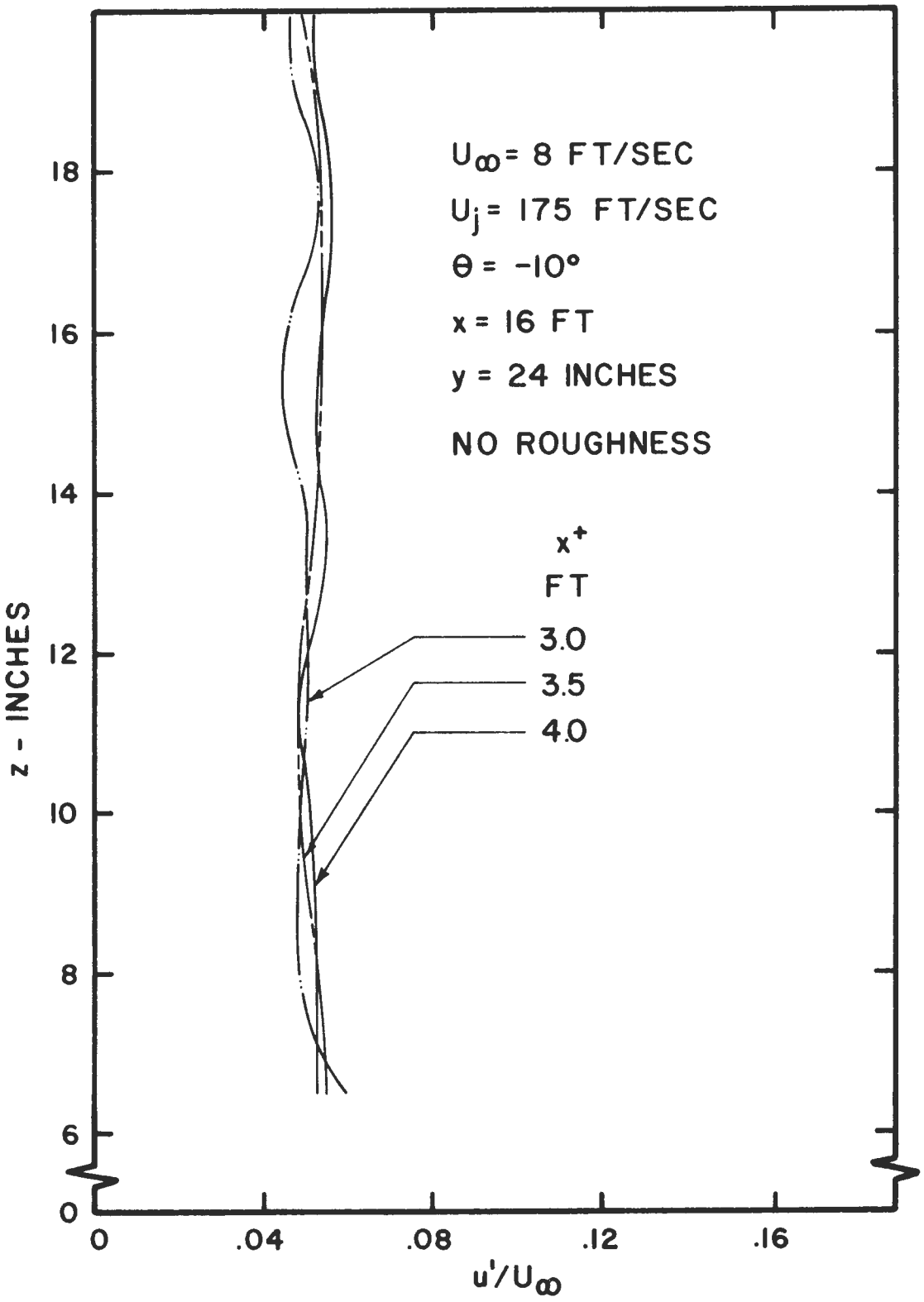

Figure 25. Effect of Position of Counter-Jet Generator With Respect to P.P. #3 on Boundary Layer Turbulence Intensity Distribution for $\theta = -10°$ at Low Free-Stream Velocity

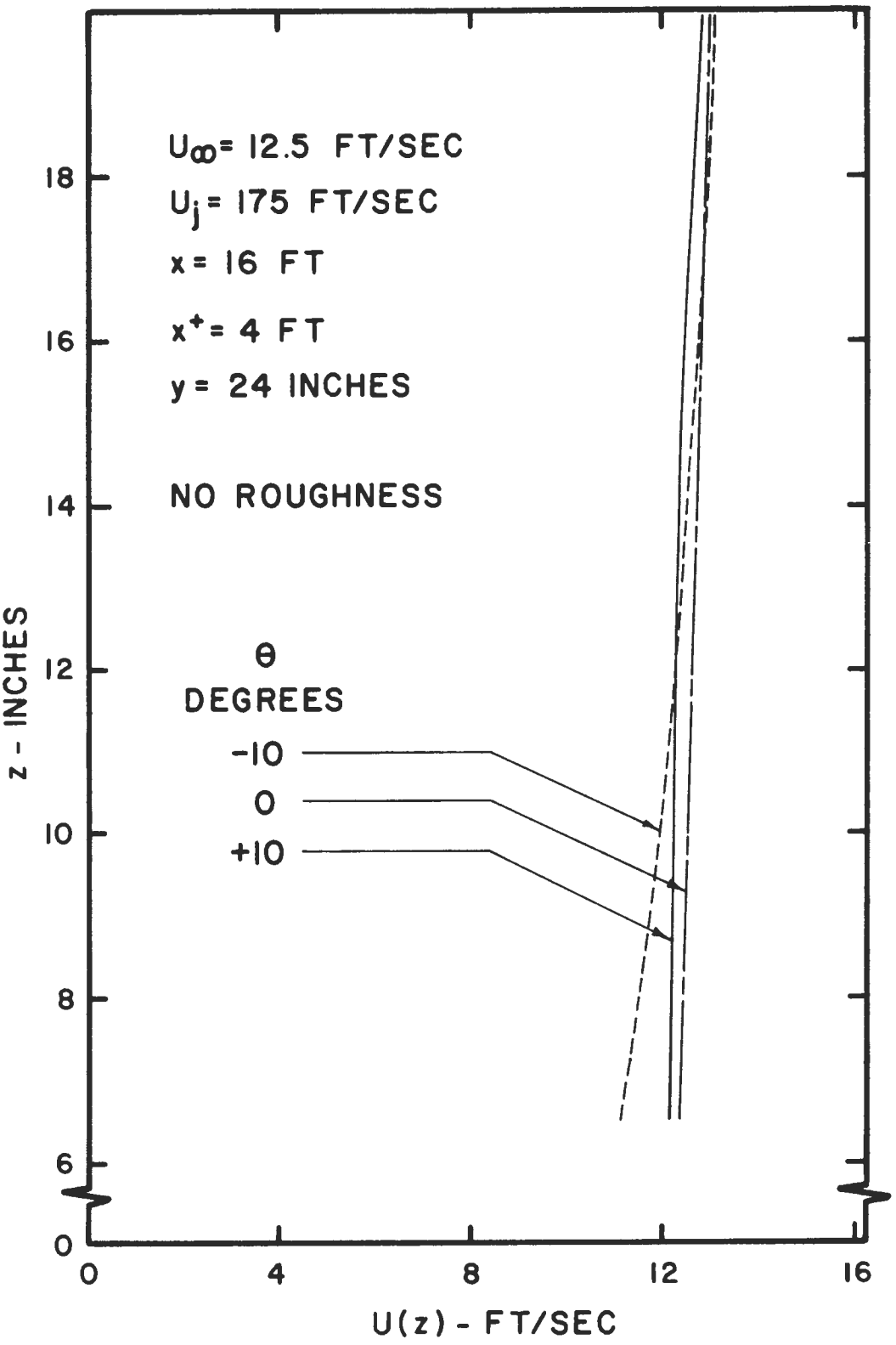

Figure 26. Effect of Counter-Jet Angle on Boundary Layer Mean Velocity Distribution

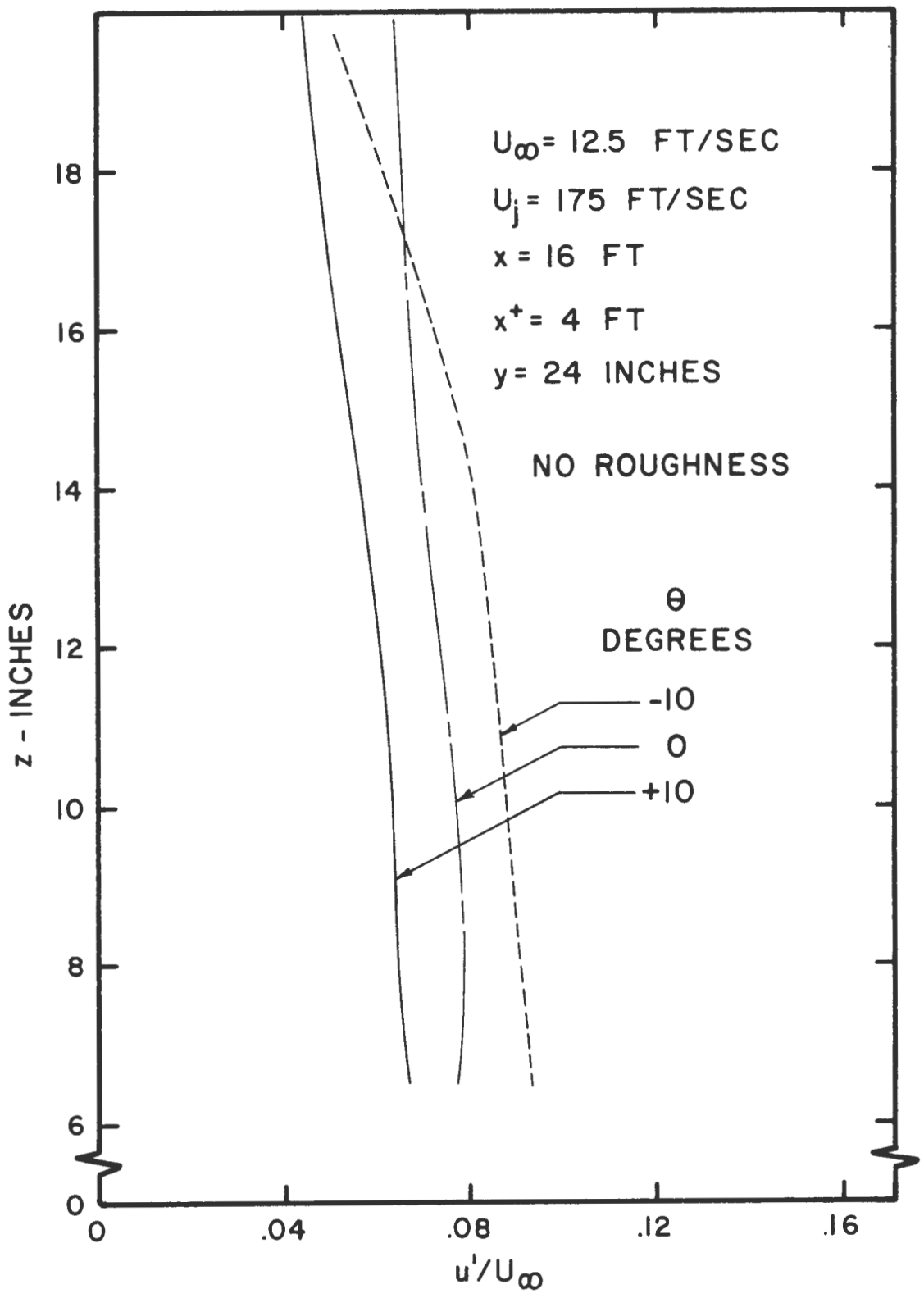

Figure 27. Effect of Counter-Jet Angle on Boundary Layer Turbulence Intensity Distribution

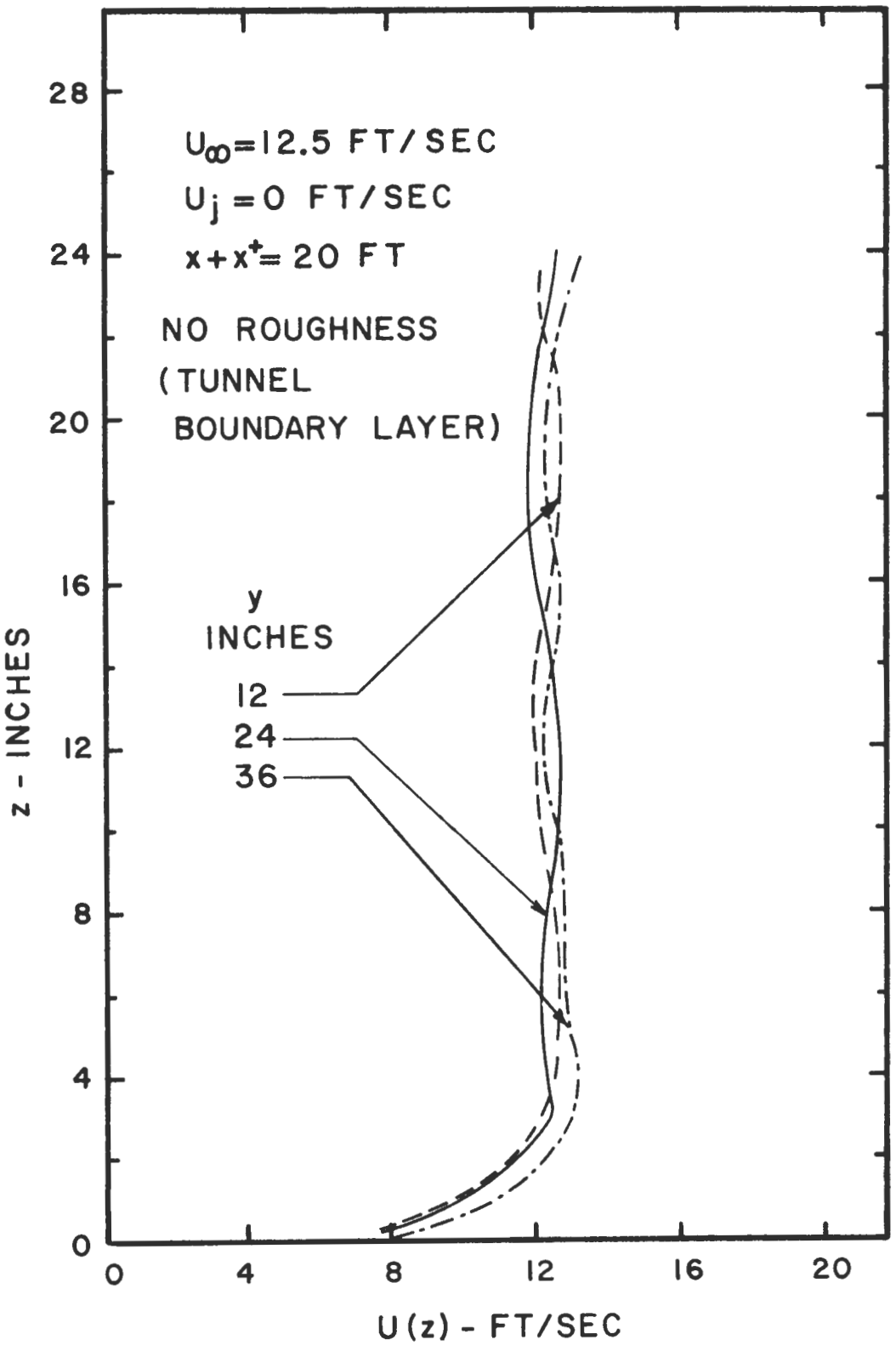

Figure 28. Transverse Uniformity of Mean Velocity Profiles of Natural Boundary Layer of Tunnel

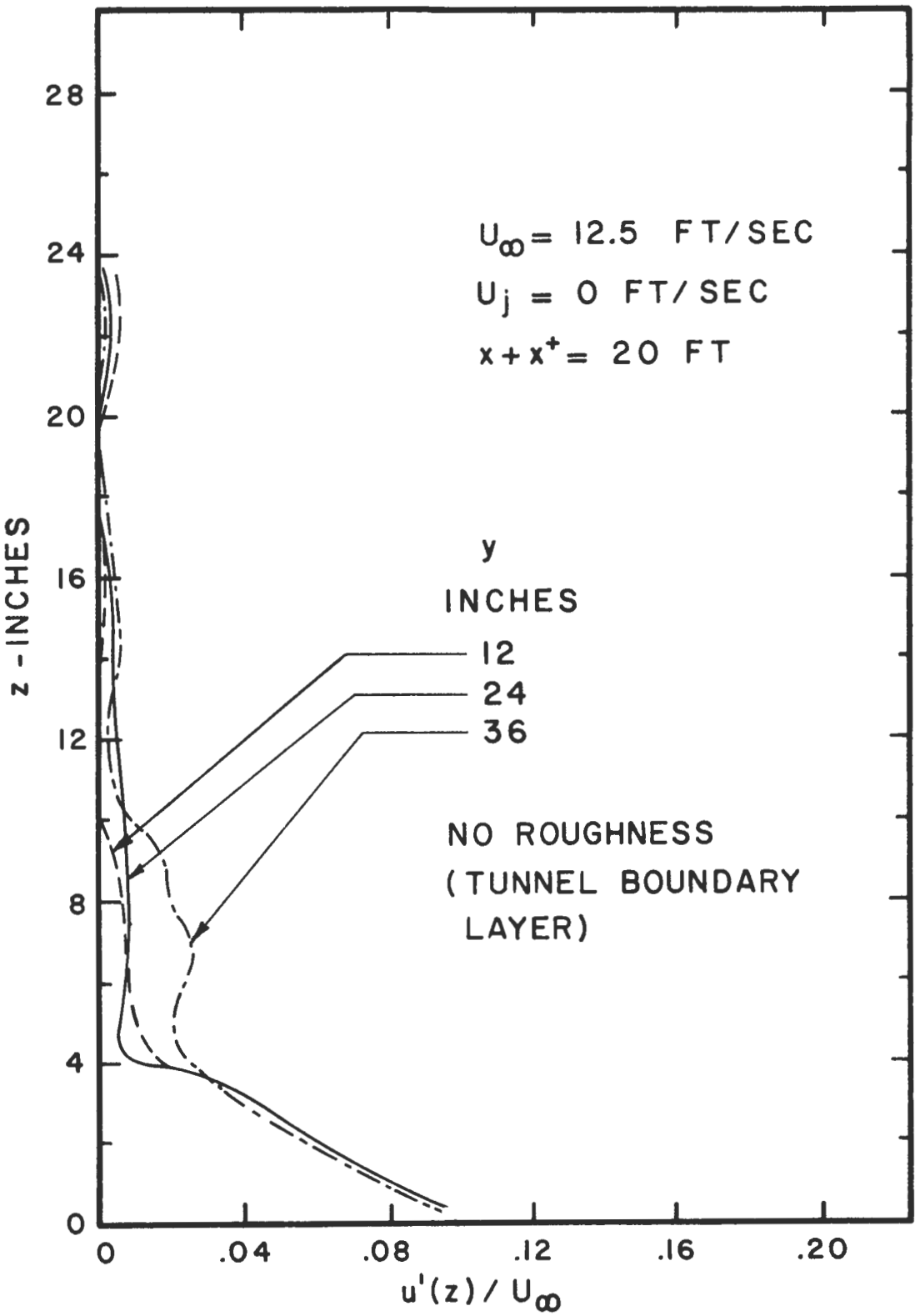

Figure 29. Transverse Uniformity of Turbulence Intensity Profiles of Natural Boundary Layer of Tunnel

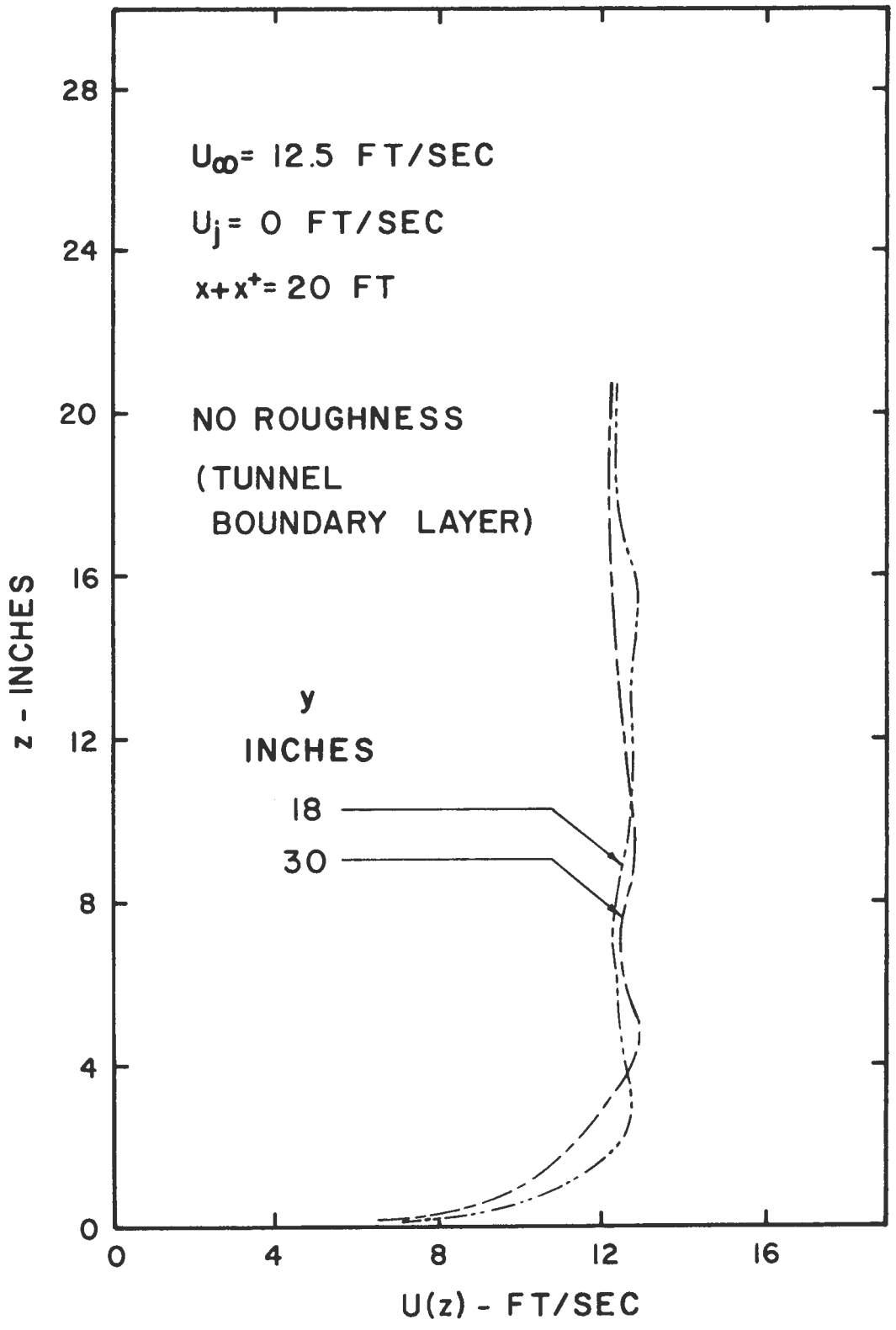

Figure 30. Transverse Uniformity of Mean Velocity Profiles of Central Portion of Natural Boundary Layer of Tunnel

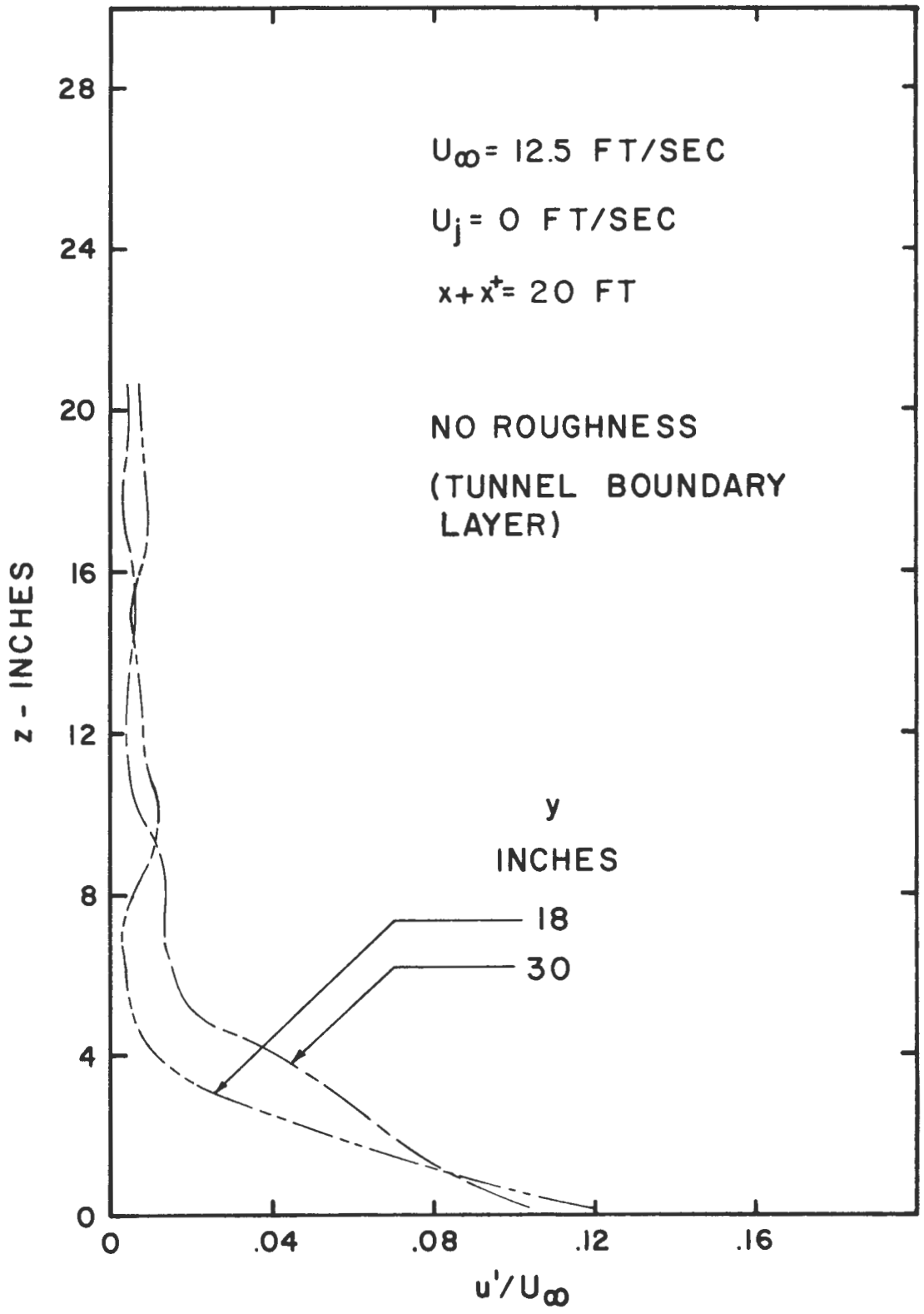

Figure 31. Transverse Uniformity of Turbulence Intensity Profiles of Central Portion of Natural Boundary Layer of Tunnel

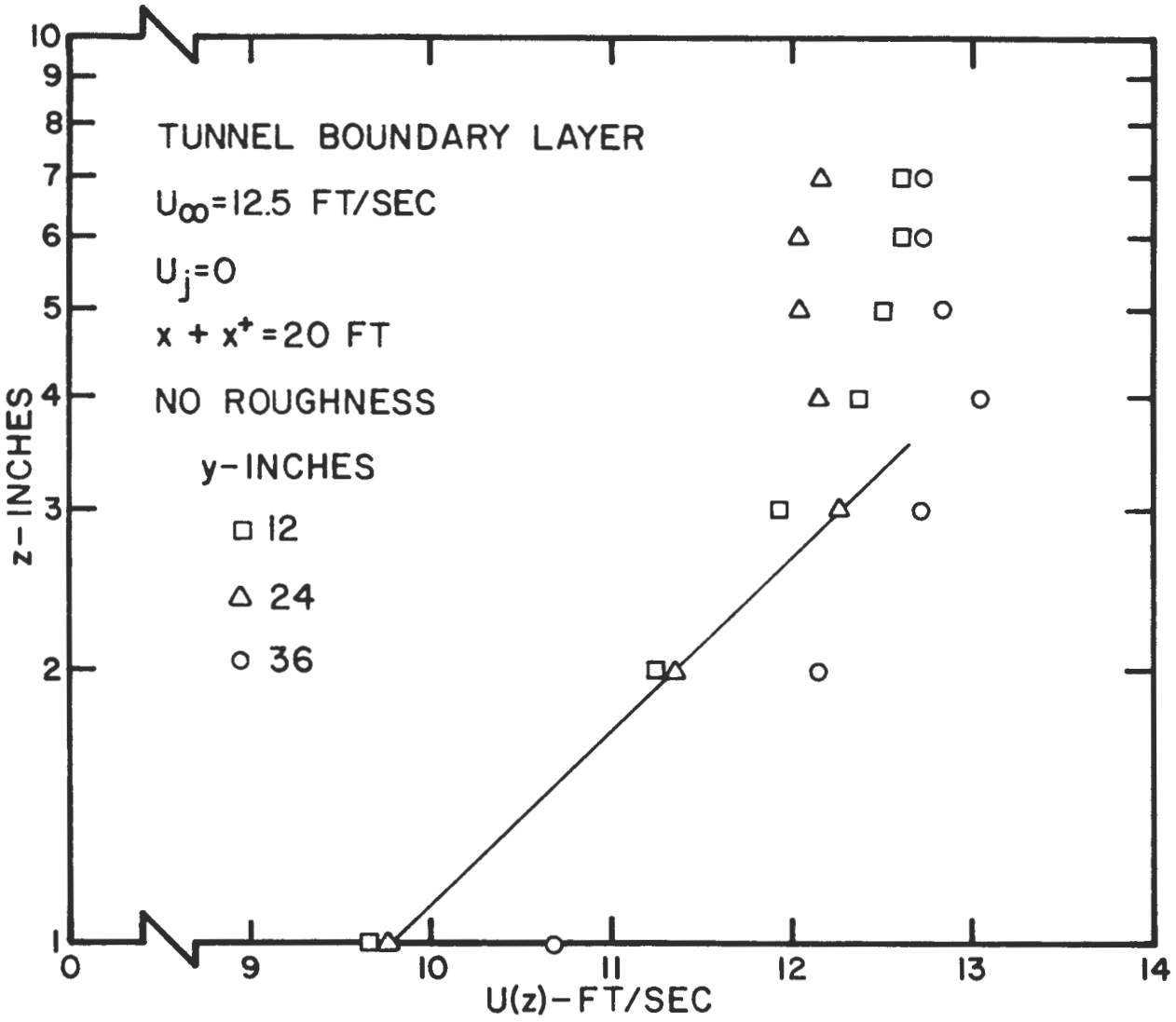

Figure 32. Log-Linear Plot of Mean Velocity Profiles of Natural Boundary Layer of Tunnel

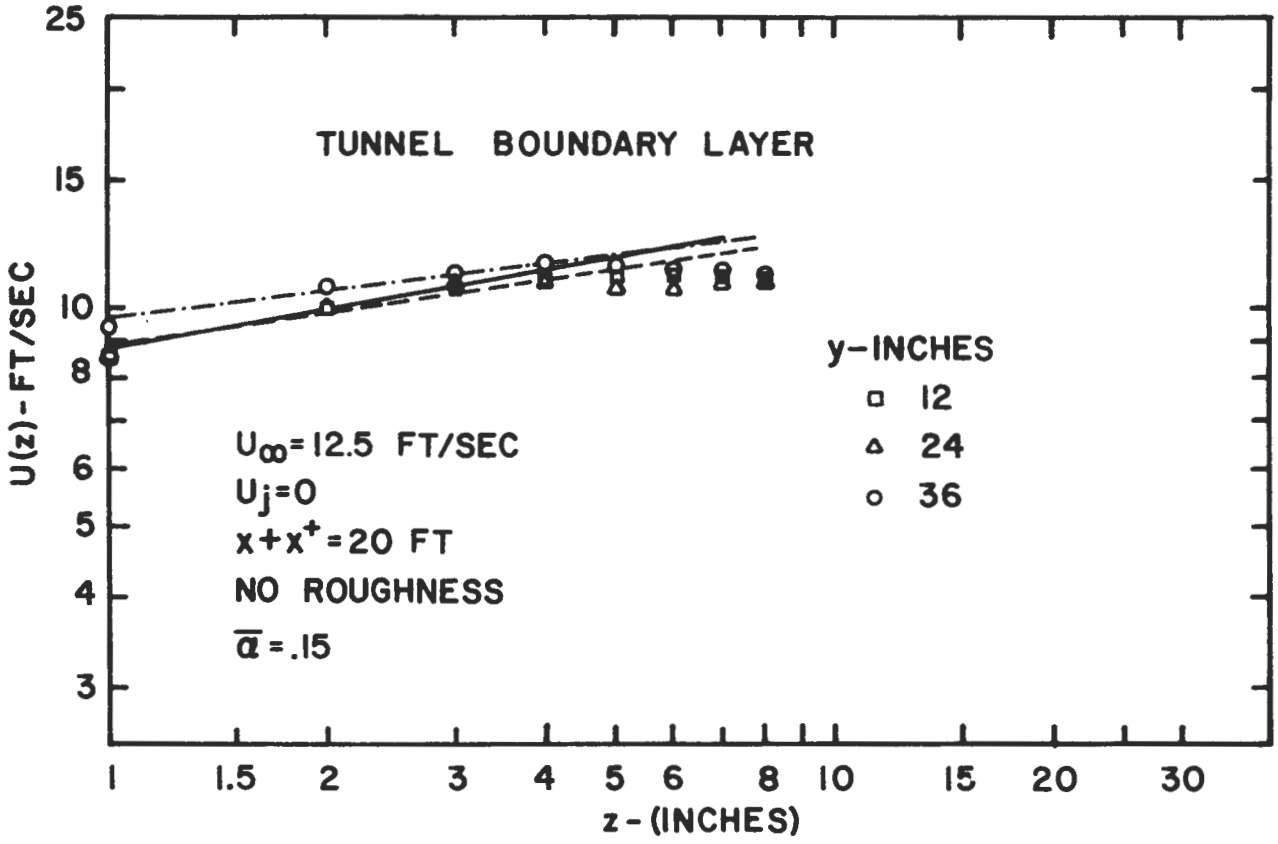

Figure 33. Log-Log Plot of Mean Velocity Profiles of Natural Boundary Layer of Tunnel

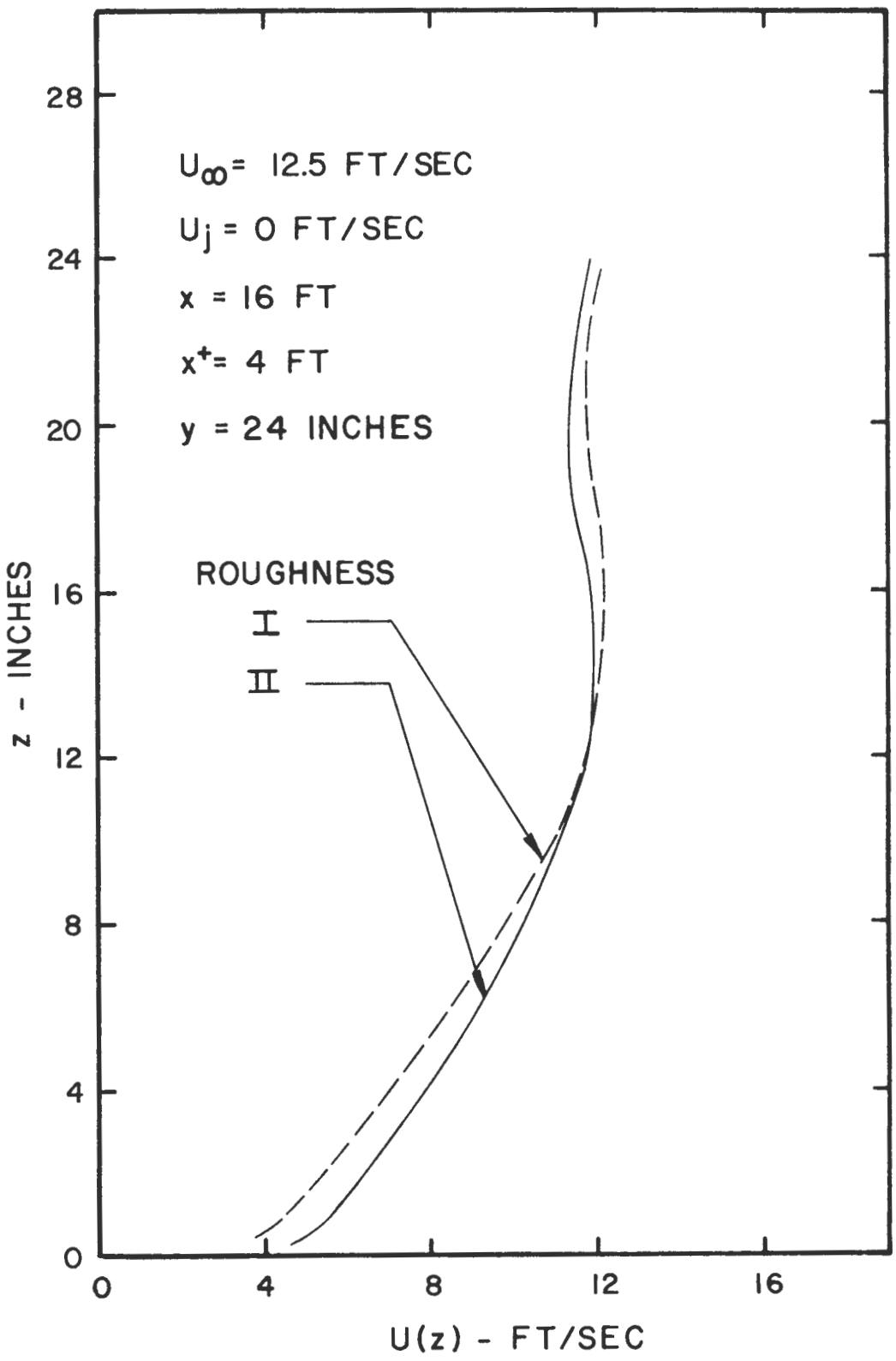

Figure 34. Mean Velocity Profiles of Roughness-Generated Boundary Layers Using Two Types of Surface Roughnesses

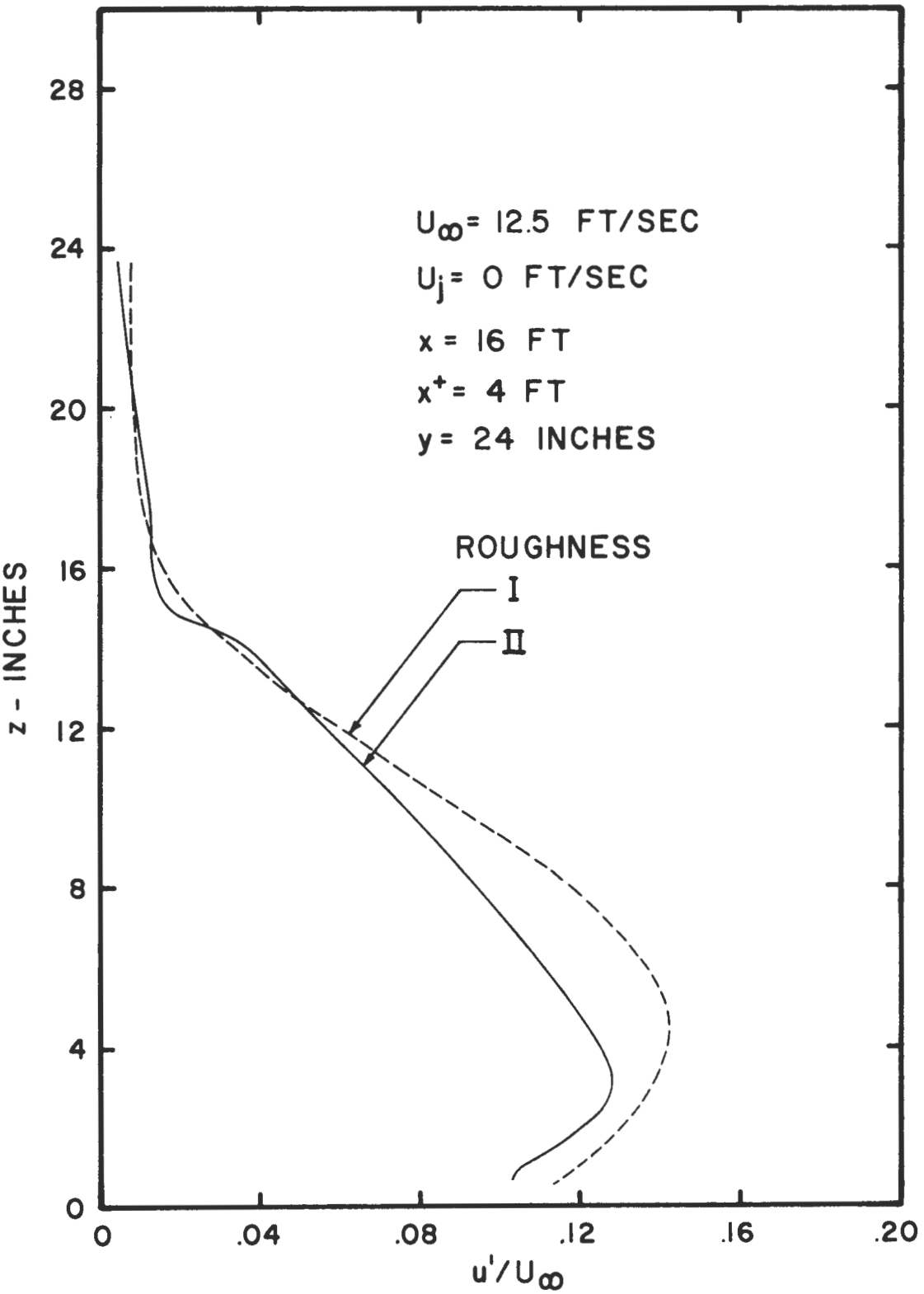

Figure 35. Turbulence Intensity Profiles of Roughness-Generated Boundary Layers Using Two Types of Surface Roughnesses

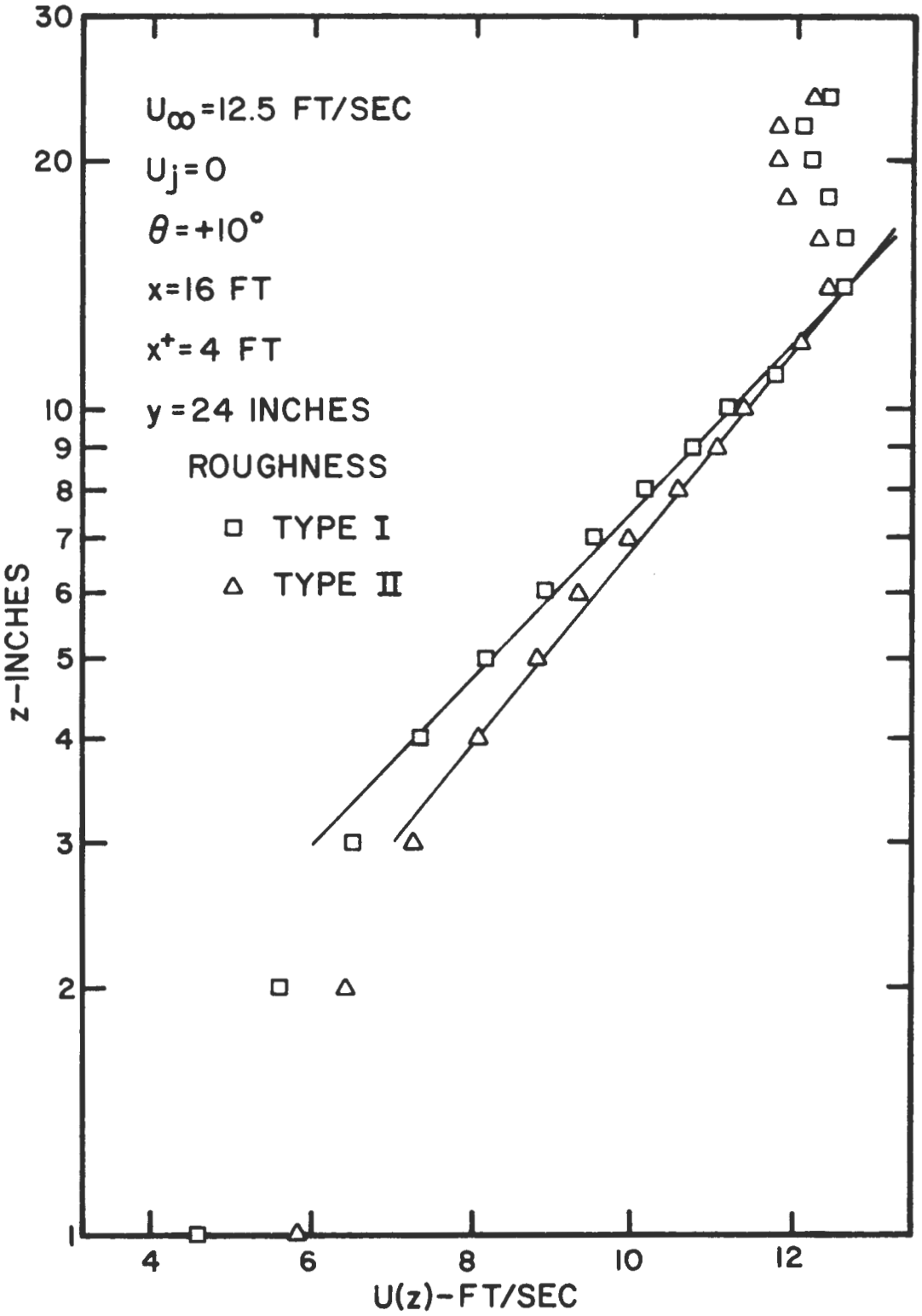

Figure 36. Log-Linear Plot of Mean Velocity Profiles of Roughness-Generated Boundary Layers Using Two Types of Surface Roughnesses

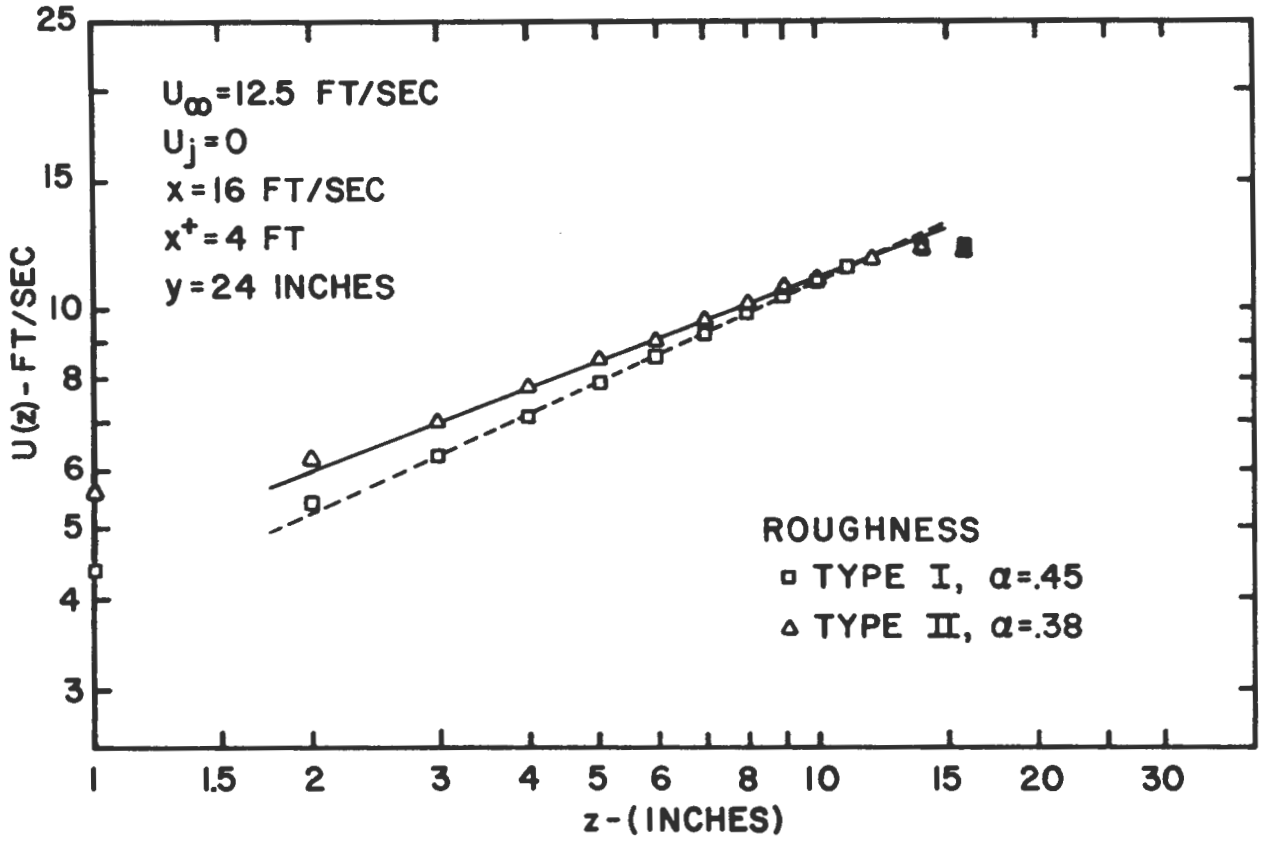

Figure 37. Log-Log Plot of Mean Velocity Profiles of Roughness-Generated Boundary Layers Using Two Types of Surface Roughnesses

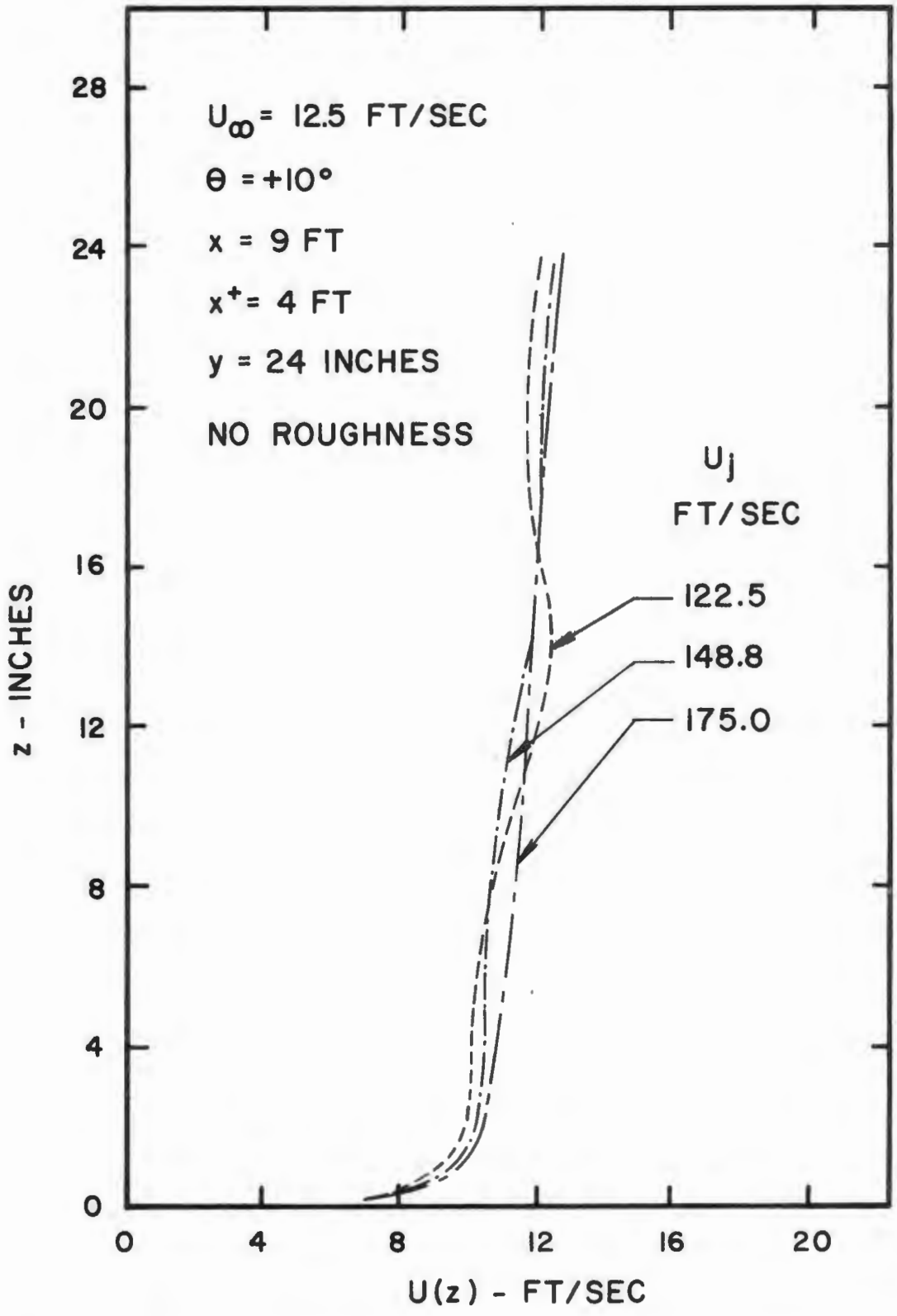

Figure 38. Effect of Counter-Jet Velocity on Boundary Layer Mean Velocity Profile at x = 9 ft.

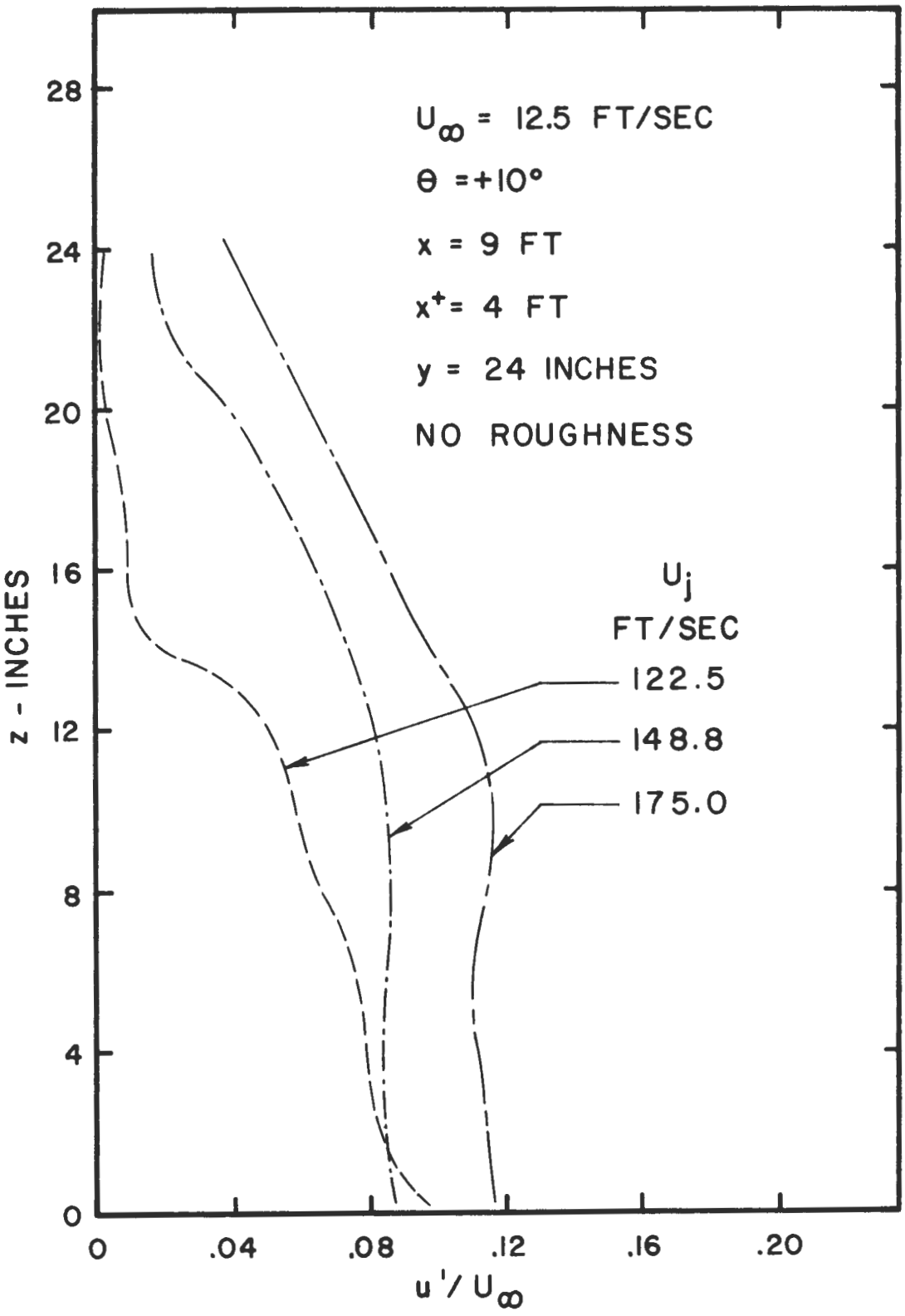

Figure 39. Effect of Counter-Jet Velocity on Boundary Layer Turbulence Intensity Profile at x = 9 ft.

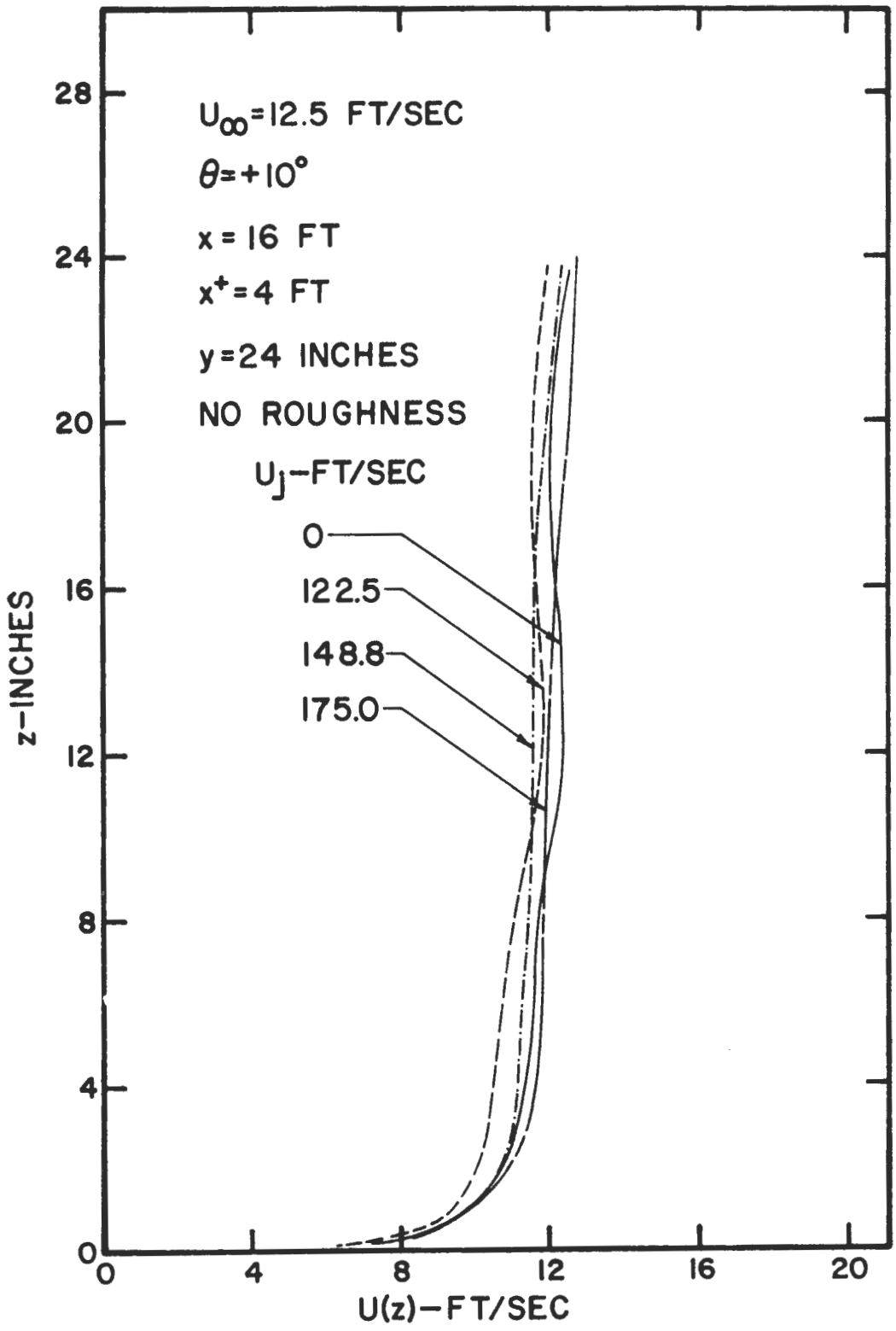

Figure 40. Effect of Counter-Jet Velocity on Boundary Layer Mean Velocity Profile at x = 16 ft.

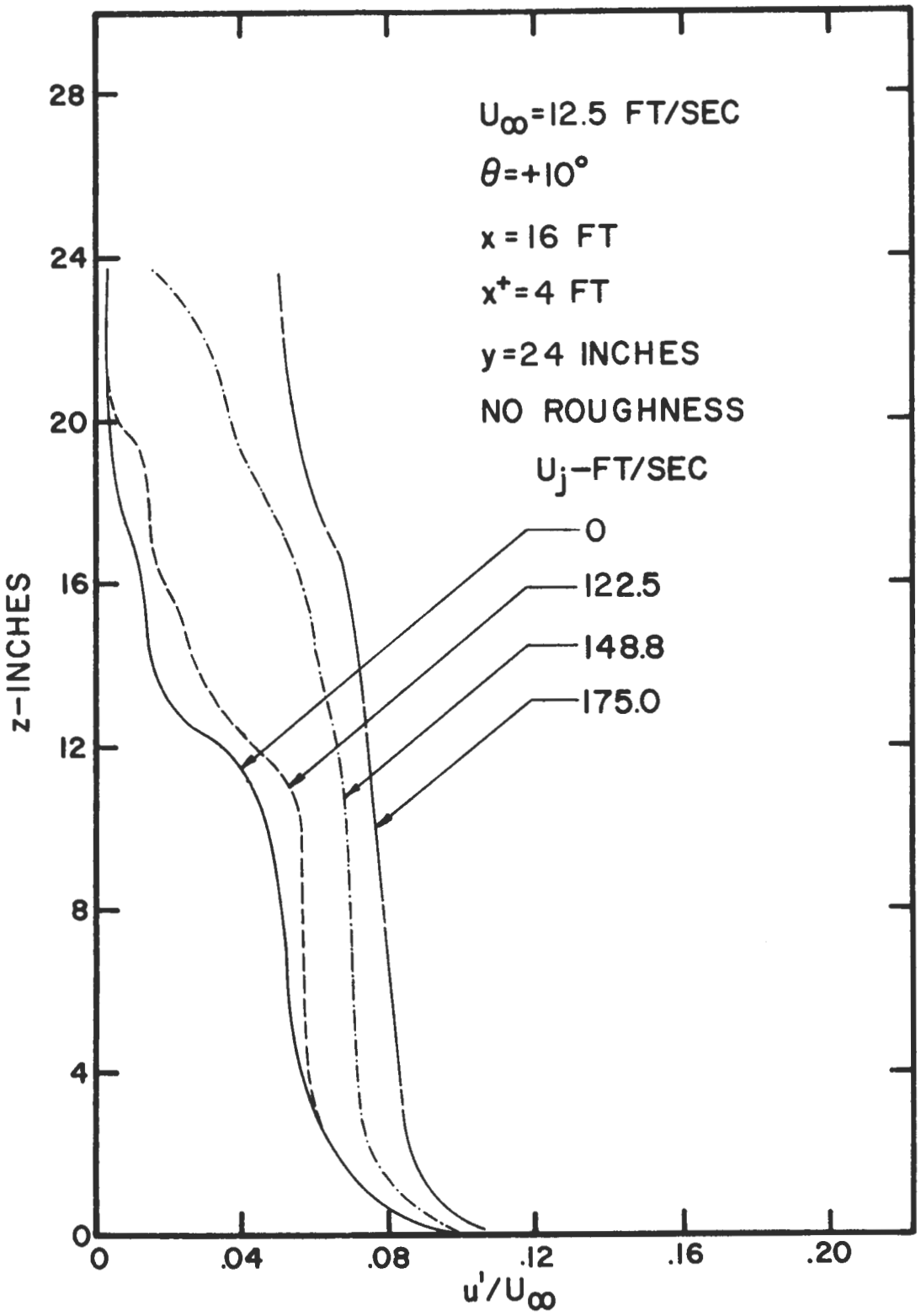

Figure 41. Effect of Counter-Jet Velocity on Boundary Layer Turbulence Intensity Profile at x = 16 ft.

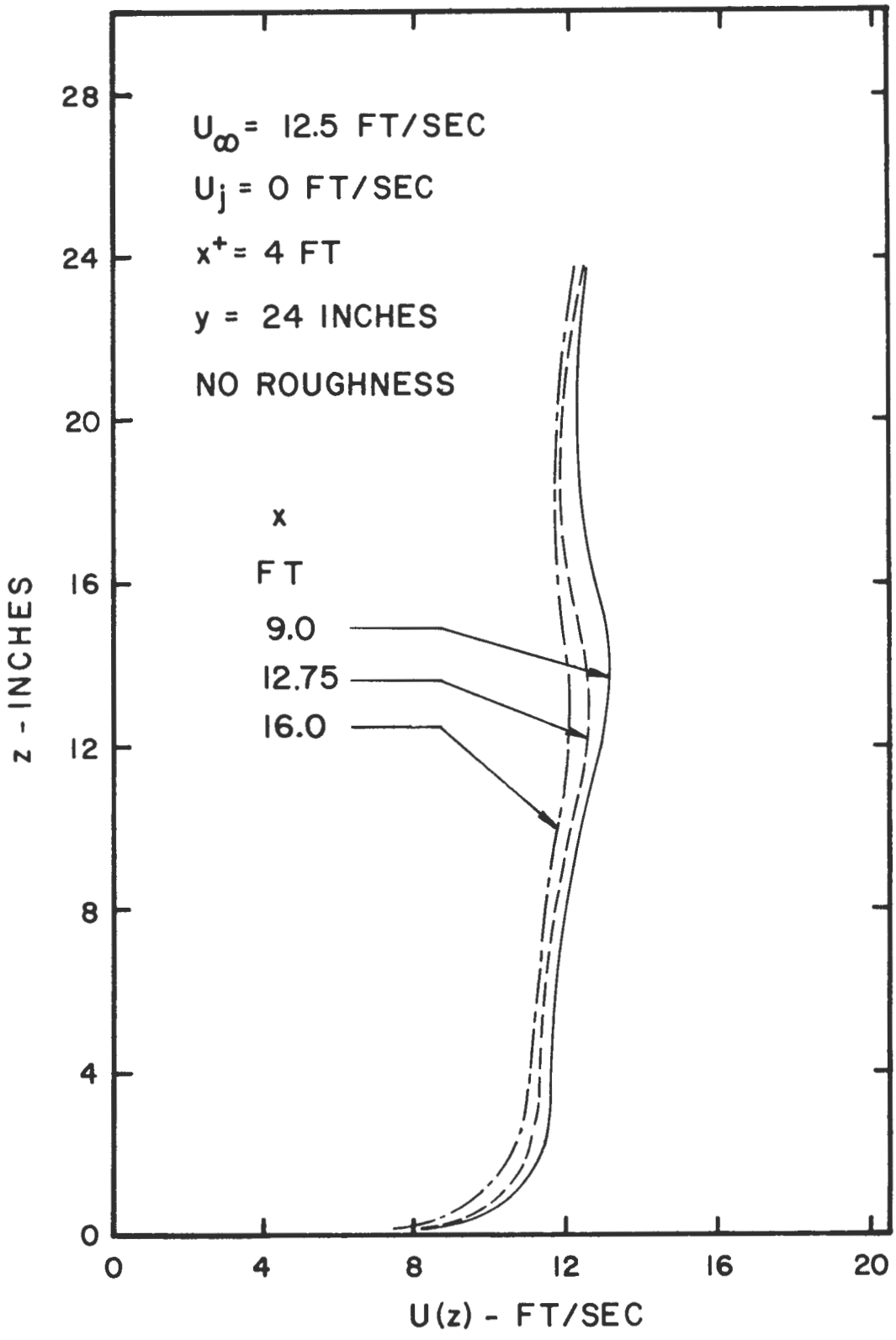

Figure 42. Downstream Development of Boundary Layer Mean Velocity Profile for U_j = 0 ft/sec

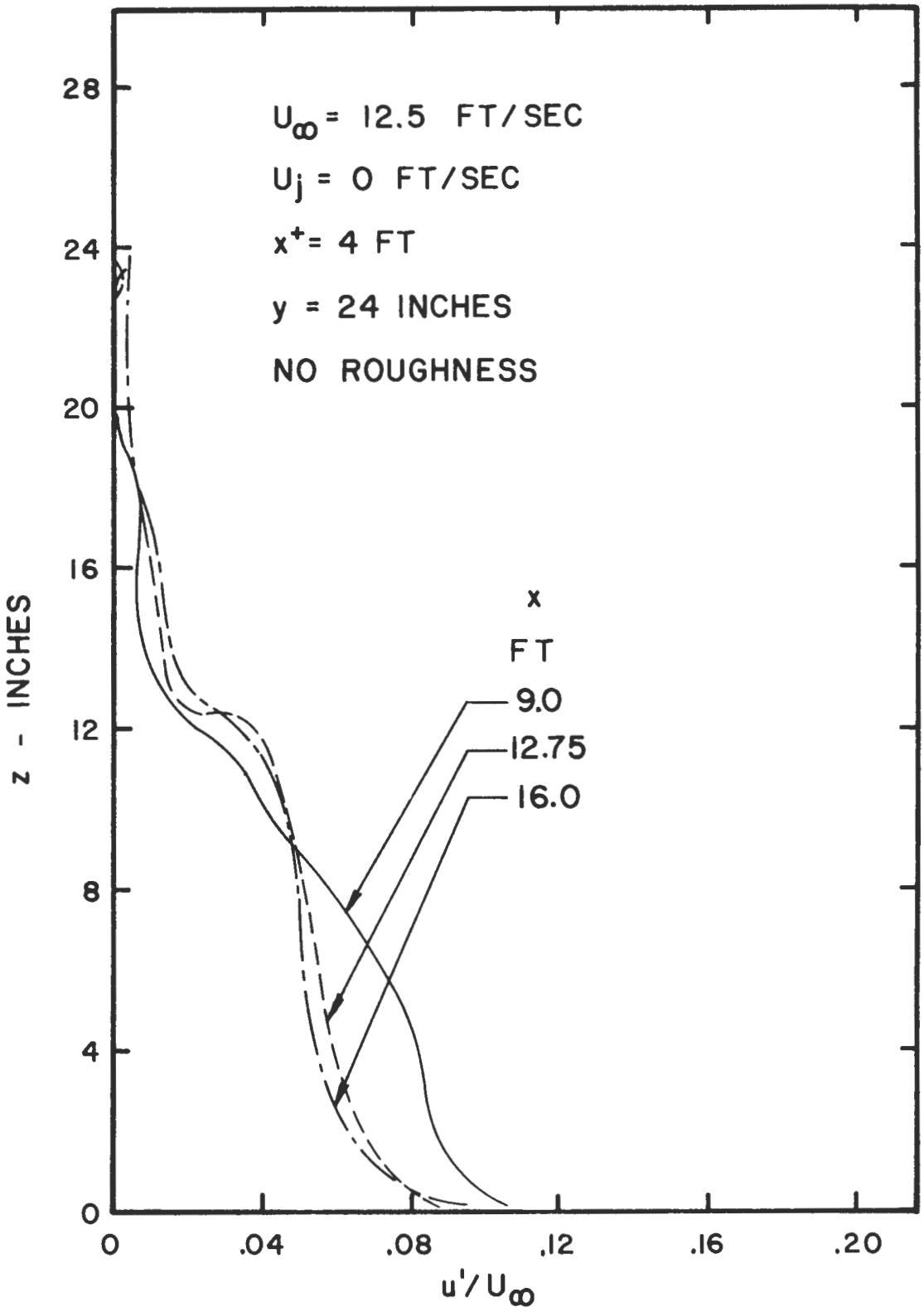

Figure 43. Downstream Development of Boundary Layer Turbulence Intensity Profile for U_j = 0 ft/sec

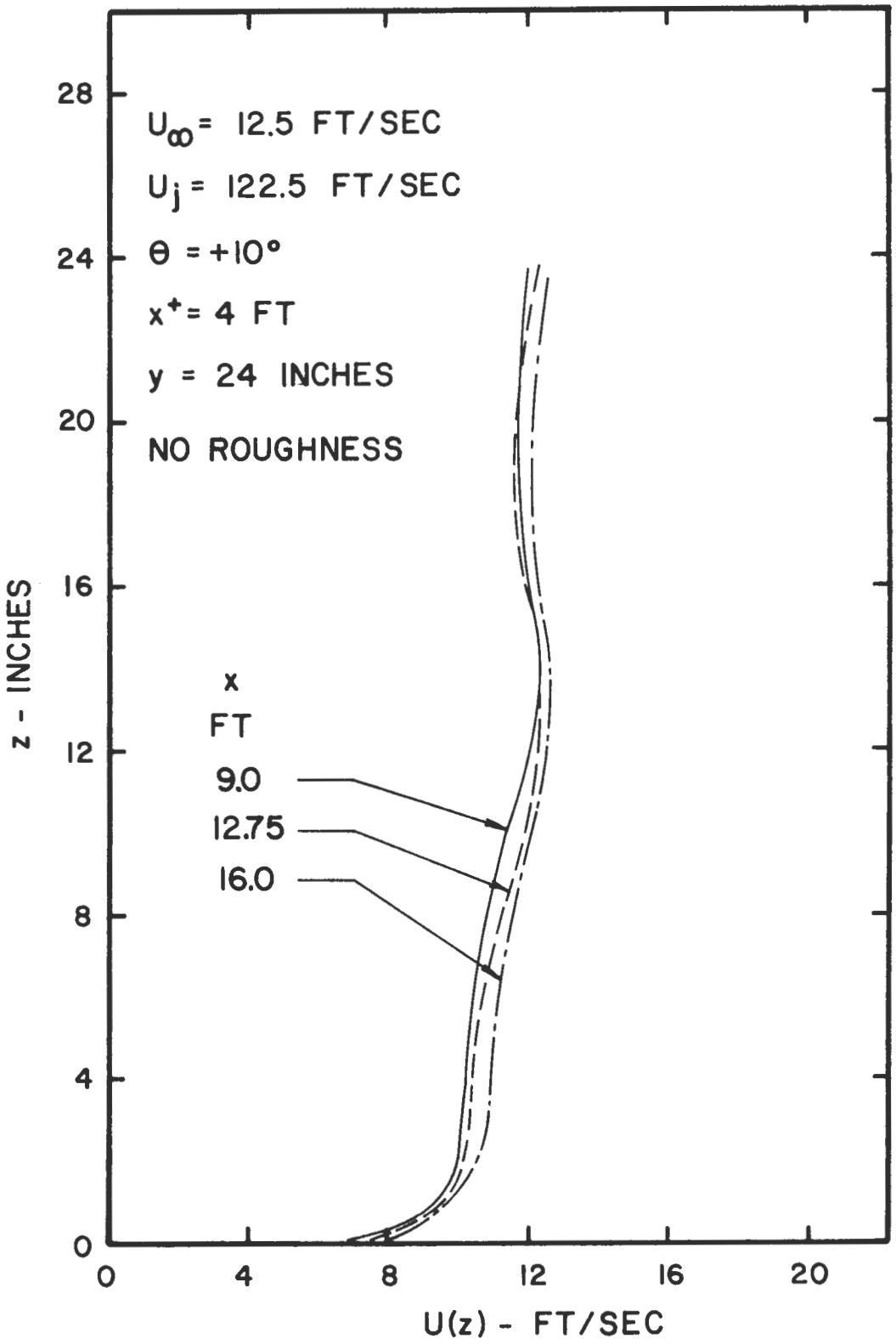

Figure 44. Downstream Development of Boundary Layer Mean Velocity Profile for U_j = 122.5 ft/sec

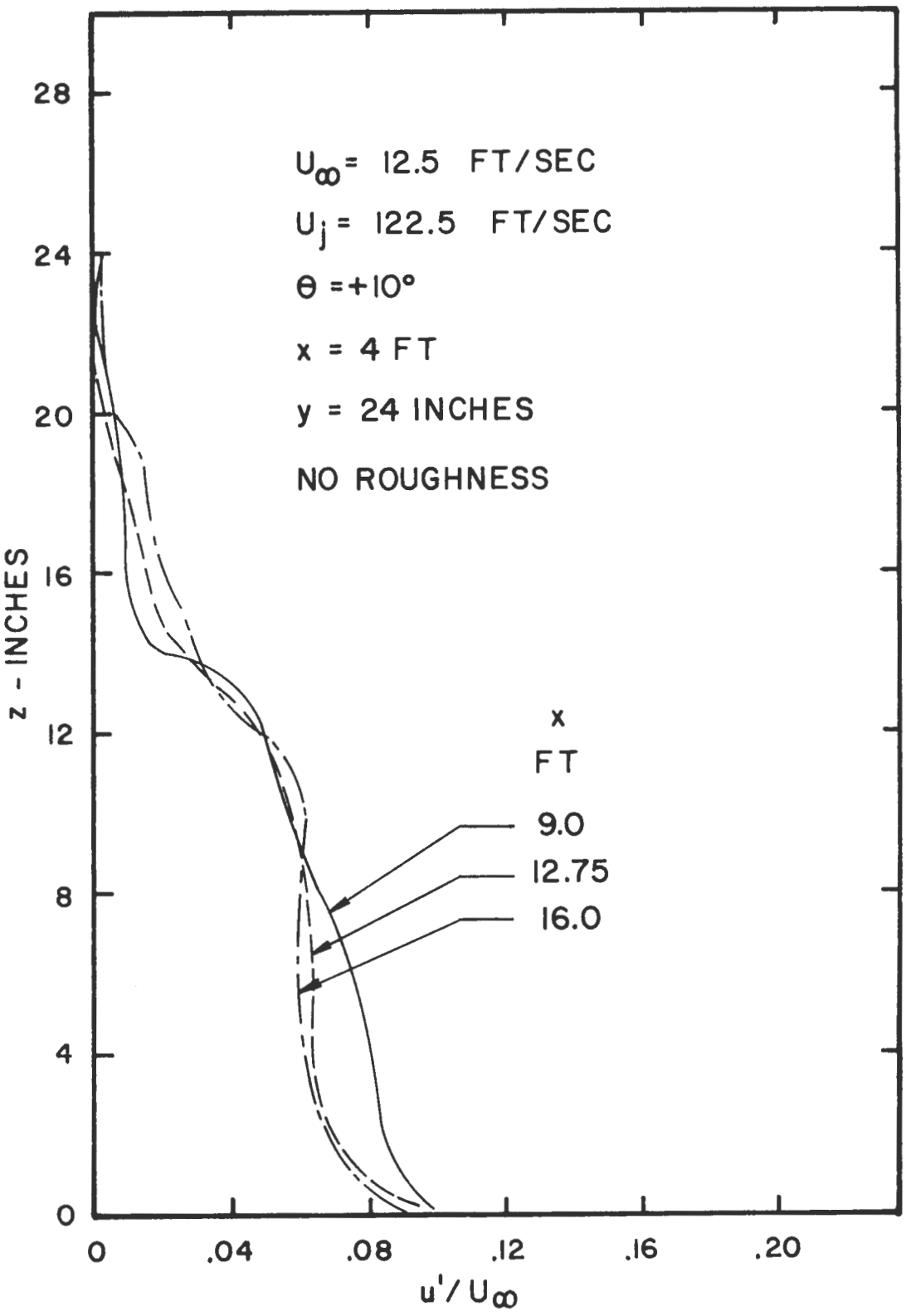

Figure 45. Downstream Development of Boundary Layer Turbulence Intensity Profile for U_j = 122.5 ft/sec

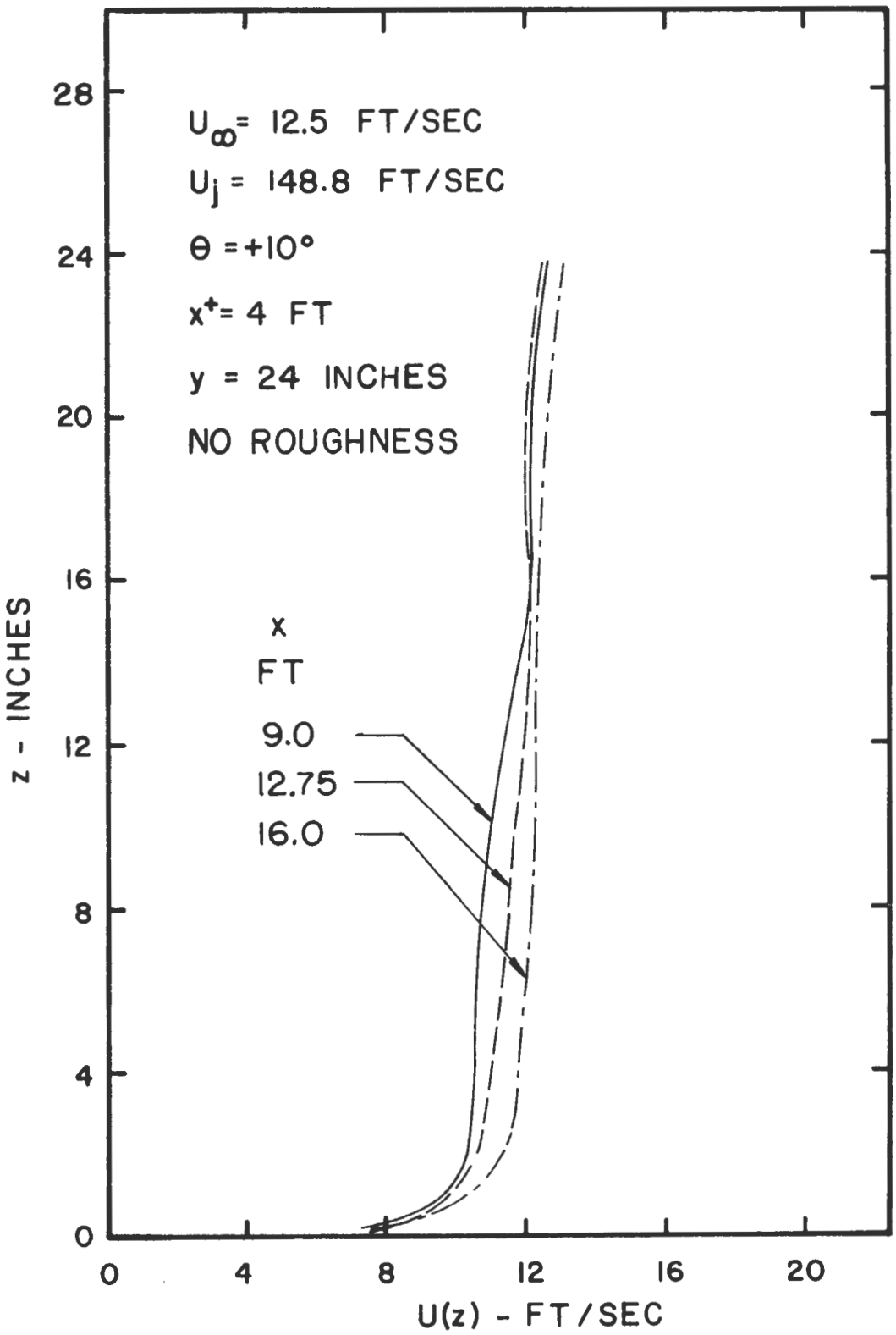

Figure 46. Downstream Development of Boundary Layer Mean Velocity Profile for U_j = 148.8 ft/sec

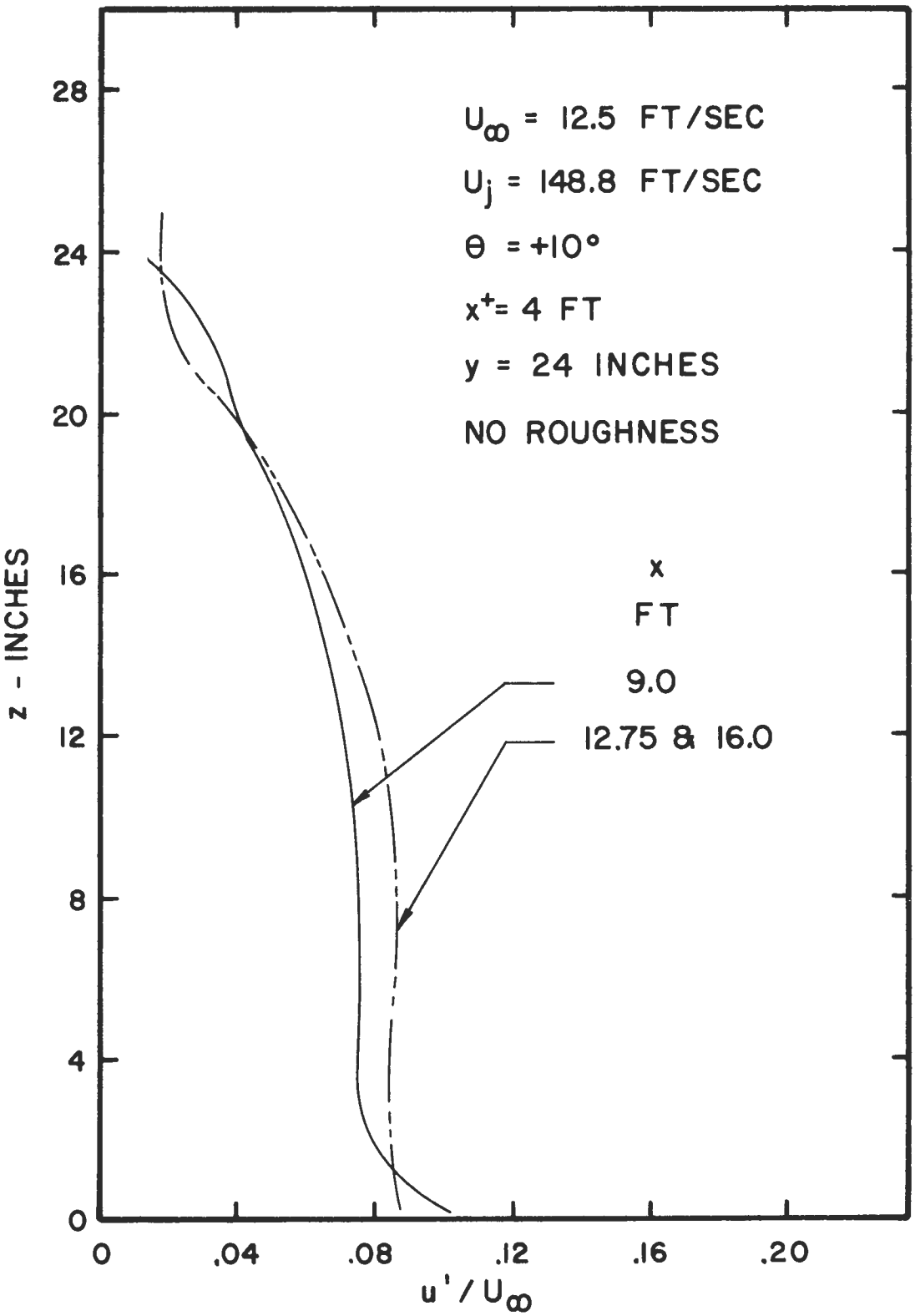

Figure 47. Downstream Development of Boundary Layer Turbulence Intensity Profile for U_j = 148.8 ft/sec

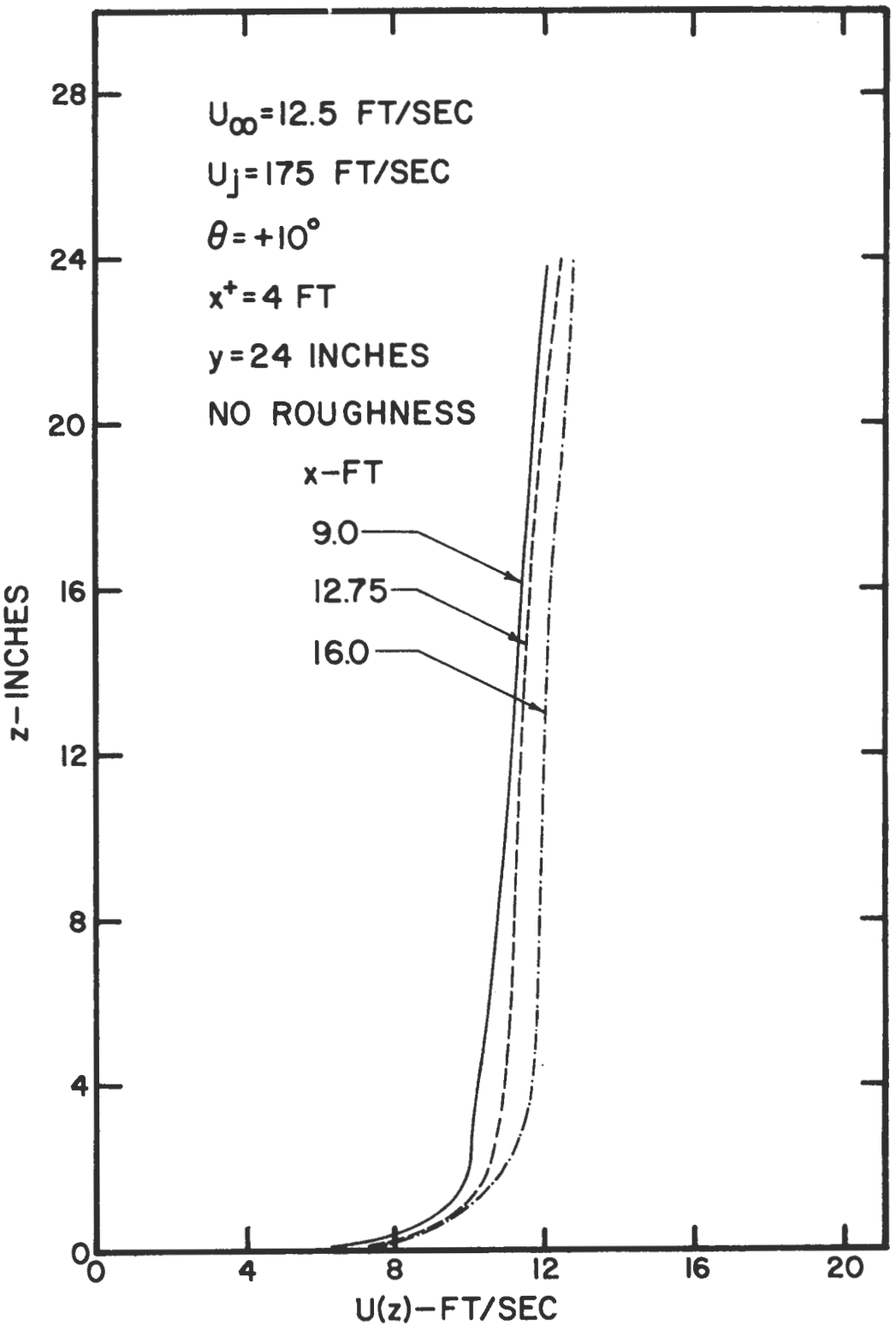

Figure 48. Downstream Development of Boundary Layer Mean Velocity Profile for U_j = 175 ft/sec

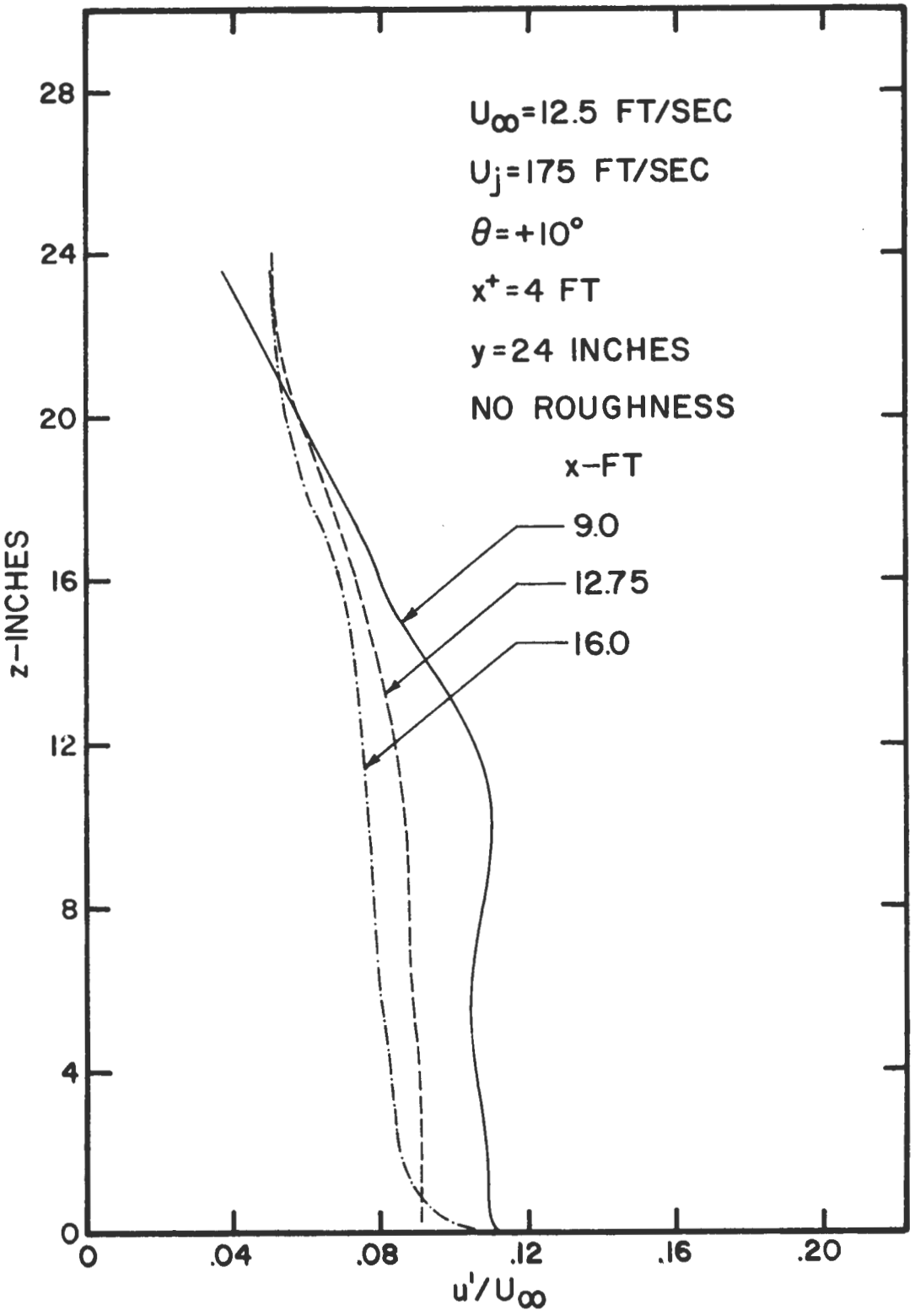

Figure 49. Downstream Development of Boundary Layer Turbulence Intensity Profile for U_j = 175 ft/sec

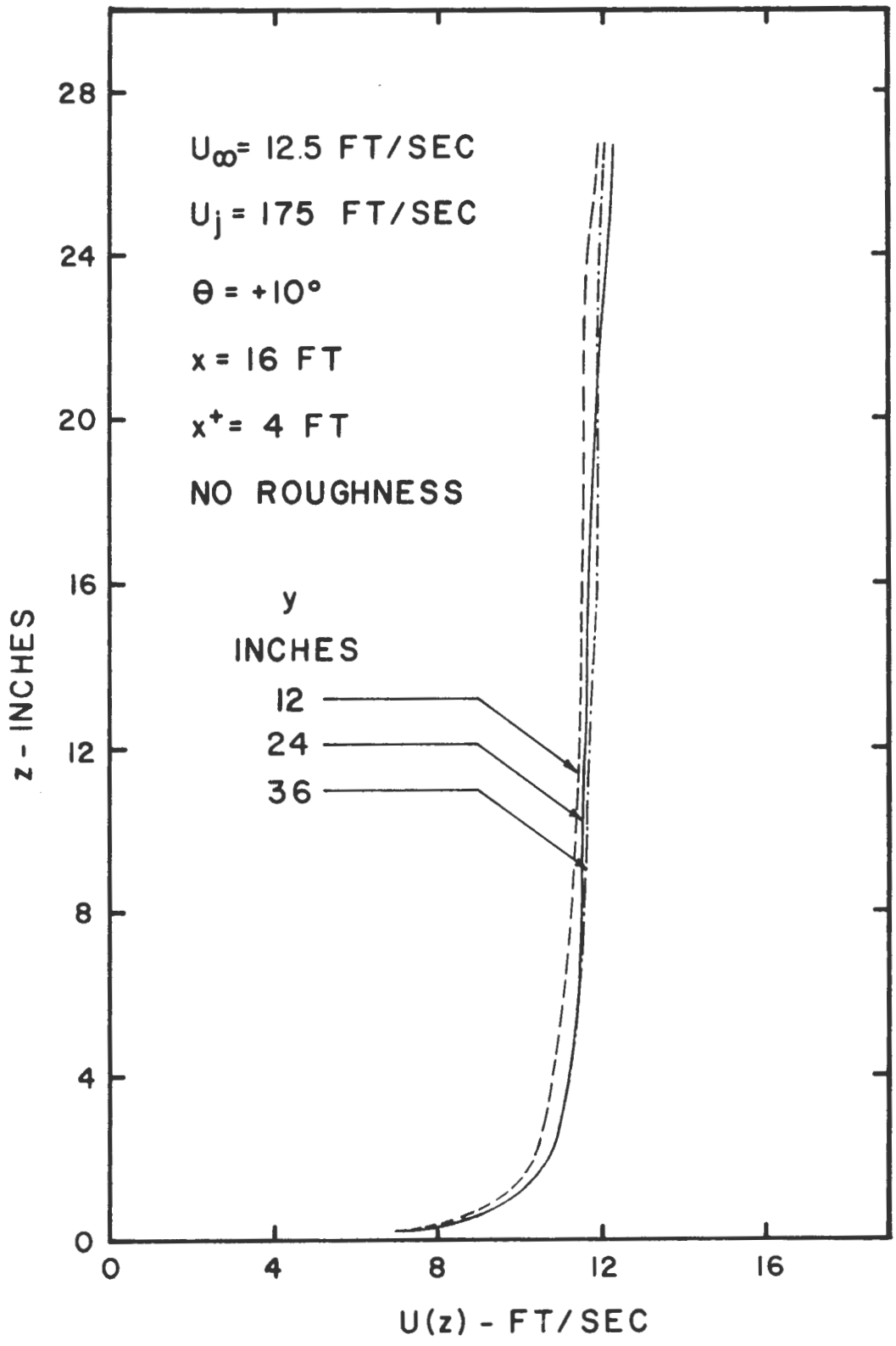

Figure 50. Transverse Uniformity of Mean Velocity Profiles of Counter-Jet Generated Boundary Layer With No Surface Roughness

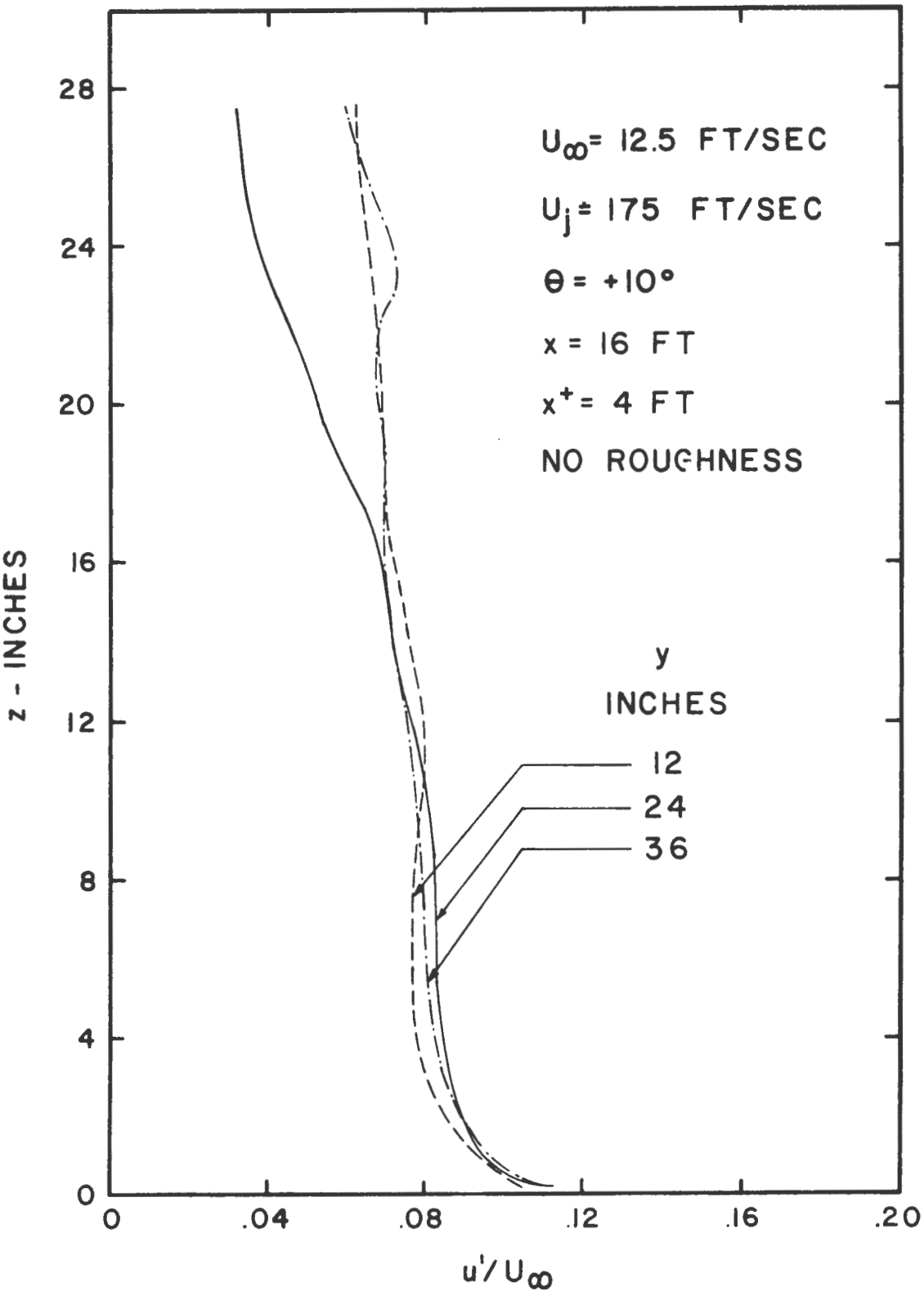

Figure 51. Transverse Uniformity of Turbulence Intensity Profiles of Counter-Jet Generated Boundary Layer With No Surface Roughness

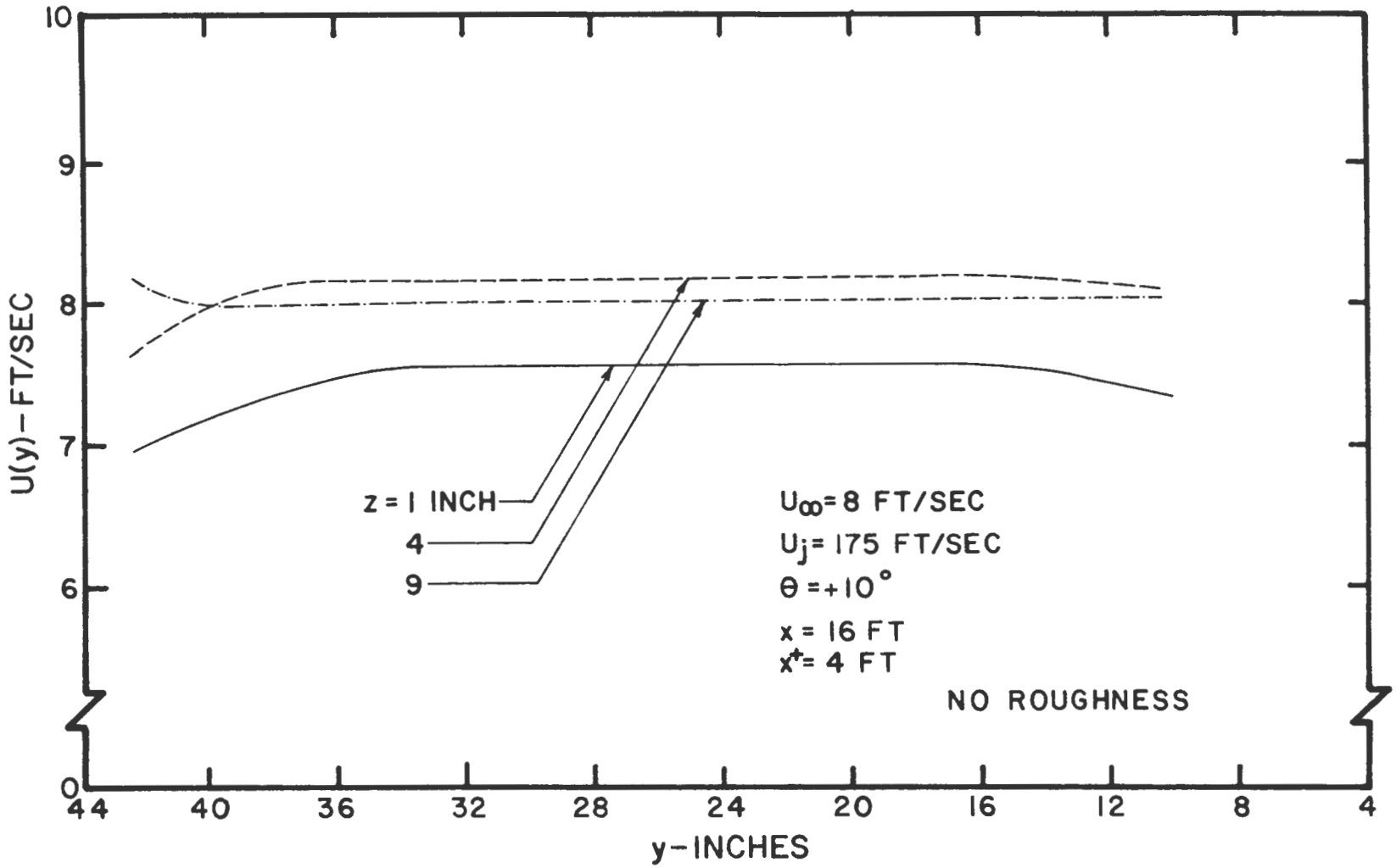

Figure 52. Transverse Profiles of Mean Velocity in a Counter-Jet Generated Boundary Layer With No Surface Roughness at Low Free-Stream Velocity

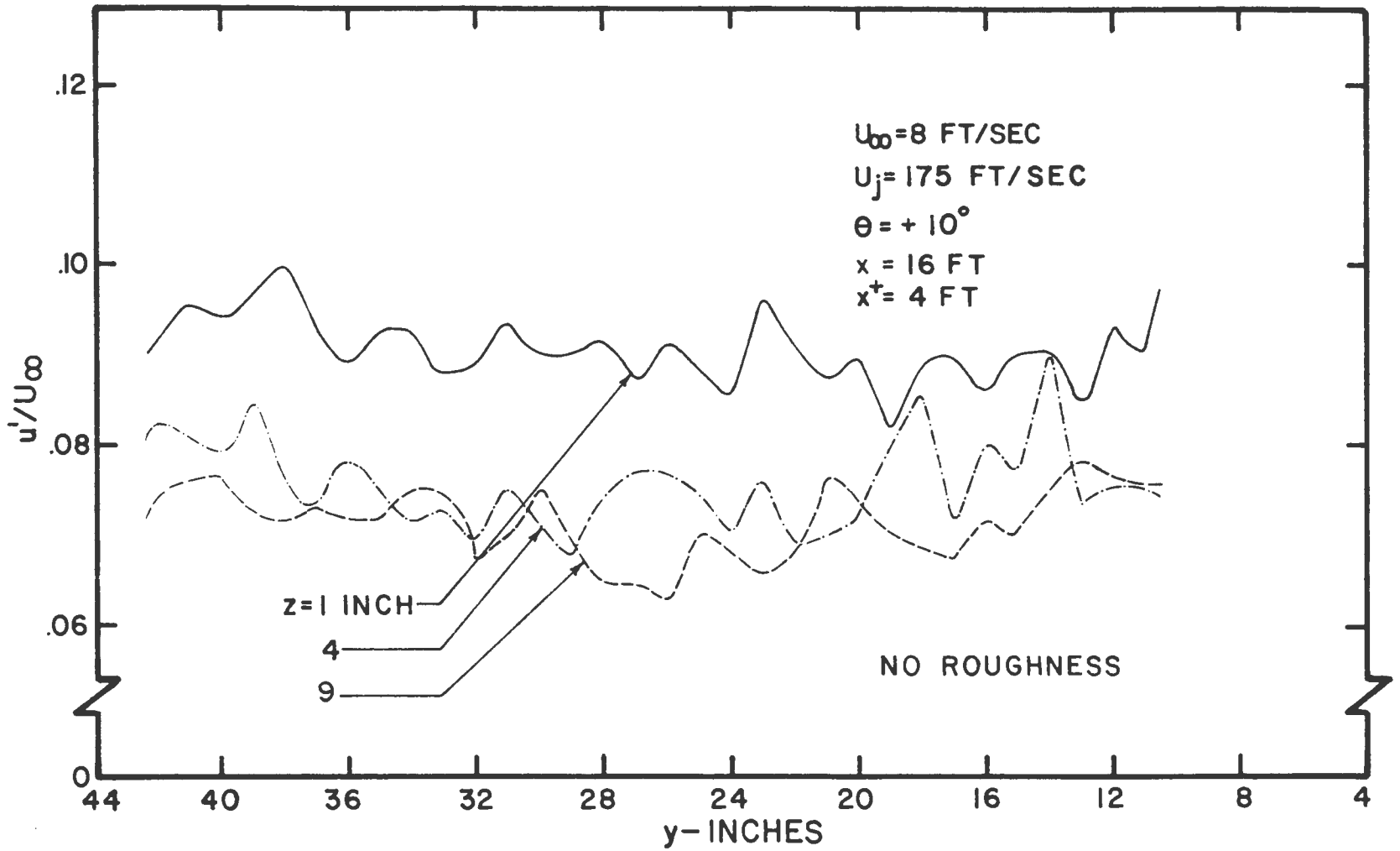

Figure 53. Transverse Profiles of Turbulence Intensity in a Counter-Jet Generated Boundary Layer With No Surface Roughness at Low Free-Stream Velocity

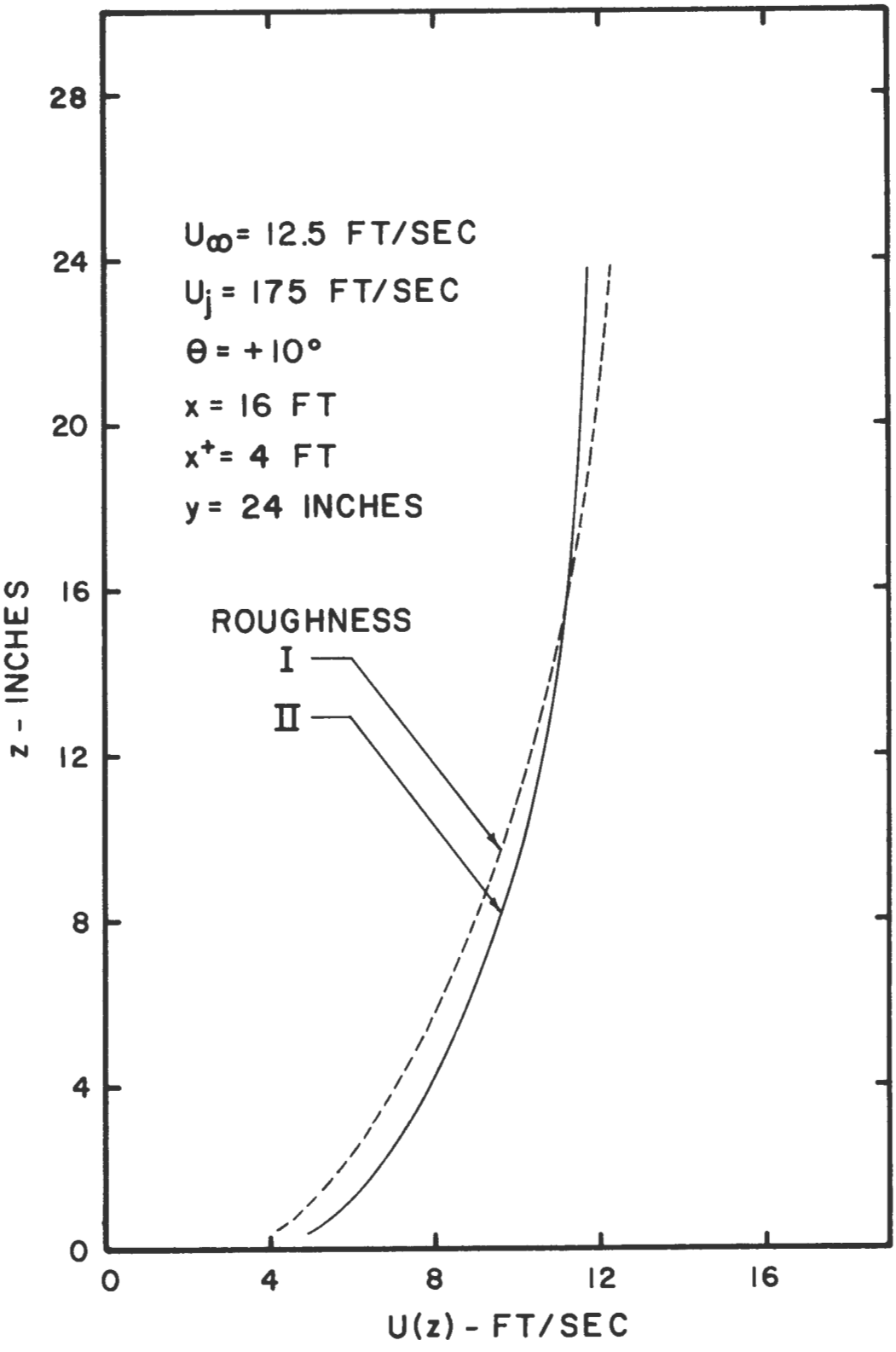

Figure 54. Mean Velocity Profiles of Counter-Jet Generated Boundary Layers Using Two Types of Surface Roughnesses

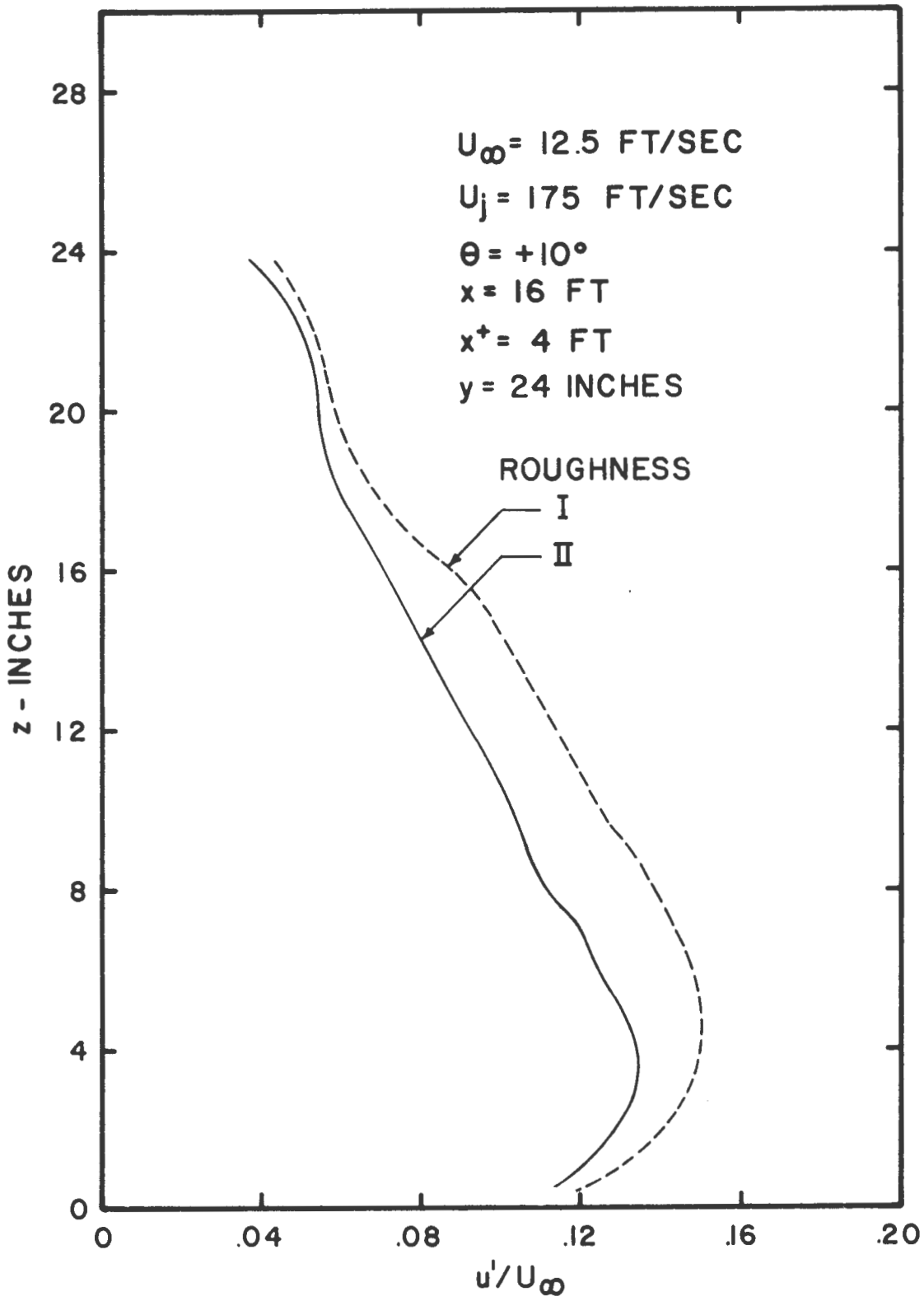

Figure 55. Turbulence Intensity Profiles of Counter-Jet Generated Boundary Layers Using Two Types of Surface Roughnesses

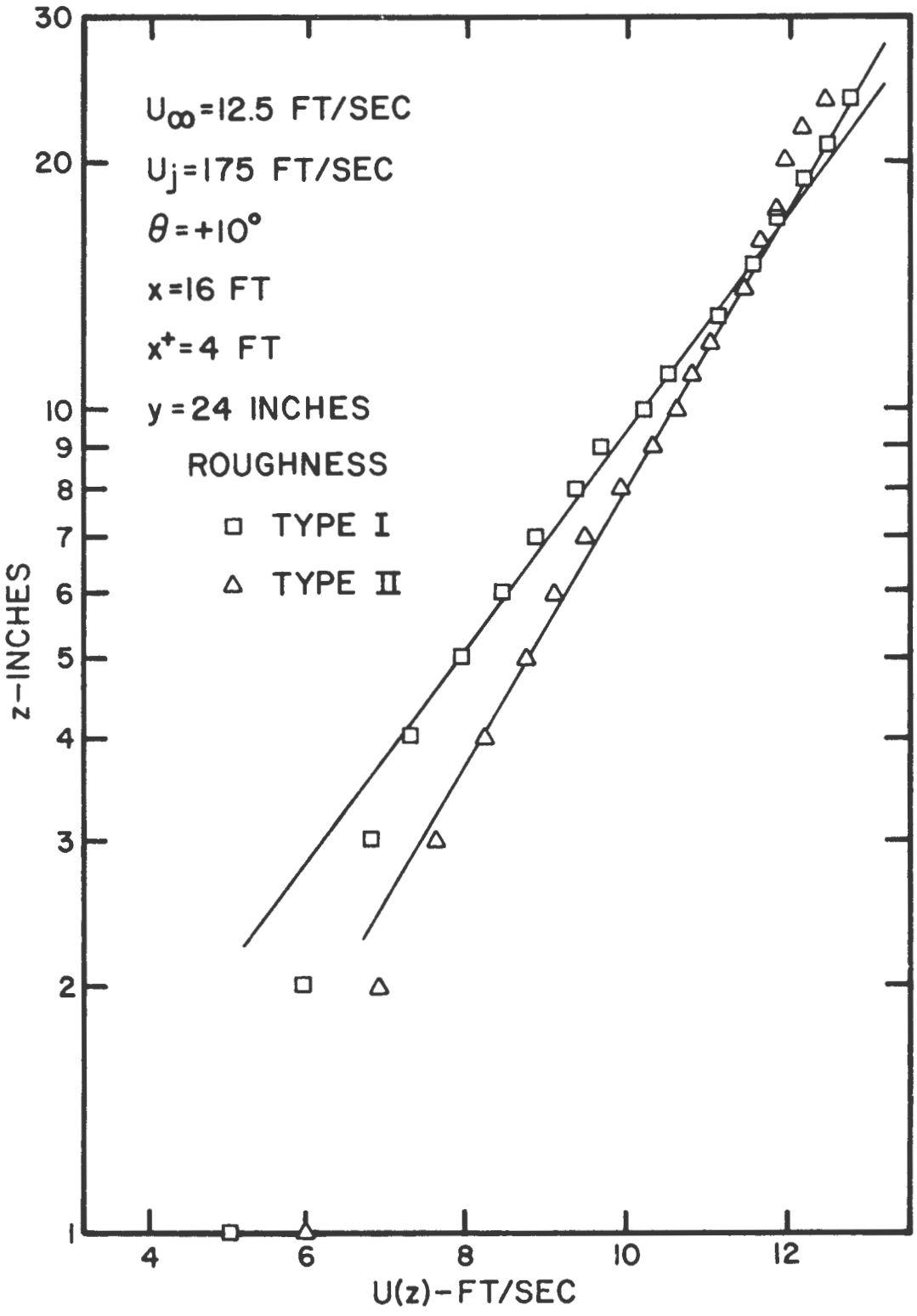

Figure 56. Log-Linear Plot of Mean Velocity Profiles of Counter-Jet Generated Boundary Layers Using Two Types of Surface Roughnesses

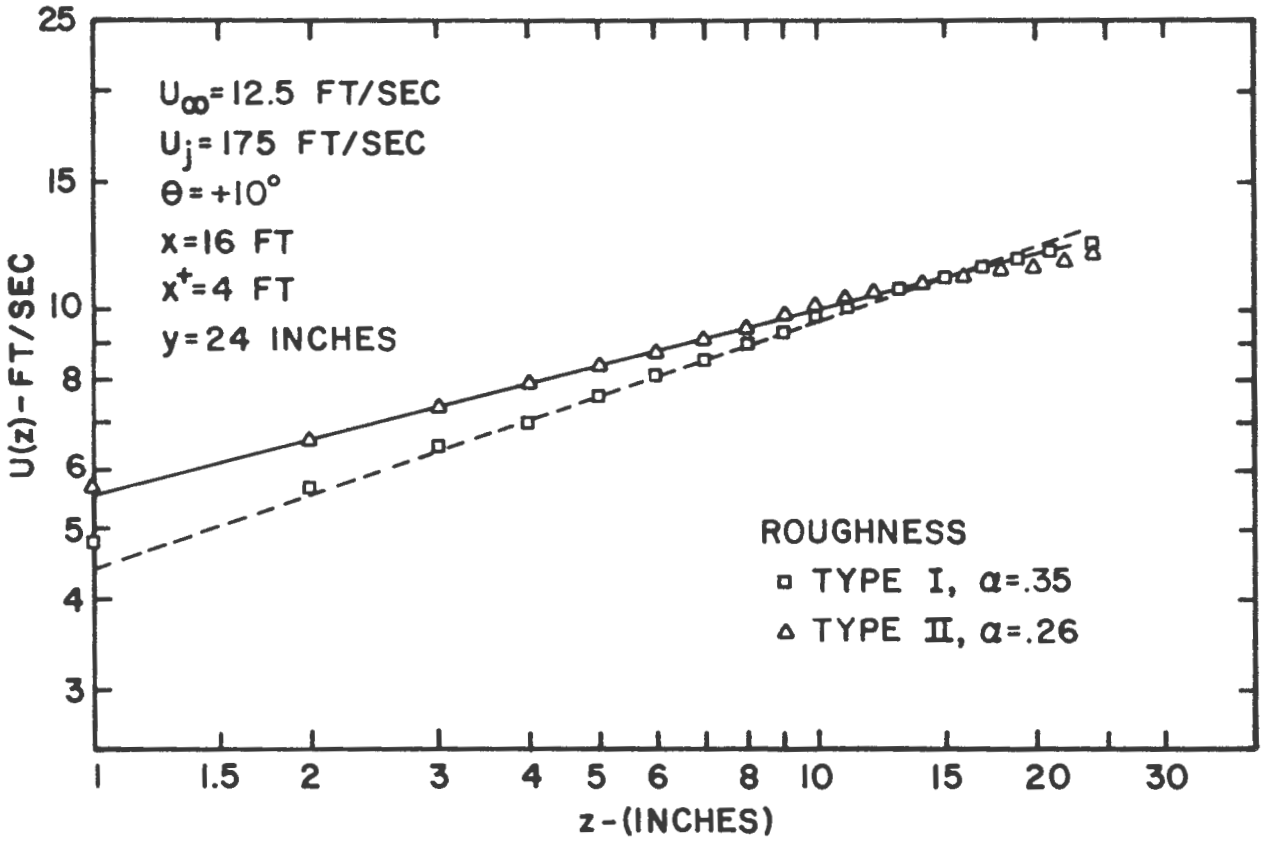

Figure 57. Log-Log Plot of Mean Velocity Profiles of Counter-Jet Generated Boundary Layers Using Two Types of Surface Roughnesses

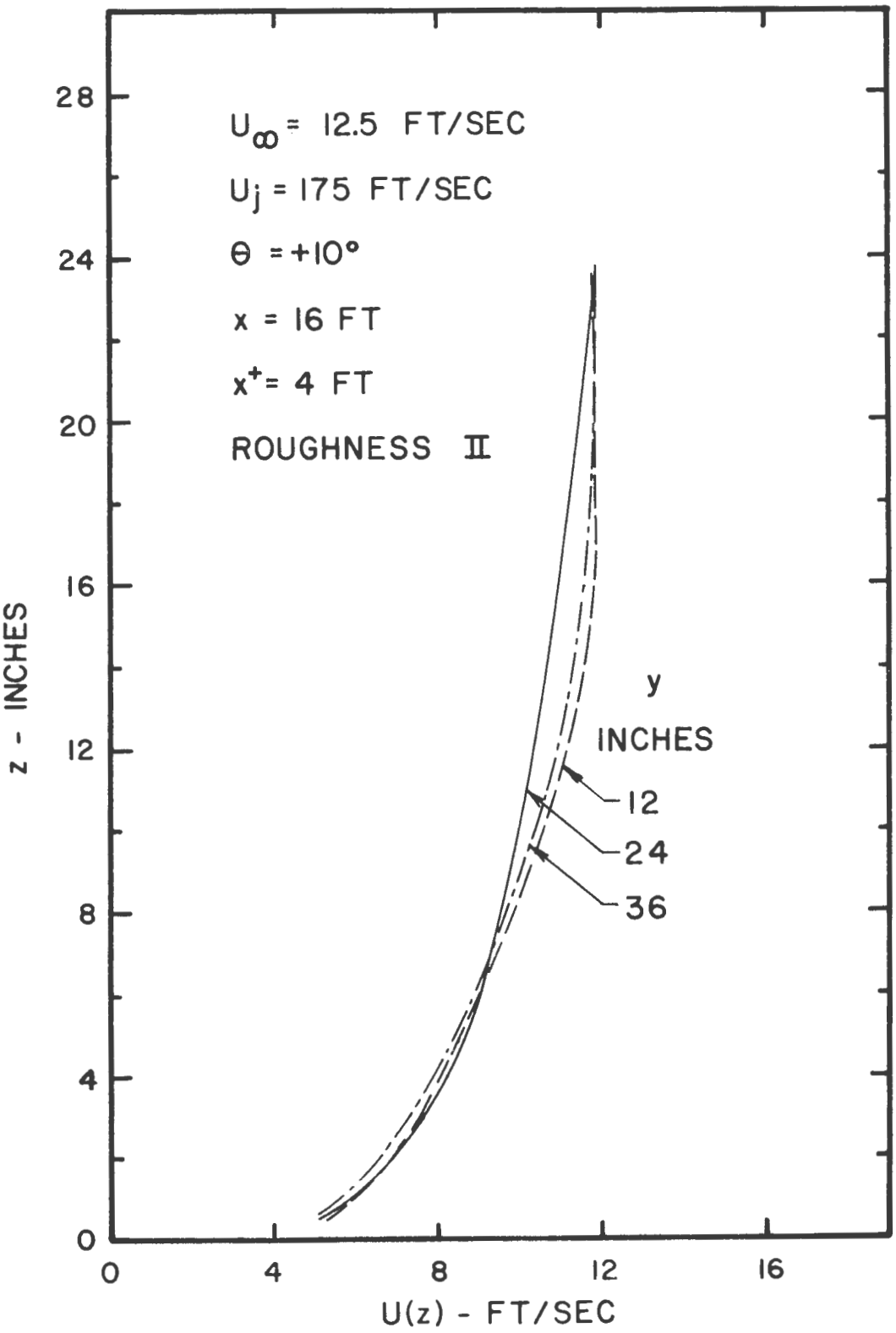

Figure 58. Transverse Uniformity of Mean Velocity Profiles of Counter-Jet Generated Boundary Layer With Surface Roughness Type II

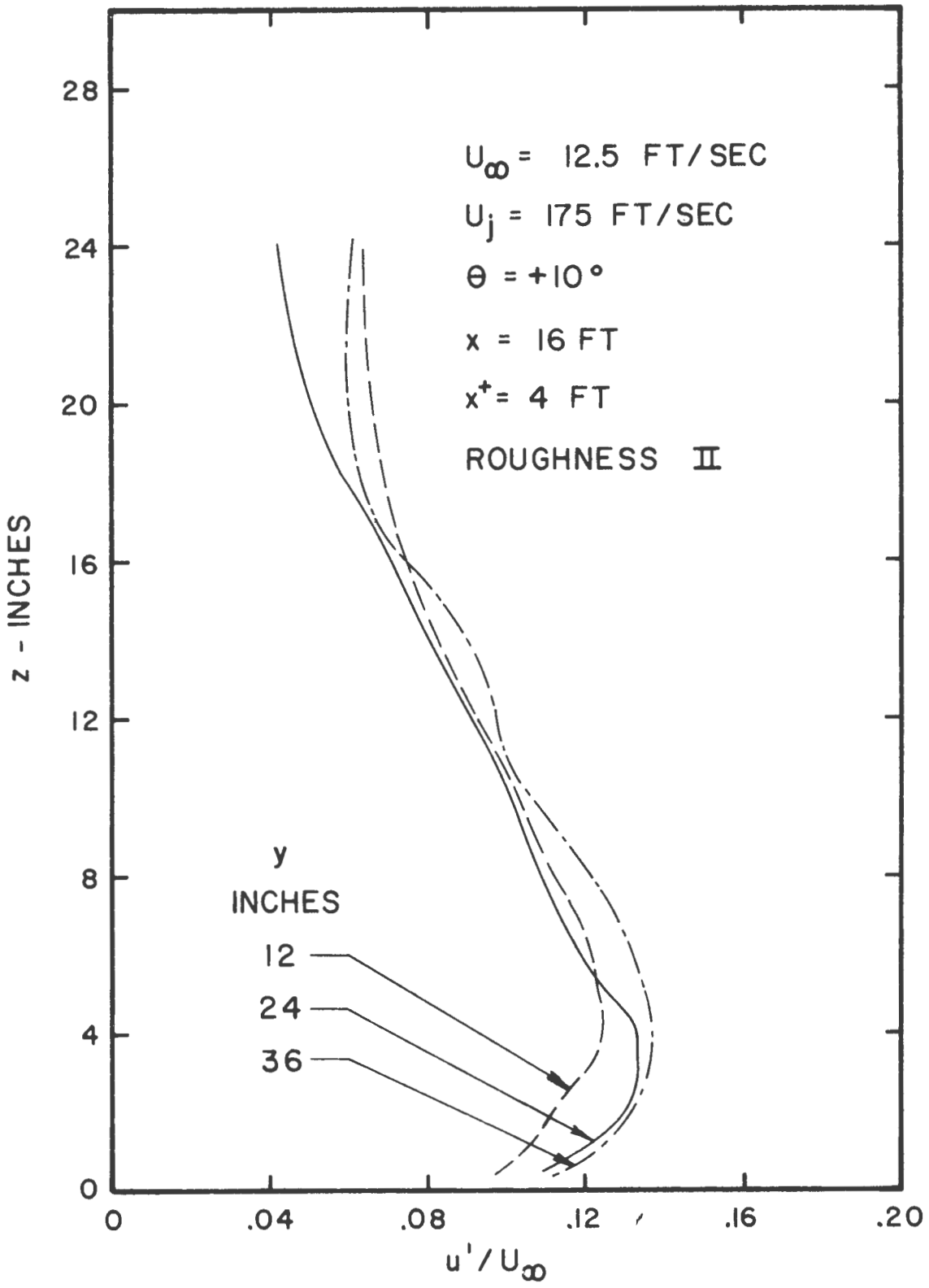

Figure 59. Transverse Uniformity of Turbulence Intensity Profiles of Counter-Jet Generated Boundary Layer With Surface Roughness Type II

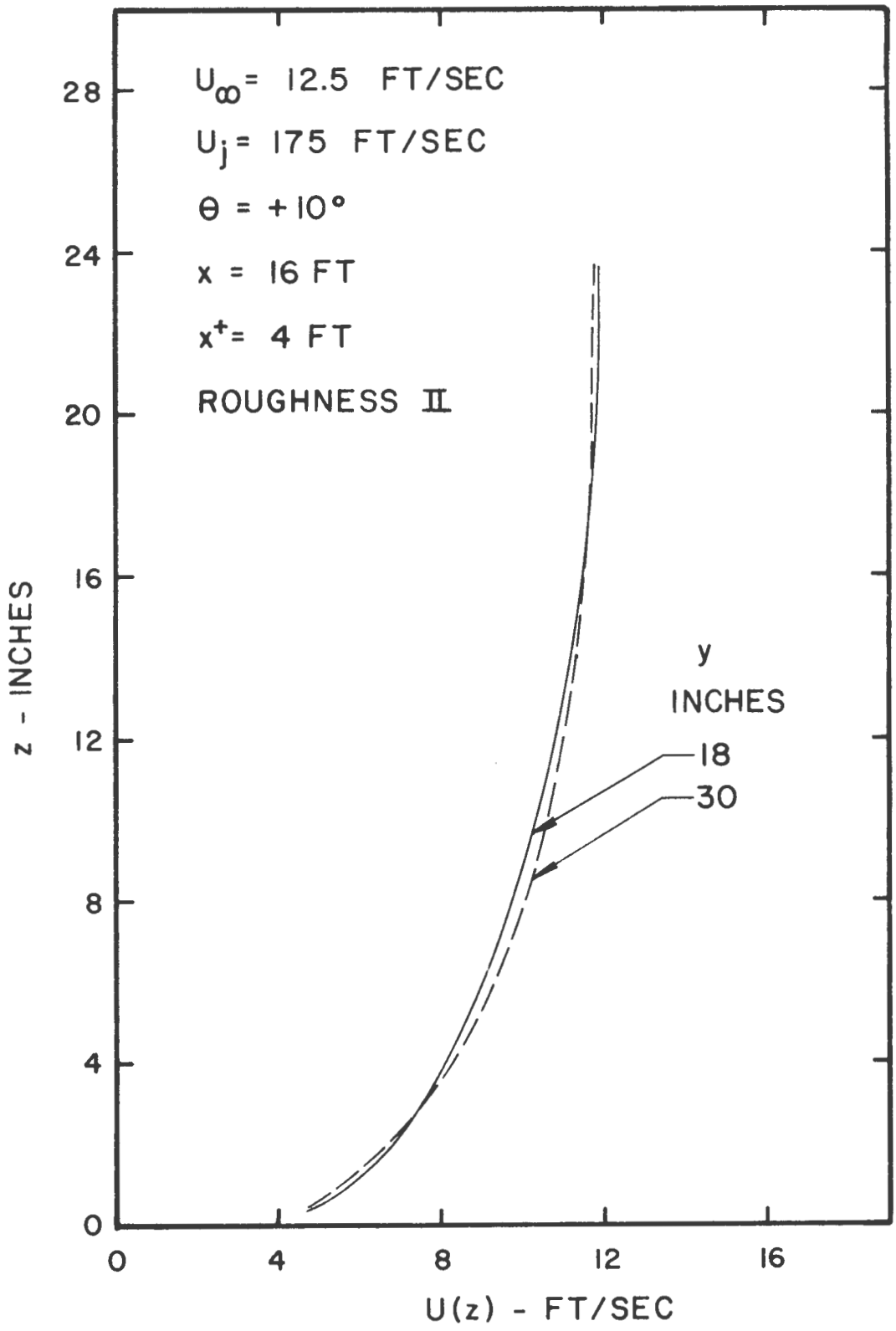

Figure 60. Transverse Uniformity of Mean Velocity Profiles of Central Portion of Counter-Jet Generated Boundary Layer With Surface Roughness Type II

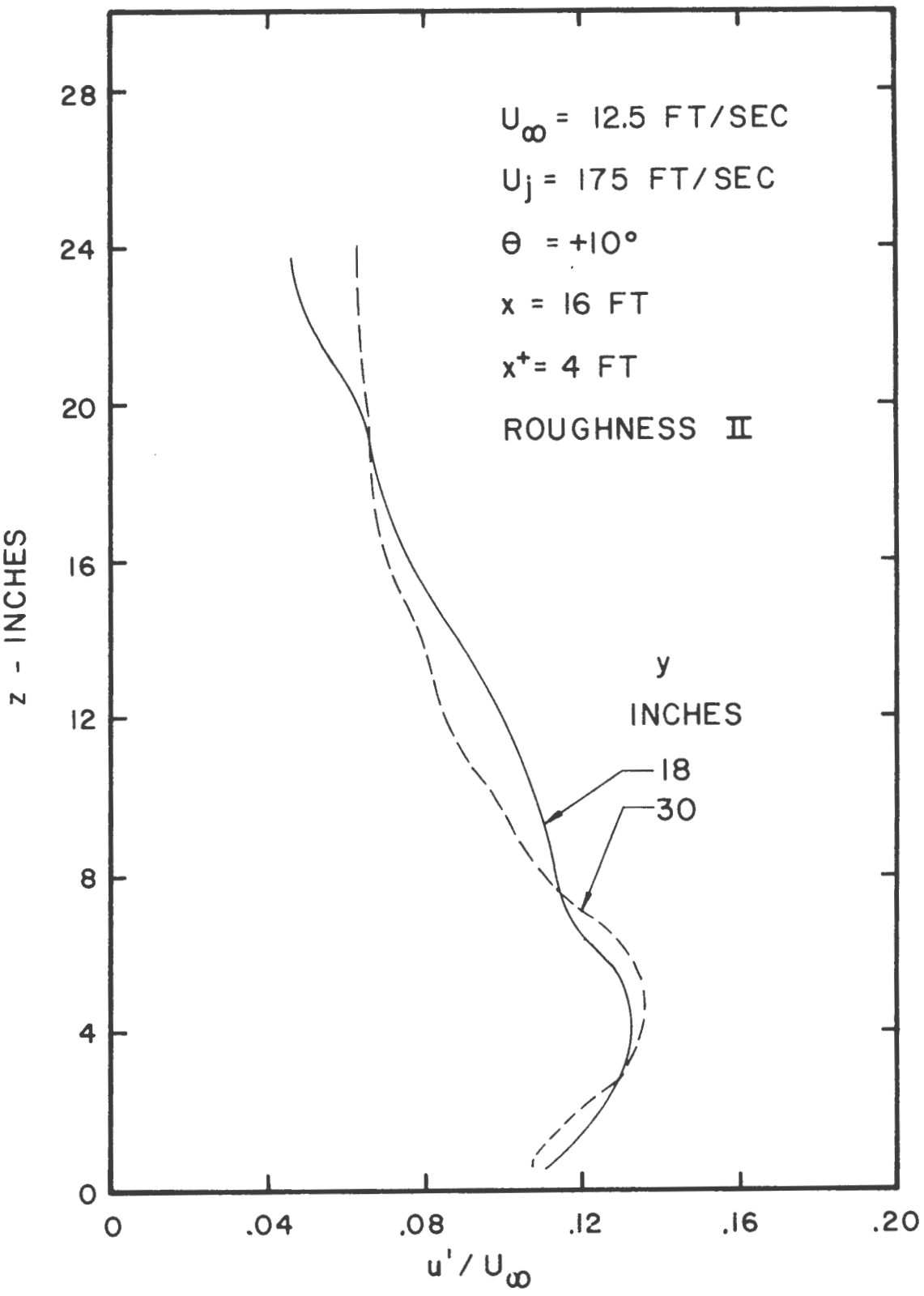

Figure 61. Transverse Uniformity of Turbulence Intensity Profiles of Central Portion of Counter-Jet Generated Boundary Layer With Surface Roughness Type II

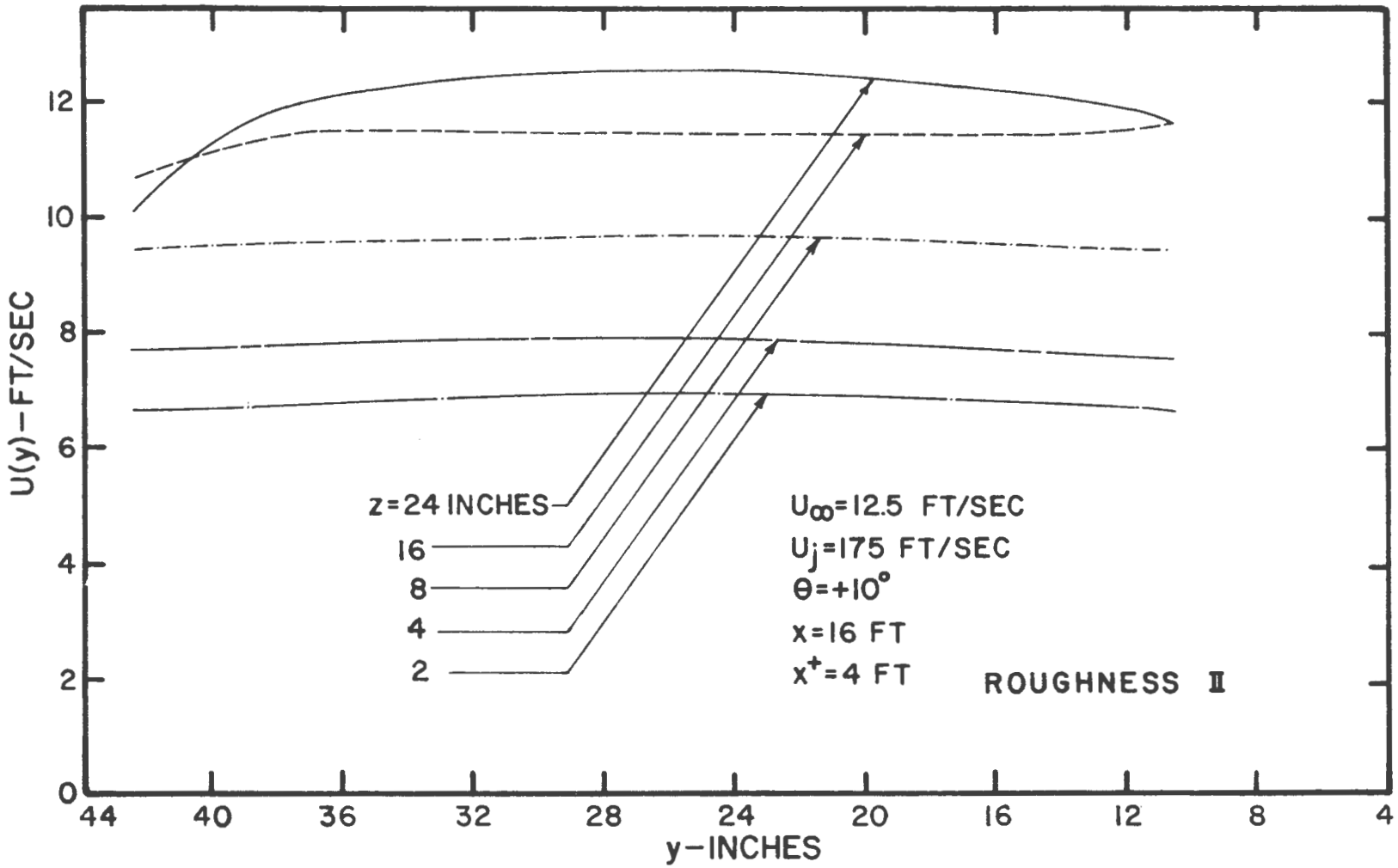

Figure 62. Transverse Profiles of Mean Velocity in Counter-Jet Generated Boundary Layer With Surface Roughness Type II

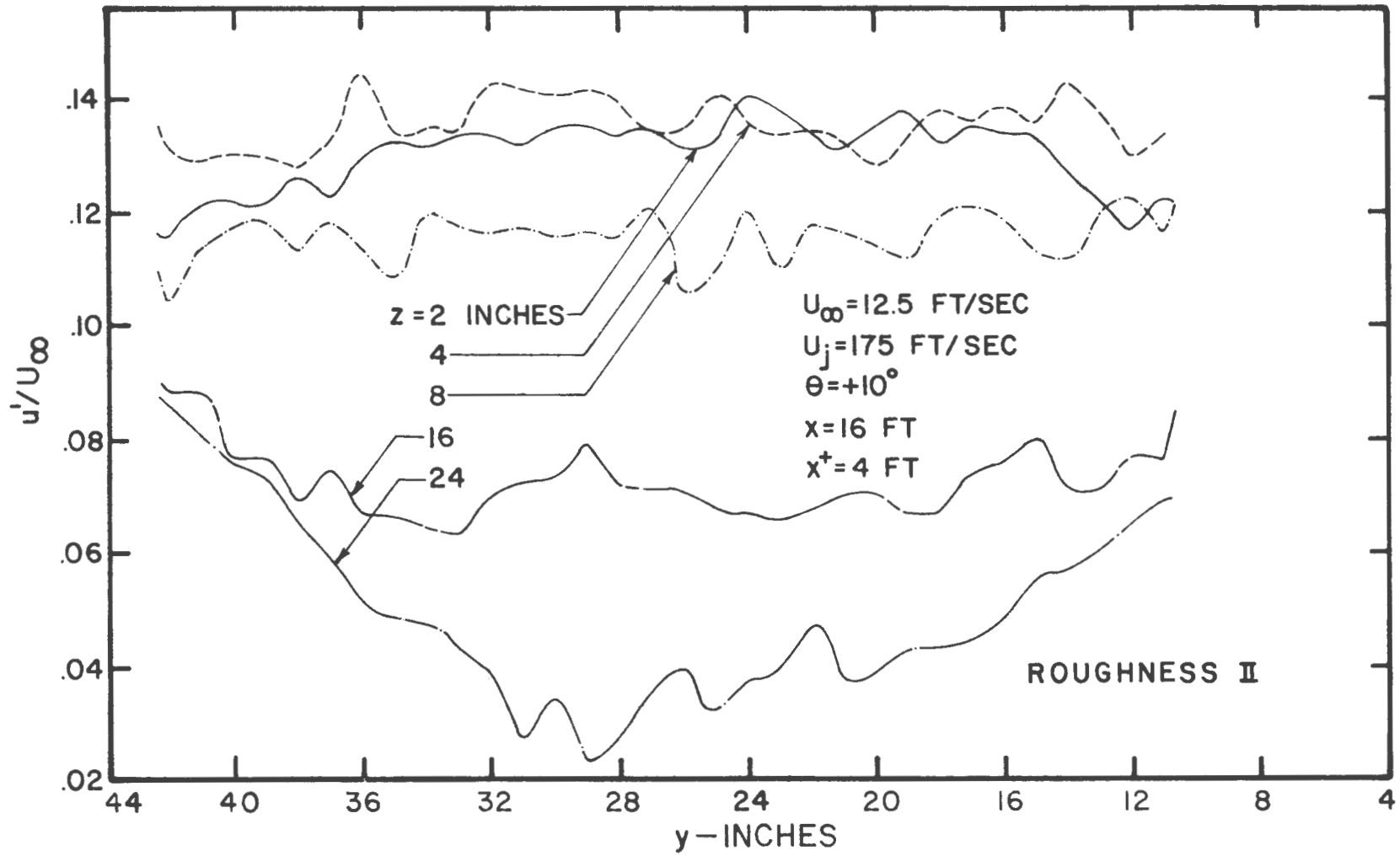

Figure 63. Transverse Profiles of Turbulence Intensity in Counter-Jet Generated Boundary Layer With Surface Roughness Type II

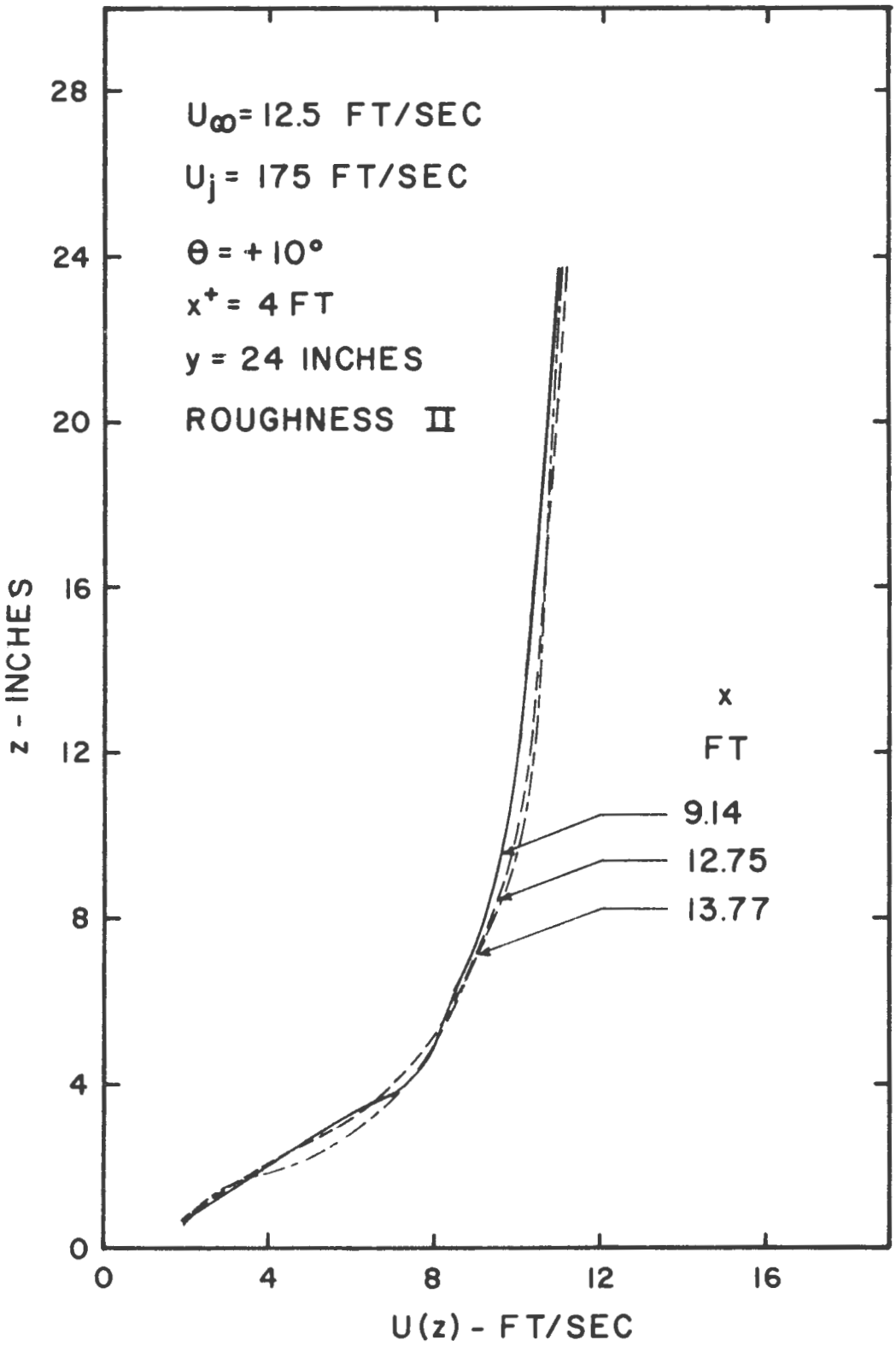

Figure 64. Downstream Development of Mean Velocity Profile of Counter-Jet Generated Boundary Layer Taken Midway Between Elements of Surface Roughness Type II

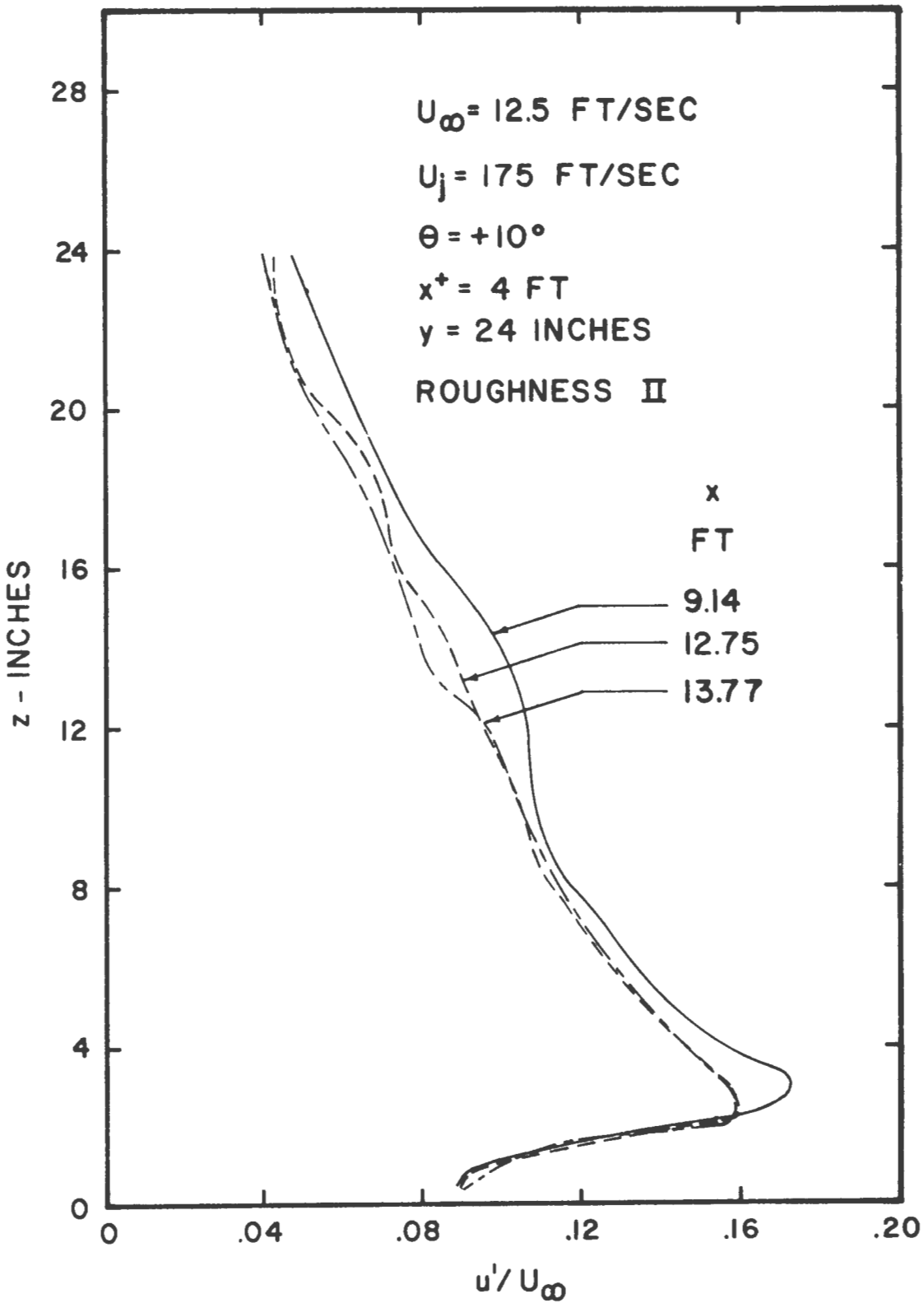

Figure 65. Downstream Development of Turbulence Intensity Profile of Counter-Jet Generated Boundary Layer Taken Midway Between Elements of Surface Roughness Type II

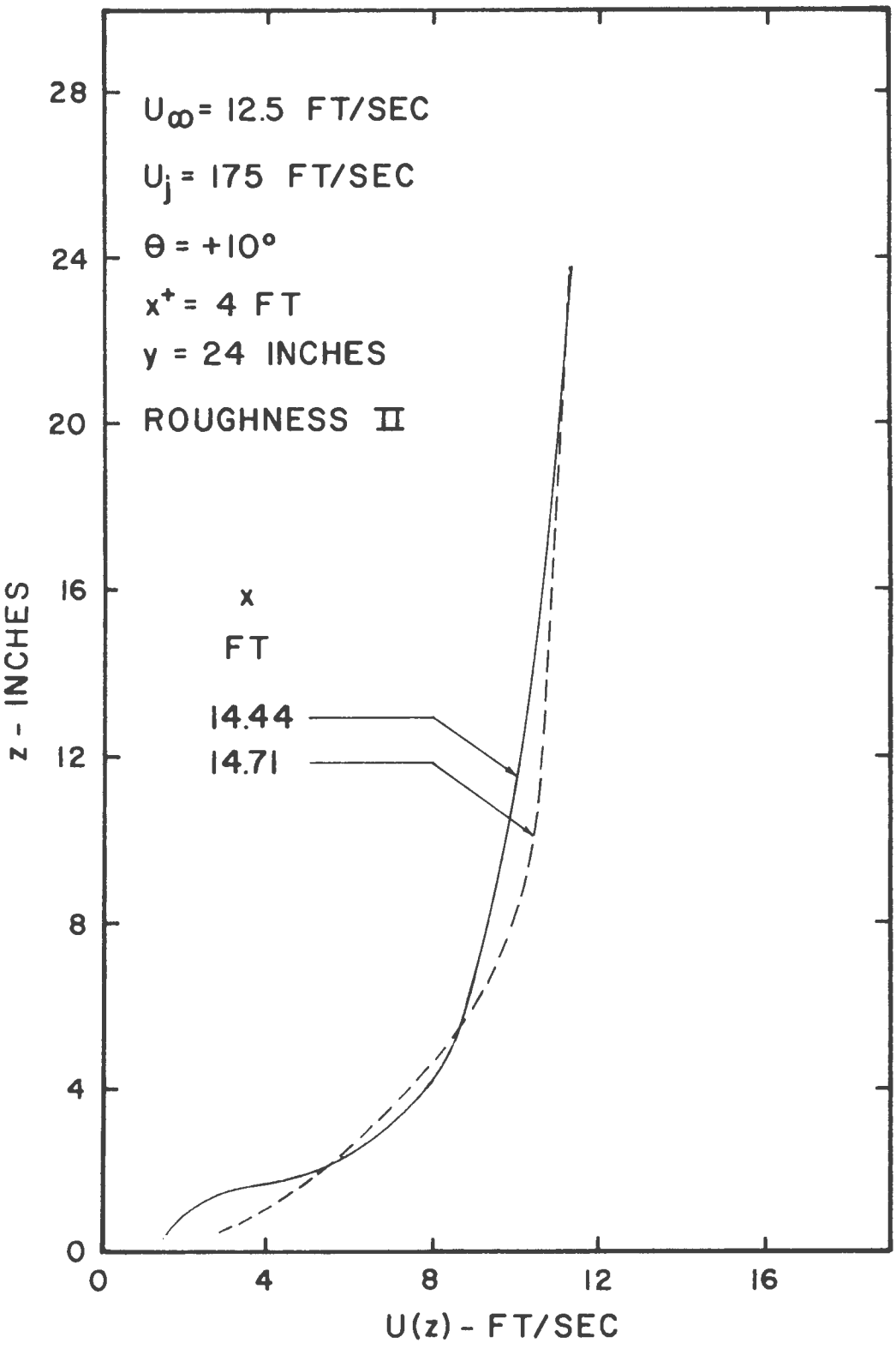

Figure 66. Development of Mean Velocity Profile of Counter-Jet Generated Boundary Layer Downstream of Last Element of Surface Roughness Type II

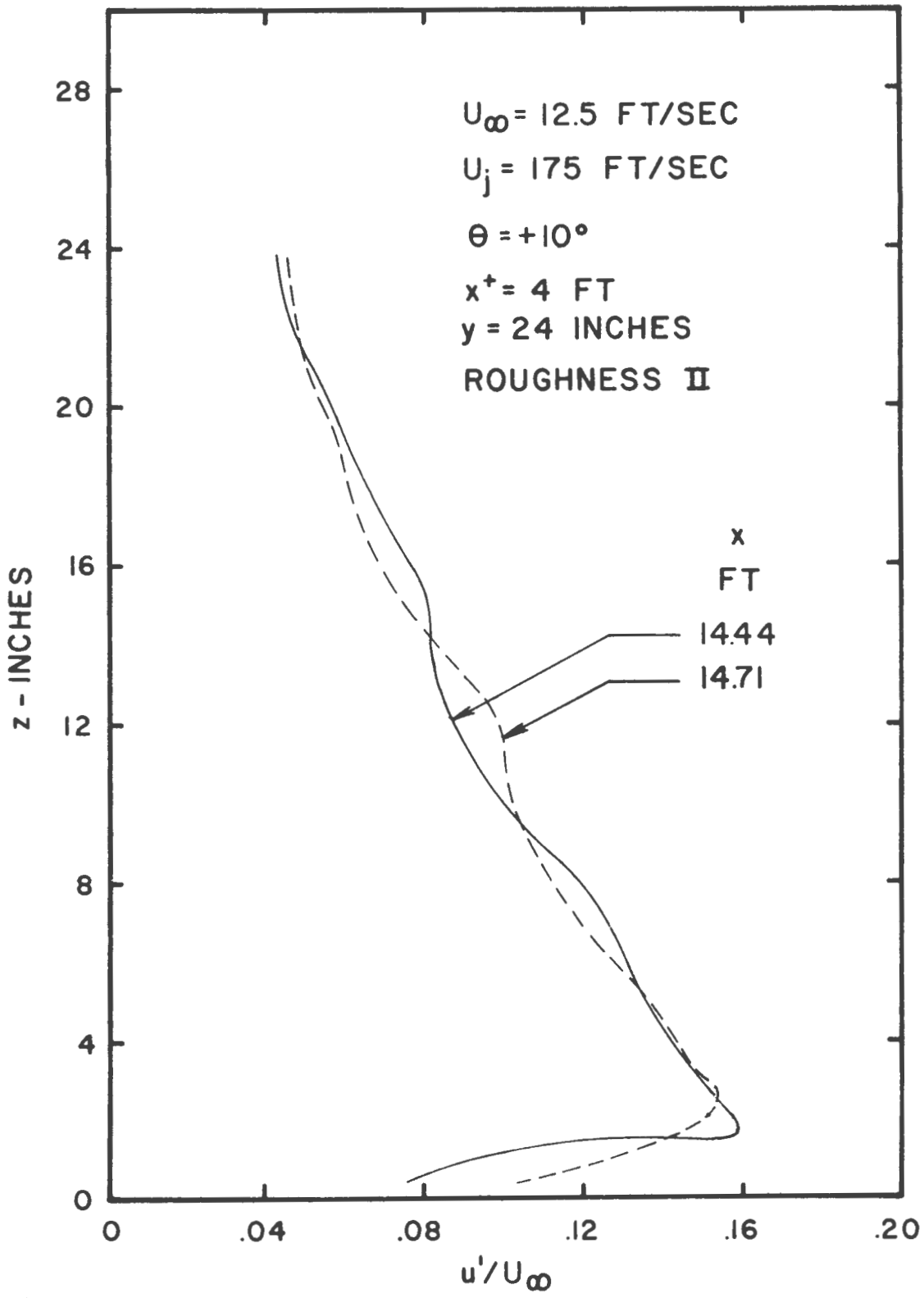

Figure 67. Development of Turbulence Intensity Profile of Counter-Jet Generated Boundary Layer Downstream of Last Element of Surface Roughness Type II

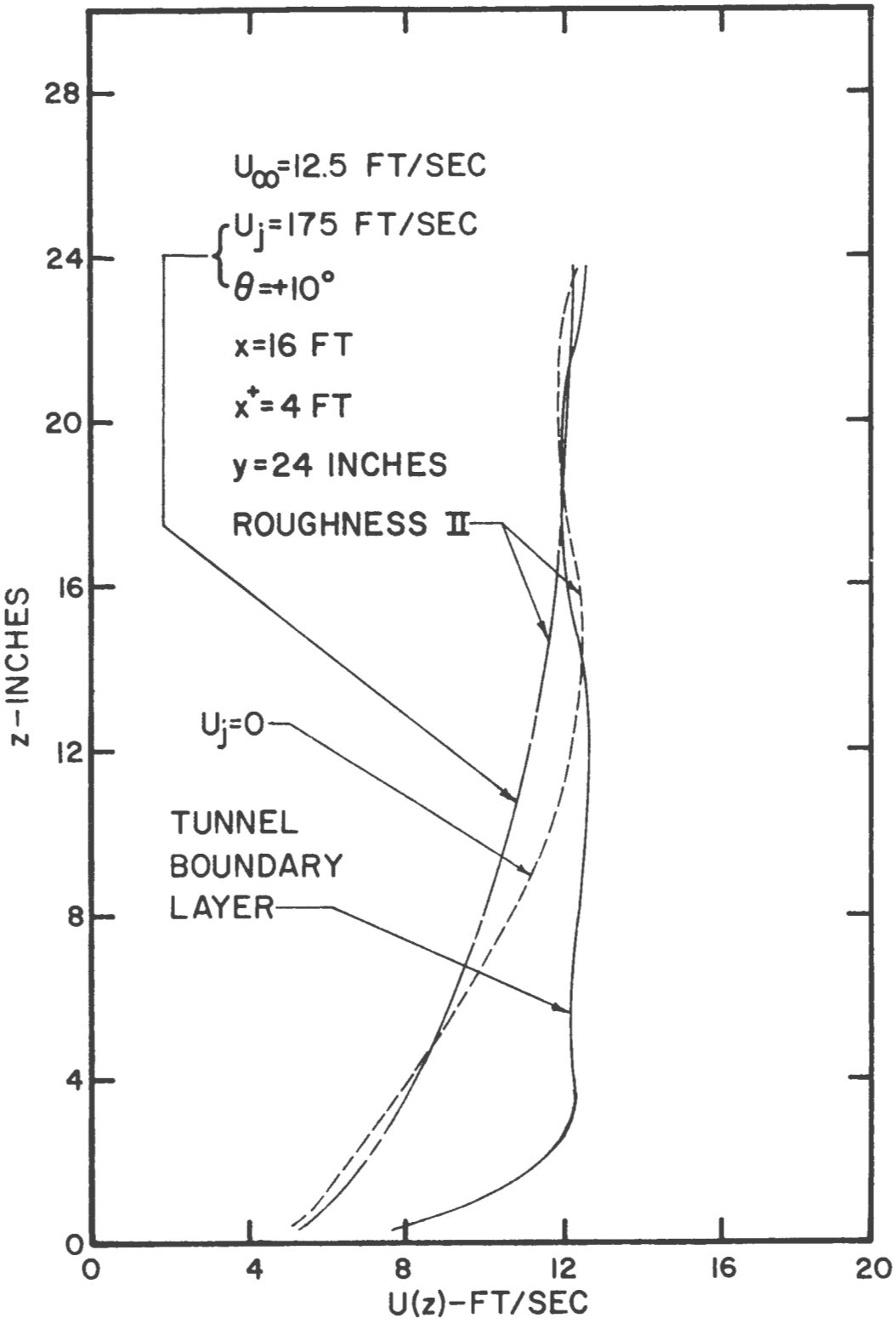

Figure 68. Mean Velocity Profiles of Boundary Layers Selected for Measurements of Flowfield Near Bluff-Body Model

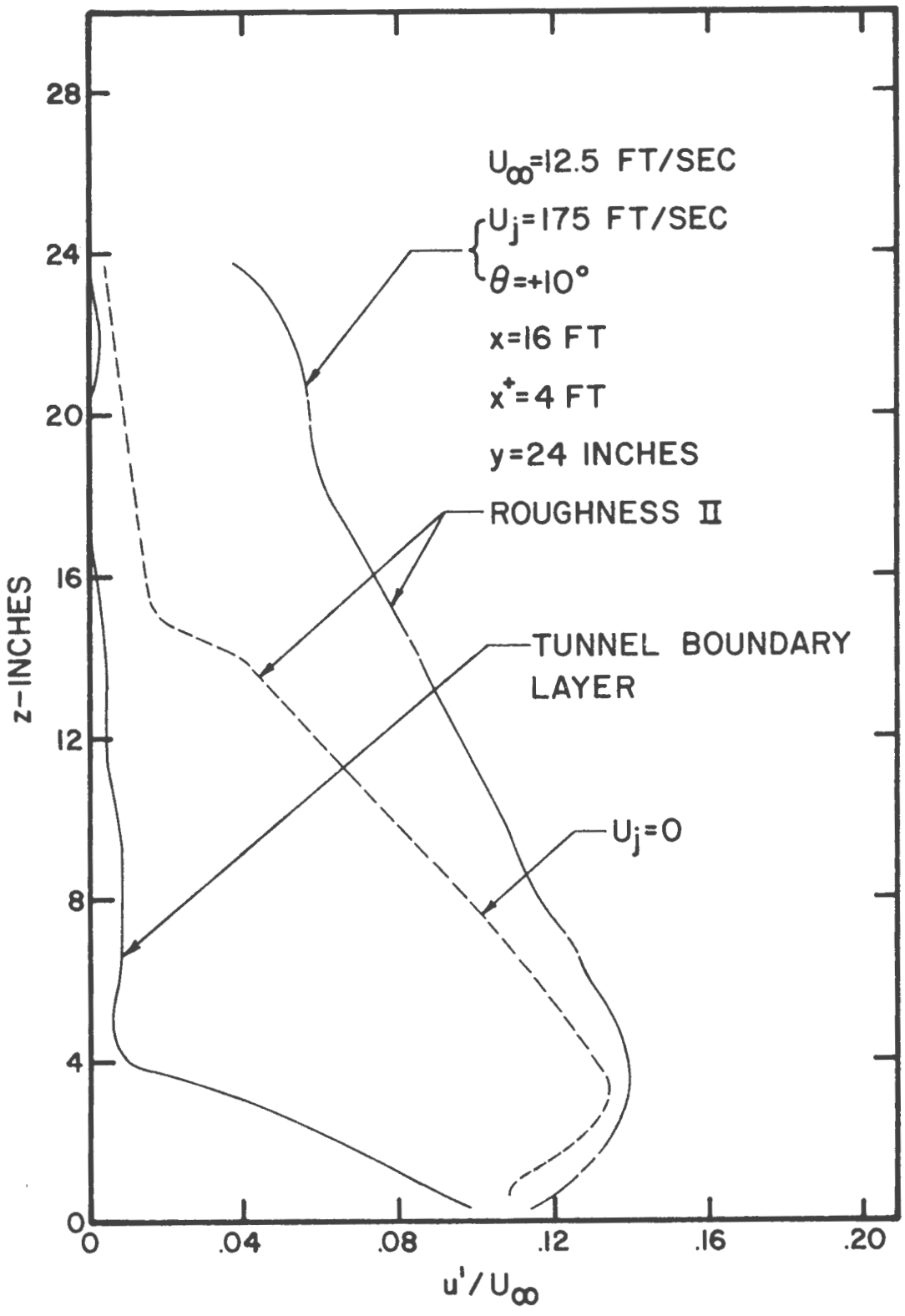

Figure 69. Turbulence Intensity Profiles of Boundary Layers Selected for Measurements of Flowfield Near Bluff-Body Model

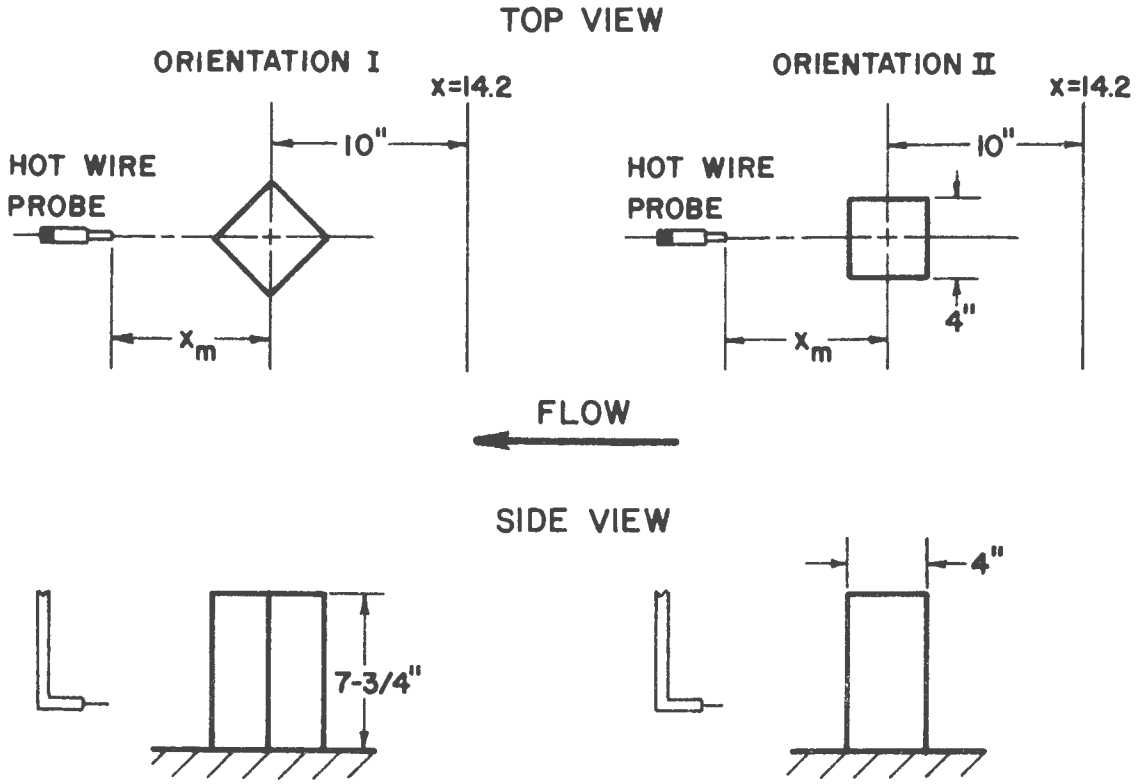

RANGE AND COORDINATES OF SURVEYS

x_m(INCHES)	0	8.75	15	0	8.75	15
y (INCHES)	24	24	24	10.6-42.4	10.6-42.4	10.6-42.4
z (INCHES)	7.9—24	.1—24	.1—24	8.13	2,4,7,8,10	2,4,7,8,10

ORIENTATION	$\left(\frac{\text{HEIGHT}}{\text{WIDTH}}\right)_{\text{MODEL}}$	MODEL CROSS-SECTION AREA (IN^2)	TUNNEL BLOCKAGE (%)
I	1.37	43.84	1.27
II	1.94	31.00	0.90

Figure 70. Schematic of Bluff-Body Model and Orientations, Including Range and Coordinates of Flowfield Surveys

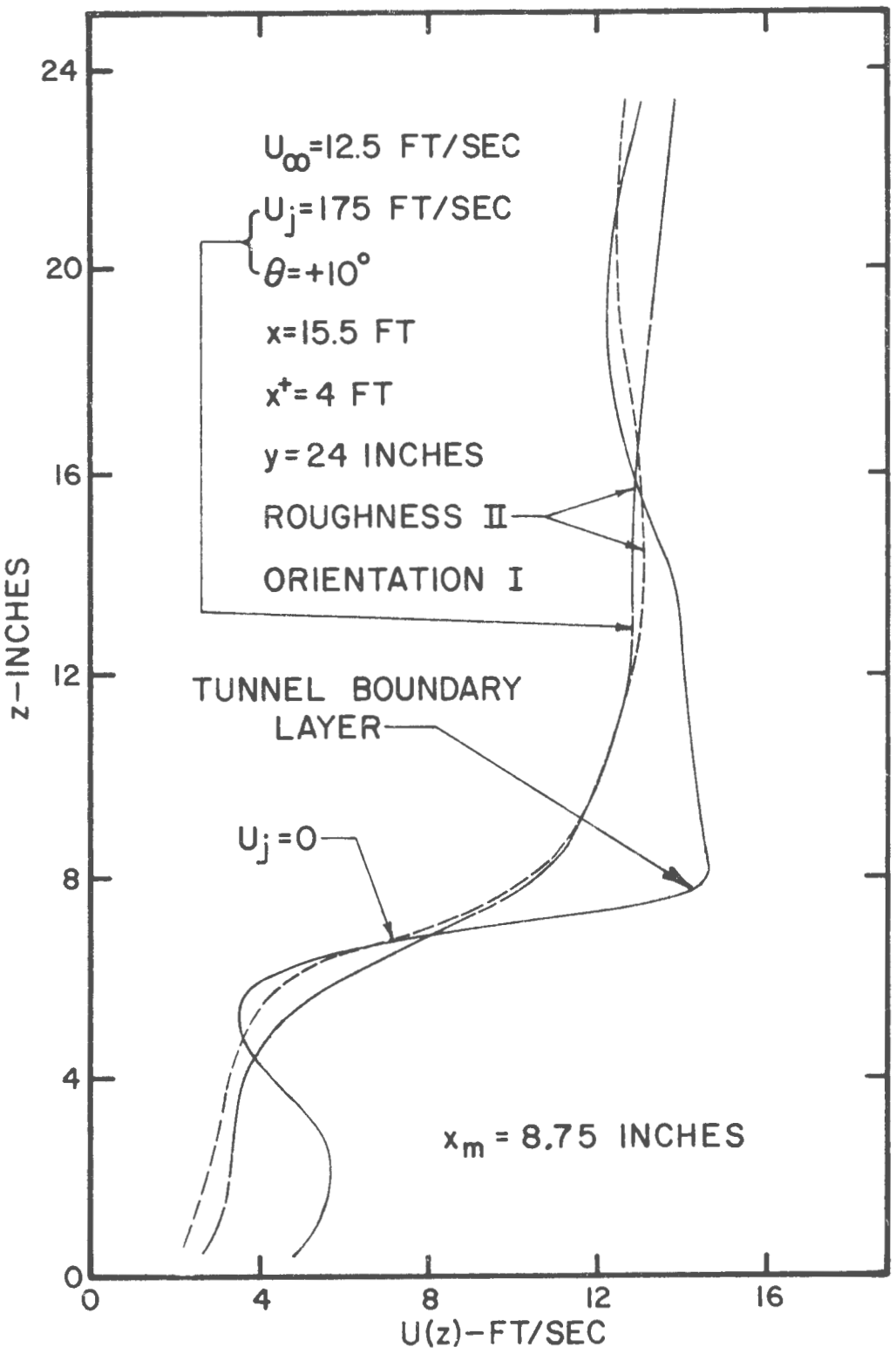

Figure 71. Vertical Mean Velocity Profiles Measured Along Model-Wake Centerline at x_m = 8.75 in. for Orientation I

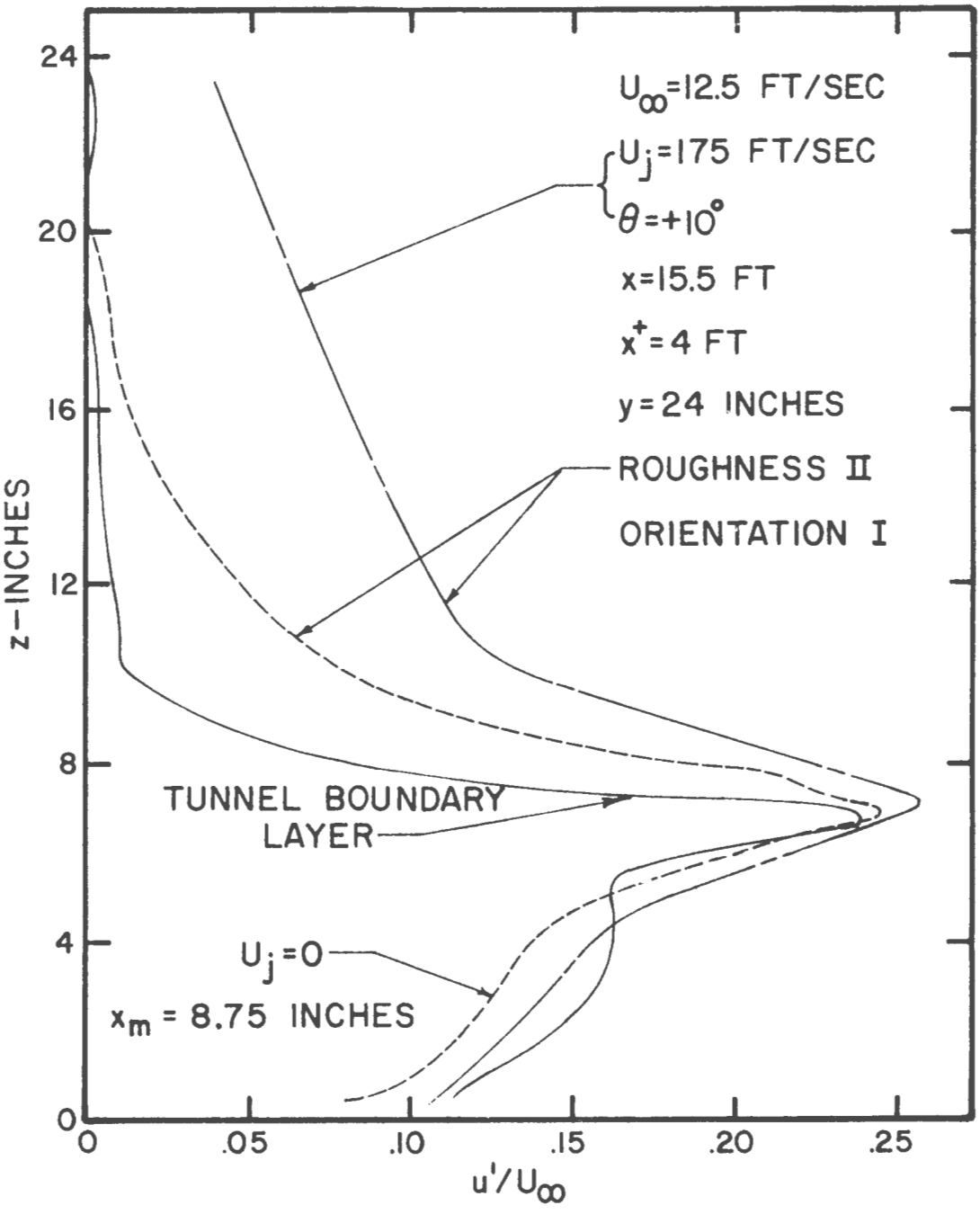

Figure 72. Vertical Turbulence Intensity Profiles Measured Along Model-Wake Centerline at x_m = 8.75 in. for Orientation I

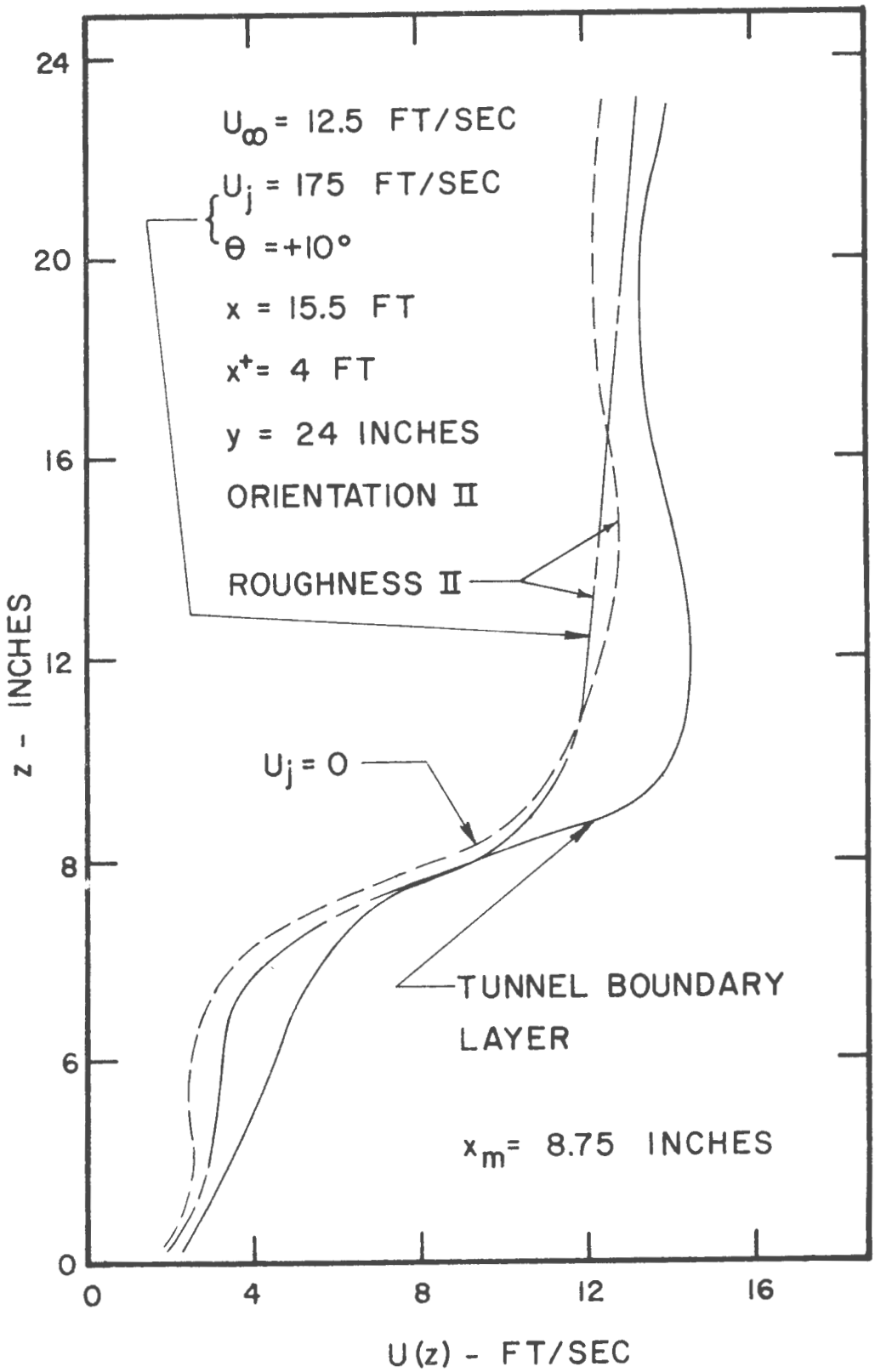

Figure 73. Vertical Mean Velocity Profiles Measured Along Model-Wake Centerline at x_m = 8.75 in. for Orientation II

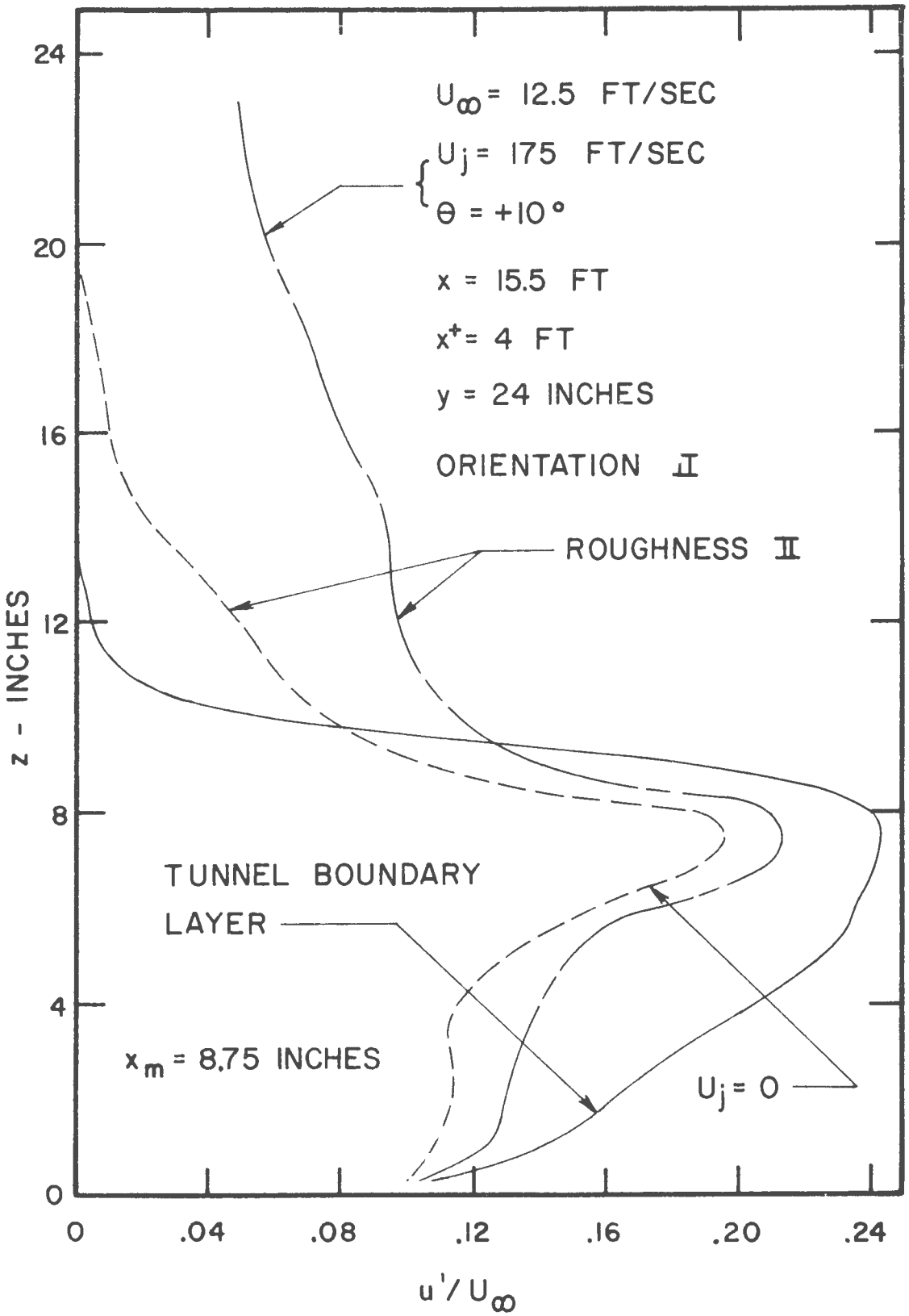

Figure 74. Vertical Turbulence Intensity Profiles Measured Along Model-Wake Centerline at x_m = 8.75 in. for Orientation II

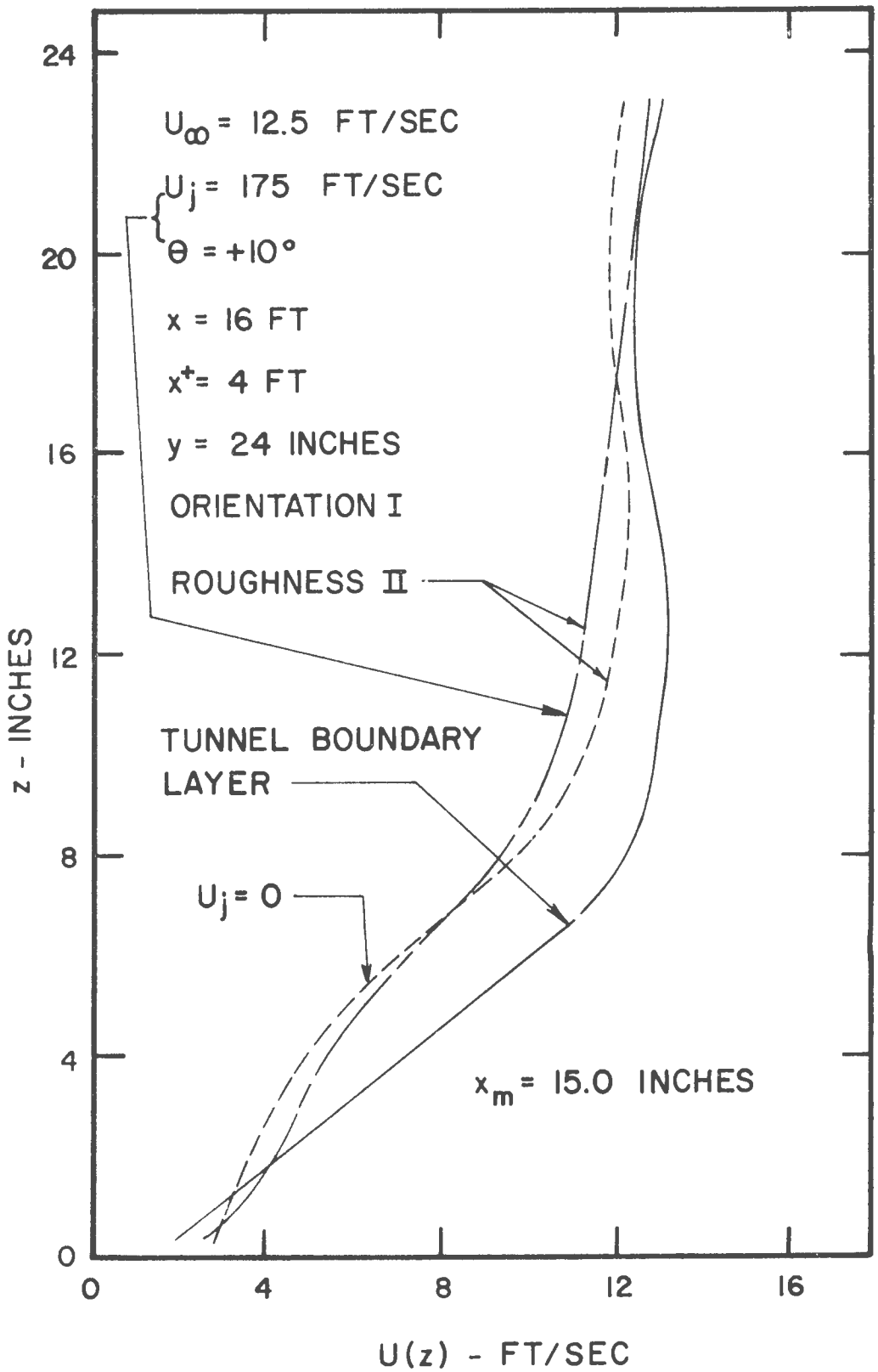

Figure 75. Vertical Mean Velocity Profiles Measured Along Model-Wake Centerline at x_m = 15.0 in. for Orientation I

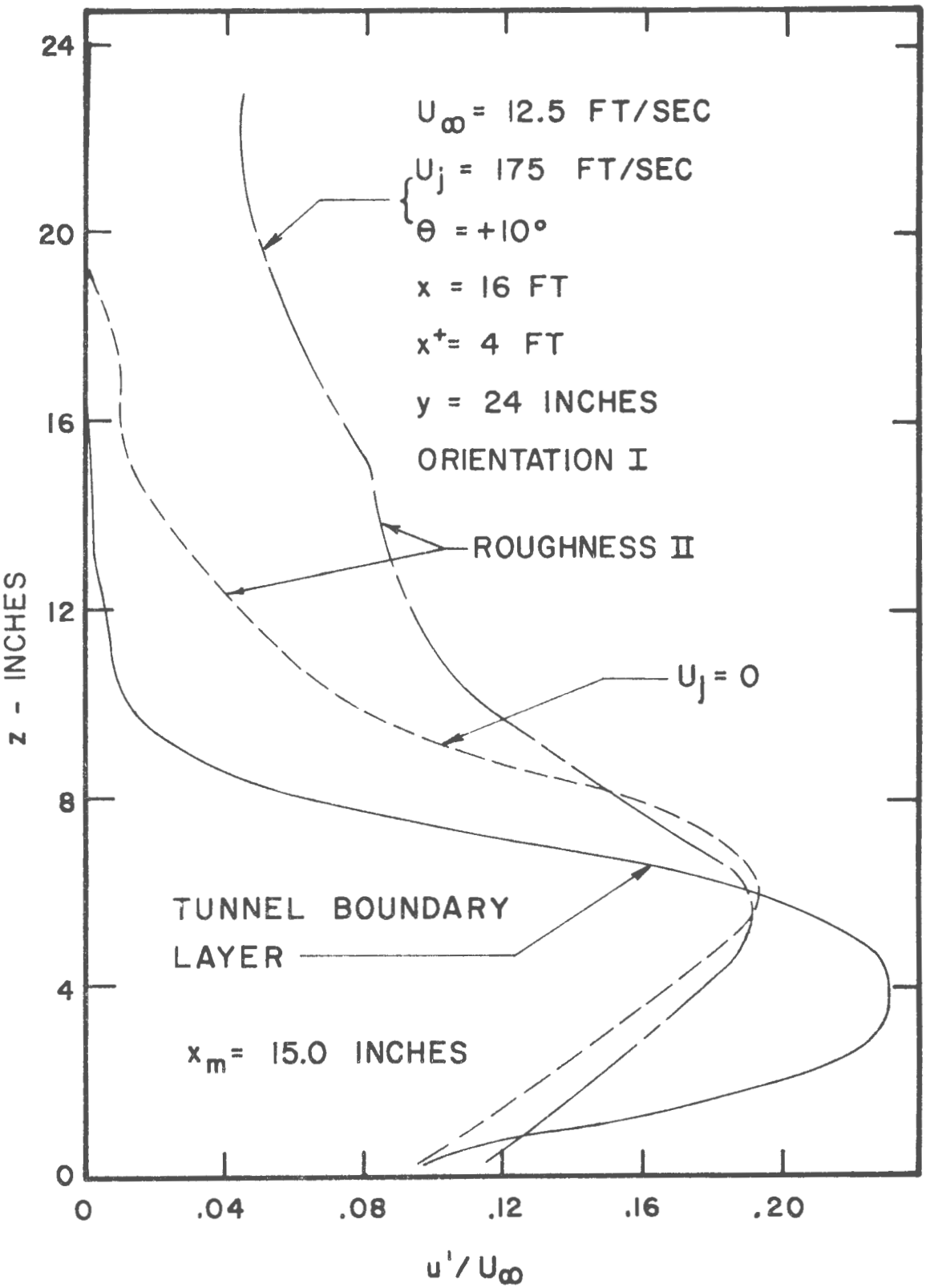

Figure 76. Vertical Turbulence Intensity Profiles Measured Along Model-Wake Centerline at x_m = 15.0 in. for Orientation I

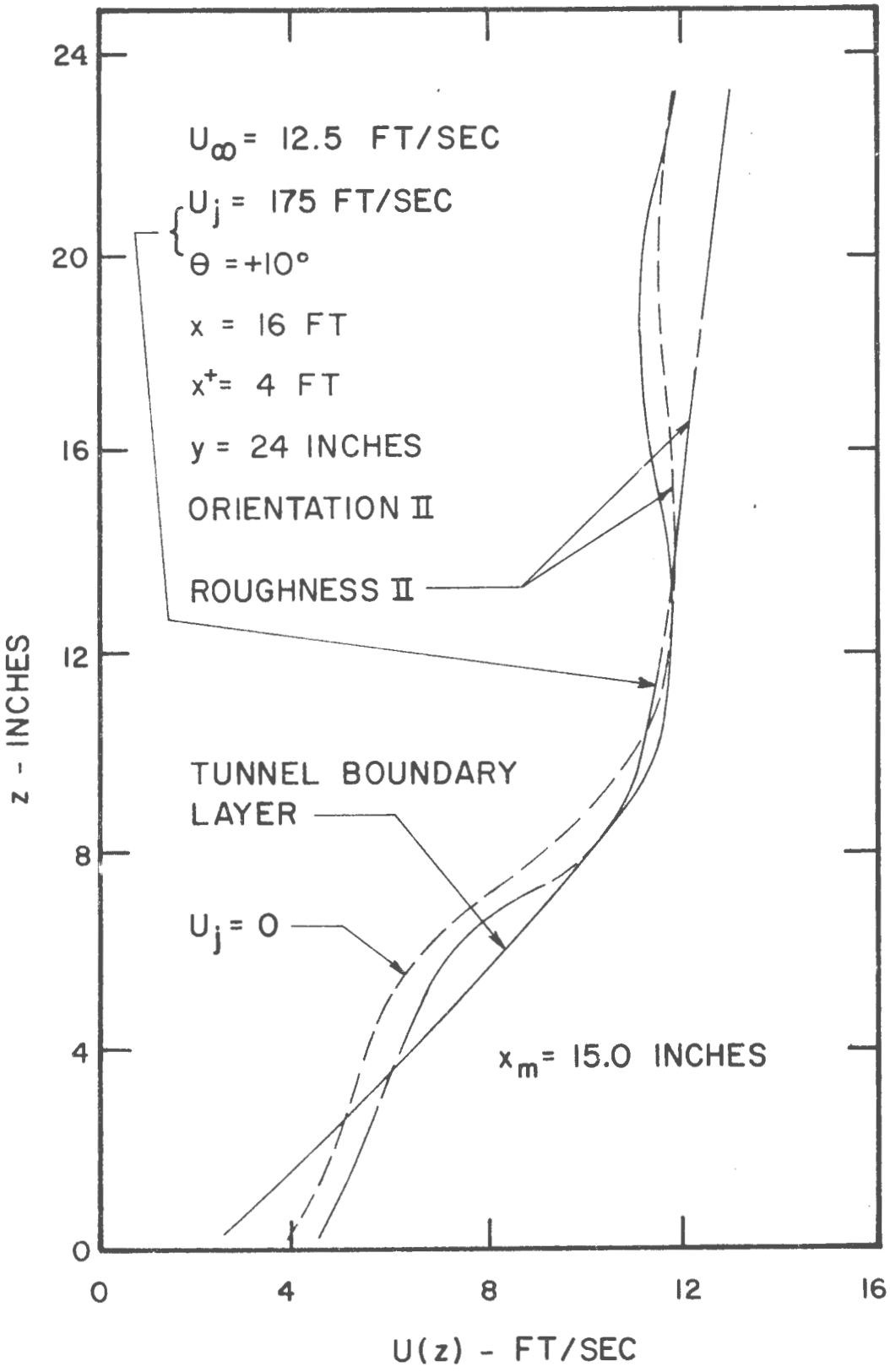

Figure 77. Vertical Mean Velocity Profiles Measured Along Model-Wake Centerline at x_m = 15.0 in. for Orientation II

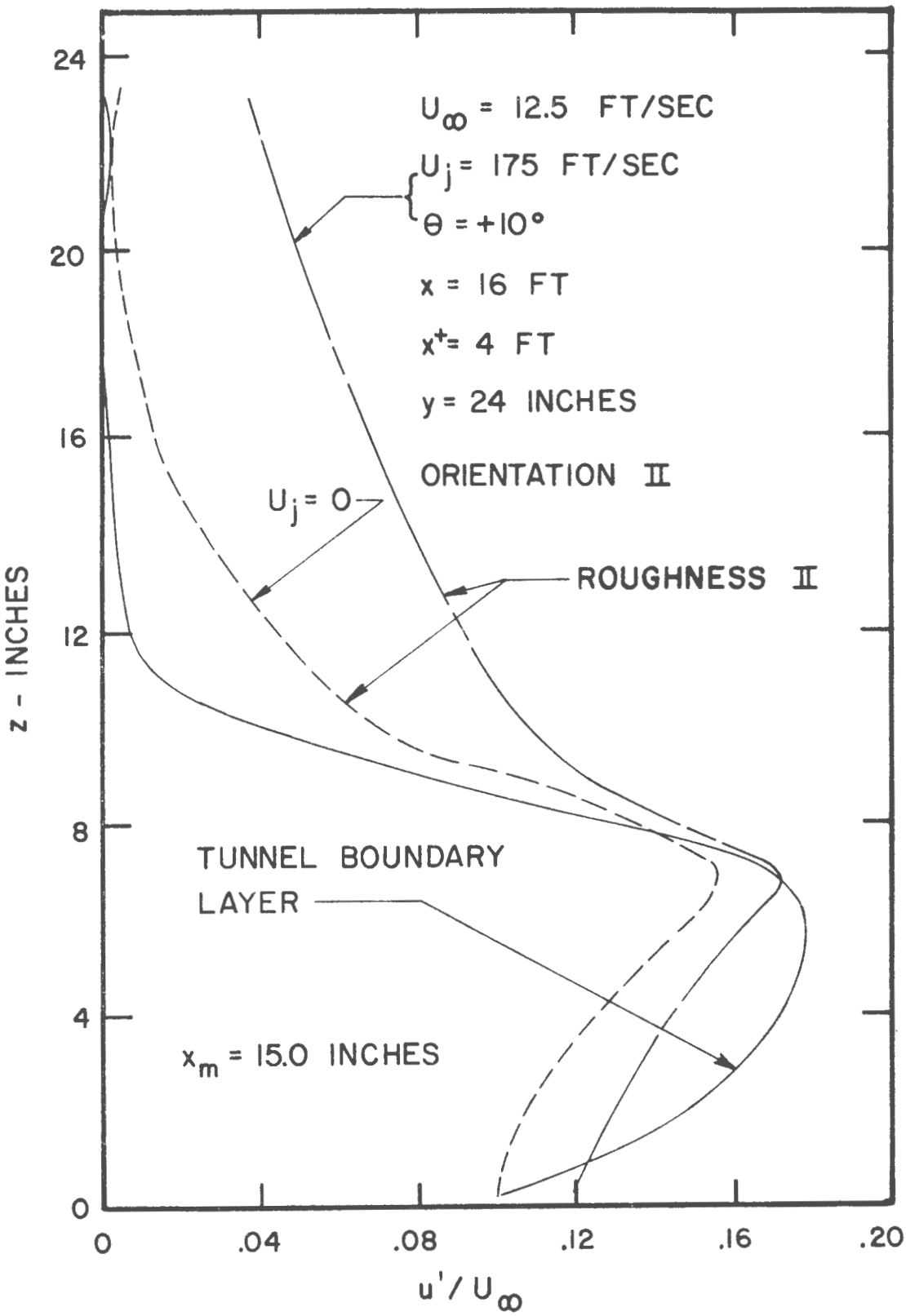

Figure 78. Vertical Turbulence Intensity Profiles Measured Along Model-Wake Centerline at x_m = 15.0 in. for Orientation II

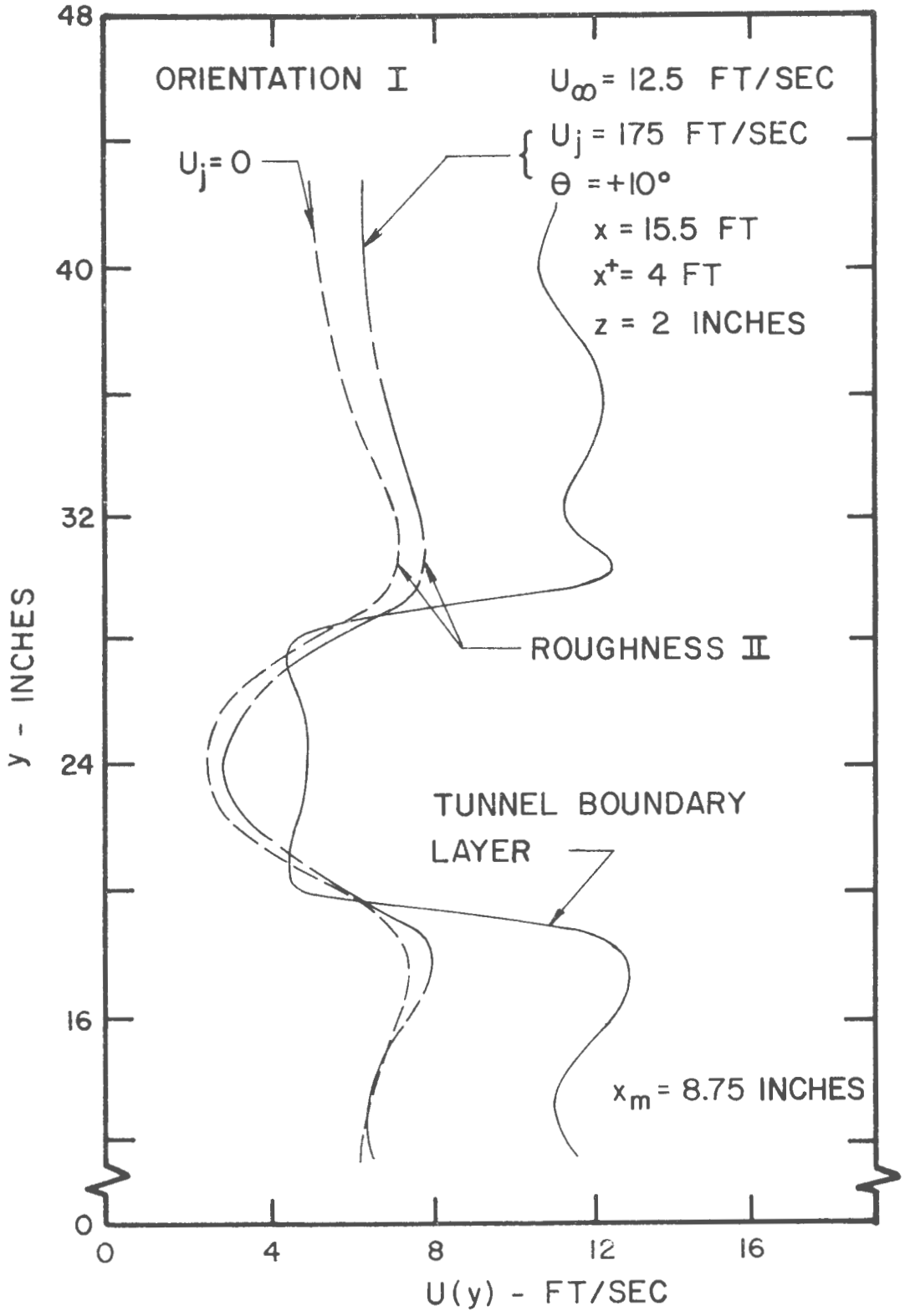

Figure 79. Transverse Mean Velocity Profiles of Model-Wake at x_m = 8.75 in. and z = 2 in. for Orientation I

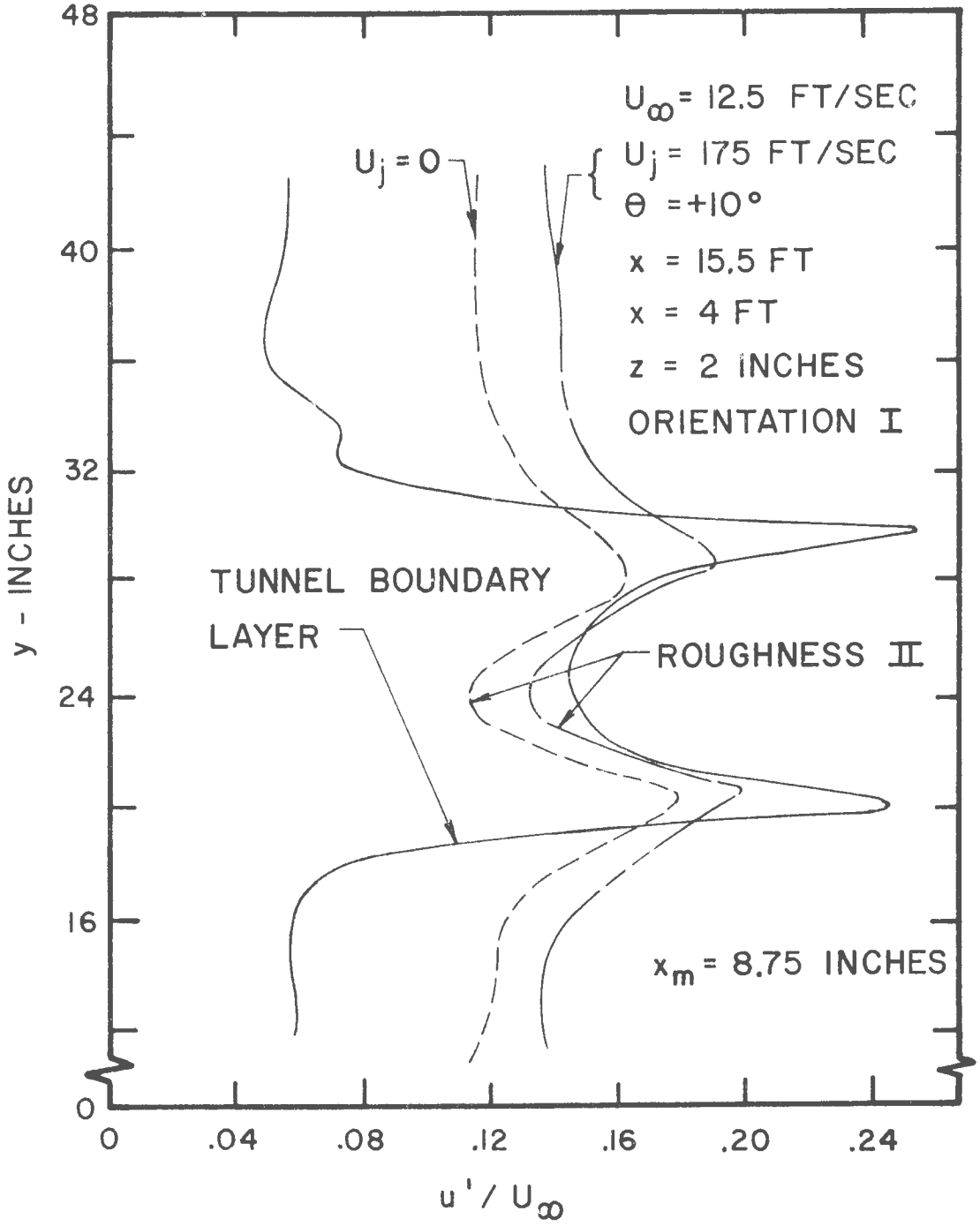

Figure 80. Transverse Turbulence Intensity Profiles of Model-Wake at x_m = 8.75 in. and z = 2 in. for Orientation I

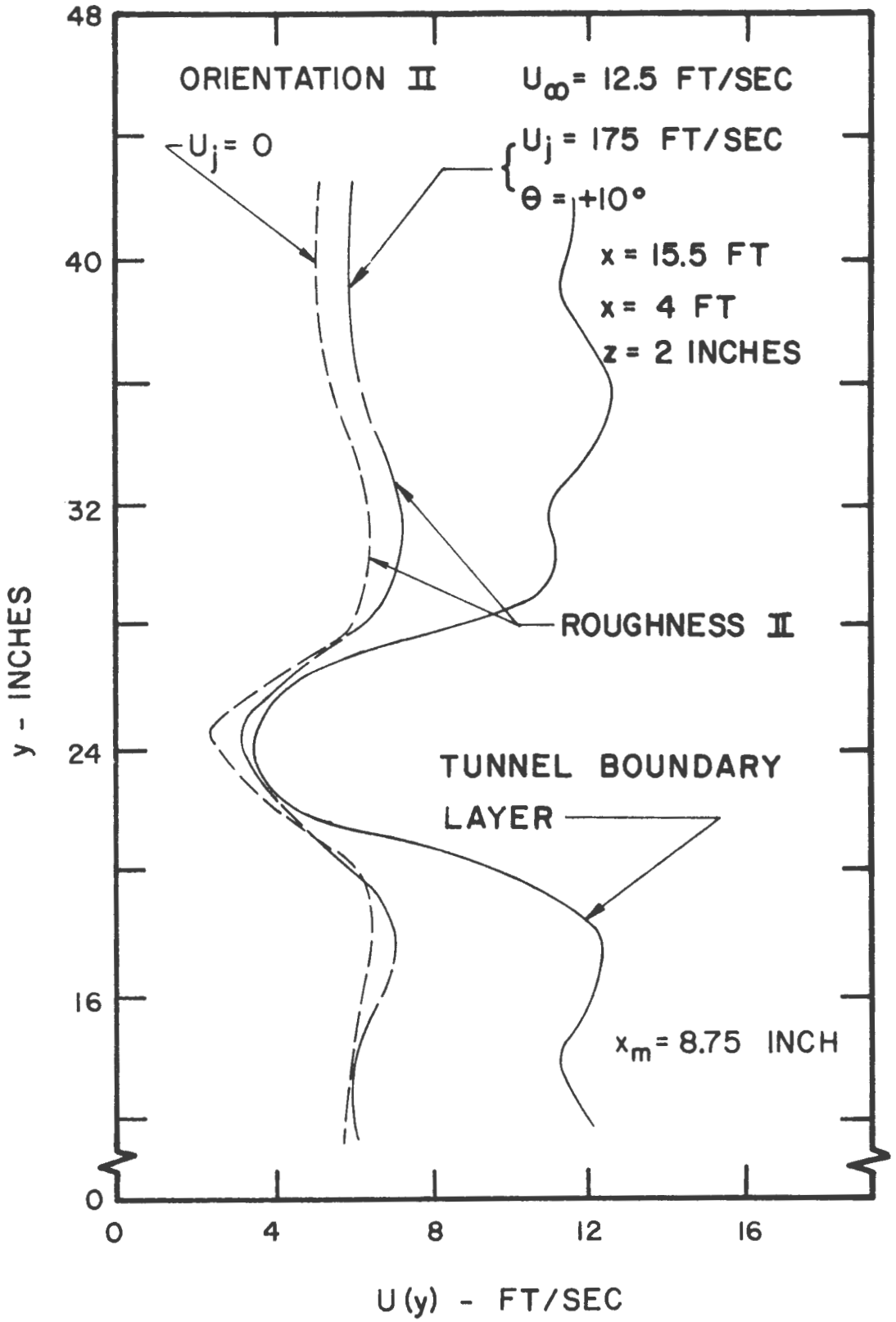

Figure 81. Transverse Mean Velocity Profiles of Model-Wake at x_m = 8.75 in. and z = 2 in. for Orientation II

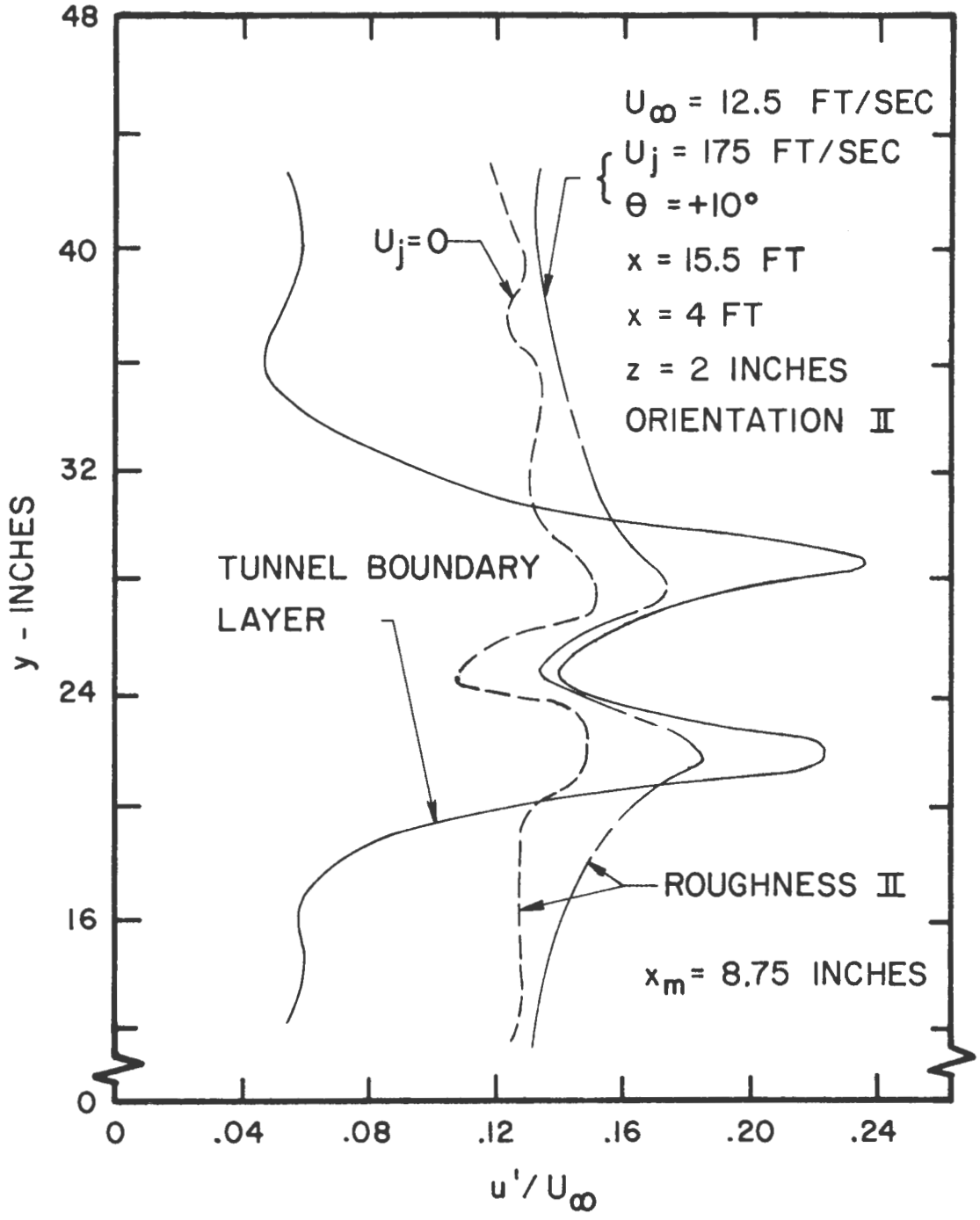

Figure 82. Transverse Turbulence Intensity Profiles of Model-Wake at x_m = 8.75 in. and z = 2 in. for Orientation II

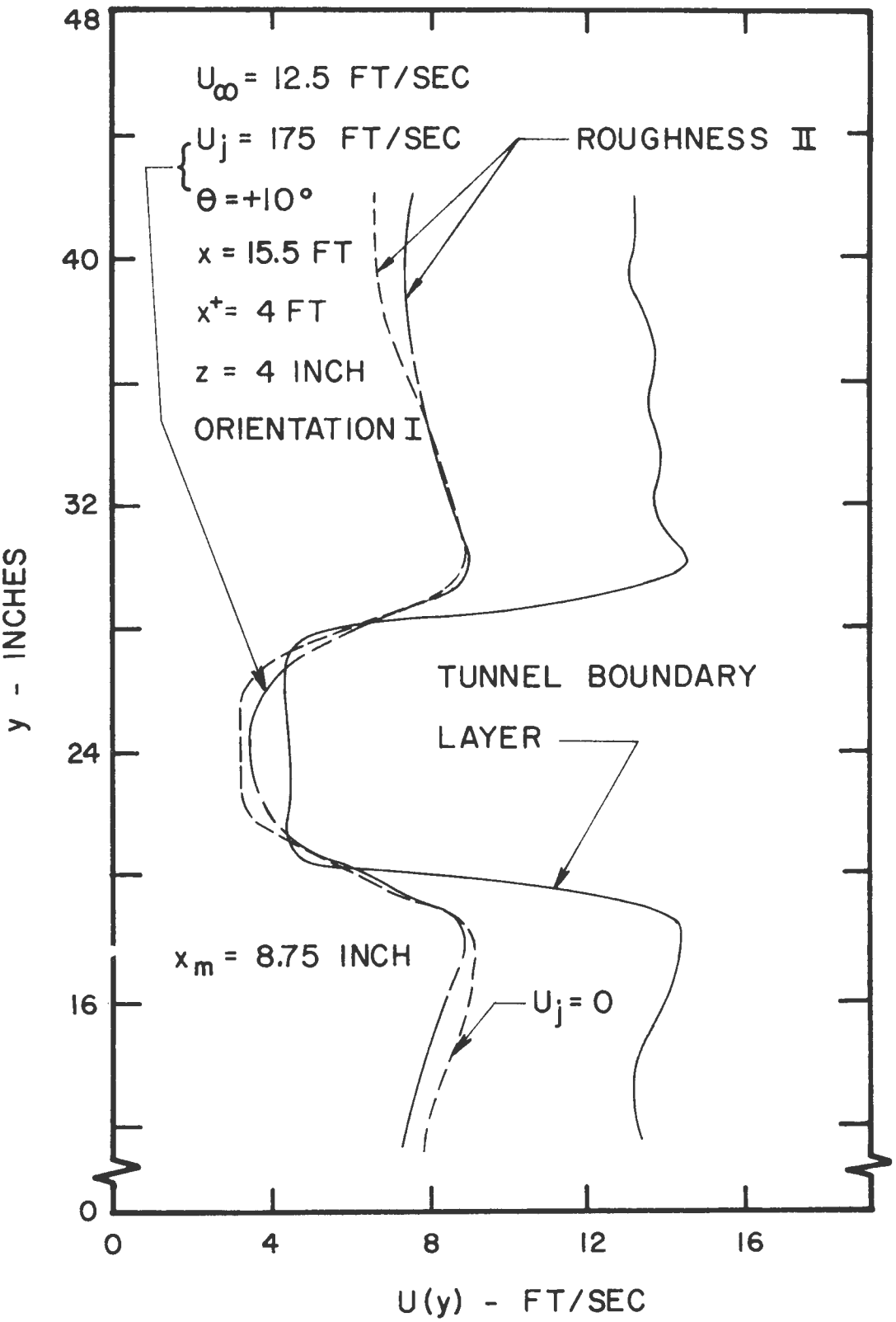

Figure 83. Transverse Mean Velocity Profiles of Model-Wake at x_m = 8.75 in. and z = 4 in. for Orientation I

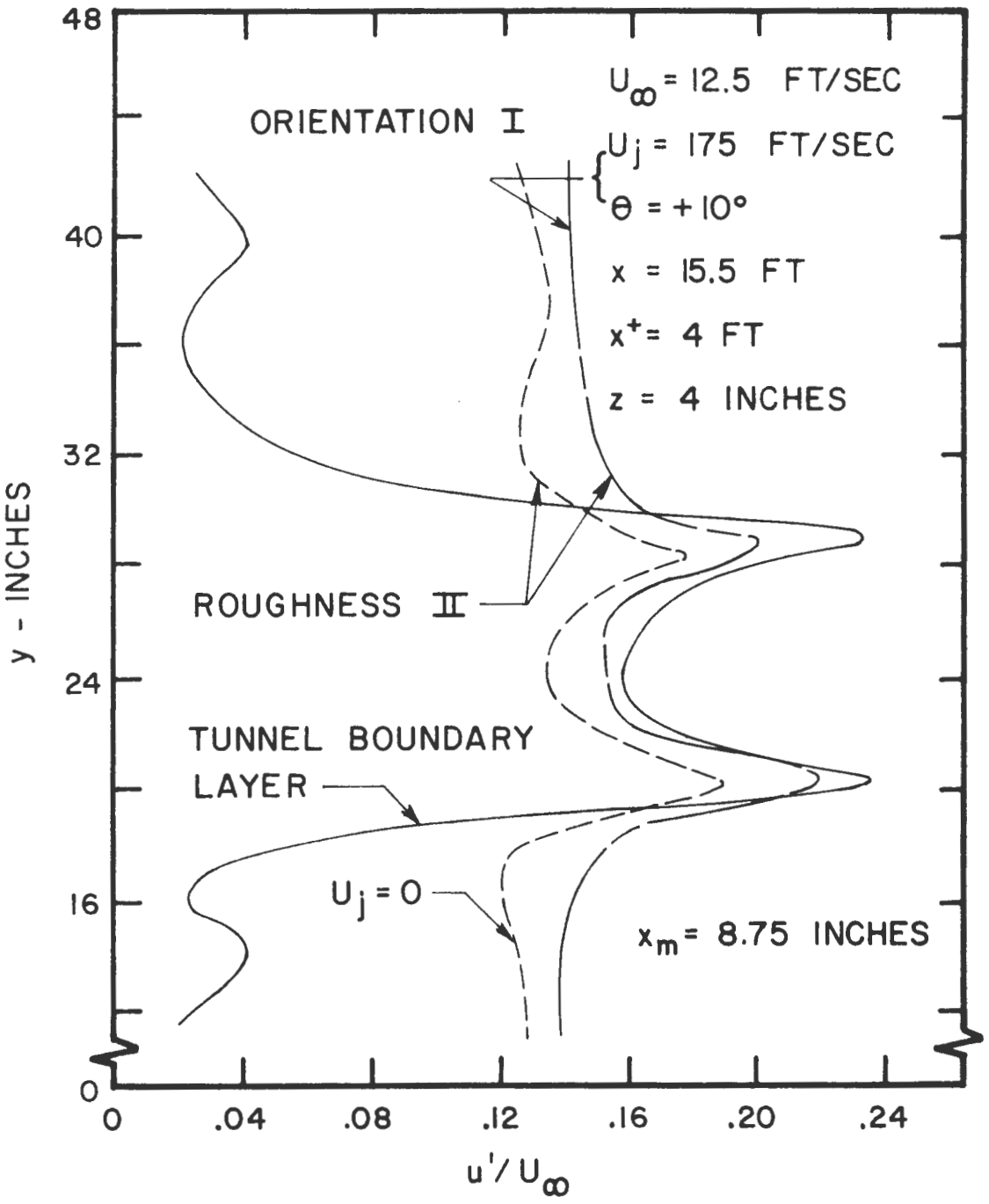

Figure 84. Transverse Turbulence Intensity Profiles of Model-Wake at x_m = 8.75 in. and z = 4 in. for Orientation I

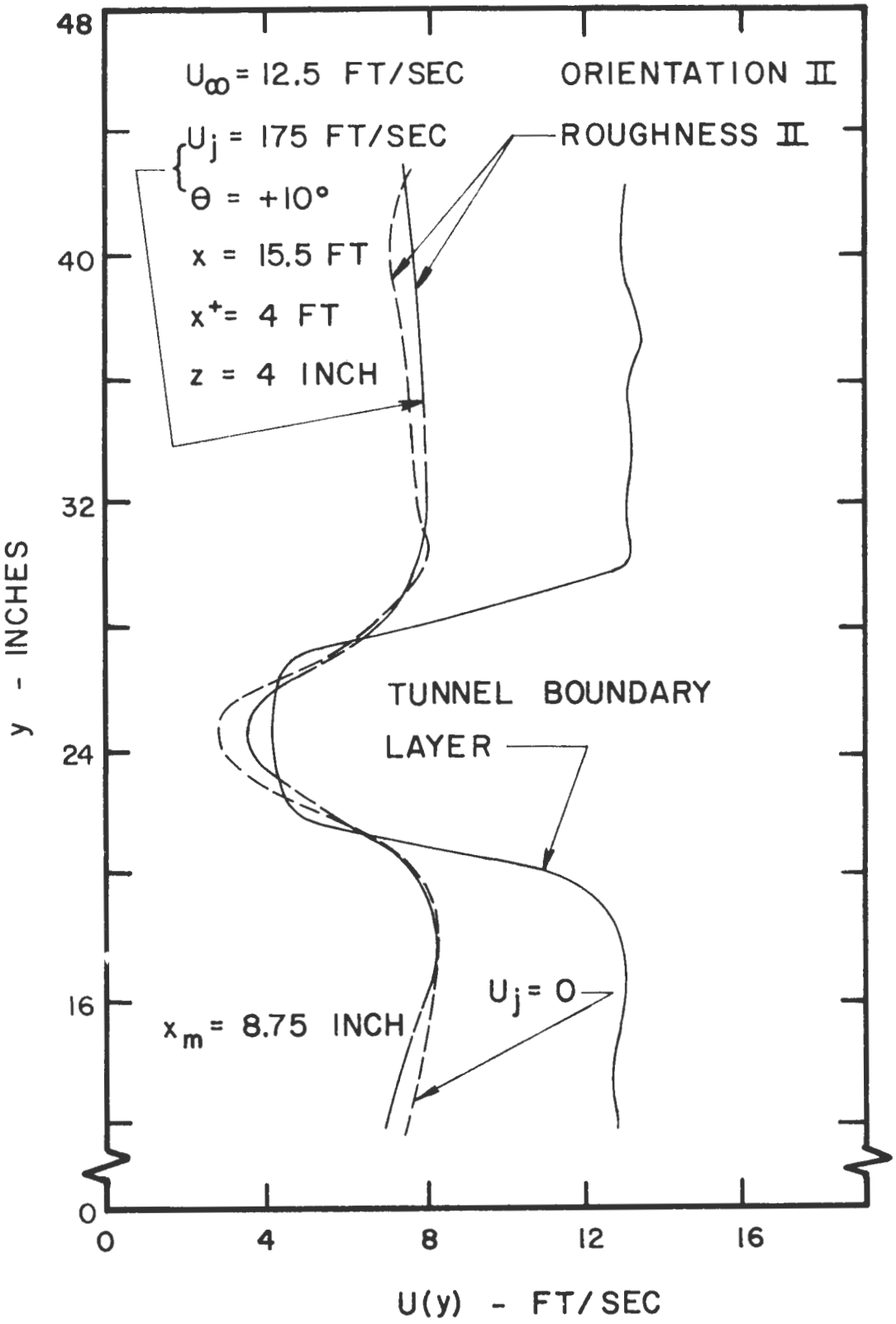

Figure 85. Transverse Mean Velocity Profiles of Model-Wake at x_m = 8.75 in. and z = 4 in. for Orientation II

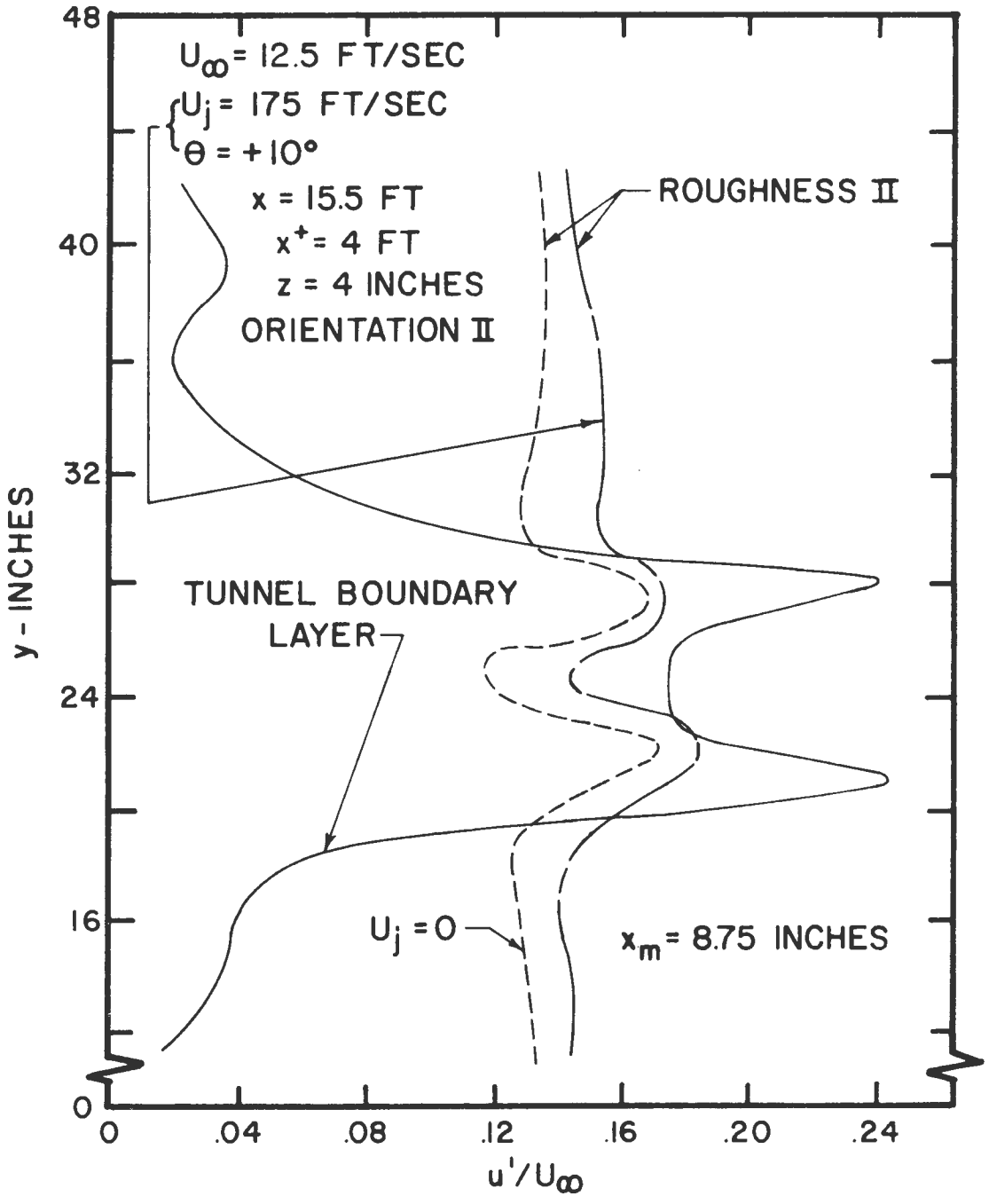

Figure 86. Transverse Turbulence Intensity Profiles of Model-Wake at x_m = 8.75 in. and z = 4 in. for Orientation II

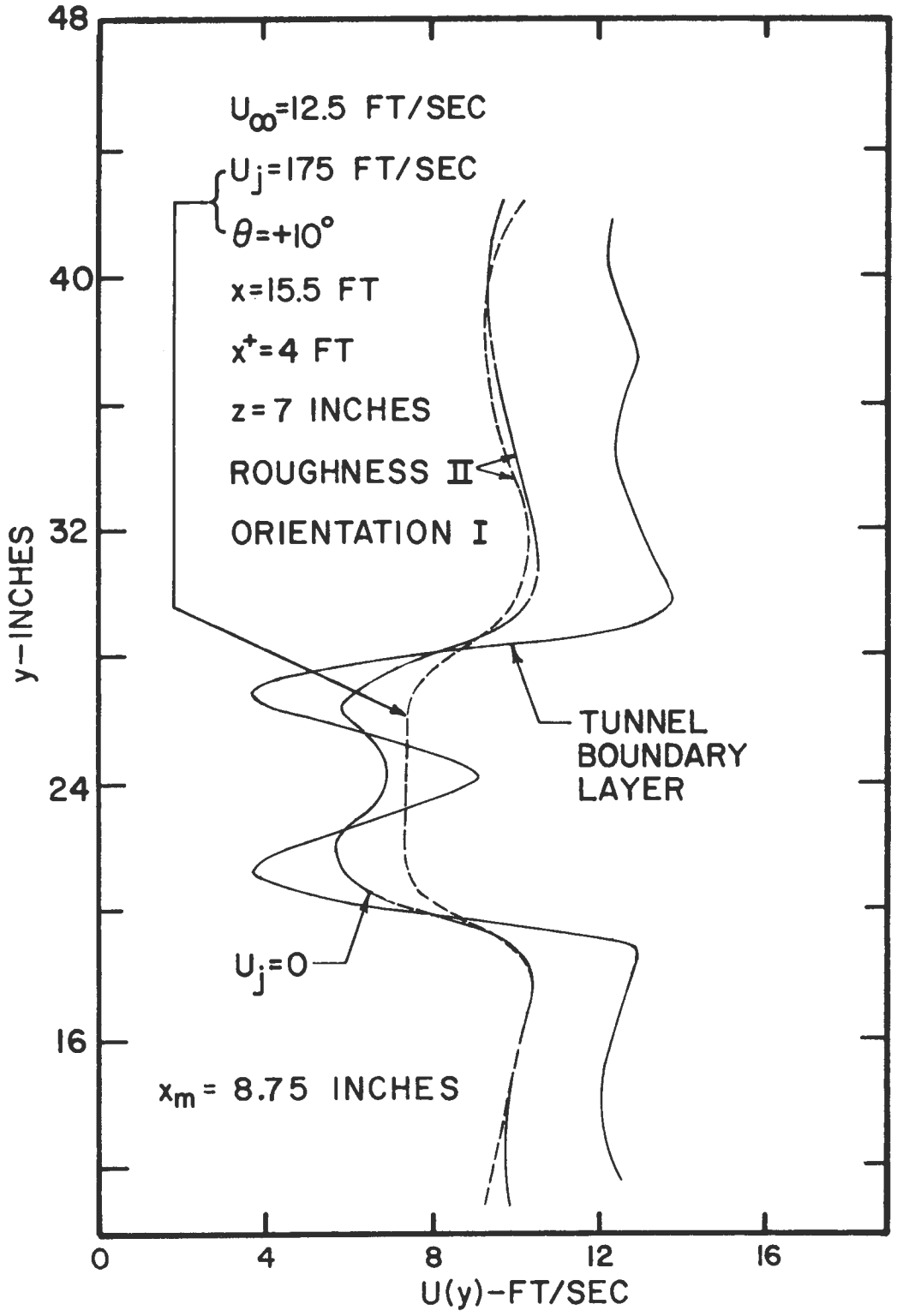

Figure 87. Transverse Mean Velocity Profiles of Model-Wake at x_m = 8.75 in. and z = 7 in. for Orientation I

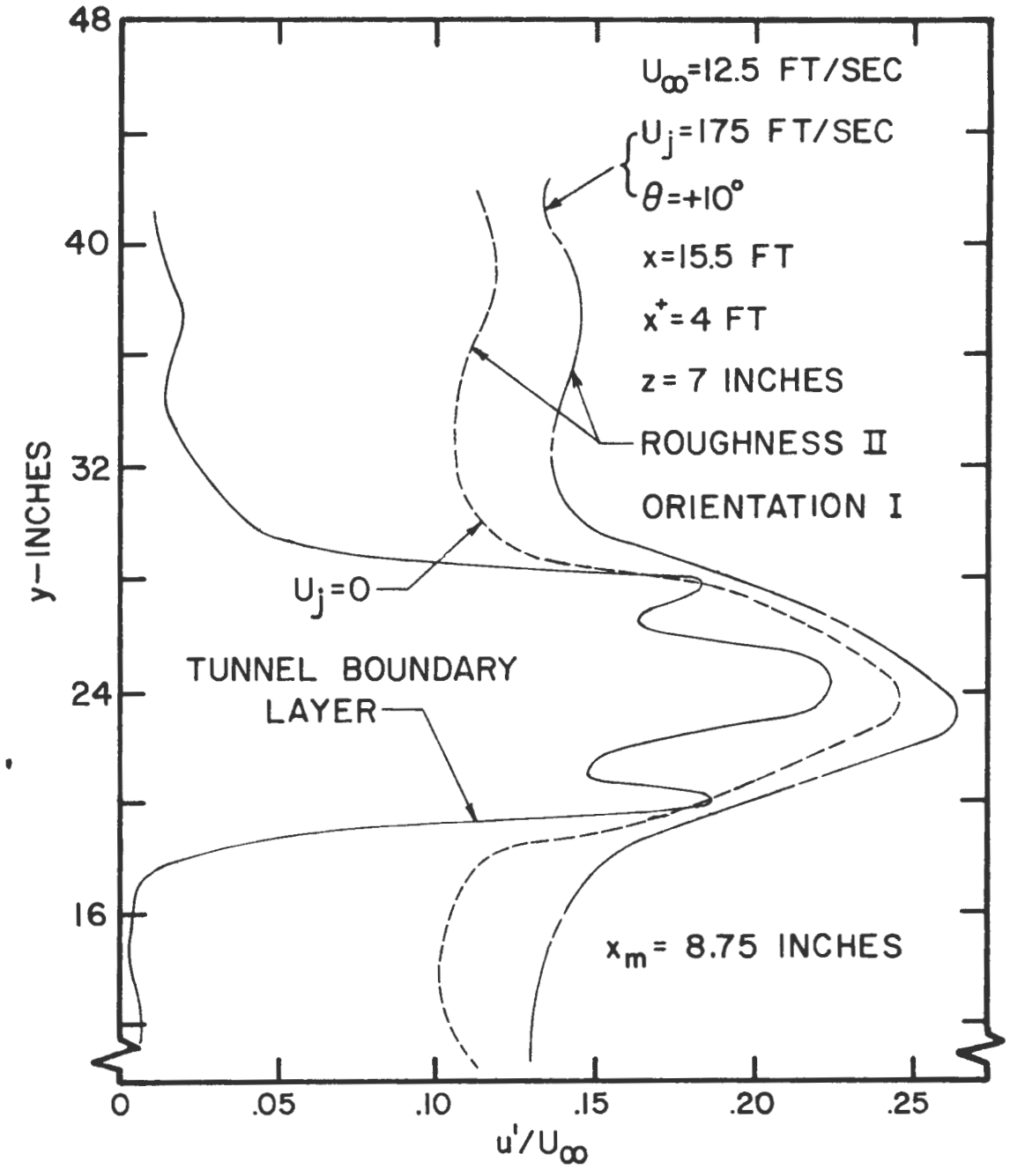

Figure 88. Transverse Turbulence Intensity Profiles of Model-Wake at x_m = 8.75 in. and z = 7 in. for Orientation I

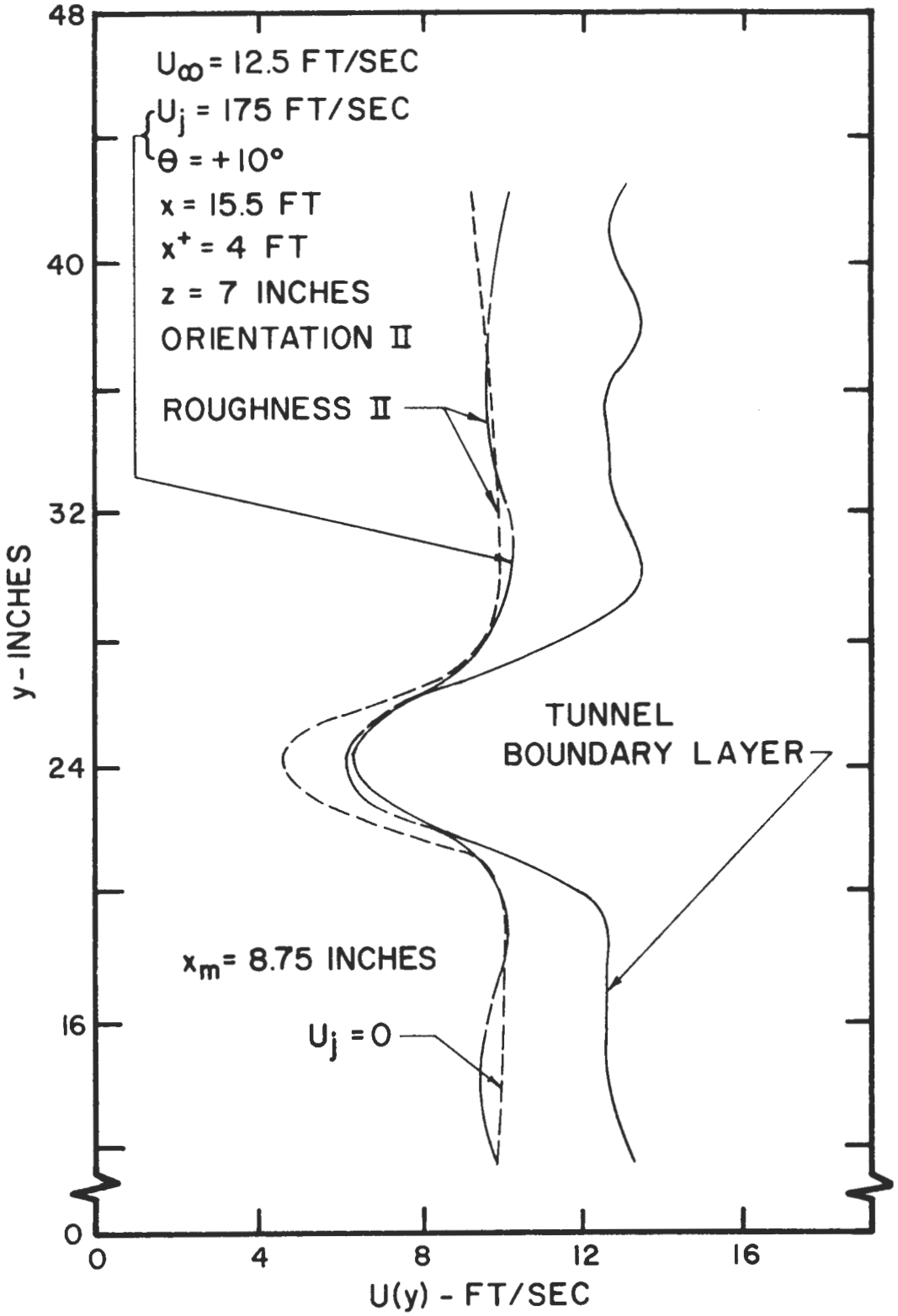

Figure 89. Transverse Mean Velocity Profiles of Model-Wake at x_m = 8.75 in. and z = 7 in. for Orientation II

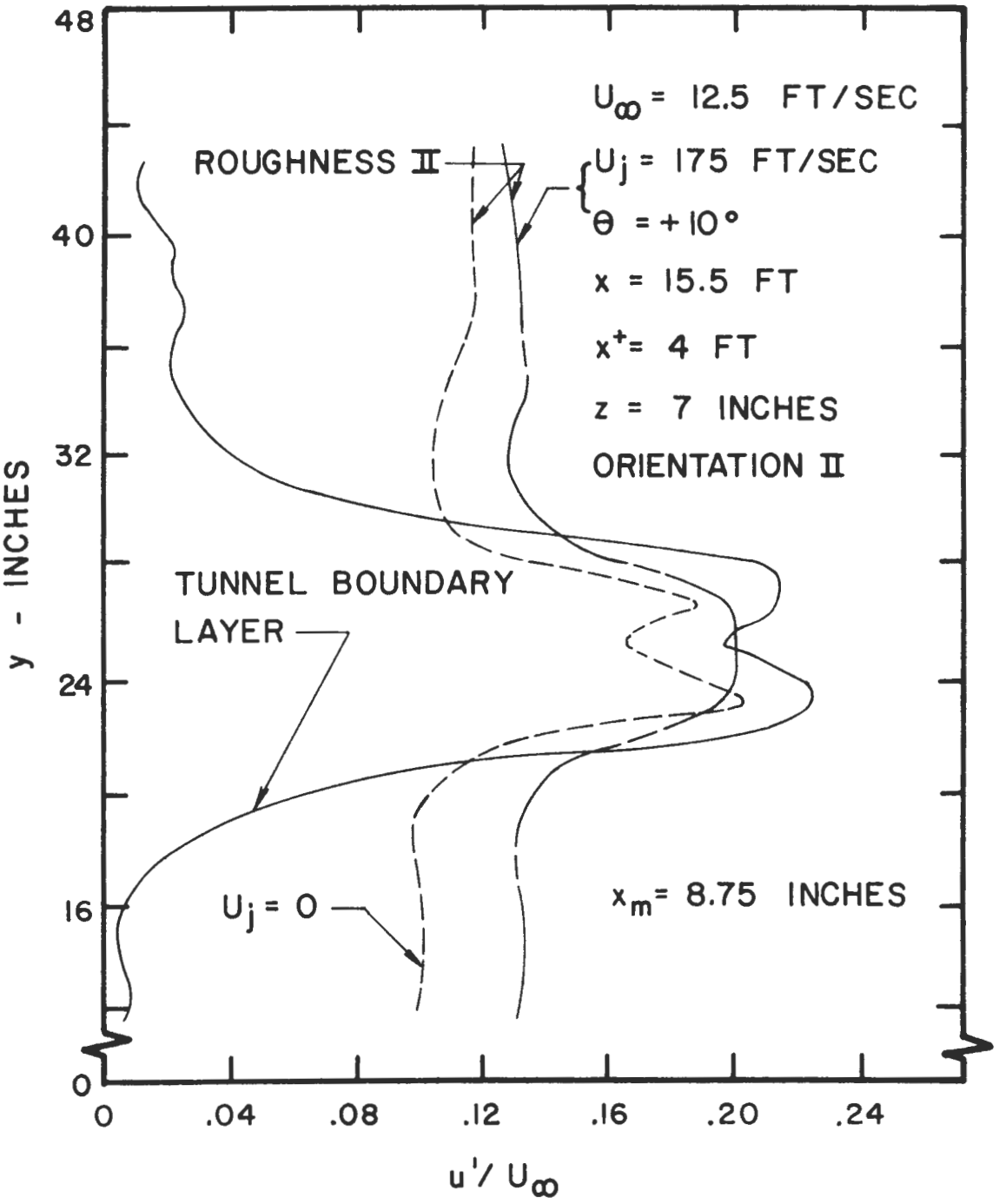

Figure 90. Transverse Turbulence Intensity Profiles of Model-Wake at x_m = 8.75 in. and z = 7 in. for Orientation II

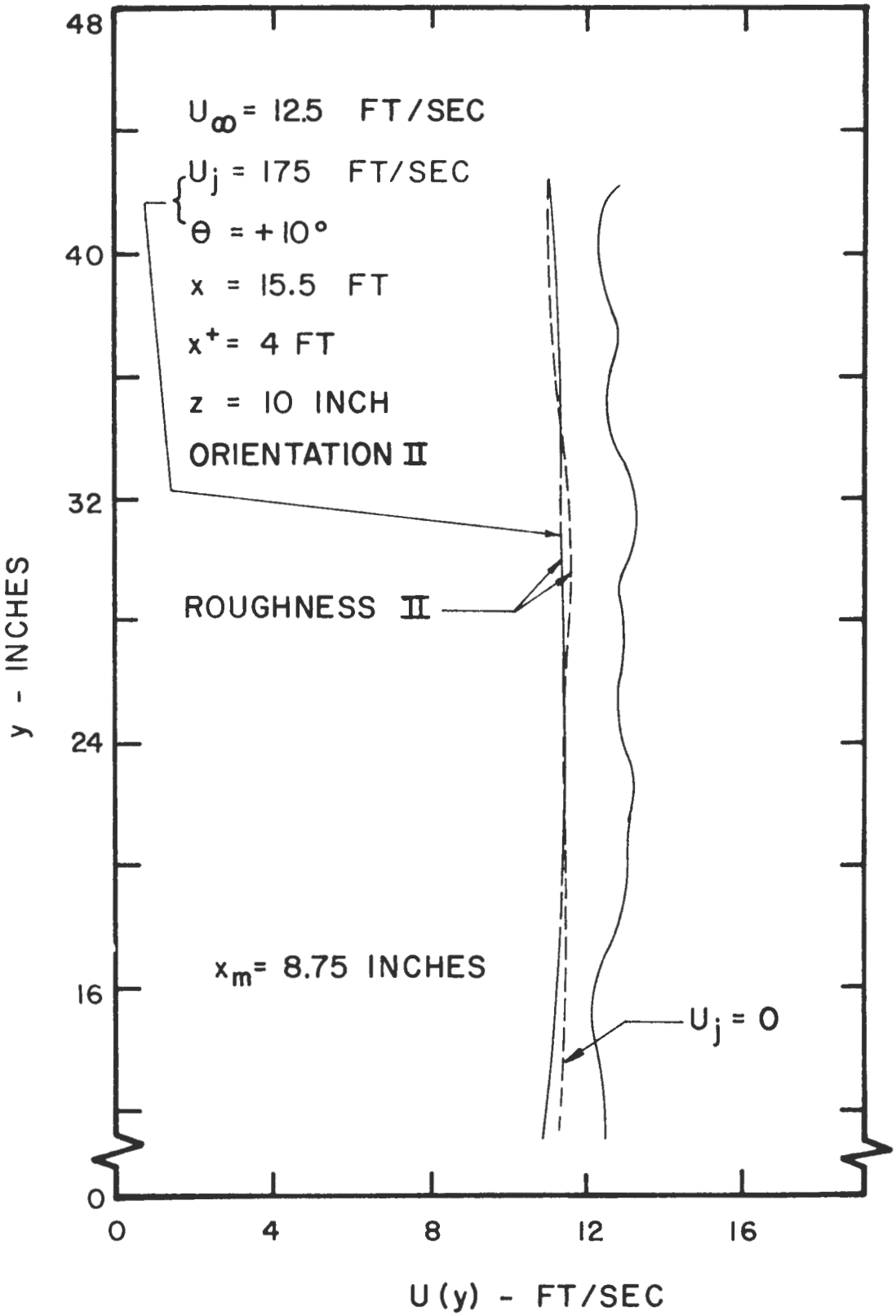

Figure 91. Transverse Mean Velocity Profiles of Model-Wake at x_m = 8.75 in. and z = 10 in. for Orientation II

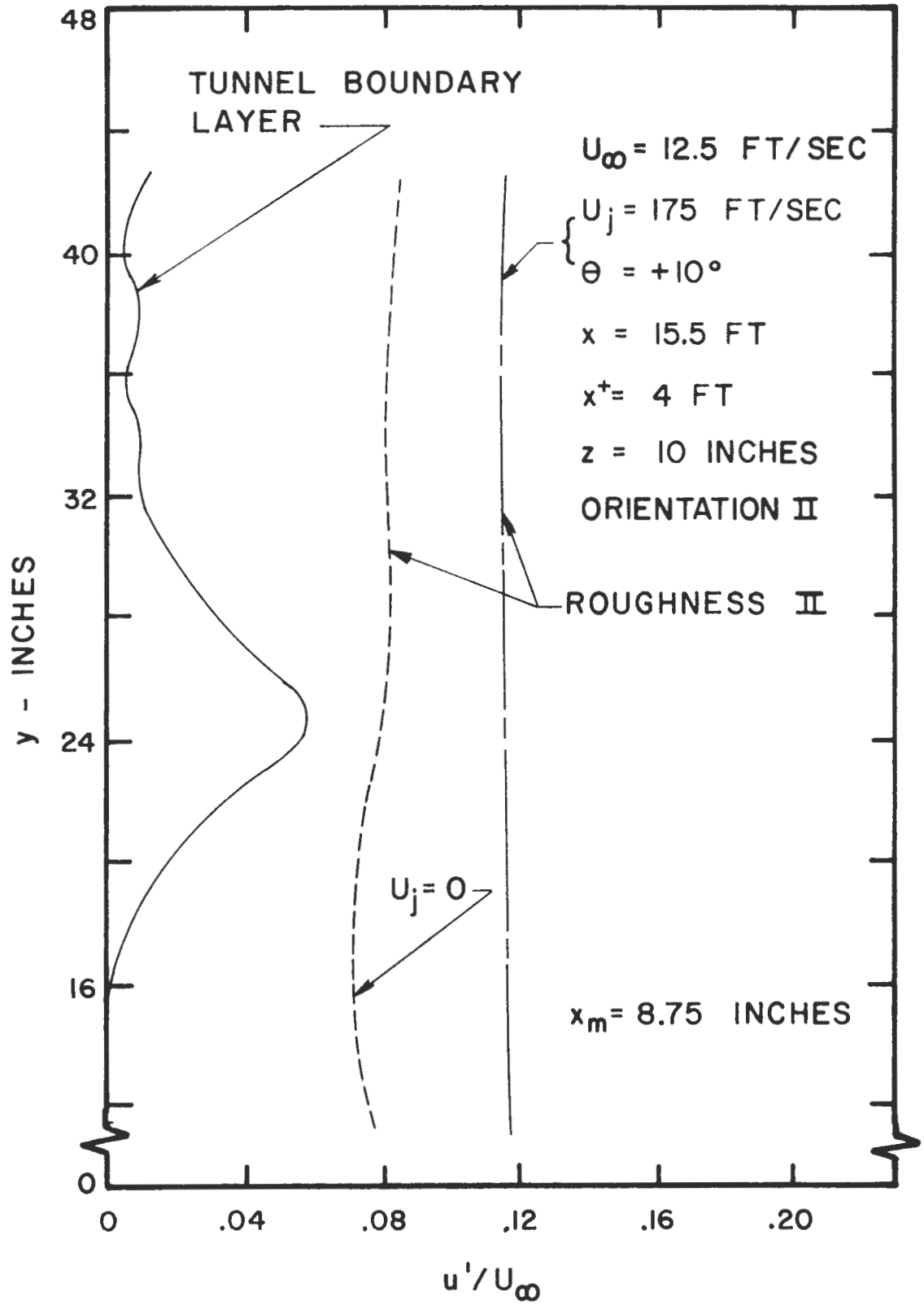

Figure 92. Transverse Turbulence Intensity Profiles of Model-Wake at x_m = 8.75 in. and z = 10 in. for Orientation II

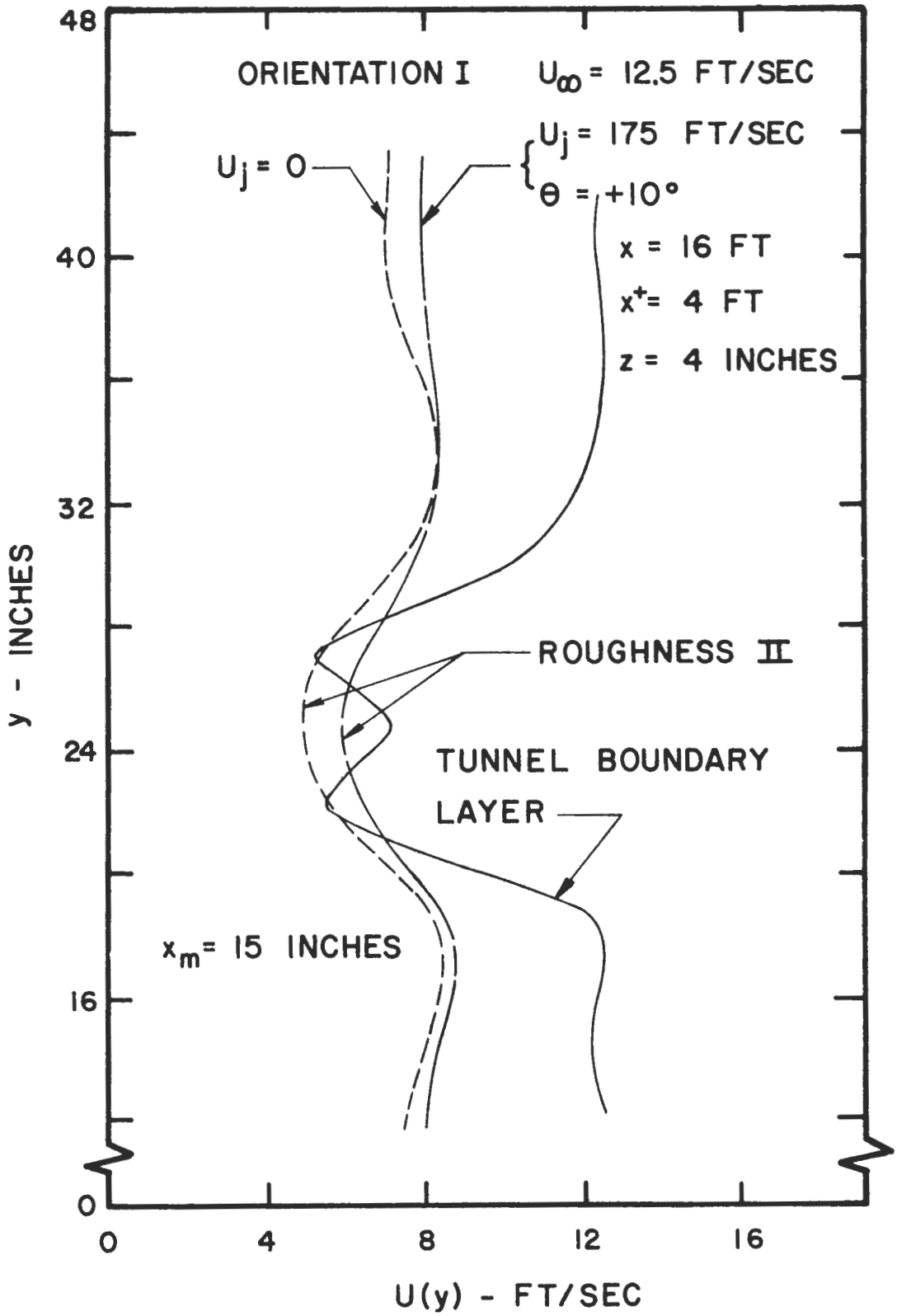

Figure 93. Transverse Mean Velocity Profiles of Model-Wake at x_m = 15.0 in. and z = 4 in. for Orientation I

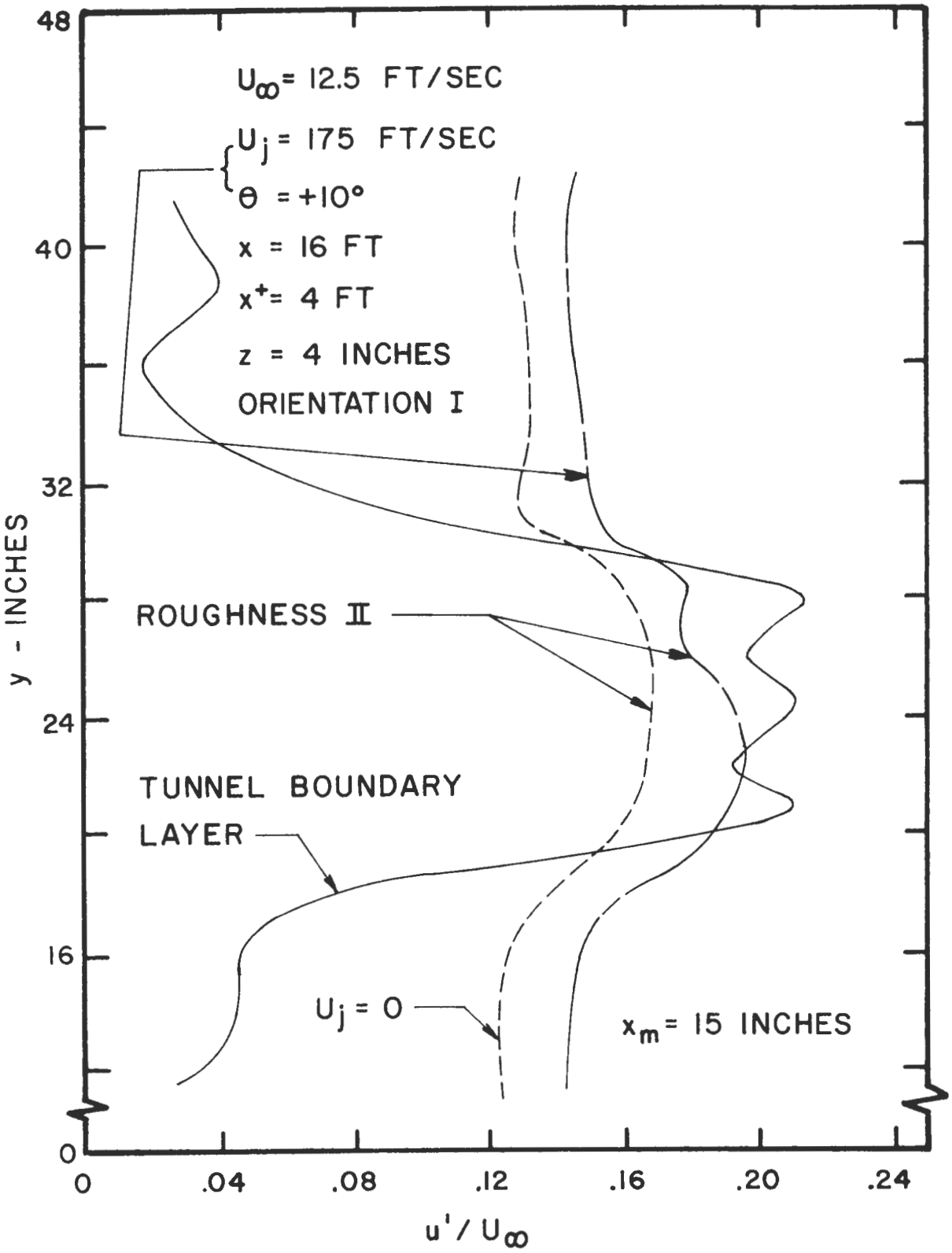

Figure 94. Transverse Turbulence Intensity Profiles of Model-Wake at x_m = 15.0 in. and z = 4 in. for Orientation I

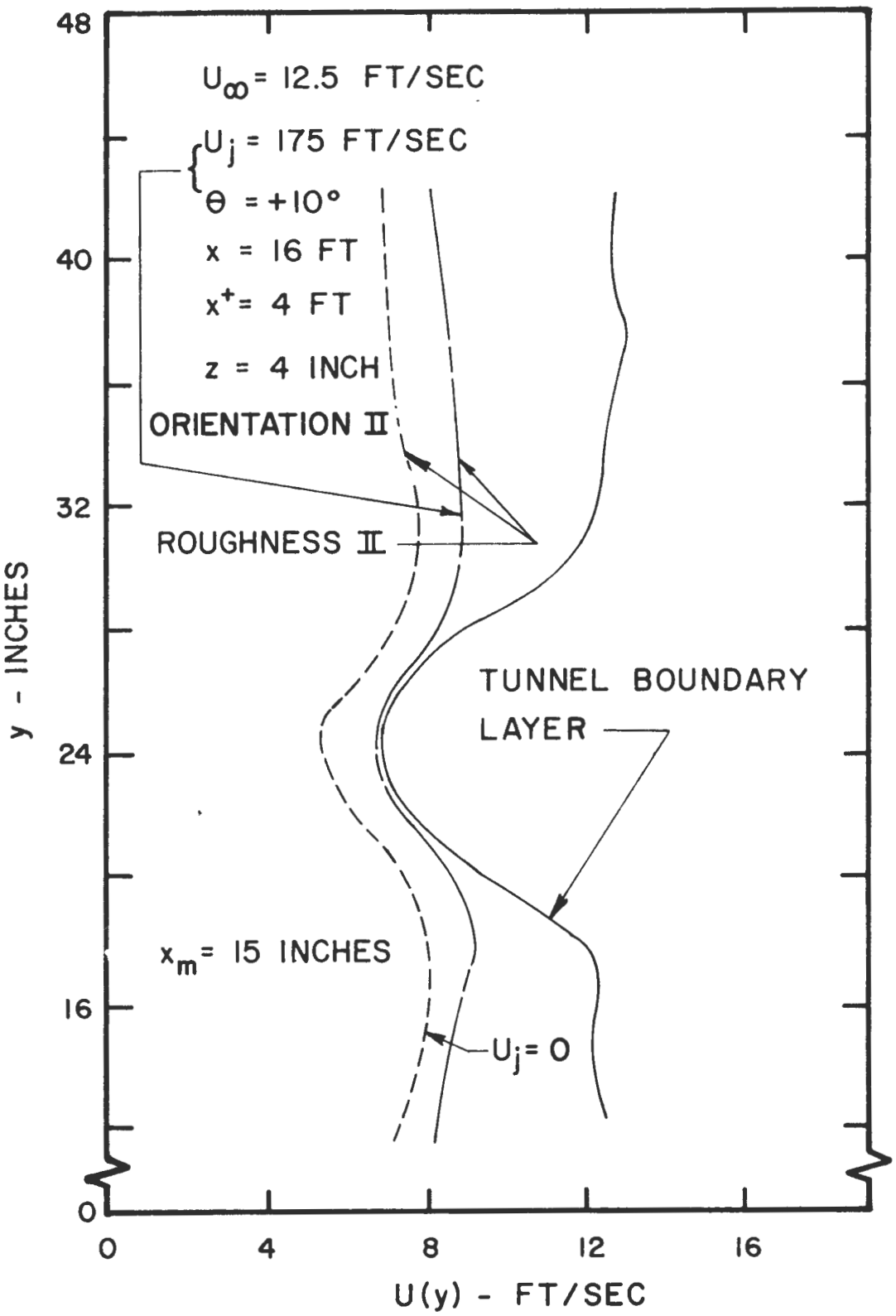

Figure 95. Transverse Mean Velocity Profiles of Model-Wake at x_m = 15.0 in. and z = 4 in. for Orientation II

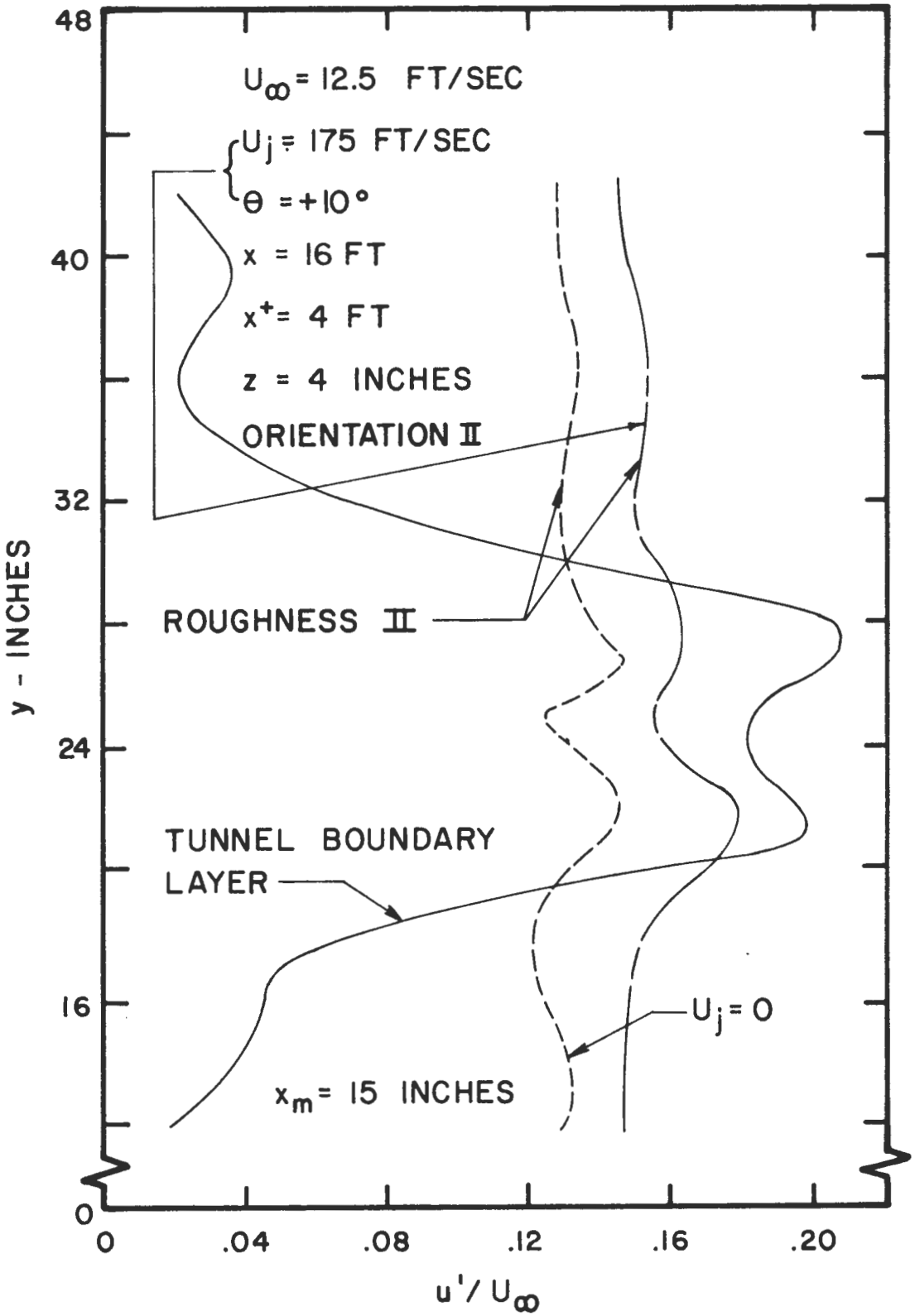

Figure 96. Transverse Turbulence Intensity Profiles of Model-Wake at x_m = 15.0 in. and z = 4 in. for Orientation II

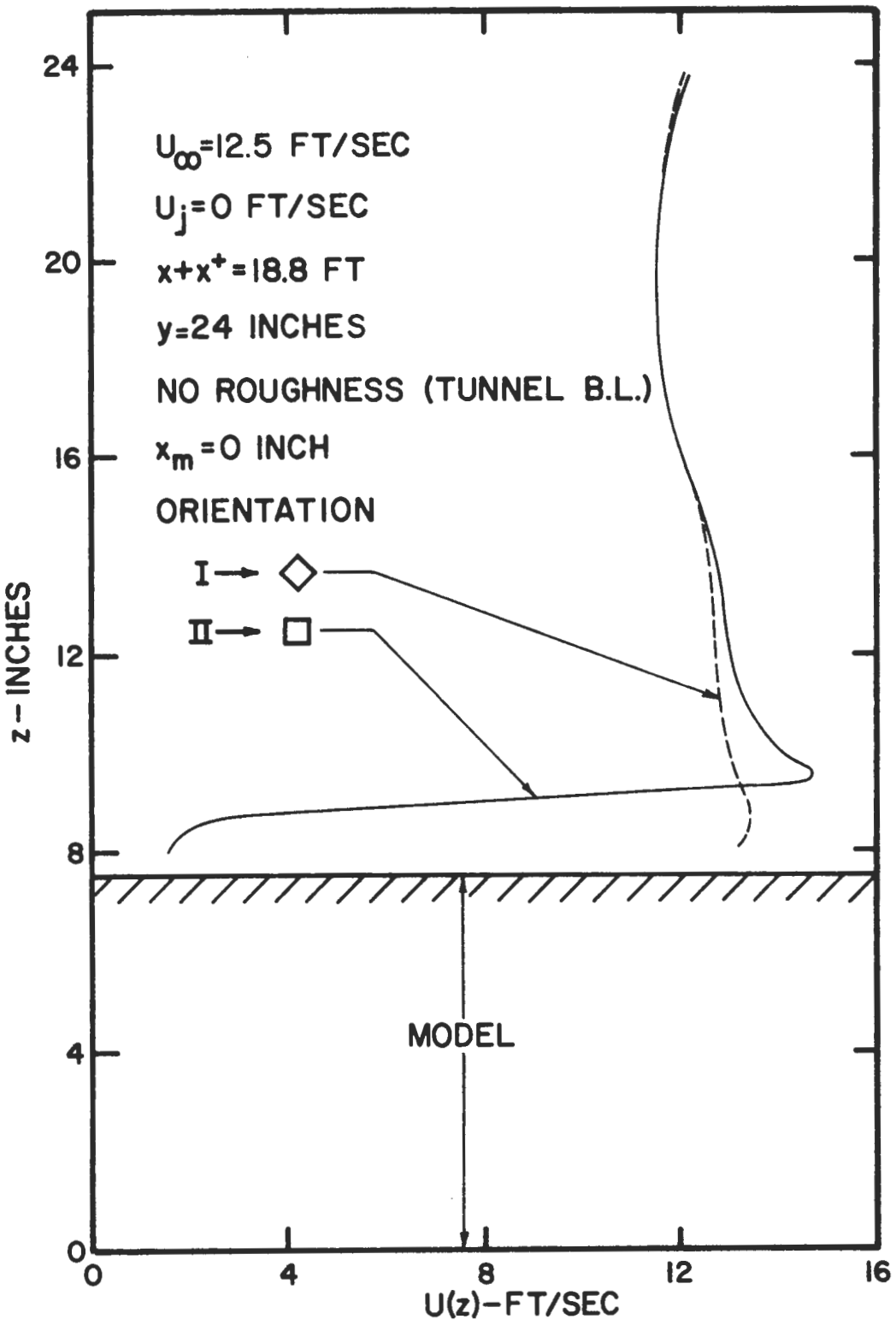

Figure 97. Vertical Mean Velocity Profiles on Top of Model for Two Wind Directions Using Tunnel Boundary Layer

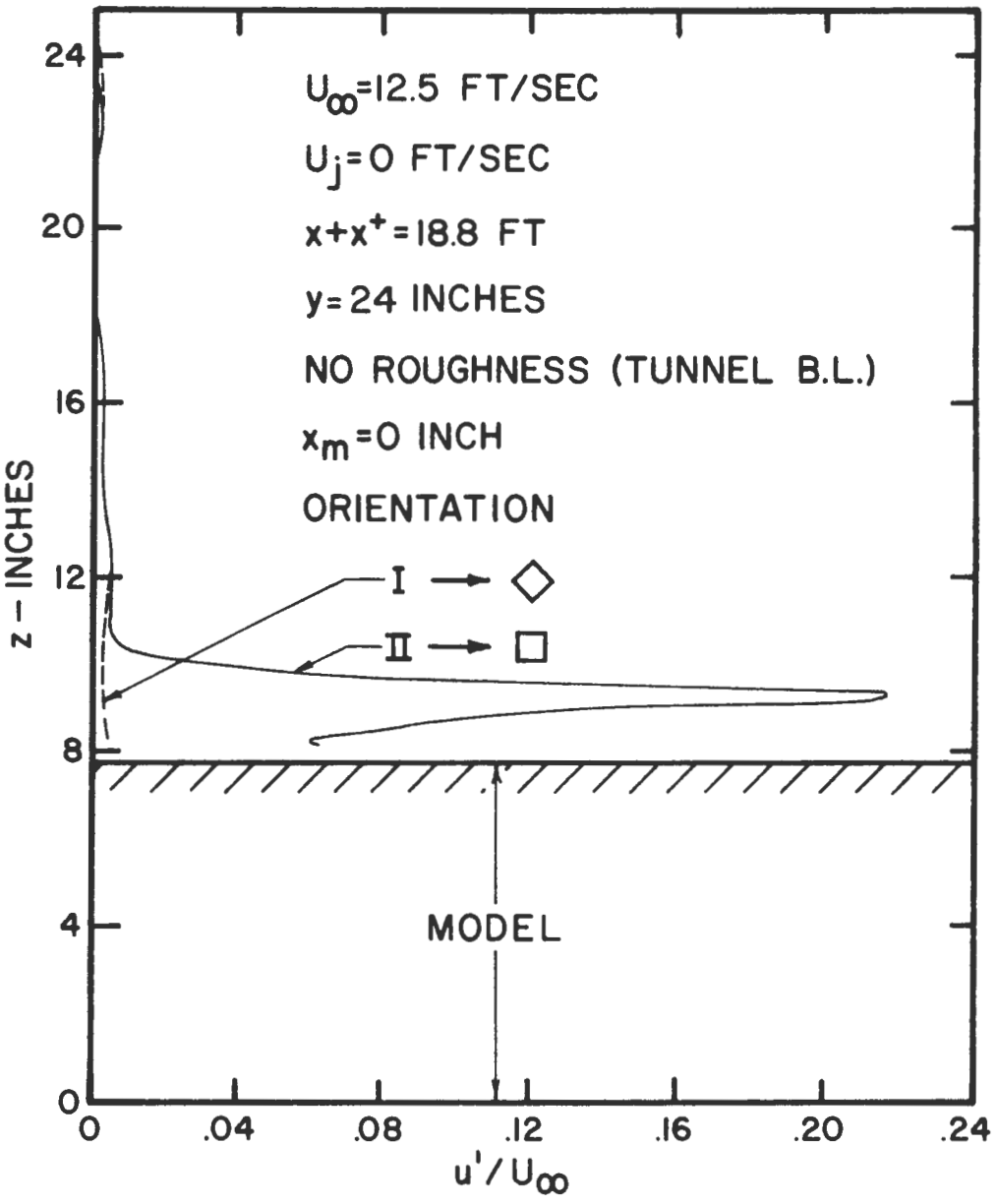

Figure 98. Vertical Turbulence Intensity Profiles on Top of Model for Two Wind Directions Using Tunnel Boundary Layer

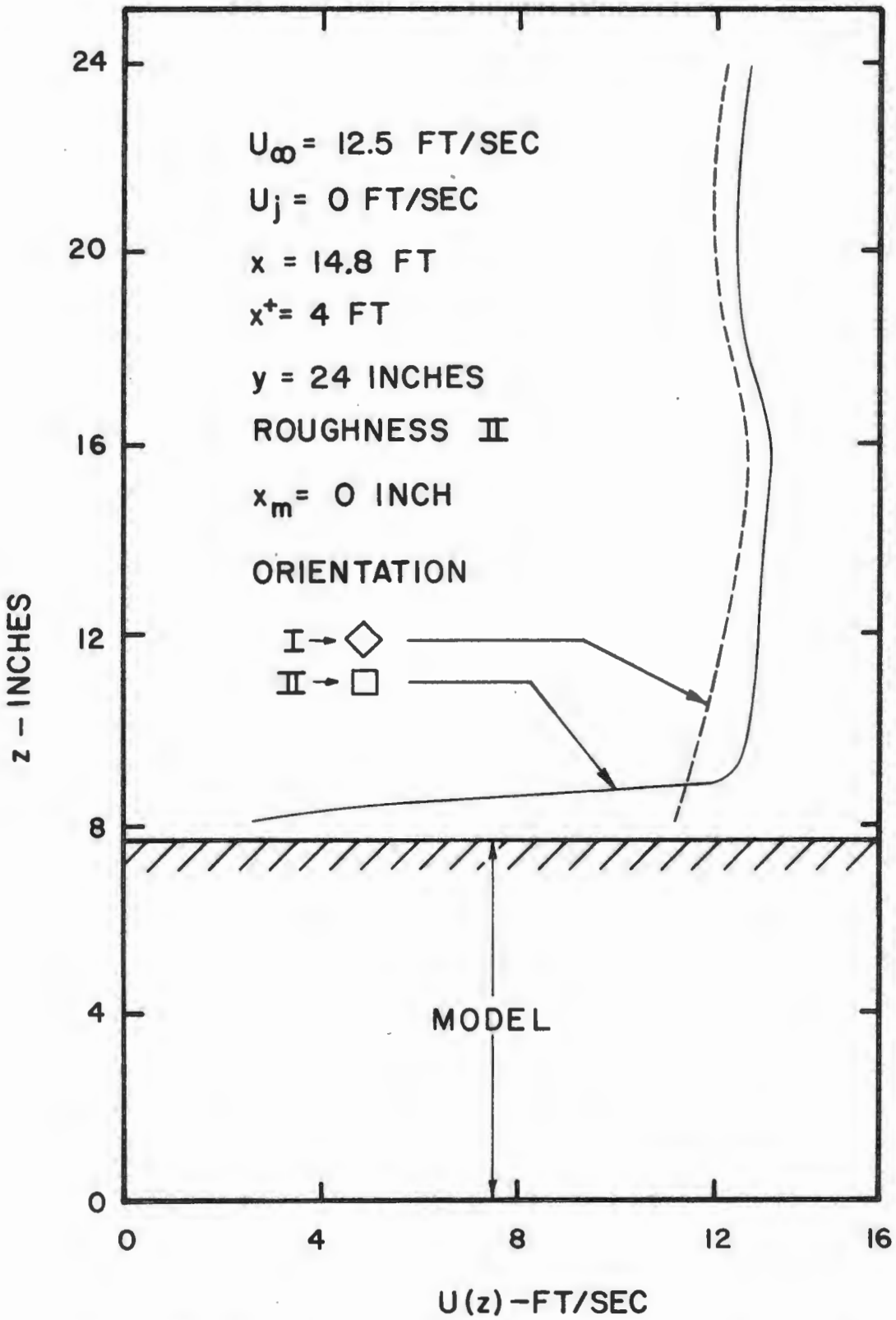

Figure 99. Vertical Mean Velocity Profiles on Top of Model for Two Wind Directions Using Roughness-Generated Boundary Layer

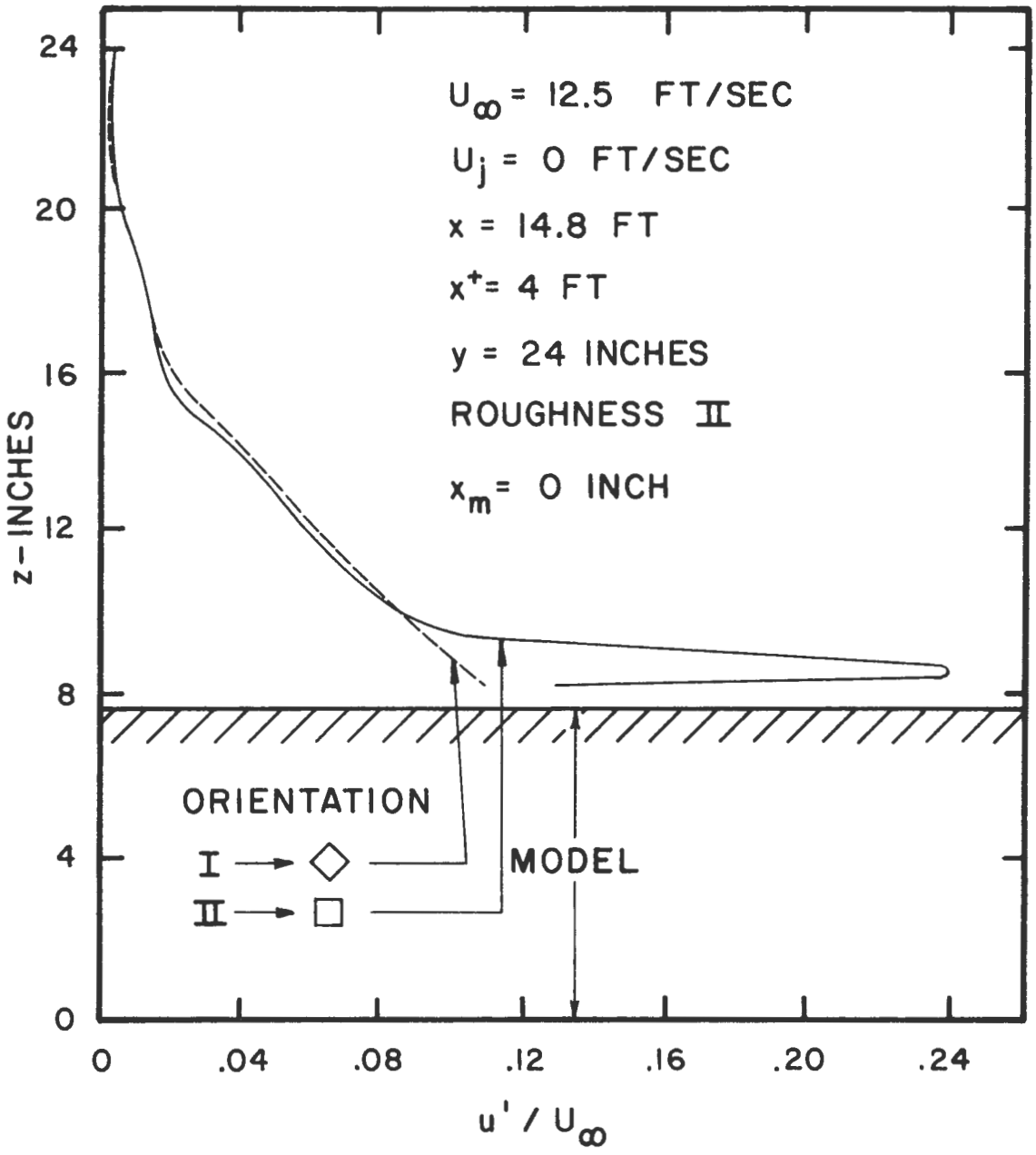

Figure 100. Vertical Turbulence Intensity Profiles on Top of Model for Two Wind Directions Using Roughness-Generated Boundary Layer

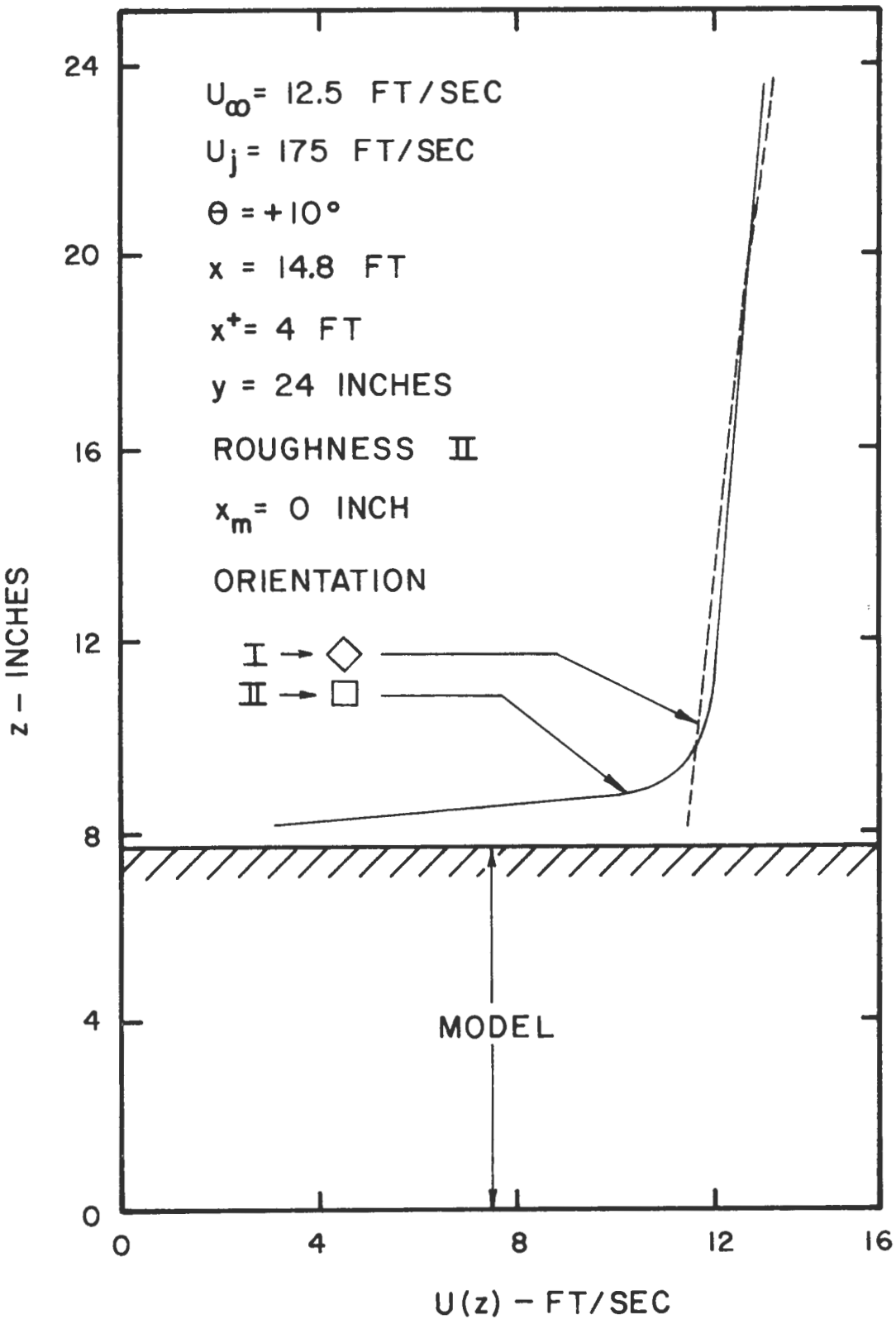

Figure 101. Vertical Mean Velocity Profiles on Top of Model for Two Wind Directions Using Counter-Jet Generated Boundary Layer

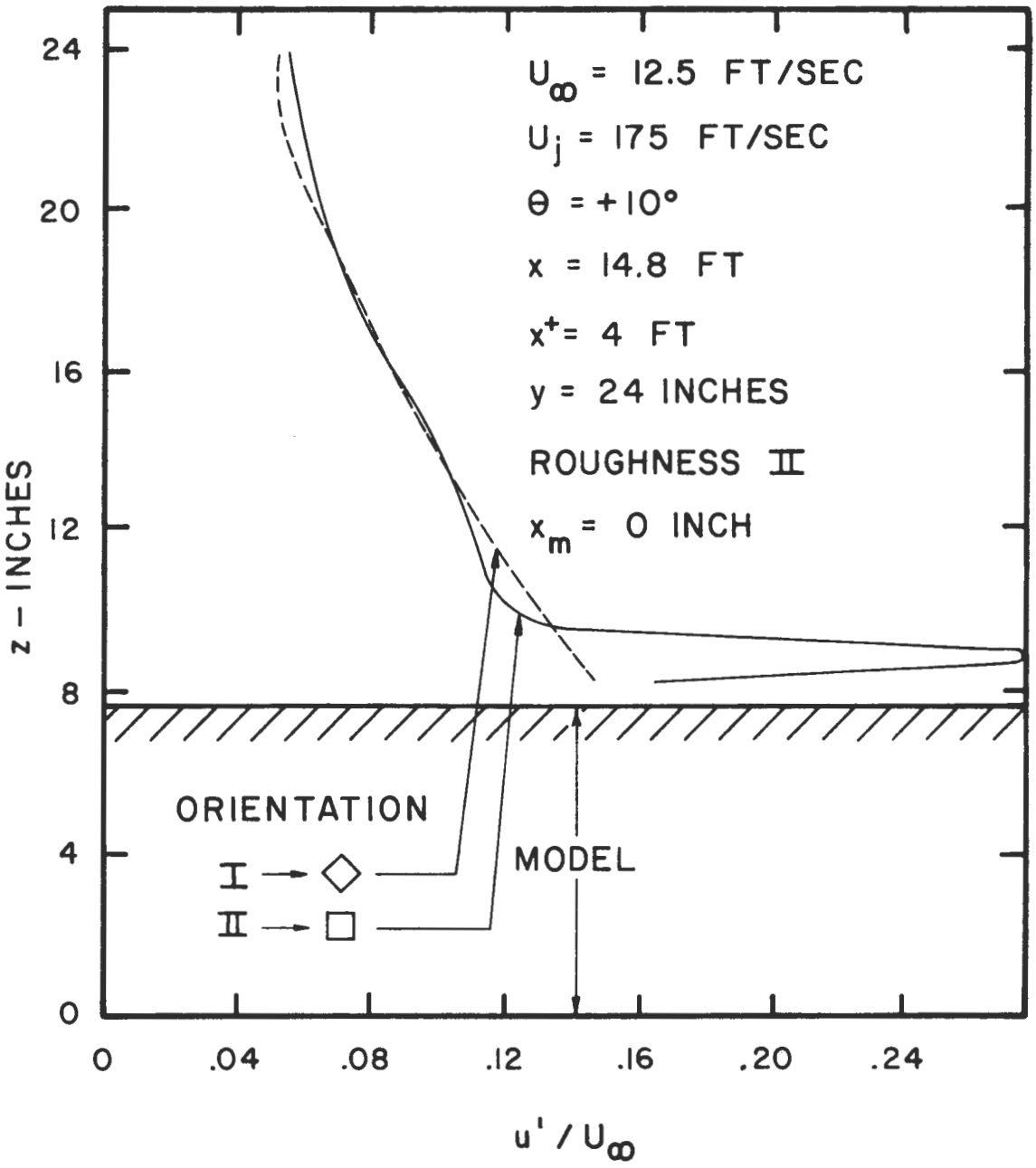

Figure 102. Vertical Turbulence Intensity Profiles on Top of Model for Two Wind Directions Using Counter-Jet Generated Boundary Layer

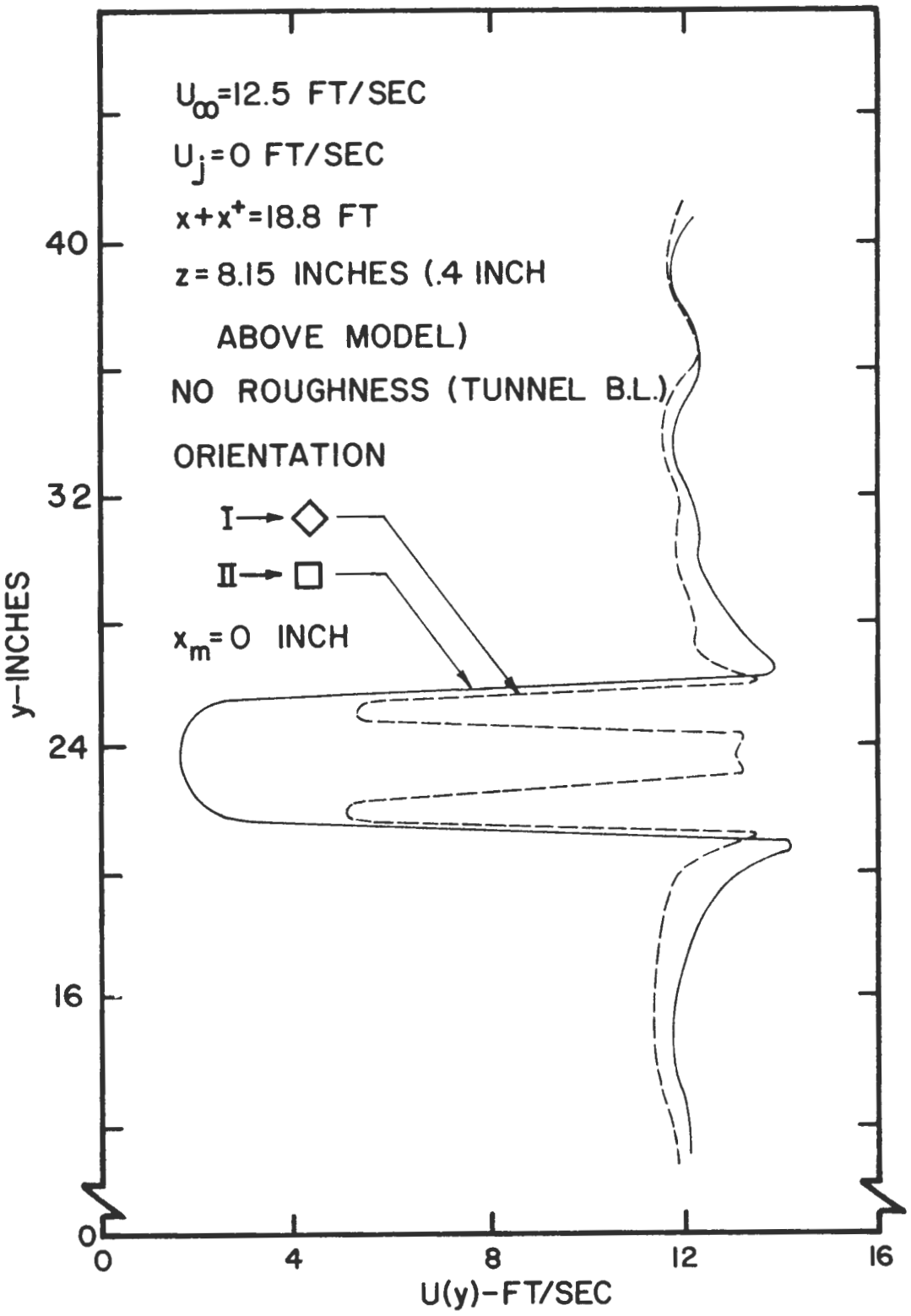

Figure 103. Transverse Mean Velocity Profiles Just Above Top of Model for Two Wind Directions Using Tnnel Boundary Layer

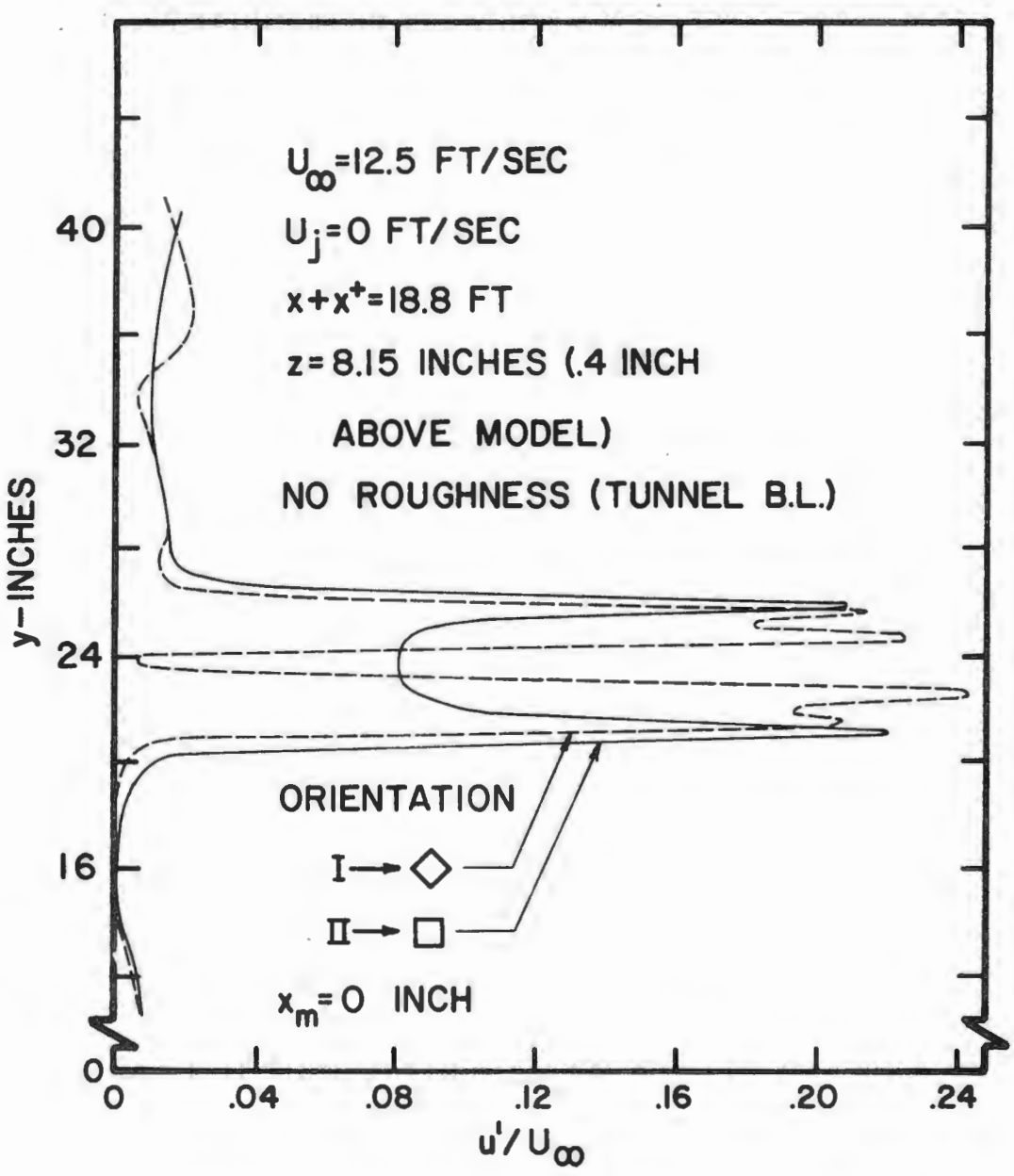

Figure 104. Transverse Turbulence Intensity Profiles Just Above Top of Model for Two Wind Directions Using Tunnel Boundary Layer

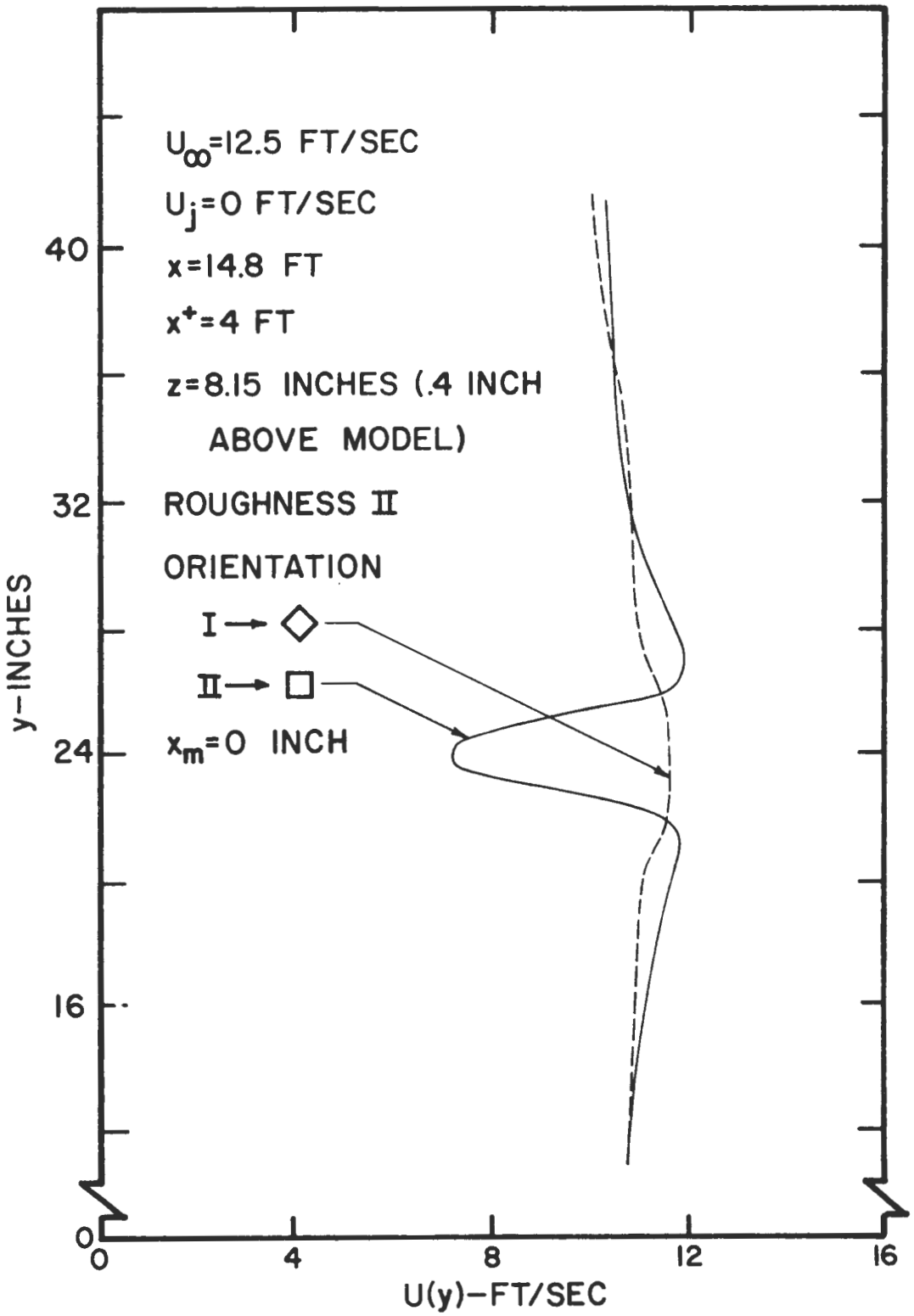

Figure 105. Transverse Mean Velocity Profiles Just Above Top of Model for Two Wind Directions Using Roughness-Generated Boundary Layer

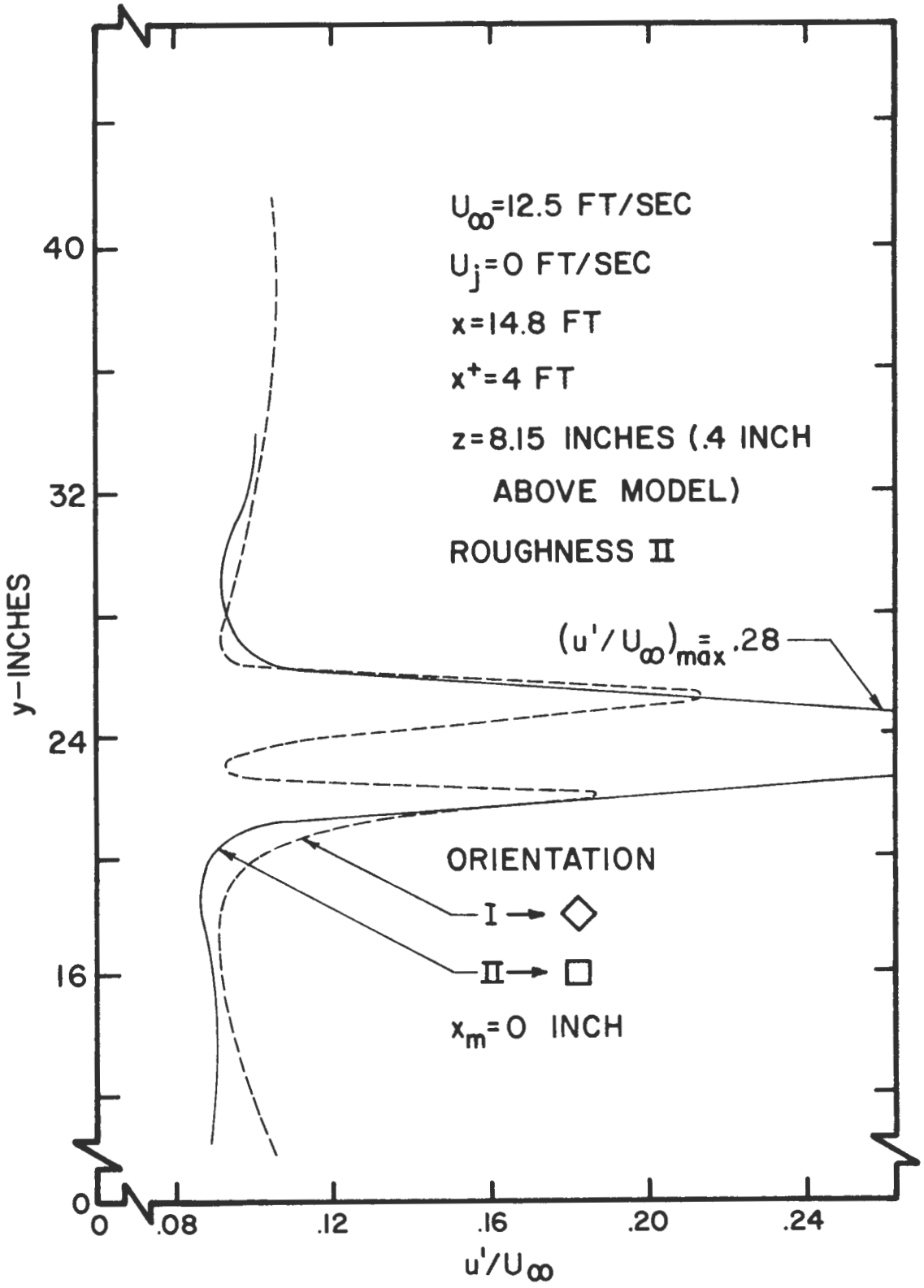

Figure 106. Transverse Turbulence Intensity Profiles Just Above Top of Model for Two Wind Directions Using Roughness-Generated Boundary Layer

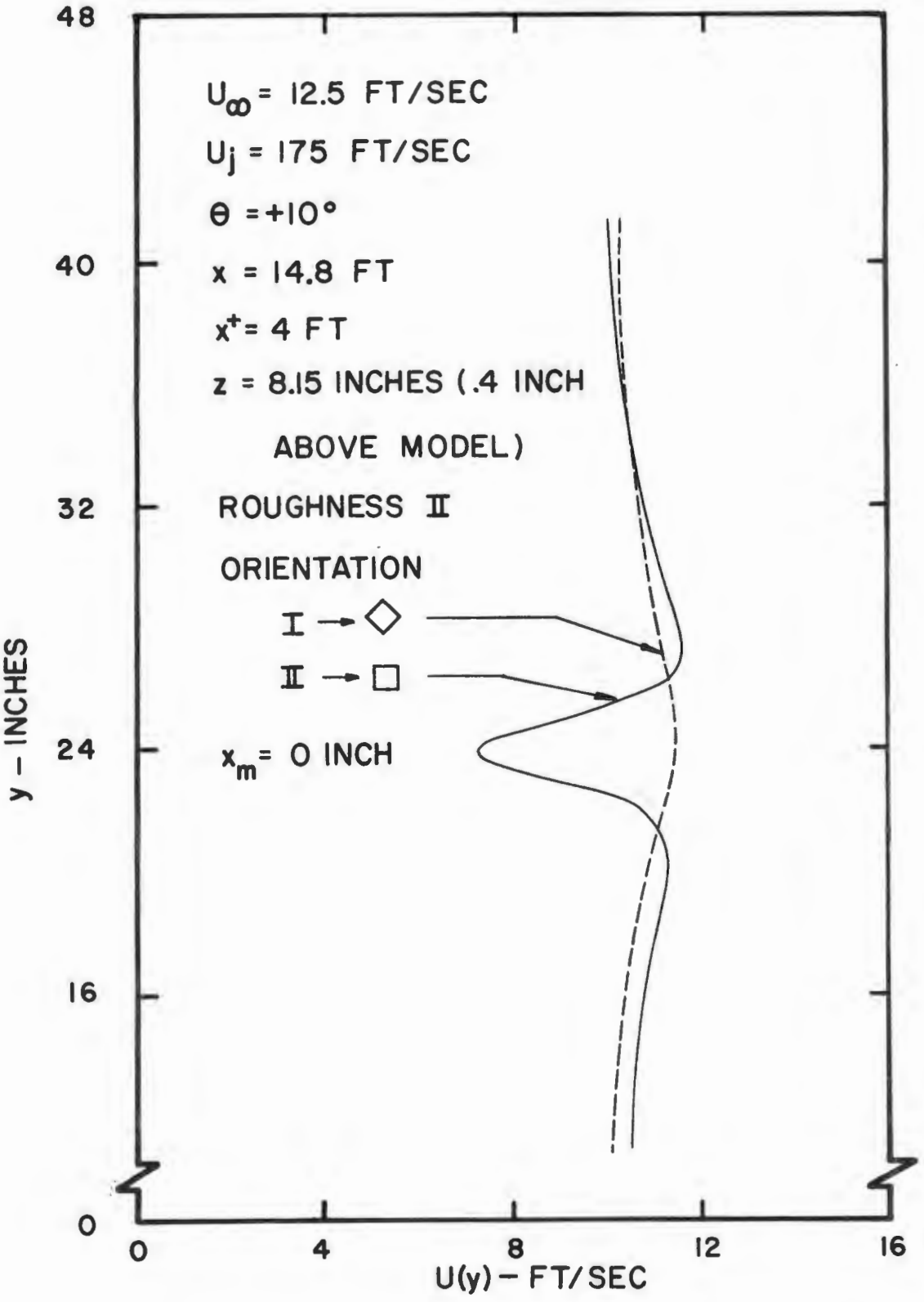

Figure 107. Transverse Mean Velocity Profiles Just Above Top of Model for Two Wind Directions Using Counter-Jet Generated Boundary Layer

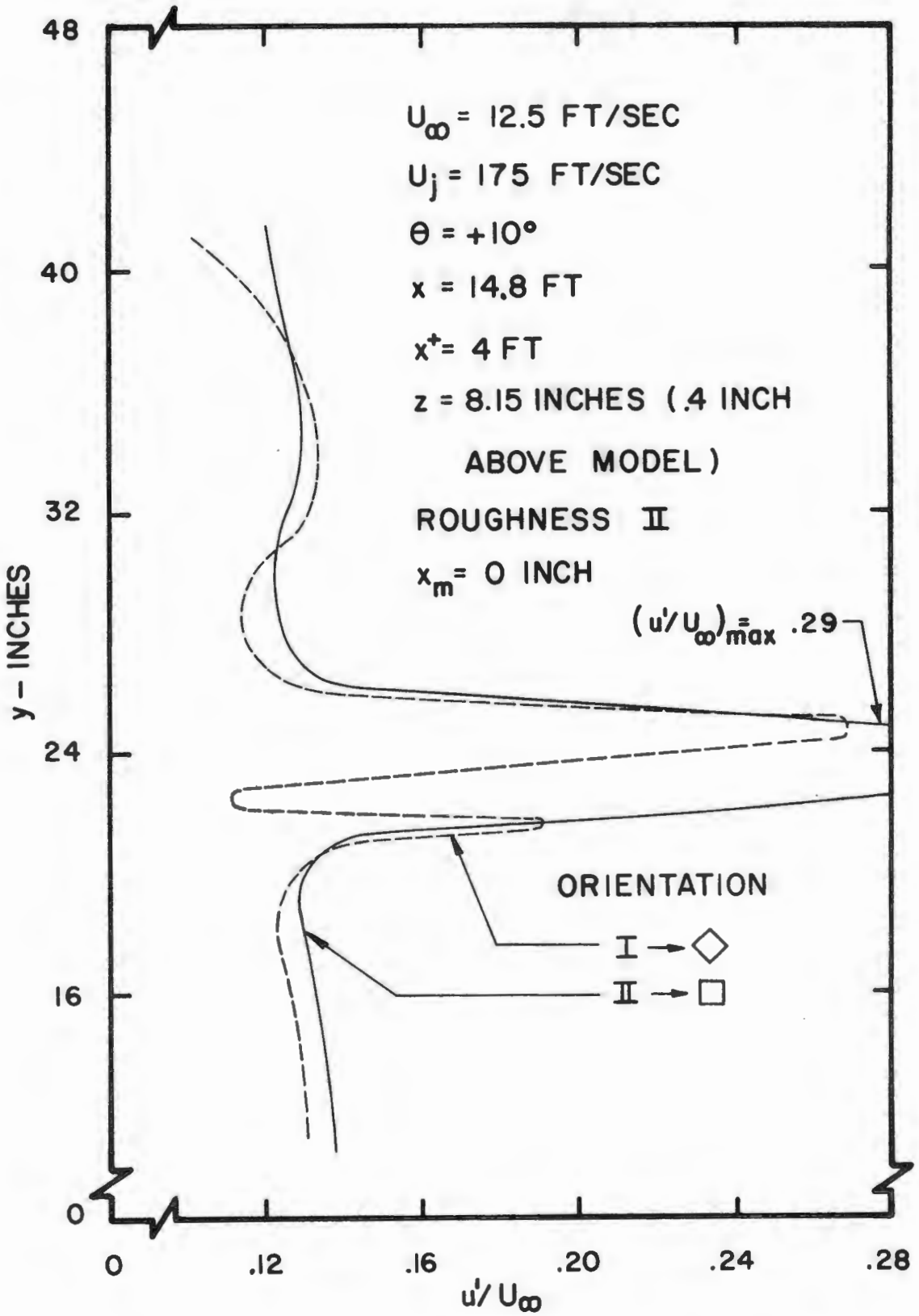

Figure 108. Transverse Turbulence Intensity Profiles Just Above Top of Model for Two Wind Directions Using Counter-Jet Generated Boundary Layer

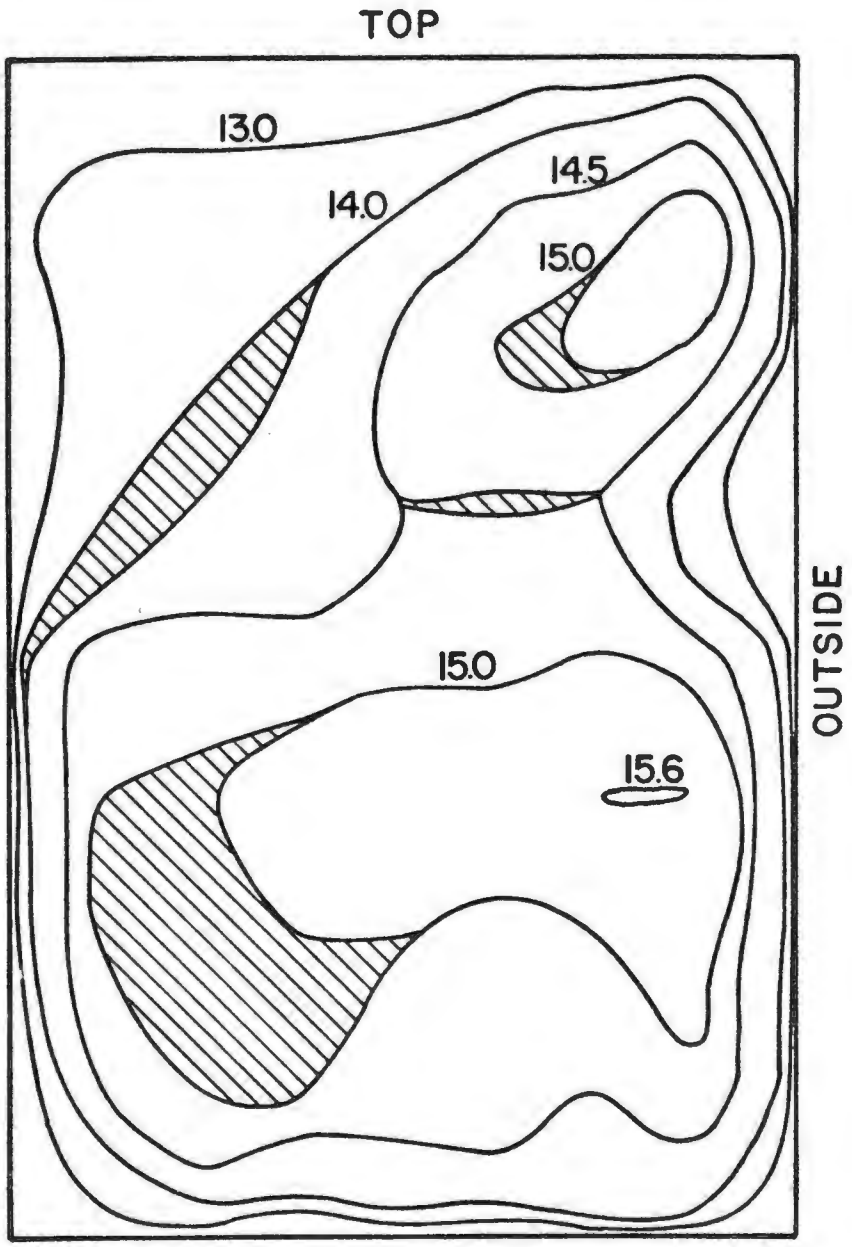

Figure 109. Free-Stream Mean Velocity Contours Obtained Between Stations XI and XII Prior to the Wind Tunnel Modifications, Fan Setting = 2; Fan r.p.m. = 750

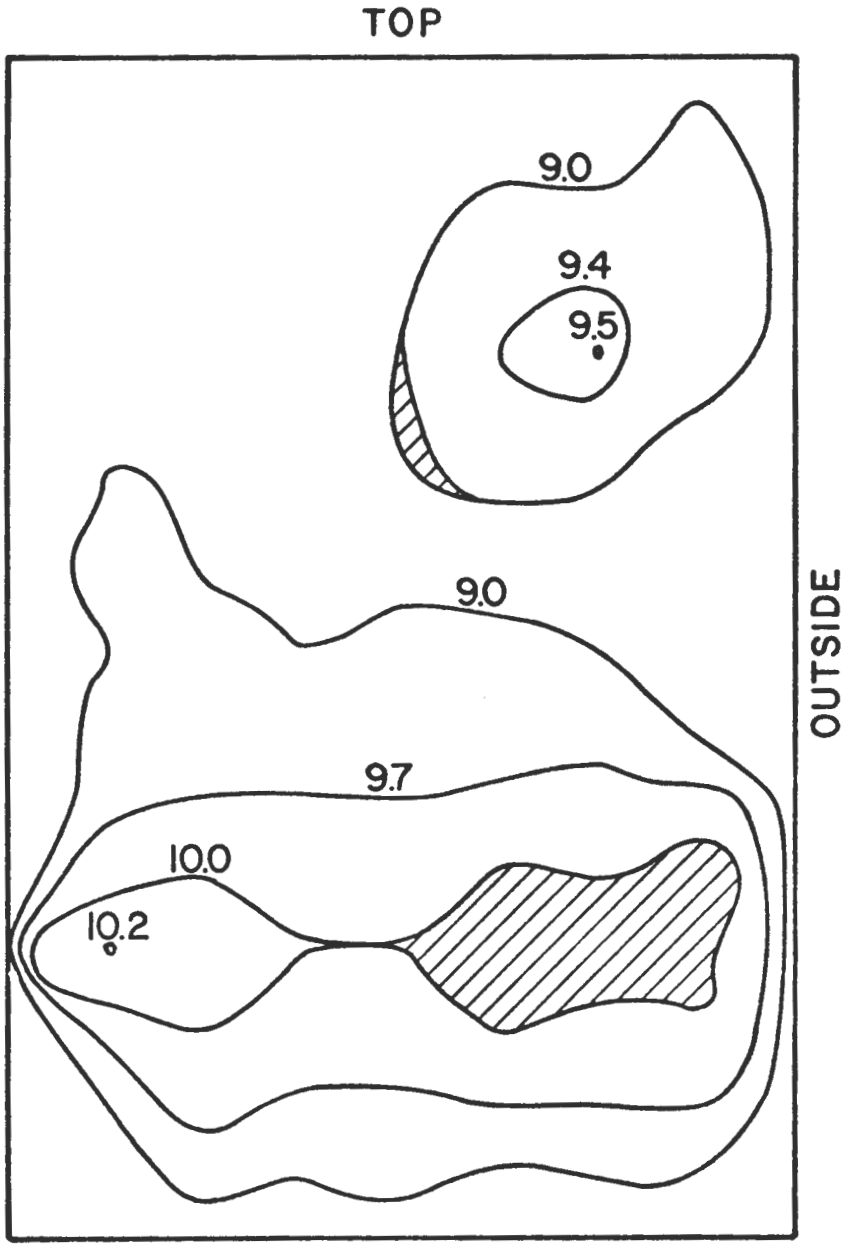

Figure 110. Free-Stream Mean Velocity Contours Obtained Between Stations XI and XII Prior to the Wind Tunnel Modifications; Fan Setting = 2, Fan r.p.m. = 570

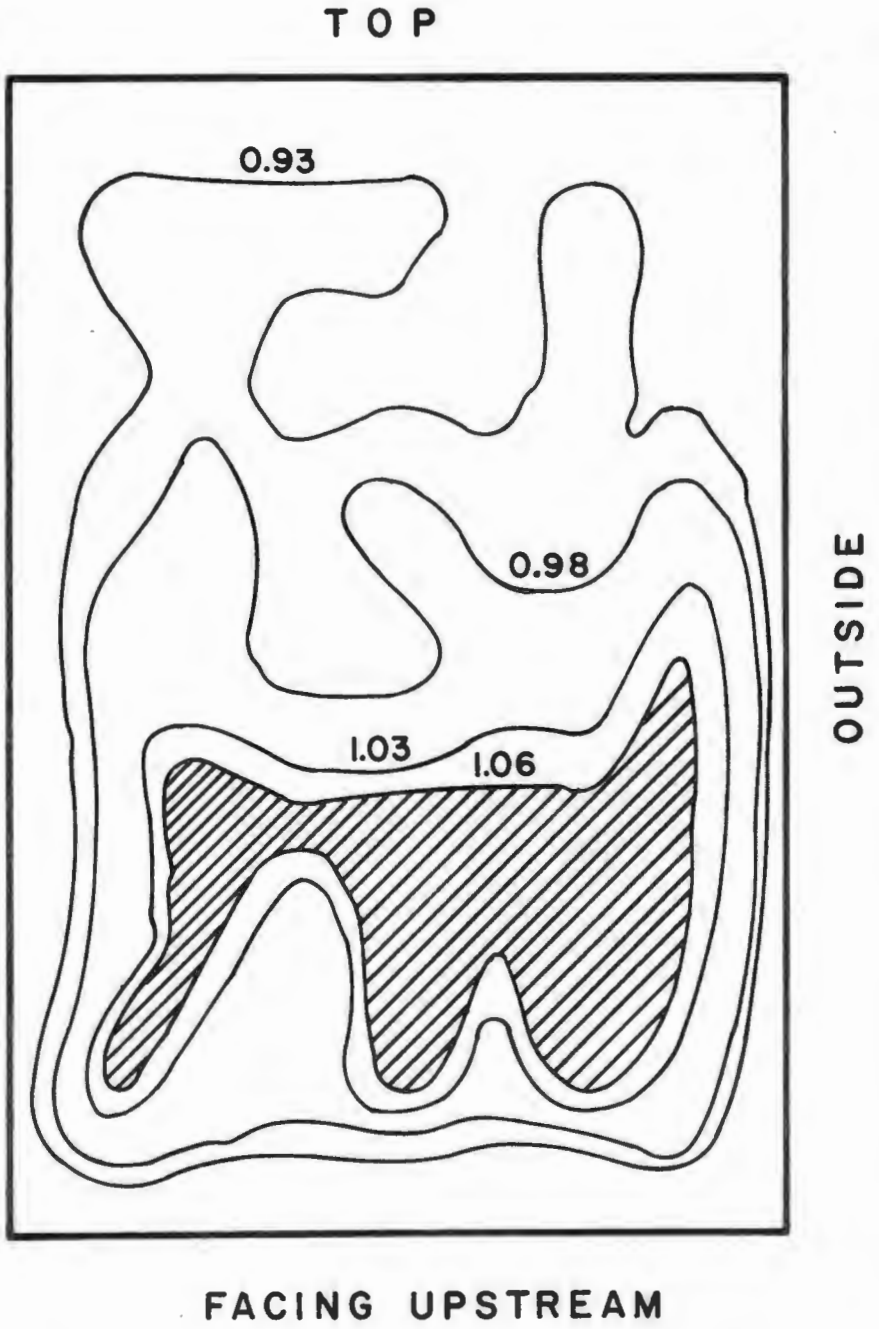

Figure 111. Non-Dimensionalized Free-Stream Mean Velocity Contours Obtained Between Stations IX and X After Wind Tunnel Modifications; Fan Setting = 2, Fan r.p.m. = 1200

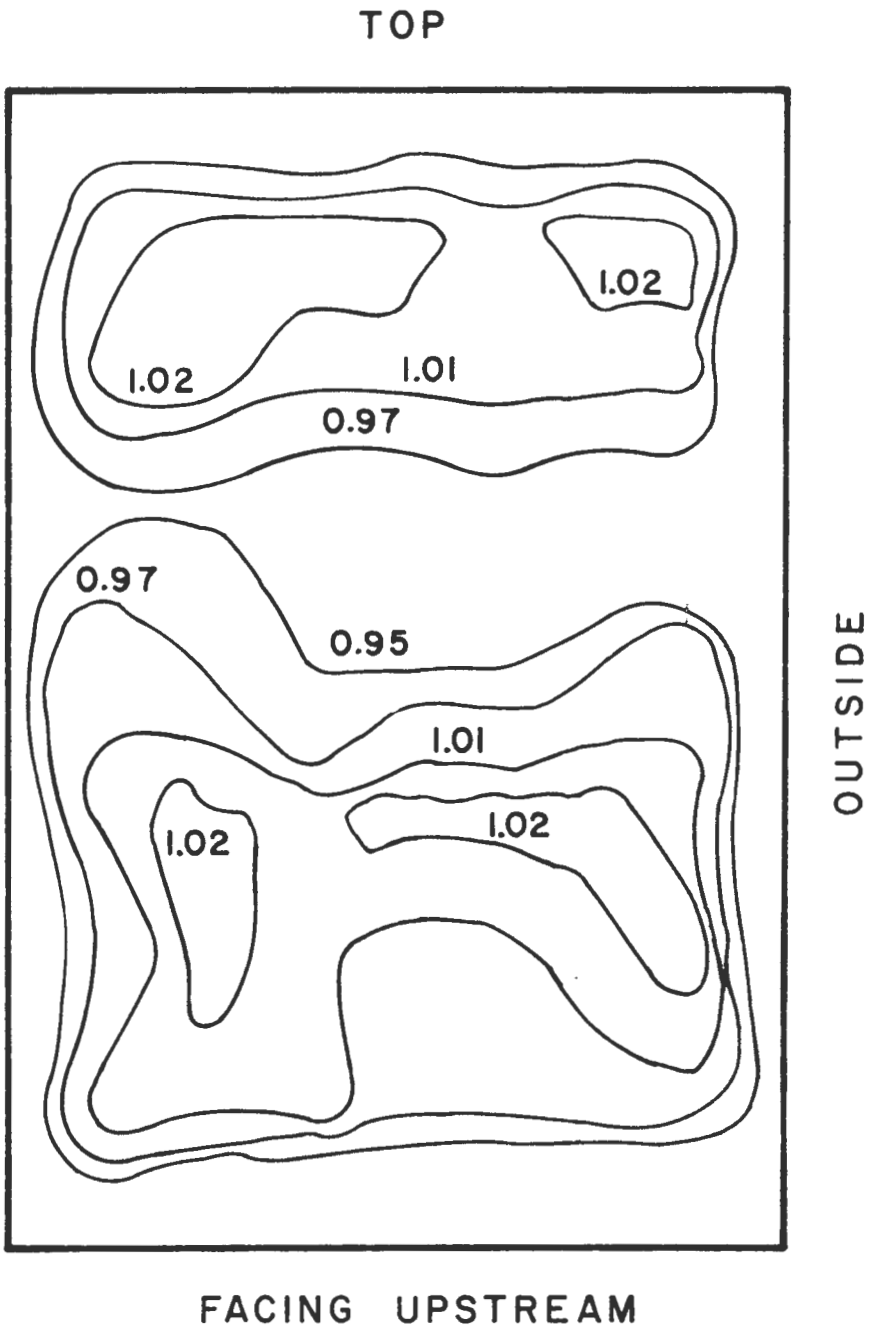

Figure 112. Non-Dimensionalized Free-Stream Mean Velocity Contours Obtained Between Stations IX and X After Wind Tunnel Modifications; Fan Setting = 2, Fan r.p.m. = 1300

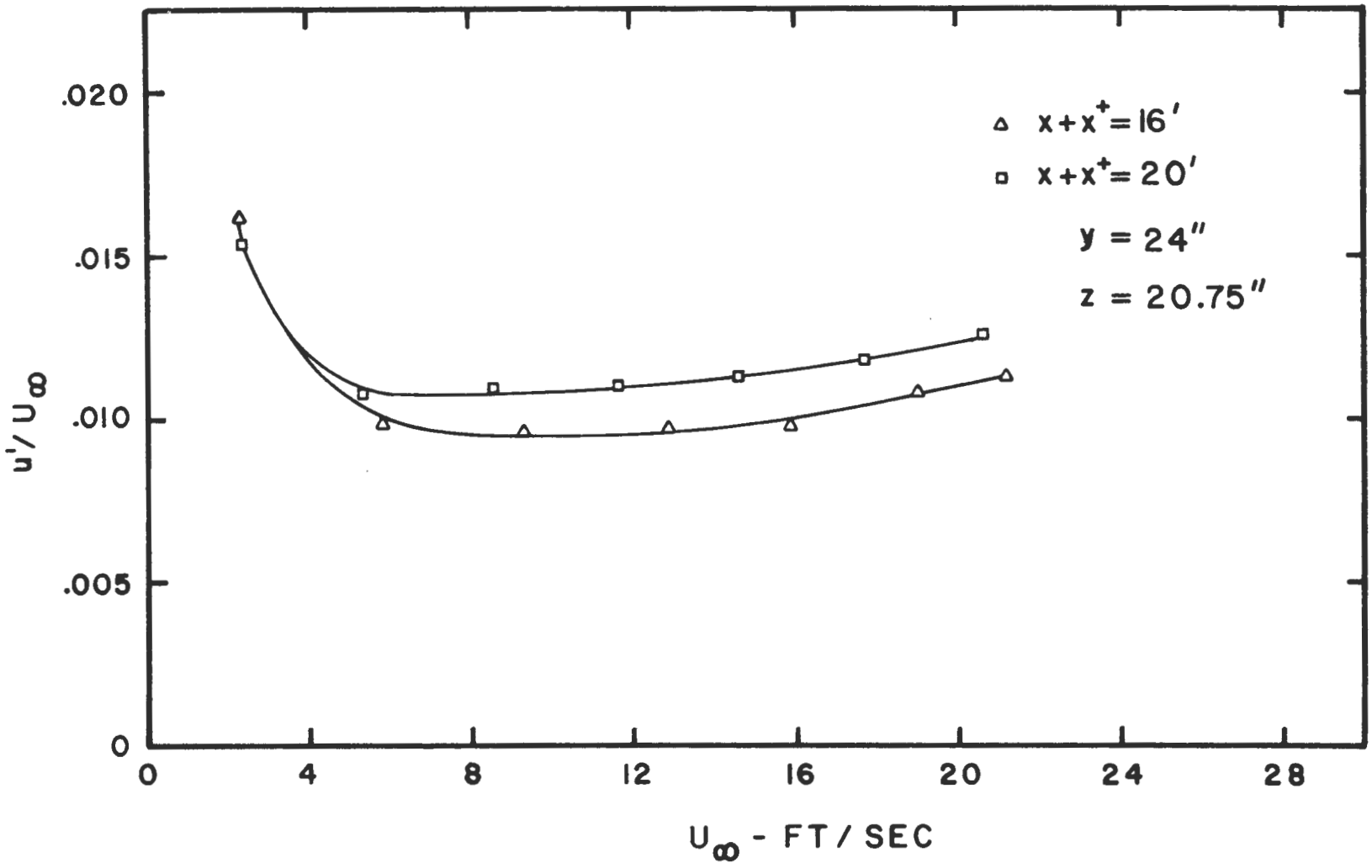

Figure 113. Free-Stream Turbulence Intensity at the Centerline of the Test Section for Various Free-Stream Mean Velocities

BIBLIOGRAPHY

1. Panofsky, H.A. 1974. "The Atmospheric Boundary Layer Below 150 Meters," Annual Review of Fluid Mechanics, Volume 6, Annual Reviews, Inc., Palo Alto, CA.

2. Teunissen, H.W. 1970. "Characteristics of the Mean Wind and Turbulence in the Planetary Boundary Layer," Institute of Aerospace Studies Review No. 32, University of Toronto, Ontario, Canada.

3. Harris, R.I. 1971. "The Nature of the Wind," Paper No. 3, The Modern Design of Wind-Sensitive Structures, CIRIA, 6 Storey's Gate, London SW1, England.

4. Plate, E. J. 1971. Aerodynamic Characteristics of Atmospheric Boundary Layers, AEC critical Review Series, USAEC Tech. Info. Center, Oak Ridge, TN.

5. Davenport, A.G. 1963. "The Relationship of Wind Structure to Wind Loading," Proceedings of Conference on Wind Effects on Buildings and Structures, National Physical Laboratory, London, England.

6. Hanna, S.R. 1969. "The Thickness of the Planetary Boundary Layer," Atmospheric Environment, Vol. 3, p. 519.

7. Cermak, J.E. 1971. "Laboratory Simulation of the Atmospheric Boundary Layer," AIAA Journal, Vol. 9, p. 1746.

8. Davenport, A.G. and N. Isyumov. 1967. "The Application of the Boundary Layer Wind Tunnel to the Prediction of Wind Loading," Paper No. 7, Proceedings of the International Research Seminar, Natural Research Council, Ottawa, Canada, University of Toronto Press, Canada.

9. Standen, N.M. 1972. "A Spire Array for Generating Thick Turbulent Shear Layers for Natural Wind Simulation in Wind Tunnels," Report No. LTR-LA-94, National Aeronautical Establishment, Canada.

10. Counihan, J. 1969. "An Improved Method of Simulating an Atmospheric Boundary Layer in a Wind Tunnel," Atmospheric Environment, Vol. 3, p. 197.

11. Counihan, J. 1970. "Further Measurements in a Simulated Atmospheric Boundary Layer," Atmospheric

Environment, Vol. 4, p. 259.

12. Sundaram, T.R., G.R. Ludwig and G.T. Skinner. 1972. "Modeling of the Turbulence Structure of the Atmospheric Surface Layer," AIAA Journal, Vol. 10, p. 743.

13. Cockrell, D.J. and B.E. Lee. 1970. "Methods and Consequences of Atmospheric Boundary Layer Simulation," Paper No. 13, AGARD C.P. No. 48.

14. Schon, J.P. and P. Mery. 1971. "A Preliminary Study of the Simulation of Neutral Atmospheric Boundary Layer Using Air Injection in a Wind Tunnel," Atmospheric Environment, Vol. 5, p. 299.

15. Teunissen, H.W. 1972. "Simulation of the Planetary Boundary Layer in a Multiple Jet Wind Tunnel," UTIAS Report No. 182, University of Toronto, Ontario, Canada.

16. Clauser, F.H. 1956. "The Turbulent Boundary Layer," Advances in Applied Mechanics, Vol. IV, Academic Press, New York, N.Y.

17. Kovasznay, L.S.G. 1972. "Turbulent Shear Flow," Symposia Mathematica, Vol. IX, p. 507, Institute Nazionale di Alta Matematica.

18. Bradshaw, P. 1971. "Variation on a Theme of Prandtl," AGARD-CP-93, No. C.

19. Whitbread, R.E. 1968. "On the Introduction of Turbulence Into Wind Tunnel Investigations," Paper No. 32, Proceedings, Symposium on Wind Effects on Buildings and Structures, Loughborough University of Technology, England.

20. Bearman, P.W. 1968. "Some Effects of Turbulence on the Flow Around Bluff Bodies," Paper No. 11, Proceedings, Symposium on Wind Effects on Buildings and Structures, Loughborough University of Technology, England.

21. Colin, P.E. and D. Olivari, Editors. 1972. Lecture Series 45 on Buildings and Structures, Von Karman Institute for Fluid Mechanics, Rhode St. Genese, Belgium.

22. Torrance, V.B. 1968. "An Investigation of the Validity of the Current Practice in Simulating the Velocity Profile of the Natural Wind in Wind Tunnels," Paper No. 13, Proceedings, Symposium

on Wind Effects on Buildings and Structures, Loughborough University of Technology, England.

23. Lemberg, R. 1973. "On the Wakes Behind Bluff Bodies in a Turbulent Boundary Layer," Research Report BLWT-3-73, The University of Western Ontario, London, Canada.

24. Nagib, H.M., M.V. Morkovin and J.T. Yung. 1974. "On Modeling of Atmospheric Surface Layers by the Counter-Jet Technique," AIAA Paper, AIAA 8th Aerodynamic Testing Conference, Bethesda, Md.

25. Gunnarsson, T.V. 1974. Implementation of the Counter-Jet Technique for Modeling of Atmospheric Surface Layers in the I.I.T. Environmental Wind Tunnel, M.S. Thesis, Illinois Institute of Technology.

26. Morkovin, M.V. 1972. "An Approach to Flow Engineering Via Functional Flow Modules," Beiträge zur Strömungsmechanik, A. Walz 65th Anniversary Volume, Deutsche Luft-und Raumfahrt Forschungsbericht 72-27.

27. Norman, R.S. 1972. On Obstacle-Generated Secondary Flows in Boundary Layers and Transition to Turbulence, Ph.D. Thesis, Illinois Institute of Technology.

28. Yung, J.T. 1972. Experiments on Jet Mixing and an Environmental Wind Tunnel Evaluation, B.S. Thesis, Illinois Institute of Technology.

29. Way, J.L., H.M. Nagib and J. Tan-atichat. 1973. "On Aeroacoustic Coupling in Free-Stream Turbulence Manipulators," Paper No. 73-1015, AIAA Aero-Acoustics Conference, Seattle, WA.

30. Loehrke, R.I. and H.M. Nagib. 1972. "Experiments on Management of Free-Stream Turbulence, AGARD Report No. 598.

31. Schubauer, G.B. and W.G. Spangenberg. 1947. "Effects of Screens in Wide Angle Diffusers," NACA Report No. 949.

32. Hinze, J.O. 1959. Turbulence, McGraw-Hill Book Company, New York, N.Y.

33. Liu, C.K., S.J. Kline and J.P. Johnston. 1966. "An Experimental Study of Turbulent Boundary Layer on Rough Walls," Report No. MD-15, Thermodynamics Division, Department of Mechanical Engineering, Stanford University.

34. Tan-atichat, J., H.M. Nagib and J.W. Pluister. 1973. "On the Interpretation of the Output of Hot-Film Anemometers and a Scheme of Dynamic Compensation for Water Temperature Variation," Proceedings of the Third Symposium on Turbulence Measurements in Liquids, Rolla, Missouri.

UNCLASSIFIED

Security Classification

DOCUMENT CONTROL DATA - R & D

(Security classification of title, body of abstract and indexing annotation must be entered when the overall report is classified)

1. ORIGINATING ACTIVITY (Corporate author) ILLINOIS INSTITUTE OF TECHNOLOGY MECHANICS & MECHANICAL & AEROSPACE ENGINEERING CHICAGO, ILLINOIS 60616	2a. REPORT SECURITY CLASSIFICATION UNCLASSIFIED 2b. GROUP

3. REPORT TITLE

MEASUREMENTS NEAR BLUFF BODIES IN TURBULENT BOUNDARY LAYERS INTENDED TO SIMULATE ATMOSPHERIC SURFACE LAYERS

4. DESCRIPTIVE NOTES (Type of report and inclusive dates)

Scientific Interim

5. AUTHOR(S) (First name, middle initial, last name)

J. TAN-ATICHAT H. M. NAGIB

6. REPORT DATE	7a. TOTAL NO. OF PAGES	7b. NO. OF REFS
May 1974	185	34

8a. CONTRACT OR GRANT NO	9a. ORIGINATOR'S REPORT NUMBER(S)
F44620-69-0022 b. PROJECT NO. 7921-04 c. 61102F d. 681307	IIT Fluids & Heat Transfer Report R74-2 9b. OTHER REPORT NO(S) (Any other numbers that may be assigned this report) AFOSR-TR-74-

10. DISTRIBUTION STATEMENT

Approved for public release, distribution unlimited.

11. SUPPLEMENTARY NOTES	12. SPONSORING MILITARY ACTIVITY
TECH, OTHER	AF Office of Scientific Research/NA 1400 Wilson Boulevard Arlington, Virginia 22209

13. ABSTRACT

The relatively new counter-jet technique is shown to be suitable for producing thick turbulent boundary layers which may be used to simulate neutral atmospheric surface layers in wind tunnels of moderate length. The increased thickness is achieved in the "I.I.T. Environmental Wind Tunnel" by providing large momentum defects at the wall through upstream-oriented, spanwise-discrete wall jets, with changeable jet velocities and controllable jet angles. This technique permits rapid alteration of reproducible boundary layers from outside the tunnel while the experiments are in progress. It is demonstrated how various mean velocity profiles (which can be represented by a wide range of power law exponents) and turbulence intensity distributions of the boundary layer are obtained at the same streamwise position using different settings of the counter-jet parameters and different types of artificial surface roughness. The transverse uniformity of these layers is also documented. Selected measurements of the flowfield near a bluff body for two wind directions in three different layers are compared in order to examine the sensitivity of measured effects to changes in the characteristics of the turbulent layers. While small changes are observed when results obtained in the two thick boundary layers are compared, large differences are noted between these and those obtained from tests in the thinner "natural" boundary layer of the tunnel. It is in this boundary layer (thickness of boundary layer equal to approximately half of the model height) that the effect of the wind direction with respect to the bluff body is most evident. The data consistently demonstrate that the higher turbulence level within the two thicker layers increases the spreading and decay rates of the wake of the model. Influence of the wind direction on the flowfield on top of the bluff body is much stronger than that due to changes in the boundary layers. Similar sensitivity to the orientation of the bluff body is observed downstream of the model at low elevations.

DD FORM 1 NOV 68 1473

UNCLASSIFIED

Security Classification